

# **INVESTIGATION OF ADVANCED PROCESSED SINGLE-CRYSTAL TURBINE BLADE ALLOYS**

**Prepared by:**

**B.J. Peters**

**C.M. Biondo**

**D.P. DeLuca**

**United Technologies Corporation**

**Pratt & Whitney**

**Government Engines & Space Propulsion**

**P.O. Box 109600**

**West Palm Beach, FL 33410-9600**

**December 1995**

**Final**

**Period of Performance from 16 December 1991 through 31 December 1995**

**Prepared for:**

**George C. Marshall Space Flight Center**

**National Aeronautics and Space Administration**

**Marshall Space Flight Center, AL 35812**

**Under Contract: NAS8-39050**



# **INVESTIGATION OF ADVANCED PROCESSED SINGLE-CRYSTAL TURBINE BLADE ALLOYS**

**Prepared by:  
B.J. Peters  
C.M. Biondo  
D.P. DeLuca**

**United Technologies Corporation  
Pratt & Whitney  
Government Engines & Space Propulsion  
P.O. Box 109600  
West Palm Beach, FL 33410-9600**

**December 1995**

**Final**


**Period of Performance from 16 December 1991 through 31 December 1995**

**Prepared for:  
George C. Marshall Space Flight Center  
National Aeronautics and Space Administration  
Marshall Space Flight Center, AL 35812**

**Under Contract: NAS8-39050**





 National Aeronautics and Space Administration		Report Document Page	
1. Report No. FR-24007		2. Government Accession No.	
3. Recipient's Catalog No.		4. Title and Subtitle Investigation of Advanced Processed Single-Crystal Turbine Blade Alloys	
5. Report Date		6. Performing Organization Code 52661	
7. Authors Program Manager: D.P. DeLuca Principal Investigators: B.J. Peters and C.M. Biondo		8. Performing Organization Report No. FR-24007	
9. Performing Organization Name and Address United Technologies Pratt & Whitney Government Engines & Space Propulsion P.O. Box 109600, West Palm Beach, FL 33410-9600		10. Work Unit No.	
11. Contract or Grant No. NAS8-39050		12. Sponsoring Agency Name and Address George C. Marshall Space Flight Center National Aeronautics and Space Administration Marshall Space Flight Center, AL 35812	
13. Type of Report and Period Covered CPFF/16 December 1991 - 31 December 1995		14. Sponsoring Agency Code	
15. Supplementary Notes			
16. Abstract <p>This investigation studied the influence of thermal processing and microstructure on the mechanical properties of the single-crystal, nickel-based superalloys PWA 1482 and PWA 1484. The objective of the program was to develop an improved single-crystal turbine blade alloy that is specifically tailored for use in hydrogen fueled rocket engine turbopumps.</p> <p>High-gradient casting, hot isostatic pressing (HIP), and alternate heat treatment (HT) processing parameters were developed to produce pore-free, eutectic-free microstructures with different <math>\gamma'</math> precipitate morphologies.</p> <p>Test materials were cast in high thermal gradient solidification (greater than 30°C/cm [137°F/in.]) casting furnaces for reduced dendrite arm spacing, improved chemical homogeneity, and reduced interdendritic pore size.</p> <p>The HIP processing was conducted in 40-cm (15.7-in.) diameter production furnaces using a set of parameters selected from a trial matrix study. Metallography was conducted on test samples taken from each respective trial run to characterize the as-HIP microstructure.</p> <p>Post-HIP alternate HT processes were developed for each of the two alloys. The goal of the alternate HT processing was to fully solution the eutectic <math>\gamma/\gamma'</math> phase islands and to develop a series of modified <math>\gamma'</math> morphologies for subsequent characterization testing. This was accomplished by slow cooling through the <math>\gamma'</math> solvus at controlled rates to precipitate volume fractions of large <math>\gamma'</math>. Post-solution alternate HT parameters were established for each alloy providing additional volume fractions of finer precipitates.</p> <p>Screening tests included tensile, high-cycle fatigue (HCF), smooth and notched low-cycle fatigue (LCF), creep, and fatigue crack growth evaluations performed in air and high pressure (34.5 MPa [5 ksi]) hydrogen at room and elevated temperature. Under the most severe embrittling conditions (HCF and smooth and notched LCF in 34.5 MPa [5 ksi] hydrogen at 20°C (68°F), screening test results showed increases in fatigue life typically on the order of 10X, when compared to the current Space Shuttle Main Engine (SSME) Alternate Turbopump (AT) blade alloy (PWA 1480).</p>			
17. Key Words (Suggested by Author[s]) PWA 1482, PWA 1484, bimodal $\gamma'$ , eutectic-free, fatigue crack, growth, high-pressure hydrogen, hydrogen embrittlement, SSME AT		18. Distribution Statement	
19. Security Classification (of this Report) Unclassified	20. Security Classification (of this Page) Unclassified	21. No. of Pages 195	22. Price



## FOREWORD

The work for this program, *Investigation of Advanced Single-Crystal Turbine Blade Alloys*, was performed under National Aeronautics and Space Administration (NASA) Contract NAS8-39050. The sponsoring agency was the NASA, George C. Marshall Space Flight Center, Marshall Space Flight Center, Alabama. The NASA Program Monitor was Deborah Diane Schmidt.

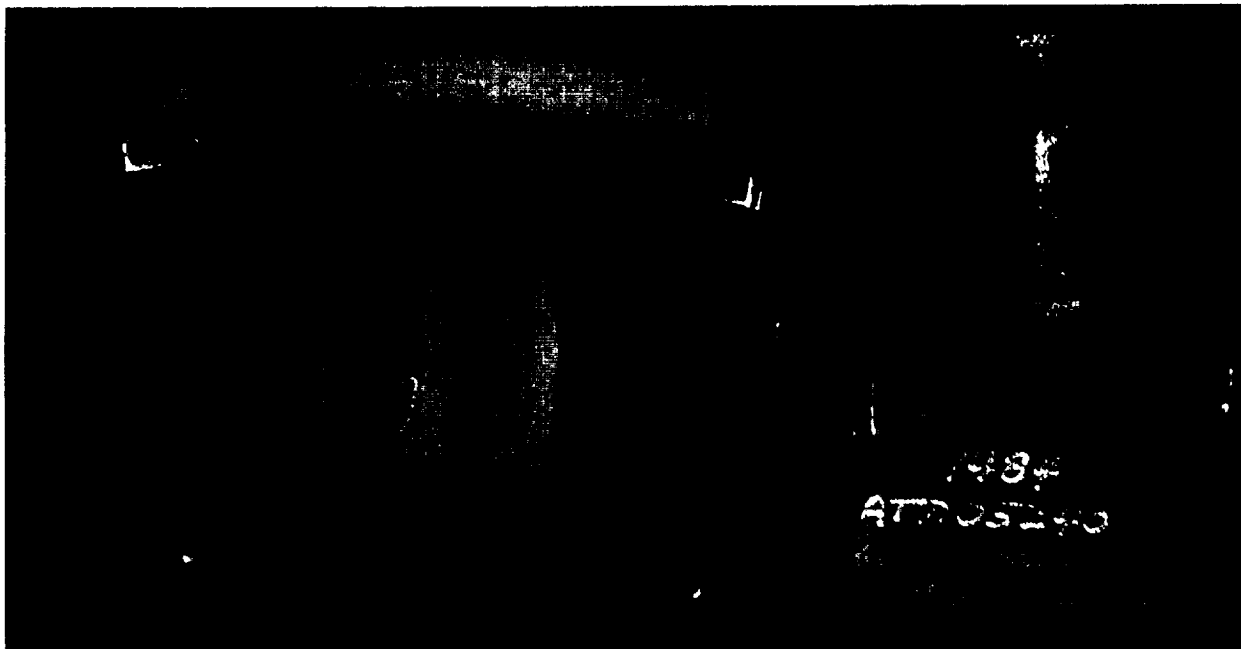
The program was conducted at the Materials and Mechanics Engineering Laboratories, Pratt & Whitney (P&W), West Palm Beach, Florida. The Principal Investigators for this program were B.J. Peters. and C.M. Biondo. The P&W Program Manager was D.P. DeLuca.



## EXECUTIVE SUMMARY

The objective of this program was to develop an advanced turbine blade alloy for use in liquid rocket turbopumps. The study focused on microstructural modifications to two single-crystal nickel-based superalloys; PWA 1484 and PWA 1482. These superalloys both exhibited significantly better durability than the blade alloys, directionally-solidified (DS) columnar-grained Mar-M246+Hf and PWA 1480, which are currently used in the National Aeronautics and Space Administration (NASA) Space Shuttle Main Engine (SSME).

The program improvements in low-cycle fatigue (LCF), high-cycle fatigue (HCF), and melt margin have provided the NASA/Pratt & Whitney (P&W) SSME Alternate Turbopump (AT) Program with a turbine blade alloy possessing an attractive balance of properties with increased durability. At the writing of this report, PWA 1484 is in various stages of test and evaluation under the ATD Program leading to its potential implementation as a turbine vane alloy in the AT High-Pressure Fuel Turbopump (HPFTP). The results of preliminary HPFTP blade and vane casting trials with the Advanced Processed PWA 1484 are shown in the following figure.



FLD130065



## CONTENTS

<i>Section</i>	<i>Page</i>
1. INTRODUCTION AND PROGRAM OBJECTIVE .....	1
1.1 INTRODUCTION .....	1
1.2 PROGRAM OBJECTIVE .....	1
2. TECHNICAL EFFORT .....	3
2.1 ALLOY SELECTION .....	3
2.2 MATERIAL PROCUREMENT .....	5
2.3 HOT ISOSTATIC PROCESS OPTIMIZATION .....	8
2.4 THERMAL TREATMENT OPTIMIZATION .....	26
2.5 HYDROGEN TEST – ALTERNATE MICROSTRUCTURE SCREENING .....	40
2.5.1 Approach .....	40
2.5.2 Results .....	54
2.5.3 Summary .....	59
2.6 PROGRAM TEST MATRIX .....	61
2.6.1 Test Matrix and Description .....	61
2.6.2 Results .....	61
2.6.3 Summary .....	86
2.7 MICROSTRUCTURAL AND FRACTOGRAPHIC ANALYSIS .....	86
2.7.1 Introduction and background .....	86
2.7.2 PWA 1484 Tensile Fractures .....	89
2.7.3 Creep Fractures .....	109
2.7.4 Fatigue Fractures .....	111
2.7.5 Crack Growth Fracture .....	132
2.7.6 Elemental Analysis/Phase Compositions/Deformation Structures .....	136
2.7.7 Summary .....	139
3. SUMMARY .....	145
3.1 PROCESSING .....	145
3.2 ALLOY CAPABILITY .....	145
3.2.1 Tensile .....	145
3.2.2 Notched Low-Cycle Fatigue .....	145
3.2.3 Crack Growth .....	146
3.3 PROGRAM TEST MATRIX .....	146
3.3.1 Yield Strength .....	146
3.3.2 Creep Stress/Rupture .....	146
3.3.3 Fatigue .....	147
3.4 MECHANISTIC ASPECTS .....	147
3.5 OVERALL SUMMARY .....	148
4. CONCLUSIONS .....	149

5. SPECIFIC RECOMMENDATIONS.....	151
APPENDIX A — HEAT CERIFICATION.....	153
APPENDIX B — TEST MATRIX SPECIMENS .....	159
APPENDIX C — NOTCHED LOW-CYCLE FATIGUE FRACTURES FROM HEAT TREATMENTS 1 THROUGH 7 PRODUCED AT 20°C (68°F) IN 34.5 MPA (5 KSI) HYDROGEN .....	165



## FIGURES

<i>Figure</i>	<i>Page</i>
1. Averaged Notched Tensile ( $K_t = 8$ ) Strength Versus Temperature for Waspaloy in Ambient Air and 34.5 MPa (5 ksi) Gaseous Helium and Hydrogen Environments .....	4
2. Strain Control LCF Results ( $R = -1$ ) Showing Degradation Due to Hydrogen for Waspaloy Versus Temperature at 1.2 percent Total Strain Range .....	4
3. As-Cast Microstructure of PWA 1482 (Top) and PWA 1484 (Bottom) .....	6
4. As-Polished Microstructure of PWA 1482 Following HIP Processing at IMT (Unetched) .....	10
5. As-Polished Microstructure of PWA 1482 Following HIP Processing at IMT (Unetched) .....	11
6. As-Polished Microstructure of PWA 1484 Following HIP Processing at IMT (Unetched) .....	12
7. As-Polished Microstructure of PWA 1484 Following HIP Processing at IMT (Unetched) .....	13
8. Typical Microstructure of PWA 1482 Following HIP and Solution Heat Treatment (Etch: AG21) .....	14
9. Typical Microstructure of PWA 1482 Following HIP and Solution Heat Treatment (Etch: AG21) .....	15
10. Typical Microstructure of PWA 1482 Following HIP and Solution Heat Treatment (Etch: AG21) .....	16
11. Typical Microstructure of PWA 1484 Following HIP and Solution Heat Treatment (Etch: AG21) .....	18
12. Typical Microstructure of PWA 1484 Following HIP and Solution Heat Treatment (Etch: AG21) .....	19
13. Typical Microstructure of PWA 1484 Following HIP and Solution Heat Treatment (Etch: AG21) .....	20
14. Typical Microstructures from PWA 1482 Test Samples HIP Processed at 1307°C (2385°F)/103 MPa (15 ksi)/4 hr (Top) and 1285°C (2345°F)/103 MPa (15 ksi)/4 hr (Bottom) .....	23
15. Typical Microstructures from PWA 1484 Test Samples HIP Processed at 1307°C (2385°F)/103MPa (15 ksi)/4 hr .....	25
16. PWA 1484 Alternate HT Microstructures .....	29
17. PWA 1484 Microstructure Produced in Thermal Treatment Optimization Studies .....	30
18. PWA 1484 Microstructure Produced in Thermal Treatment Optimization Studies .....	31
19. PWA 1484 Microstructure Produced in Thermal Treatment Optimization Studies .....	32
20. PWA 1484 Microstructure Produced in Thermal Treatment Optimization Studies .....	33
21. PWA 1484 Microstructure Produced in Thermal Treatment Optimization Studies .....	34
22. PWA 1484 Microstructure Produced in Thermal Treatment Optimization Studies .....	35
23. PWA 1484 Microstructure Produced in Thermal Treatment Optimization Studies .....	36
24. PWA 1482 Alternate HT 4 .....	38
25. PWA 1482 Alternate HT 6 .....	39
26. Remote Blast Cells Housing High-Pressure Environment Test Machines .....	40
27. Gas Control Console and Television Monitors .....	41
28. High-Pressure Environmental LCF/HCF Test Machine; Pressure Vessel Open .....	42
29. View of Typical LCF Specimen Installed in Extensometer .....	42

30.	Automated Crack Growth Rate Control and Data Acquisition System.....	44
31.	Tensile Stress-Strain Specimen.....	45
32.	Creep Rupture Specimen.....	46
33.	Double Notch LCF Specimen .....	48
34.	Low-Cycle Fatigue Specimen for Air Testing .....	49
35.	High-Pressure Environment LCF Specimen.....	50
36.	Typical LCF Test With Mean Strain of Zero.....	51
37.	High-Cycle Fatigue Specimen (Smooth $K_t = 1.0$ ) .....	52
38.	Crack Growth Rate Specimen.....	53
39.	Tensile Yield and Ultimate Data for PWA 1484 HT Trials, Tested at 20°C (68°F) in 34.5 MPa (5 ksi) Hydrogen With Comparison to PWA 1480 Yield Data for Same Condition .....	56
40.	Tensile Ductility Data for PWA 1484 HT Trials Tested at 20°C (68°F) in 34.5 MPa (5 ksi) Hydrogen With Comparison to PWA 1480 Ductility Data for Same Condition.....	56
41.	Load Controlled LCF Screening Results for [001] Oriented PWA 1484 Double Notch specimens Tested in 34.5 MPa (5 ksi) Hydrogen at 0.167 Hz, 20°C (68°F), $R = 0.05$ , 620.55 MPa (90 ksi), $K_t = 2.18$ ; Comparison to the Means of DS MAR-M-246+Hf and PWA 1480 Tested Under the Same Condition ....	58
42.	Comparison of Double Notch LCF Data for Different HTs of PWA 1484, Tested at Room Temperature in 34.5 MPa (5 ksi) Hydrogen, $R = 0.05$ .....	58
43.	Crack Growth Screening Results for [001] Oriented PWA 1484 Specimens Tested in 34.5 MPa (5 ksi) Hydrogen at 0.167 Hz, 20°C (68°F), $R = 0.05$ , $K_t = 2.18$ ; Comparison of PWA 1484, HTs 4 and 6 with PWA 1480 .....	60
44.	Tensile Engineering Stress/Strain Results for [001] Oriented PWA 1482 and PWA 1484 Tested in 34.5 MPa (5 ksi) Hydrogen at 20°C (68°F) .....	65
45.	Tensile Engineering Stress/Strain Results for [001] Oriented PWA 1482 and PWA 1484 Tested in Air and 34.5 MPa (5 ksi) Hydrogen at 649°C (1200°F) .....	65
46.	Tensile Engineering Stress/Strain Results for [001] Oriented PWA 1484 Tested in Air at 649°C (1200°F), 760°C (1400°F), and 871°C (1600°F) .....	66
47.	Air 0.2 percent Yield Properties Versus Temperature for PWA 1489 and [001] Oriented PWA 1480, PWA 1482, and PWA 1484 .....	66
48.	34.5 MPa (5 ksi) Hydrogen 0.2 percent Yield Properties Versus Temperature for PWA 1489 and [001] Oriented PWA 1480, PWA 1482, and PWA 1484 .....	67
49.	Air Ultimate Strength Properties Versus Temperature for PWA 1489 and [001] Oriented PWA 1480, PWA 1482, and PWA 1484 .....	67
50.	34.5 MPa (5 ksi) Hydrogen Ultimate Strength Properties Versus Temperature for PWA 1489 and [001] Oriented PWA 1480, PWA 1482, and PWA 1484 .....	68
51.	Air Percent Elongation Versus Temperature for PWA 1489 and [001] Oriented PWA 1480, PWA 1482, and PWA 1484 .....	68
52.	34.5 MPa (5 ksi) Hydrogen Percent Elongation Versus Temperature for PWA 1489 and [001] Oriented PWA 1480, PWA 1482, and PWA 1484 .....	69

53.	Air Percent Reduction in Area Versus Temperature for PWA 1489 and [001] Oriented PWA 1480, PWA 1482, and PWA 1484 .....	69
54.	34.5 MPa (5 ksi) Hydrogen Percent Reduction in Area Versus Temperature for PWA 1489 and [001] Oriented PWA 1480, PWA 1482, and PWA 1484 .....	70
55.	Air 871°C (1600°F) Creep Properties at 413.7 MPa (60 ksi) for [001] Oriented PWA 1480, PWA 1482, and PWA 1484 .....	73
56.	Load Controlled HCF Results for [001] Oriented PWA 1482 Specimens Tested in 34.5 MPa (5 ksi) Hydrogen at 0.167 Hz, 20°C (68°F), R = -1 .....	75
57.	Load Controlled HCF Results for [001] Oriented PWA 1484 Specimens Tested in 34.5 MPa (5 ksi) Hydrogen at 0.167 Hz, 20°C (68°F), R = -1 .....	75
58.	Alloy Comparison of Mean Curves 34.5 MPa (5 ksi) Hydrogen HCF Results Smooth Specimens Tested at 20/30 Hz, 20°C (68°F), R = -1 .....	76
59.	Load Controlled LCF Results for [001] Oriented PWA 1482 Double Notch Specimens Tested at 0.167 Hz, 20°C (68°F), R = 0.05, Kt = 2.18 .....	78
60.	Load Controlled LCF Results for [001] Oriented PWA 1484 Double Notch Specimens Tested at 0.167 Hz, 20°C (68°F), R = 0.05, Kt = 2.18 .....	78
61.	Alloy Comparison of Mean Curves Air Load Controlled LCF Results Double Notch Specimens Tested at 0.167 Hz, 20°C (68°F), R = 0.05, Kt = 2.18 .....	79
62.	Alloy Comparison of Mean Curves 34.5 MPa (5 ksi) Hydrogen Load Controlled LCF Results Double Notch Specimens Tested at 0.167 Hz, 20°C (68°F), R = 0.05, Kt = 2.18 .....	79
63.	Strain Controlled LCF Results for [001] Oriented PWA 1482 Specimens Tested at 0.167 Hz, 20°C (68°F), R = -1 .....	83
64.	Strain Controlled LCF Results for [001] Oriented PWA 1484 Specimens Tested at 0.167 Hz, 20°C (68°F), R = -1 .....	83
65.	Alloy Comparison of Mean Curves Air Strain Control LCF Results Smooth Specimens Tested at 0.167 Hz, 20°C (68°F), R = -1 .....	84
66.	Alloy Comparison of Mean Curves 34.5 MPa (5 ksi) Hydrogen Strain Control LCF Results Smooth Specimens Tested at 0.167 Hz, 20°C (68°F), R = -1 .....	84
67.	Fatigue Crack Growth Results for [001] Oriented PWA 1484 Tested in 34.5 MPa (5 ksi) Hydrogen at 0.167 Hz, 20°C (68°F), R = 0.1 Compared to PWA 1480 Data and Model for Same Condition.....	85
68.	Microscopic Fracture Modes Dictate Crack Growth Behavior in Single-Crystals; Matrix Failure Prevails in Near Threshold Region (Left) and Is Shown Idealized and Fractographically Above the Data; In Region II, Propagation Is by Microscopic (111) Failure On the Size Order of the $\gamma$ Precipitate.....	88
69.	Partially Restoring Normal Air Fracture Mode in PWA 1480 Under Hydrogen Embrittlement Conditions Has a Pronounced Effect on Crack Growth Rate in Hydrogen.....	89
70.	Overall View of PWA 1484 HT 1; Fracture Origin (Center of Photo) Is Matrix Failure; Conditions – PWA 1484 HT 1, 20°C (68°F), 34.5 MPa (5 ksi), Hydrogen, Tensile.....	90
71.	Overall View of PWA 1484 HT 2; Fracture Origin Is at Streaks of Matrix Failure; Conditions – PWA 1484 HT 2, 20°C (68°F), 34.5 MPa (5 ksi), Hydrogen, Tensile.....	91

72.	Overall View of PWA 1484 HT 4; Fracture Is Noncrystallographic (Macroscopically) (Note Lenticular Crack at Upper Right); Conditions – PWA 1484 HT 4, 20°C (68°F), 34.5 MPa (5 ksi) Hydrogen, Tensile .....	91
73.	Flat Fracture Nominally Parallel to (001) Occurs in Primary $\gamma'$ Microscopic (111) Fracture Occurs in Surrounding Cuboidal $\gamma'$ ; Conditions – PWA 1484 HT 4, 20°C (68°F), 34.5 MPa (5 ksi) Hydrogen, Tensile .....	92
74.	Fine Lenticular Cracking in Same Specimen Is Nominally Parallel To (001) and in Some Cases Can Be Resolved as Interprecipitate; Conditions – PWA 1484 HT 4, 20°C (68°F), 34.5 MPa (5 ksi) Hydrogen, Tensile .....	92
75.	Larger Cracks in Same Specimen; Onset of this Form of Cracking Appears To Be Stress Intensity Dependent; Conditions – PWA 1484 HT 4, 20°C (68°F), 34.5 MPa (5 ksi) Hydrogen, Tensile .....	93
76.	Lenticular Cracking in Cast $\gamma'$ Superalloys in Hydrogen; This Example is Equiaxed Alloy, HIP Microcast MAR-M-247 (Notched LCF in 34.5 MPa (5 ksi) Hydrogen, 20°C (68°F) .....	93
77.	Lenticular Cracking in DS MAR-M-246+Hf (Notched LCF in 34.5 MPa [5 ksi] Hydrogen, 20°C [68°F]) Showing Prominent Lenticular Cracks .....	94
78.	Overall View of PWA 1484 HT 6; Fracture Is Noncrystallographic (Macroscopically); Conditions – PWA 1484 HT 6, 20°C (68°F), 34.5 MPa (5 ksi) Hydrogen, Tensile.....	94
79.	Detail of $\gamma'$ Fracture Nominally Parallel to (001), But Decidedly Rough (Increased Crack Path Tortuosity), Microscopic (111) Fracture Outlines Primary $\gamma'$ ; Conditions – PWA 1484 HT 6, 20°C (68°F), 34.5 MPa (5 ksi) Hydrogen, Tensile.....	95
80.	Overall View of PWA 1484 HT 4 Tested in Air at Room Temperature Showing Prominent Macroscopic (111) Planes; Conditions – PWA 1484 HT 4, 20°C (68°F), Air, Tensile .....	96
81.	Detail of Crystallographic Fracture Plane from Previous Fracture, Nominally Parallel to (111); Conditions – PWA 1484 HT 4, 20°C (68°F), Air, Tensile .....	96
82.	High-Magnification View of (111) Fracture Surface Shows More Roughness Than Conventional Microstructures Exhibit; Conditions – PWA 1484 HT 4, 20°C (68°F), Air, Tensile.....	97
83.	Overall View of PWA 1484 HT 6 Tested in Air at Room Temperature Showing Prominent Macroscopic (111) Planes; Conditions – PWA 1484 HT 6, 20°C (68°F), Air, Tensile .....	97
84.	High-Magnification View of (111) Fracture Surface Shows High Degree of Roughness Versus Conventional Microstructures; Conditions – PWA 1484 HT 6, 20°C (68°F), Air, Tensile .....	98
85.	Overall View of PWA 1484 HT 4 Tested in Air at Room Temperature Showing Single (111) Planar Fracture; Conditions – PWA 1484 HT 4, 650°C (1200°F), Air, Tensile.....	99
86.	High-Magnification View of (111) Fracture Surface Shows Oxidized $\gamma$ Phase and Roughness Associated With Bimodal $\gamma'$ ; Conditions – PWA 1484 HT 4, 650°C (1200°F), Air, Tensile .....	99
87.	Overall View of PWA 1484 HT 6 Tested in Air at 650°C (1200°F) Showing Two Intersecting (111) Fracture Planes (Typical of Elevated Single-Crystal Tensile Failures); Conditions – PWA 1484 Microstructure HT 6, 650°C (1200°F), Air, Tensile .....	100
88.	Detail of (111) Fracture Surface Shows Oxidized $\gamma$ Phase and Marked Roughness; Conditions – PWA 1484 HT 6, 650°C (1200°F), Air, Tensile .....	100
89.	High-Magnification Study of (111) Fracture Surface Shows Unoxidized Primary $\gamma'$ and Marked Roughness; Conditions – PWA 1484 HT 6, 650°C (1200°F), Air, Tensile .....	101

90.	Overall View of PWA 1484 HT 6 Tested in 650°C (1200°F) Hydrogen Showing Prominent Macroscopic (111) Planes Intersecting at Center of Specimen; Overall Appearance Does Not Differ from 650°C (1200°F) Air Fracture; Conditions – PWA 1484 HT 6, 650°C (1200°F), Hydrogen, Tensile.....	102
91.	High-Magnification View of (111) Fracture Surface Shows High Degree of Ductility in $\gamma$ Phase Versus 650°C (1200°F) Air Tests; Conditions – PWA 1484 HT 6, 650°C (1200°F) Hydrogen, Tensile.....	102
92.	Overall View of PWA 1484 HT 4 Tested in 650°C (1200°F) Hydrogen Showing Prominent Macroscopic (111) Planes and Steps (Detailed in Subsequent Figures; Conditions – PWA 1484 HT 4, 650°C (1200°F), Hydrogen, Tensile.....	103
93.	High-Magnification View of Step on (111) Fracture Surface; Dark Area at Center Is Analyzed in Figure 94; Conditions – PWA 1484 HT 4, 650°C (1200°F), Hydrogen, Tensile .....	103
94.	Back Scattered Electron Image of Field Shown Figure 93 Shows Localized Area of Precipitated Carbide; Conditions – PWA 1484 HT 4, 650°C (1200°C), Hydrogen, Tensile .....	104
95.	Overall View of Tensile Failure Shows Localized Areas of Hydrogen Affected Fracture in the Form of Flat Feathery Areas at Perimeter (Detailed in Subsequent Figures); Condition – PWA 1482 HT 4, 20°C (68°F), Hydrogen, Tensile .....	105
96.	Closeup View of Localized Areas of Hydrogen Affected Fracture from Figure 95; This Is Typical Hydrogen Tensile Fractures; Conditions – PWA 1482 HT 4, 20°C (68°F), Hydrogen, Tensile.....	105
97.	At 400X, Microstructure Can Be Discerned Because of Differential Fracture Modes in Primary Versus Fine Cuboidal $\gamma$ ; At low stress intensity ( $\Delta K$ ), Fracture Is Nearly All Nominally (001); As $\Delta K$ Increases, Fine Cuboidal Precipitates Begin To Fracture Along (111) Planes Delineating Larger Primary $\gamma$ ; Conditions – PWA 1482 HT 4, 20°C (68°F), Hydrogen, Tensile. ....	106
98.	At 4000X, Behavior Described in Figure 97 Can Be Discerned; Fine Cuboidal $\gamma$ Appears White and Larger Primary $\gamma$ is dark; Conditions – PWA 1482 HT 4, 20°C (68°F), Hydrogen, Tensile .....	106
99.	Overall View of Tensile Failure Produced in 650°C (1200°F) Air Shows Typical Prominent (111) Intersecting Crystallographic Planes; Conditions – PWA 1482 HT 4, 650°C (1200°F), Air, Tensile .....	107
100.	Cellular Appearance of (111) Fracture Plane Is a Result of Microstructure and Appears To Be Associated With Unusual Roughness (Presumed Beneficial Under Conditions Where Octahedral Crack Initiation Is a Concern); Conditions – PWA 1482 HT 4, 650°C (1200°F), Air, Tensile .....	107
101.	Overall View of 650°C (1200°F) Tensile Fracture Produced in 34.5 MPa (5 ksi) Hydrogen Showing Typical (111) Crystallographic Fracture; Conditions – PWA 1482 HT 4, 650°C (1200°F), Hydrogen, Tensile .....	108
102.	High-Magnification View of (111) Fracture Suggests Some Structure Within Primary $\gamma$ ; Conditions – PWA 1482 HT 4, 650°C (1200°F), Hydrogen, Tensile .....	108
103.	Overall View of Creep/Stress Rupture Fracture Produced in Air Showing Mixed Noncrystallographic and (111) Crystallographic Fracture; Conditions – PWA 1482 HT 6, 871°C (1600°F), Air, Creep/Stress Rupture .....	109
104.	High-Magnification View of Stress Rupture Fracture Details; Conditions – PWA 1482 HT 6, 871°C (1600°F), Air, Creep/Stress Rupture.....	110
105.	Overall View of Creep/Stress Rupture Fracture Produced in Air Shows Noncrystallographic Macroscopically and (111) Crystallographic Fracture Microscopically in Figure 106; Conditions – PWA 1484 HT 6, 871°C (1600°F), Air, Creep/Stress Rupture .....	110

106.	High-Magnification View of Stress Rupture Fracture Details Shows Large Area of (111) Fracture; Conditions – PWA 1484 HT 6, 871°C (1600°F), Air, Creep/stress Rupture .....	111
107.	Stage I Crack Initiation at Discrete (111) Crystallographic Facet (10 x 30 micron); Conditions – PWA 1484 HT 2, Notched LCF, 20°C (68°F), 34.5 MPa (5 ksi) Hydrogen, Magnification 1000X .....	112
108.	Isolated Microscopic (111) $\gamma'$ Fracture Among Predominantly Matrix Failure; Conditions – PWA 1484 HT 2, Notched LCF, 20°C (68°F), 34.5 MPa (5 ksi) Hydrogen, Magnification 10,000X 1132109. Crystallographic Fatigue Crack Origins and Microscopic (111) Fracture in Fine Cuboidal $\gamma'$ ; Conditions – PWA 1482 HT 4, Notched LCF, 20°C (68°F), 34.5 MPa (5 ksi) Hydrogen .....	113
110.	Lenticular (001) Cracking Cutting Large Primary $\gamma'$ ; Conditions – PWA 1482 HT 4, Notched LCF, 20°C (68°F), 34.5 MPa (5 ksi) Hydrogen .....	113
111.	In Some Cases Secondary Cracks Appeared To Be Skirting Primary $\gamma'$ ; Conditions – PWA 1482 HT 6, Notched LCF, 20°C (68°F), 34.5 MPa (5 ksi) Hydrogen .....	114
112.	Replica TEM of PWA 1482 HT 6 Was Compared to Previous Fracture in Figure 111 and Subsequent Figure 113 To Confirm Cracks Skirting Primary $\gamma'$ ; Magnification Is 22,000X .....	114
113.	Replica TEM of Primary $\gamma'$ Fracture Features Show Interprecipitate Cracking; Conditions – PWA 1482 HT 6, Notched LCF, 20°C (68°F), 34.5 MPa (5 ksi) Hydrogen; Magnification Is 22,000X .....	115
114.	Replica TEM of Primary $\gamma'$ Fracture Surface Suggests Microscopic (111) Fracture and Perhaps Some Type of Structure Within Precipitate; Conditions – PWA 1482 HT 6, Notched LCF, 20°C (68°F), 34.5 MPa (5 ksi) Hydrogen; Magnification Is 22,000X .....	116
115.	SEM Imagery of Primary $\gamma'$ Fracture Surfaces Suggests Structure Within Large Primary $\gamma'$ (Possibly $\gamma$ Phase Retrograde Solubility) .....	116
116.	Thin Foil TEM Shows No Presence of $\gamma$ Within Primary $\gamma'$ ; Fine Cuboidal Precipitates Are at the Upper Left; Interfacial Dislocations Outline Primary $\gamma'$ and Appear Tangled; Arrangement of Dislocations Within Primary $\gamma'$ Show Some Correlation With Fractographic Structures Shown in Figure 111; PWA 1484 HT 3; Magnification is 50,000X .....	117
117.	High-Magnification FEM Images Taken From Etched Metallographic Sections Show No Reprecipitated $\gamma$ Within Primary $\gamma'$ ; PWA 1484 HT 3 .....	117
118.	Overall View of Notched LCF Air Fracture (20°C [68°F]) Shows Typical (111) Fracture; Conditions – PWA 1484 HT 4, Notched LCF, 20°C (68°F), Air .....	118
119.	High-Magnification View of Microscopic (111) Fracture in Areas That Macroscopically Appear Noncrystallographic; Conditions – PWA 1484 HT 4, Notched LCF, 20°C (68°F), air .....	119
120.	Similar to Previous Fracture in Figure 115; Overall View of Notched LCF Air Fracture Shows Typical (111) Fracture; Conditions – PWA 1484 HT 6, Notched LCF, 20°C (68°F), Air .....	119
121.	Primary and Fine Precipitates Show Differential Fracture in This High-magnification View of Microscopic (111) Fracture; These Areas Macroscopically Appear Noncrystallographic; Conditions – PWA 1484 HT 6, Notched LCF, 20°C (68°F), Air .....	120
122.	(111) Fracture Planes Typical of 20°C (68°F) Single-Crystal Fractures Produced in Air; Conditions – PWA 1484 HT 4, 20°C (68°F), Air, Controlled Strain LCF .....	121

123.	Detail of Origin Area from Figure 122; Conditions – PWA 1484 HT 4, 20°C (68°F), Air, Controlled Strain LCF .....	121
124.	Hexagonal Crack Front on Large (111) Plane Results from <110> Slip Directions Intersecting (111) Plane; No Point Source Was Detected at Origin; Conditions – PWA 1484 HT 6, 20°C (68°F), Air, Controlled Strain LCF, Magnification 10X .....	122
125.	Microscopic Appearance of (111) Fracture Planes; Conditions – PWA 1484 HT 6, 20°C (68°F), Air, Controlled Strain LCF.....	122
126.	Overall of Strain Control LCF Fracture Produced in Room Temperature Hydrogen; Fatigue Origin Is at Stage I Crystallographic Facet; Enlarged in Figure 127; Dark Oval Shape at Right Is Secondary Grain; Conditions – PWA 1482 HT 4, 20°C (68°F), 34.5 MPa (5 ksi) Hydrogen, Controlled Strain LCF, Magnification 30X .....	123
127.	Microscopic (111) Facet Initiated Crack in Figure 126; Note Fatigue “Thumbail” Crack Front Radiating from (111) Face; Conditions – PWA 1482 HT 6, 20°C (68°F), 34.5 MPa (5 ksi) hydrogen, Controlled Strain LCF, Magnification 50X.....	123
128.	Transverse Metallographic Section Through Specimen Gage Shown in Figure 127 Reveals Secondary Grain; Conditions – PWA 1482 HT 6, 20°C (68°F), 34.5 MPa (5 ksi) Hydrogen, Controlled Strain LCF, Magnification 60X .....	124
129.	Longitudinal Metallographic Section Through Specimen Gage Shown in Figure 128 Reveals Secondary Grain; Conditions – PWA 1482 HT 6, 20°C (68°F), 34.5 MPa (5 ksi) Hydrogen, Controlled Strain LCF, Magnification 12X .....	124
130.	Overall View of Strain Control LCF Fracture Produced in Room Temperature Hydrogen; Conditions – PWA 1482 HT 4, 20°C (68°F), 34.5 MPa 5 ksi) Hydrogen, Controlled Strain LCF, Magnification 10X .....	125
131.	Enlargement of Origin Area from Figure 130 Shows Increasing Roughness as Stress Intensity Increases; Conditions – PWA 1482 HT 4, 20°C (68°F), 34.5 MPa (5 ksi) Hydrogen, Controlled Strain LCF 1266132. Fatigue Crack Origin from Figure 131 Shows Extremely Flat Fracture and Apparent Machining Marks at Specimen Edge; Conditions – PWA 1482 HT 4, 20°C (68°F), 34.5 MPa (5 ksi) Hydrogen, Controlled Strain LCF .....	126
133.	Overall View of Strain Control LCF Fracture Produced in Room Temperature Hydrogen; Fatigue Origin Was Nonspecific (No Point Source Present); Flat Smooth Surface Characteristic of Hydrogen Fractures Is Absent; Conditions – PWA 1482 HT 6, 20°C (68°F), 34.5 MPa (5 ksi) Hydrogen, Controlled Strain LCF.....	126
134.	High-Magnification Details of $\gamma'$ Fracture Modes Near Suspected Origin in Figure 133; Dark Shape at Lower Left and Right Are Primary $\gamma'$ ; Note High Degree of Roughness Surrounding These Features; Conditions – PWA 1482 HT 6, 20°C (68°F), 34.5 MPa (5 ksi) Hydrogen, Controlled Strain LCF .....	127
135.	Further Study of Primary $\gamma'$ from Figure 134 Shows Pronounced Ridges and (111) Facets Covering Areas Where Fine Cuboidal $\gamma'$ Reside; Conditions – PWA 1482 HT 6, 20°C (68°F), 34.5 MPa (5 ksi) Hydrogen, Controlled Strain LCF.....	127
136.	Detail from Lower Right of Figure 134; Interprecipitate (Primary $\gamma'$ ) (111) Fracture Mode Is Not Well Resolved and Appears Distorted; Regardless, This Topography Represents More Tortuous Crack Path Than That Offered by Conventional Fine Uniform Cuboidal $\gamma'$ Structure; Conditions – PWA 1482 HT 6, 20°C (68°F), 34.5 MPa (5 ksi) Hydrogen, Controlled Strain LCF .....	128

137.	PWA 1484 HT 4 Controlled Strain LCF Crack Origin Area Shows Relatively Flat Fracture; Stress Intensity (K) Dependent Increasing Roughness Is Clearly Seen; Conditions – PWA 1484 HT 4, 20°C (68°F), 34.5 MPa (5 ksi) Hydrogen, Controlled Strain LCF .....	128
138.	PWA 1484 HT 4 HCF Overall View; Crack Origin Area (At Top) Shows Relatively Flat Fracture; Conditions – PWA 1484 HT 4, 20°C (68°F), 34.5 MPa (5 ksi) Hydrogen, R = -1.0 HCF ..... 1329139.HCF Crack Initiation at 100 um Long (111) Facet from Figure 135; Conditions – PWA 1484 HT 4, 20°C (68°F), 34.5 MPa (5 ksi) Hydrogen, R = -1.0 HCF .....	130
140.	PWA 1482 HT 6 HCF Overall View; Crack Origin Area (At Left) Shows Prominent (111) Fracture; Conditions – PWA 1482 HT 6, 20°C (68°F), 34.5 MPa (5 ksi) Hydrogen, R = -1.0 HCF .....	130
141.	HCF Crack Initiation at 1mm (0.039 in.) Long (111) Facet from Figure 136; Conditions – PWA 1482 HT 6, 20°C (68°F), 34.5 MPa (5 ksi) Hydrogen, R = -1.0 HCF .....	131
142.	PWA 1484 HT 6 HCF Overall View; Crack Origin Area (At Right) Shows Prominent (111) Fracture; Conditions – PWA 1484 HT 6, 20°C (68°F), 34.5 MPa (5 ksi) Hydrogen, R = -1.0 HCF .....	131
143.	HCF Crack Initiation at 200 um Long (111) Facet From Figure 142; Conditions – PWA 1484 HT 6, 20°C (68°F), 34.5 MPa (5 ksi) Hydrogen, R = -1.0 HCF .....	132
144.	Fatigue Crack Growth in Hydrogen at Low Stress Intensity; Note Crack Front from Air Precrack at Top of Micrograph; Micromechanical Damage Was Extensive With Propagation on Multiple Parallel Planes; Crack Advance Was Extremely Rapid; Conditions – PWA 1484 HT 1, Fatigue Crack Growth in 20°C (68°F), 34.5 MPa (5 ksi) Hydrogen, R = 0.1, 0.16 Hz.....	133
145.	Microscopic Fracture Mode from Figure 144 Shows Failure Along Multiple Layers of $\gamma'$ ; Conditions – PWA 1484 HT 1, Fatigue Crack growth in 20°C (68°F), 34.5 MPa (5 ksi) Hydrogen, R = 0.1, 0.16 Hz .....	133
146.	Microscopic Fracture Mode from Figure 145 Etched in This Case Shows Layers of $\gamma'$ Exhibiting “Stepped” Appearance Associated With Matrix Failure; Conditions – PWA 1484 HT 1, Fatigue Crack Growth in 20°C (68°F), 34.5 MPa (5 ksi) Hydrogen, R = 0.1, 0.16 Hz.....	134
147.	SEM Mode from Scanning Transmission Electron Microscope (STEM) in High Voltage Backscatter Electron Imaging Shows Disposition of $\gamma$ Phase (Blotches on Top of Upper Layer of Precipitates) and Step as Described in Figure 146.....	134
148.	FEM Imaging of HT 4 Shows Planar Fracture in Primary $\gamma'$ (Dark Flat “X” Shape at Center) Surrounded by (111) Crystallographic Fracture in Fine Cuboidal $\gamma'$ .....	135
149.	Enlargement of Primary $\gamma'$ from Figure 148; PWA 1484 HT 4; Orthogonal Metallographic Sections Show Precipitate Is Ripened Octet Elongated in $\langle 111 \rangle$ Directions (Appearing To Be $\langle 110 \rangle$ in This $\langle 001 \rangle$ View); Conditions – Fatigue Crack Growth in 34.5 MPa (5 ksi), 20°C (68°F), Hydrogen.....	135
150.	Center of Octet (from Figure 149) Shows (111) Matrix Failure Revealed by Sunken “Stepped” Fracture; PWA 1484 HT 4; Conditions – Fatigue Crack Growth in 34.5 MPa (5 ksi), 20°C (68°F), Hydrogen .....	136
151.	Atomic Force Microscopy (AFM) of Fatigue Crack Growth Fracture Produced in Room Temperature 34.5 MPa (5 ksi) Hydrogen; Enlargement of primary $\gamma'$ from Figure 150; In This Case, the “Step” Is Elevated by Approximately 0.2 mm; (111) Matrix Failure Appears at Right Corner of Step; Blotches on Precipitate Surface Are $\gamma$ Phase (as in Figure 147); PWA 1484 HT 6.....	137
152.	$\gamma/\gamma'$ Phase Composition gradients for Ni and Cr in PWA 1484 HT 4; $\gamma/\gamma'$ Interface Is at zero nanometers .....	140
153.	$\gamma/\gamma'$ Phase Composition Gradients for Al and Ta in PWA 1484 HT 4; $\gamma/\gamma'$ Interface Is at zero nanometers .....	141



154.	Fine Cuboidal $\gamma'$ Covers Lower Left Half of Micrograph; Overaged Octet (Primary $\gamma'$ ) At Upper Right; Octet/g Interface Is Delineated by High Dislocation Concentration; Numerous Dislocations Can Be Observed Within Octet; Conditions – Controlled Strain LCF, $\Delta\epsilon_t = 1.5\%$ , $20^\circ\text{C}$ ( $68^\circ\text{F}$ ), 34.5 MPa (5 ksi) Hydrogen, $R = -1$ , Load Axis $\langle 001 \rangle$ , Zone Axis Approximately $\langle 001 \rangle$ , Magnification 20,000X .....	142
155.	Higher Magnification of Interface Shows Concentrated Dislocations at Octet/ $\gamma$ Interface (Left) and Near Absence of Dislocations in Cuboidal $\gamma/\gamma'$ Array; Conditions – Controlled Strain LCF, $\Delta\epsilon_t = 1.5\%$ , $20^\circ\text{C}$ ( $68^\circ\text{F}$ ), 34.5 MPa (5 ksi) Hydrogen, $R = -1$ Load Axis $\langle 001 \rangle$ , Zone Axis Approximately $\langle 001 \rangle$ , Magnification 30,000X, .....	143
156.	Dislocation Structures Within Primary g, Cuboidal $\gamma'$ Can Be Observed at Upper Right Bounded by Dislocation Tangles at Interface With Octet; Deformation Substructures Within Octet Are Coincident With Fractographic Details Previously Discussed in Paragraph 2.7.4 – Fatigue Fractures; Conditions – Controlled Strain LCF, $\Delta\epsilon_t = 1.5\%$ , $20^\circ\text{C}$ ( $68^\circ\text{F}$ ), 34.5 MPa (5 ksi) Hydrogen, $R = -1$ Load Axis $\langle 001 \rangle$ , Magnification 30,000X, Zone Axis Approximately $\langle 001 \rangle$ .....	144
157.	Heat Treatment 1 .....	167
158.	Heat Treatment 2 .....	168
159.	Heat Treatment 3 .....	169
160.	Heat Treatment 4 .....	170
161.	Heat Treatment 5 .....	171
162.	Heat Treatment 6 .....	172
163.	Heat Treatment 7 .....	173



## TABLES

<i>Table</i>	<i>Page</i>
1. Composition of PWA 1482 and PWA 1484 (Wt%) .....	5
2. Cast Single-Crystal Test Material Requirements .....	7
3. Creep-Stress Rupture Heat Certification Test Results .....	7
4. Matrix for HIP Trials .....	8
5. PWA 1482 Visual Inspection Results .....	21
6. Revert PWA 1482 Test Material Procurement .....	24
7. Summary of Final HIP Parameters Used on PWA 1482 and PWA 1484 Test Material .....	26
8. PWA 1484 Alternate HT Processing .....	27
9. PWA 1484 Alternate HTs for Screening Tests .....	28
11. PWA 1482 Alternate HT Processing Parameters .....	37
10. Microstructural Summary of PWA 1484 Alternate HT .....	37
12. Alternate Microstructure Screening Test Matrix Performed on PWA 1484 in 34.5 MPa Hydrogen at 20°C (68°F) Number of Tests .....	54
13. Summary of Tensile Data for PWA 1484 Alternate Microstructure Screening Studies With Testing in 34.5 MPa (5 ksi) Hydrogen at 20°C (68°F) .....	55
14. Load Controlled LCF Alternate Microstructure Screening Results for [001] Oriented PWA 1484 Double Notch Specimens Tested in 34.5 MPa (5 ksi) Hydrogen at 0.167 Hz, 20°C (68°F), R = 0.05, Kt = 2.18 ..57	
15. Crack Growth Alternate Microstructure Screening Results for [001] Oriented PWA 1484 Compact Tension Specimens Tested in 34.5 MPa (5 ksi) Hydrogen at 0.167 Hz, 20°C (68°F), R = -1 .....	59
16. Program Test Matrix .....	62
17. Tensile Results for [001] Oriented PWA 1482 .....	63
18. Tensile Results for [001] Oriented PWA 1484 .....	64
19. Creep Rupture Results for [001] Oriented PWA 1482 Tested at 413.7 MPa (60 ksi) .....	72
20. Creep Rupture Results for [001] Oriented PWA 1484 Tested at 413.7 MPa (60 ksi) .....	72
21. Load Controlled HCF Results for [001] Oriented PWA 1482 Specimens Tested in 34.5 MPa (5 ksi) Hydrogen at 30 Hz, 20°C (68°F), R = -1 .....	74
22. Load Controlled HCF Results for [001] Oriented PWA 1484 Specimens Tested in 34.5 MPa (5 ksi) Hydrogen at 30 Hz, 20°C (68°F), R = -1 .....	74
23. Load Controlled LCF Results for [001] Oriented PWA 1482 Double Notch Specimens Tested at 0.167 Hz, 20°C (68°F), R = 0.05, Kt = 2.18 .....	77
24. Load Controlled LCF Results for [001] Oriented PWA 1484 Double Notch Specimens Tested at 0.167 Hz, 20°C (68°F), R = 0.05, Kt = 2.18 .....	77
25. Strain Controlled Results for [001] Oriented PWA 1482 Tested at 0.167 Hz, 20°C (68°F), R = -1 .....	81
26. Strain Controlled Results for [001] Oriented PWA 1484 Tested at 0.167 Hz, 20°C (68°F), R = -1 .....	82

27.	Fatigue Crack Growth Testing of [001] Oriented PWA 1484 Compact Tension Specimens Tested in 34.5 MPa (5 ksi) Hydrogen at 0.167 Hz, 20°C (68°F), R = -1 .....	85
28.	Phase Composition Gradients in $\alpha$ and Fine Cudoidal $\gamma$ From PWA 1484 HT 4 .....	138

## 1. INTRODUCTION AND PROGRAM OBJECTIVE

### 1.1 INTRODUCTION

Cast nickel-based superalloys are the materials of choice for turbine airfoils in advanced, liquid hydrogen fueled rocket engine turbopumps. Current Space Shuttle Main Engine (SSME) turbopumps employ the directionally-solidified (DS), columnar-grained Mar-M-246+Hf alloy for turbine blade applications. The extreme thermal shock, vibration, and mechanical loading, combined with the high-pressure hydrogen environment, have produced airfoil cracking in test articles and engines, thus resulting in durability and safety concerns. Advanced turbopump designs that are currently under development<sup>1</sup> rely on PWA 1480 cast single-crystal blades to improve durability of the airfoils. Significant durability improvements over the DS Mar-M-246+Hf alloy are indicated by specimen and thermal shock rig testing. However, it appears that substantial improvements to current single-crystal properties can be achieved through alloy selection and modification, and through development of improved processing methods. Such improvements could dramatically increase turbine airfoil durability and safety for both the SSME and advanced or derivative rocket engines.

### 1.2 PROGRAM OBJECTIVE

The objective of this program was to develop advanced processed single-crystal alloys for turbine airfoil applications in liquid-fueled rocket engine turbopumps. To accomplish this objective, the program studied two cast single-crystal alloy compositions, the development and optimization of hot isostatic pressing (HIP) and thermal treatments for the two alloys, and the evaluation of key mechanical properties of the resultant materials in both air and high-pressure gaseous hydrogen environments.

---

<sup>1</sup> *SSME Alternate Turbopump Development Program*, NASA-MSFC Contract NAS8-36801.



## 2. TECHNICAL EFFORT

### 2.1 ALLOY SELECTION

Pratt & Whitney (P&W) selected PWA 1482 and PWA 1484 as the two single-crystal materials for investigation in this program. The selection of these two alloys was based on a material trade study in which comparisons of mechanical properties, processability, and castability were made of several P&W and commercially available investment cast nickel-based superalloys. The material trade study was conducted with input from Space Shuttle Main Engine (SSME) Design and Project Engineering personnel at P&W to assist in defining a set of critical material requirements for evaluation. Relative material capabilities were compared for specific properties, such as thermal shock capability in hydrogen, room temperature high-cycle fatigue (HCF) in hydrogen, impact resistance, notch low-cycle fatigue (LCF) in hydrogen, 871°C (1600°F) creep, modulus of elasticity, and density. From these comparisons, it became apparent that the single-crystal alloys offered the best overall balance of thermal shock capability, fatigue strength, and creep resistance.

Trade study comparisons of other P&W and commercially available single-crystal alloys did not show any significant processing or mechanical property advantages over the two selected alloys. The PWA 1480 material was not selected as an alloy for this program because of the concerns about the relatively narrow heat treatment (HT) window. The narrow range between the gamma prime ( $\gamma'$ ) solvus and incipient melt temperatures would make processing with hot isostatic pressing (HIP) and full solutioning more difficult than with the selected PWA 1482 and PWA 1484 alloys.

The alloys Rene' N-5 and AF-56 were also considered. Results of room temperature tensile tests in helium and hydrogen for several single-crystal alloys have been reported by NASA.<sup>2</sup> All of the alloys showed reduced tensile strengths in hydrogen as compared to helium, but the degree of reduction varied considerably. Based on the ratio of notched tensile strengths in hydrogen to helium, the alloys AF-56 and Rene' N-5 ranked highest (with a ratio of 0.84) followed by PWA 1480, RR2000, and Rene' N-4 (with notch ratios of 0.46 to 0.49). The remaining six materials had notch strengths of 0.36 or below.

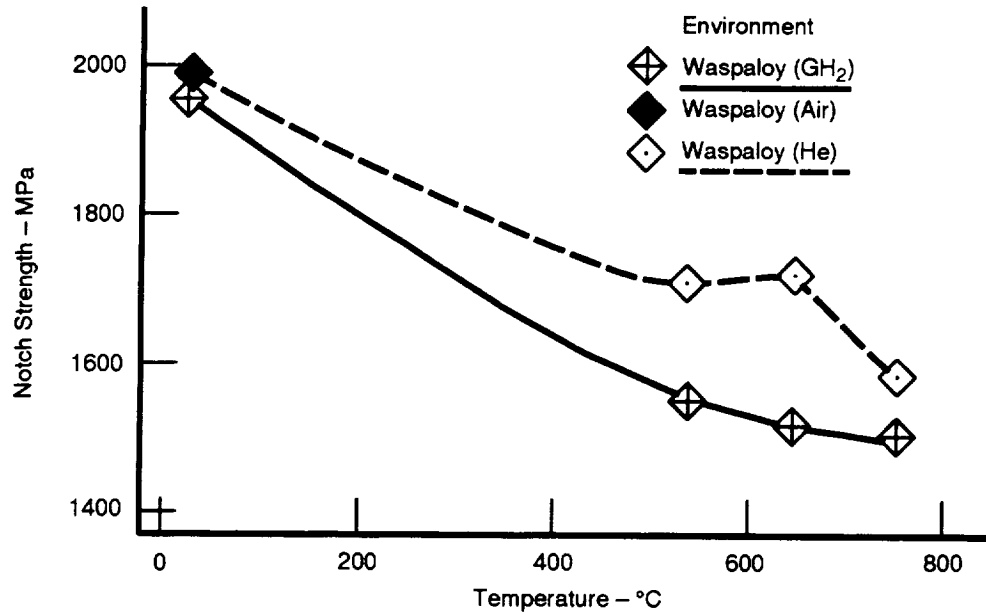
Tests of four wrought nickel-based superalloys, however, have shown that trends in notch tensile strength ratios are not necessarily indicative of trends in smooth LCF behavior.<sup>3</sup> Results of notch tensile tests and smooth fatigue tests, as a function of temperature, are shown for Waspaloy in Figures 1 and 2. Note that the notch tensile strength would indicate some hydrogen effects at all temperatures, with most significant reductions in the 540° to 650°C range (1000° to 1200°F), and the least effects at room temperature. The fatigue results, on the other hand, show substantial effects due to hydrogen at room temperature, and little or no effect on life in the 540° to 650°C (1000° to 1200°F) range. Similar results were observed for the other three alloys, and for crack growth behavior performed for the SSME-Alternate Turbopump Development (ATD) Program.<sup>4</sup> Consequently, the notch tensile results for the single-crystal alloys were used primarily as an indicator of hydrogen susceptibility, rather than as a firm alloy selection criterion for the program.

Rene' N-5 was eliminated from selection because it is a yttrium-containing alloy, which presents both casting difficulties and processing concerns. One desirable option for evaluation is full solutioning heat treatment to eliminate or minimize eutectic regions. However, it is doubtful that an yttrium-containing alloy can be fully solutioned without melting of the yttride phase below the eutectic  $\gamma/\gamma'$  solvus temperature. In addition, a yttrium-free version of Rene' N-5 would be similar in composition and material properties to PWA 1484. Due to these factors, and a lack of hands on experience with Rene' N-5 at P&W, Rene' N-5 was eliminated from consideration. The AF-56 alloy is similar in composition to a hot corrosion-resistant single-crystal alloy that is designated as PWA 1483.

<sup>2</sup> Dreshfield, R.L. and Parr, R.A.: *Application of Single-Crystal Superalloys for Earth-to-Orbit Propulsion Systems*; AIAA/SAE/ASME/ASME 23rd Joint Propulsion Conference, San Diego, CA, 23 June to 2 July, 1987 (Reprint as NASA TM 89877).

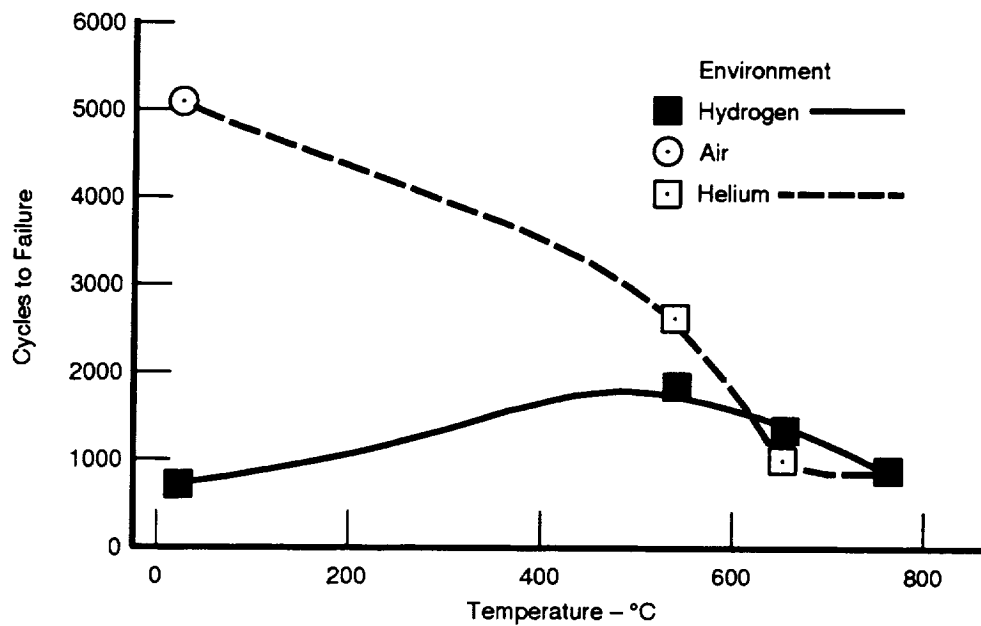
<sup>3</sup> Cowles, B.A. and Warren, J.R.: *Evaluation of Powder Metallurgy Alloys in Hydrogen*; P&W FR-19613-2, 2nd Annual Report; NASA Contract NAS8-36553, 30 September 1987 to 25 September 1988.

<sup>4</sup> *SSME Alternate Turbopump Development Program*, NASA-MSFC Contract NAS8-36801.



73753

Figure 1. Averaged Notched Tensile ( $K_t = 8$ ) Strength Versus Temperature for Waspaloy in Ambient Air and 34.5 MPa (5 ksi) Gaseous Helium and Hydrogen Environments



73752

Figure 2. Strain Control LCF Results ( $R = -1$ ) Showing Degradation Due to Hydrogen for Waspaloy Versus Temperature at 1.2 percent Total Strain Range



Based on experience with PWA 1483, no mechanical property or processing advantage could be associated with the selection of AF-56 over PWA 1482 or PWA 1484.

The Canon Muskegon single-crystal alloys, CMSX-2 and CMSX-4, were considered as candidates. Because the alloys did not offer any apparent mechanical property advantages over PWA 1482 and PWA 1484, CMSX-2 and CMSX-4 were not selected. Both PWA 1482 and PWA 1484 are the primary alloys of choice because they offer the best combination of mechanical properties, castability, and processibility.

PWA 1482 and PWA 1484 are  $\gamma$  strengthened single-crystal superalloys based on the Ni-Cr-Al system. The composition of PWA 1482 and PWA 1484 are provided in Table 1. The microstructures consist of cuboidal  $\gamma$  precipitates (approximately 60 percent by volume) in a continuous matrix. The precipitate size ranges from 0.35 - 0.50 micron and is an ordered face centered cubic (FCC) phase based on  $\text{Ni}_3\text{Al}(\text{Ti})$ . The microstructure also consists of microporosity and  $\gamma/\gamma'$  eutectic phase islands that form in the interdendritic regions during the last stages of solidification. Typical as-cast microstructures for PWA 1482 and PWA 1484 are shown in Figure 3.

Table 1. Composition of PWA 1482 and PWA 1484 (Wt%)

	Ni	Cr	Co	Mo	W	Re	Ta	Ti	Al	Hf
PWA 1482	Bal	9.0	5.0	1.0	6.8	—	6.0	1.0	5.5	0.1
PWA 1484	Bal	5.0	10.0	2.0	6.0	3.0	8.8	—	5.0	0.1

## 2.2 MATERIAL PROCUREMENT

Pratt & Whitney solicited single-crystal material quotes from several production casting suppliers for the test specimen geometries that are required for this program. Quotes were provided by the following:

- Howmet Dover Casting Division
- PCC Airfoils, Inc.
- Pratt & Whitney's Rapid Prototype Casting Laboratory (RPCL).

Pratt & Whitney elected to place the purchase order with the RPCL after reviewing the supplier quotes, delivery schedules, and technical proposals. The RPCL pioneered the single-crystal solidification process in 1975 and has produced thousands of investment cast single-crystal castings in support of P&W engine programs, Government contracts, and Independent Research and Development (IR&D) technical efforts over the past 25 years. They have extensive experience casting the two single-crystal alloys, PWA 1482 and PWA 1484, that were selected for use in this program.

A purchase order was placed with the RPCL for the high-gradient, single-crystal test material as outlined in Table 2. All test material was cast with the [001] crystallographic axis, parallel to the test specimen axis (length dimension) within 10 degrees of the primary orientation. Additionally, each of the test slabs had a [100] secondary crystallographic axis aligned with respect to the rectangular faces of the block. The test material requirements represented sufficient quantities to allow for 50 percent specimen attrition due to machining, thermal treatment, and mechanical test errors.

The RPCL placed a purchase order with Special Metals to produce two 227-kg (500-lb) heats of each respective alloy. Two heats from each alloy provided a statistical sampling from multiple heats for subsequent mechanical property testing evaluations. The use of multiple heats also provided more information on heat-to-heat influences (chemistry variation) on alloy thermal processibility during subsequent tasks in the program.

Special Metals produced the two 227-kg (500-lb) heats of PWA 1482 and PWA 1484 and shipped the alloys to the RPCL as 6.99-cm (2.75-in.) diameter ingots for subsequent remelting during the casting process. Special Metals performed compositional analyses and provided certification sheets for each of the respective heats that cer-

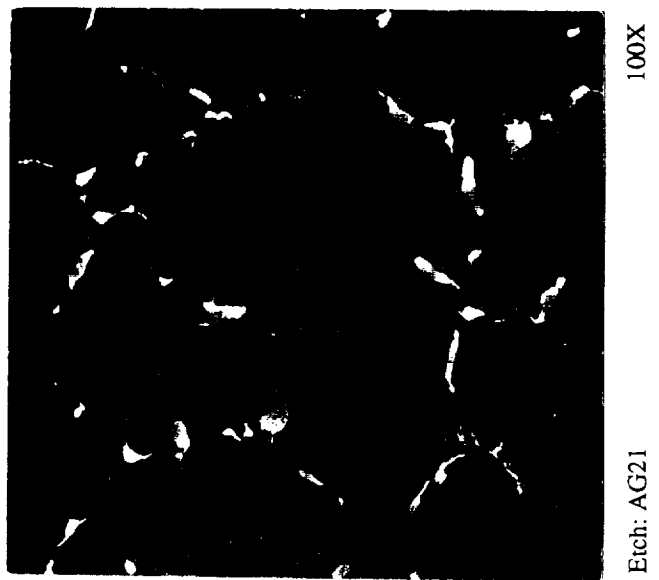
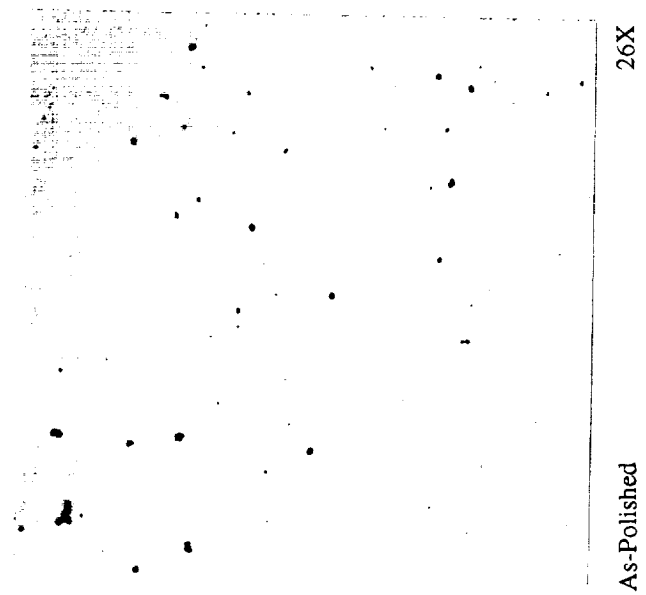
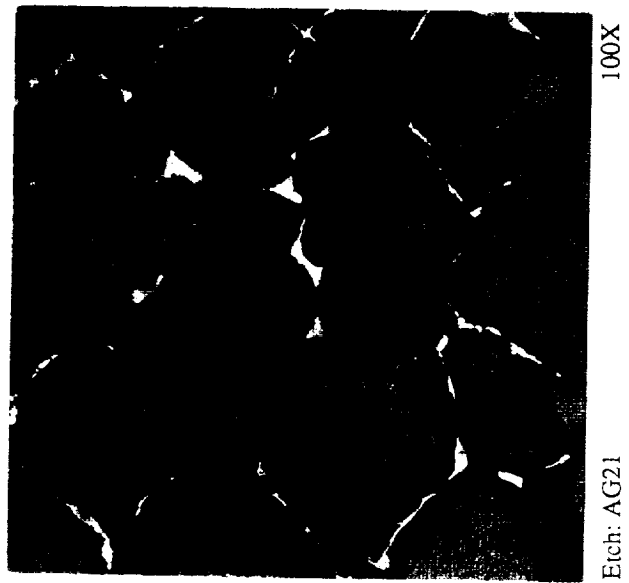
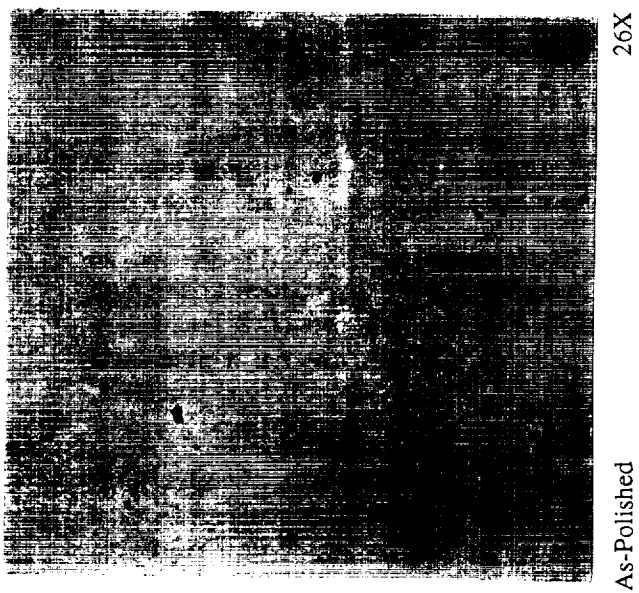


*Figure 3. As-Cast Microstructure of PWA 1482 (Top) and PWA 1484 (Bottom)*

*Table 2. Cast Single-Crystal Test Material Requirements*

<i>Quantity</i>	<i>Alloy Type</i>	<i>Specimen Configuration</i>
128	PWA 1482	1.59-cm (0.625-in.) Diameter x 17.78-cm (7-in.) Length
75	PWA 1482	1.91-cm (0.750-in.) Diameter x 17.78-cm (7-in.) Length
12	PWA 1482	3.81-cm (1.5-in.) Wide x 1.59-cm (0.625-in.) Thick x 15.24-cm (6-in.) Length
128	PWA 1484	1.59-cm (0.625-in.) Diameter x 17.78-cm (7-in.) Length
75	PWA 1484	1.91-cm (0.75-in.) Diameter x 17.78-cm (7-in.) Length
12	PWA 1484	3.81-cm (1.5-in.) Wide x 1.59-cm (0.625-in.) Thick x 15.24-cm (6-in.) Length

tified the alloy chemistries. Each of the respective alloy heat certification sheets are provided in Appendix A – *Heat Certification*. Each of the heats provided by Special Metals met the PWA 1482 and PWA 1484 compositional requirements as specified in P&W's purchase order.

After receipt of the ingot material from Special Metals, the RPCL cast a chemistry verification test bar mold for each heat and performed an alloy specification mechanical property test that is required by P&W Materials Control Laboratory (MCL) prior to release of the alloy heats. This particular test for the release of single-crystal alloy heats is a creep-stress rupture test at the condition specified below for each alloy:

- **PWA 1482:**

Specimens that are maintained at 982°C (1800°F), while a load sufficient to produce an initial axial stress of 247 MPa (36,000 psi) is continually applied, will not rupture in less than 40 hours. The percentage of plastic extension that is measured at 20 hours will not be higher than 2 percent. The specimen will be tested to rupture. Elongation after rupture, when measured at room temperature, will not be less than 10 percent.

- **PWA 1484:**

Specimens maintained at 1010°C (1850°F), while a load sufficient to produce an initial axial stress of 261 MPa (38,000 psi) is continually applied, will not rupture in less than 40 hours. Time to 1 percent creep will be reported and will not be less than 13 hours. Specimen will be tested to rupture. Elongation after rupture, when measured at room temperature, will not be less than 10 percent.

The Creep-Stress rupture tests results for each heat are presented in Table 3. The test results for each alloy heat met the specification requirements and was considered acceptable by MCL for release to the NASA program.

*Table 3. Creep-Stress Rupture Heat Certification Test Results*

<i>Alloy</i>	<i>Special Metals Heat Number</i>	<i>RPCL Heat Number</i>	<i>Time to 1 percent Creep (hr)</i>	<i>Creep at 20 hr (%)</i>	<i>Rupture Life (hr)</i>	<i>Elongation at Rupture (%)</i>
1 - PWA 1482	D54223	P1030	NR*	0.629	82.4	21.3
2 - PWA 1482	D54224	P1032	NR*	0.658	85.6	27.2
3 - PWA 1484	D54228	P1033	32.0	NR*	64.5	24.1
4 - PWA 1484	D54229	P1034	29.6	NR*	75.0	34.5

\* Not Required.

All of the test material produced for this program was cast using a solidification furnace at the RPCL that was capable of producing a thermal gradient in excess of 66°C/cm (300°F/in.). NASA requested that all test material be produced using a solidification process that was capable of producing a thermal gradient of 30°C/cm (137°F/in.). The RPCL verified the performance of their casting furnace early in the program by thermocoupling an initial mold of 1.91-cm (0.75-in.) diameter test bars and analyzing the data that was generated during the solidification cycle.

This mold of 1.91-cm (0.75-in.) diameter PWA 1484 test bars was cast with platinum-rhodium thermocouples affixed at 3.8-cm (1.5-in.) intervals along the length of the bar. Analysis of the data collected during casting was processed using a software package called *PROCESS*, which was developed at PWA to calculate solidification gradients during the directional solidification process. Analysis of these data revealed that the measured solidification gradient exceeded the minimum gradient requirement of 30°C/cm (137°F/in.) specified in the proposal.

Following a review of the data from the instrumented molds with the NASA technical monitor, authorization was given to the RPCL to proceed with casting of the entire lot of test material.

Following casting of the test material, one mold of 1.59-cm (0.625-in.) diameter test bars (12 pieces) of each alloy was shipped to P&W's RPCL for use in the HIP cycle optimization task. The remaining test material at the RPCL was held in the as-cast condition for subsequent thermal processing, until the results of the HIP optimization task were completed.

## 2.3 HOT ISOSTATIC PROCESS OPTIMIZATION

A series of HIP trials were conducted on the 1.59-cm (0.625-in.) diameter test bars of each alloy. The goal of the HIP optimization trials was to define a set of HIP parameters for each alloy that produced a pore-free homogenous microstructure. A secondary goal of the HIP trials was to determine if full eutectic  $\gamma/\gamma'$  solutioning could be accomplished during the HIP HT cycle. The trials were conducted in series at progressively higher temperatures to explore the effect of temperature on the degree of pore closure and alloy homogenization.

The HIP trials were conducted at Industrial Materials Technology (IMT), an approved HIP vendor qualified to process production cast turbine hardware. Optimization trials were conducted in one of IMT's small subscale HIP vessels with a working hot zone of 15.24 cm (6.0 in.) diameter by 25.4 cm (10.0 in.) length. This HIP HT furnace had a maximum attainable hot zone temperature of 1343°C (2450°F). Temperature control during each HIP trial was provided by an imbedded monitor thermocouple that was positioned within the furnace hot zone adjacent to the test pieces. A series of six HIP trials were conducted according to the matrix outlined in Table 4. One 1.59-cm (0.625-in.) diameter by 17.78-cm (7-in.) length test bar of each alloy was included in the HIP runs as outlined in Table 4.

Table 4. Matrix for HIP Trials

Trial	Temperature		Pressure		Time (hr)	Alloy
	°C	(°F)	MPa	(ksi)		
1	1274	(2325)	103	(15)	4	PWA 1482
2	1285	(2345)	103	(15)	4	PWA 1482, PWA 1484
3	1296	(2365)	103	(15)	4	PWA 1482, PWA 1484
4	1307	(2385)	103	(15)	4	PWA 1482, PWA 1484
5	1318	(2405)	103	(15)	4	PWA 1482, PWA 1484
6	1329	(2425)	103	(15)	4	PWA 1484

Previous HIP experience with both PWA 1482 and PWA 1484 has established that a cycle of 1296°C (2365°F) at 103 MPa (15 ksi) for 4 hours is effective in eliminating subsurface microporosity in each alloy. PWA 1484 is currently HIP'ed in production for certain advanced airfoil applications using a HIP cycle of 1296°C (2365°F). The additional HIP trials above and below 1296°C (2365°F) were conducted to investigate the effective processing window for the respective alloys, while taking into the account the overall microstructural processing goals stated previously in this subsection.

Each HIP trial was performed under an argon atmosphere to prevent any environmental interaction between the castings and the atmosphere. Minimizing contaminants in the argon was critical because of the high temperatures and long cycle times involved. By diffusing into the alloy during the HIP cycle, impurities may oxidize or otherwise contaminate the alloy; therefore, impurities must be carefully controlled. Carbide contamination is a serious problem that is sometimes encountered during HIP cycles. This is especially true in low-carbon single-crystal alloys that contain strong carbide-forming elements, such as titanium or tantalum. Carbon, if present in sufficient quantity, can diffuse to depths of 600 to 1300 microns (0.025 to 0.050 in.) during the HIP cycle, forming stable carbides that will significantly degrade fatigue capability. Since single crystals are susceptible to carbon contamination, it is critical that all sources of carbon (i.e., such as pump oils) be eliminated from the HIP chamber, and that clean argon gas be used in each run. In addition, test bars for each respective HIP run were placed within an alumina crucible with a loosely fit refractory sheetmetal lid to provide additional line-of-sight shielding. Each HIP cycle was run using a specially designed ramp temperature/pressurization schedule, which has been demonstrated in production PWA 1484 trials to minimize recrystallization (RX). This is especially important in the higher temperature HIP trials, where the alloys may be prone to RX.

All the test material used in the HIP study was grain etched in the P&W materials laboratory following the HIP cycle and visually inspected for evidence of RX. Post-HIP visual inspection did not reveal any evidence of surface RX on PWA 1482 and PWA 1484 test bars that were used in this study.

Metallographic analysis was performed on samples of PWA 1482 and PWA 1484 following HIP and grain inspection. Samples were initially reviewed in the as-polished condition following HIP processing and compared with baseline microstructures from an as-cast specimen.

Metallography performed on as-polished samples of PWA 1482 indicated that complete pore closure was achieved during each of the five HIP trials used for this alloy. Post-HIP microporosity was not observed at any HIP temperature. Microstructures from an as-cast PWA 1482 specimen and samples following HIP processing are shown in Figures 4 and 5.

Metallography performed on PWA 1484 indicated that complete pore closure was observed on samples HIP'ed at 1296°C (2365°F) and above. Some residual microporosity was still evident in the samples HIP'ed at 1285°C (2345°F) as shown in Figure 6. Microstructures from an as-cast PWA 1484 specimen and from samples following the HIP cycles are shown in Figures 6 and 7. No subsurface carbide contamination was observed in any PWA 1482 and PWA 1484 samples following the HIP cycles.

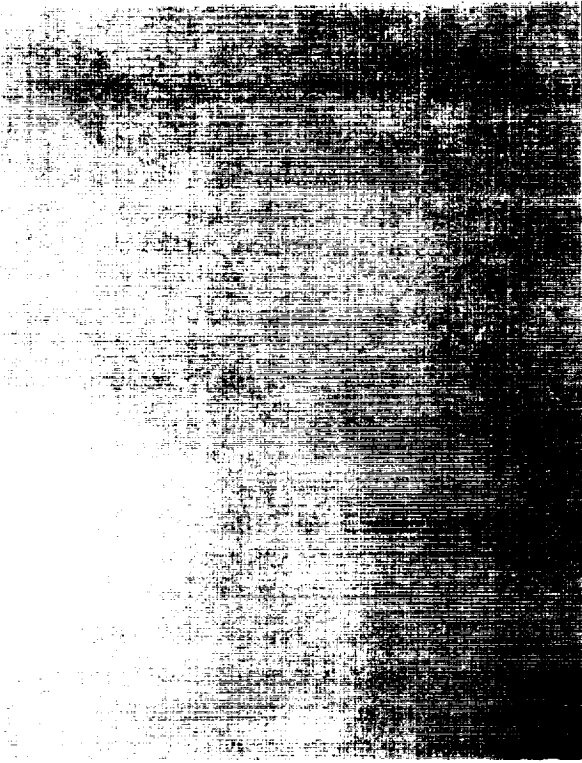
After studying metallography from samples in the as-polished condition, each sample was etched to document microstructures following HIP processing. Metallography from as-HIP'ed samples of PWA 1482 are shown in Figures 8 through 10. This metallography indicates that minimal eutectic  $\gamma/\gamma'$  solutioning is observed during HIP at temperatures of 1296°C (2365°F) and below. HIP cycles at temperatures of 1307°C (2385°F) and 1318°C (2405°F) resulted in appreciable eutectic solutioning. Nearly 100 percent of the  $\gamma/\gamma'$  eutectic phase islands were solutioned at 1318°C (2405°F). No evidence of incipient melting or RX was observed in any PWA 1482 samples.

After coupons were sectioned from each bar for metallography following the HIP cycles, the remaining test bar lengths were solution heat treated to determine whether complete eutectic solutioning was achieved. Post-HIP solution heat treated microstructures of PWA 1482 are shown in Figures 8 through 10. This metallography indicates that complete eutectic solutioning was achieved in all samples irrespective of the level of eutectic solutioning that occurred during the HIP cycles. This metallography also indicates that no additional microporosity or RX was



As-Cast

20X



HIP at 1274°C (2325°F)/103 MPa (15 ksi)/4 hr

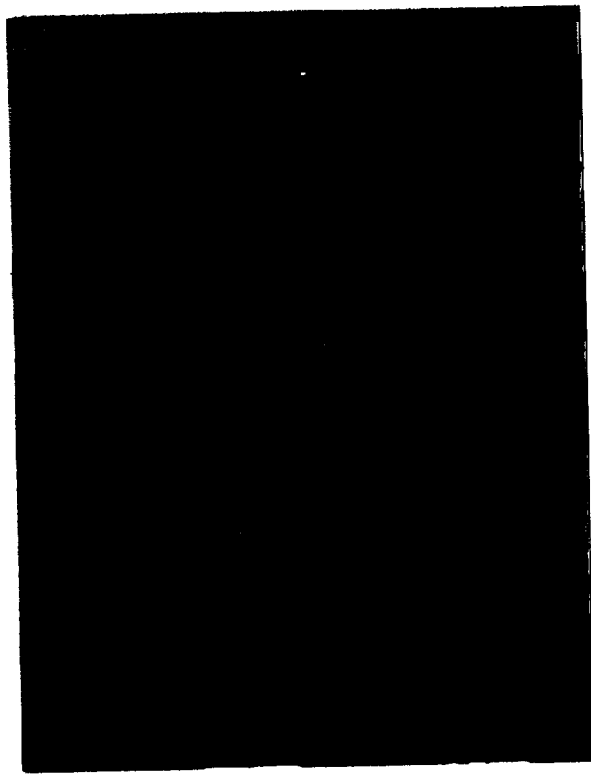
20X



HIP at 1285°C (2345°F)/103 MPa (15 ksi)/4 hr

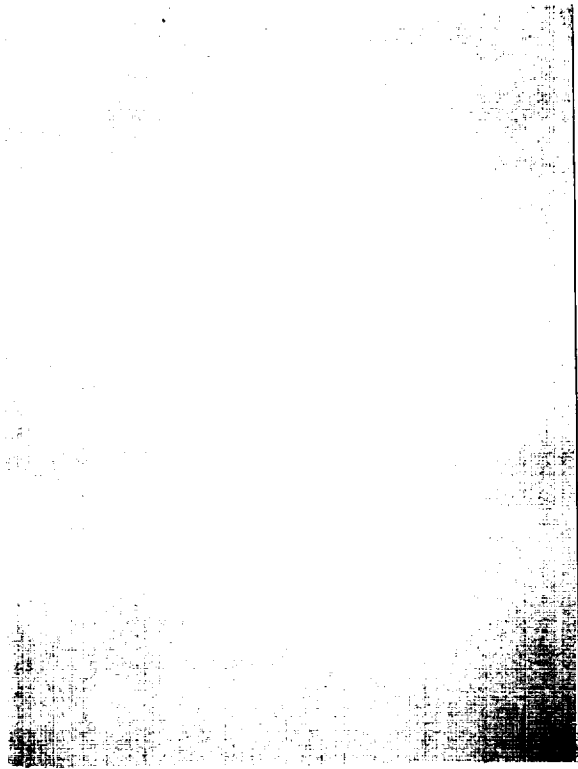
20X

Figure 4. As-Polished Microstructure of PWA 1482 Following HIP Processing at IMT (Unetched)



HIP at 1296°C (2365°F)/103 MPa (15 ksi)/4 hr

20X



HIP at 1307°C (2385°F)/103 MPa (15 ksi)/4 hr

20X



HIP at 1318°C (2405°F)/103 MPa (15 ksi)/4 hr

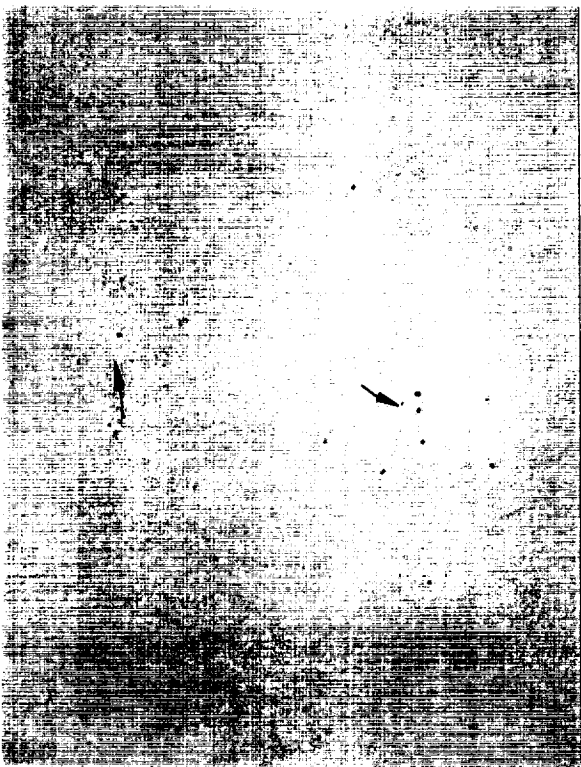
20X

*Figure 5. As-Polished Microstructure of PWA 1482 Following HIP Processing at IMT (Unetched)*



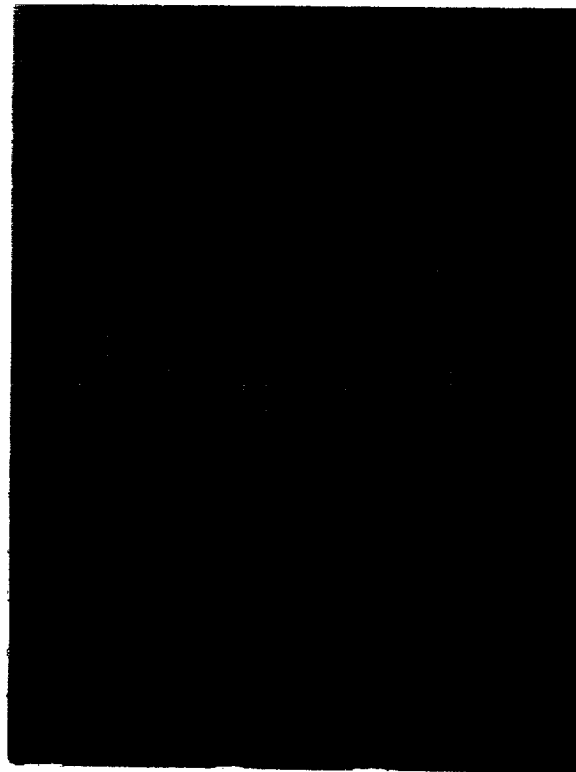
As-Cast

20X



HIP at 1285°C (2345°F)/103 MPa (15 ksi)/4 hr

20X



HIP at 1296°C (2365°F)/103 MPa (15 ksi)/4 hr

20X

Figure 6. As-Polished Microstructure of PWA 1484 Following HIP Processing at IMT (Unetched)





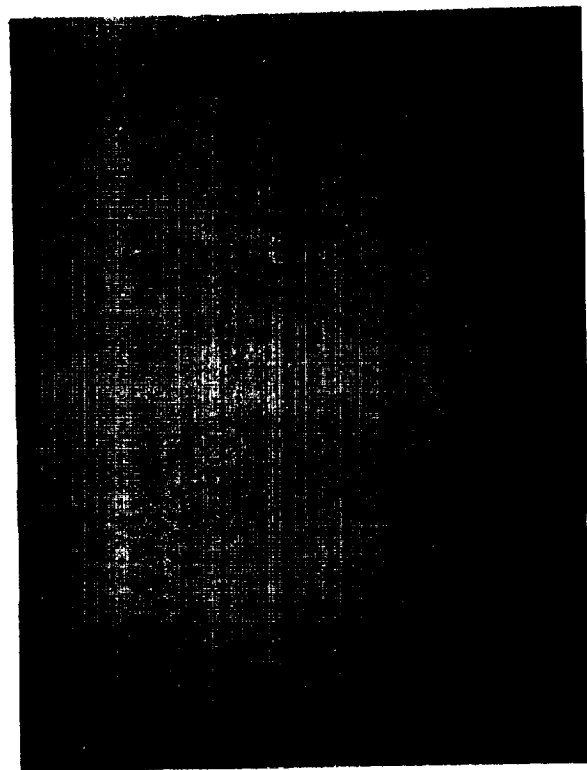
20X

HIP at 1318°C (2405°F)/103 MPa (15 ksi)/4 hr



20X

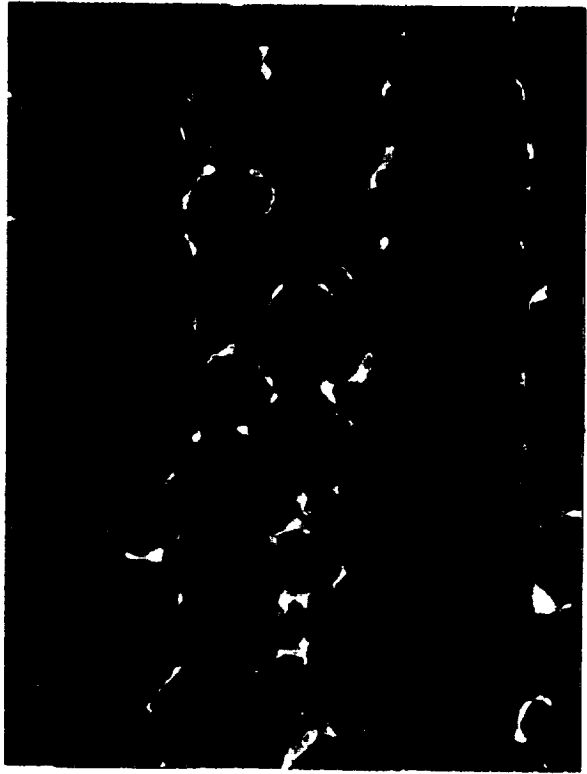
HIP at 1307°C (2385°F)/103 MPa (15 ksi)/4 hr



20X

HIP at 1330°C (2425°F)/103 MPa (15 ksi)/4 hr

Figure 7. As-Polished Microstructure of PWA 1484 Following HIP Processing at IMT (Unetched)



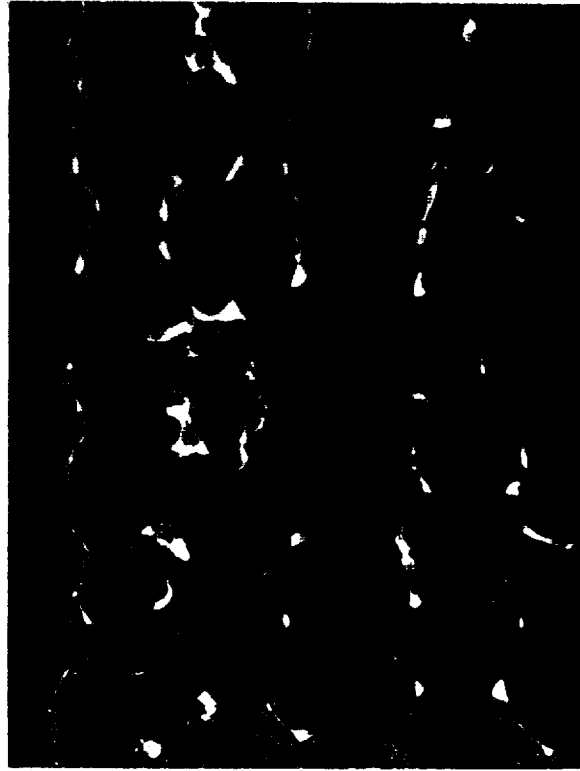
As-Cast

100X



As-Cast

200X



HIP at 1274°C (2325°F)/103 MPa (15 ksi)/4 hr

100X



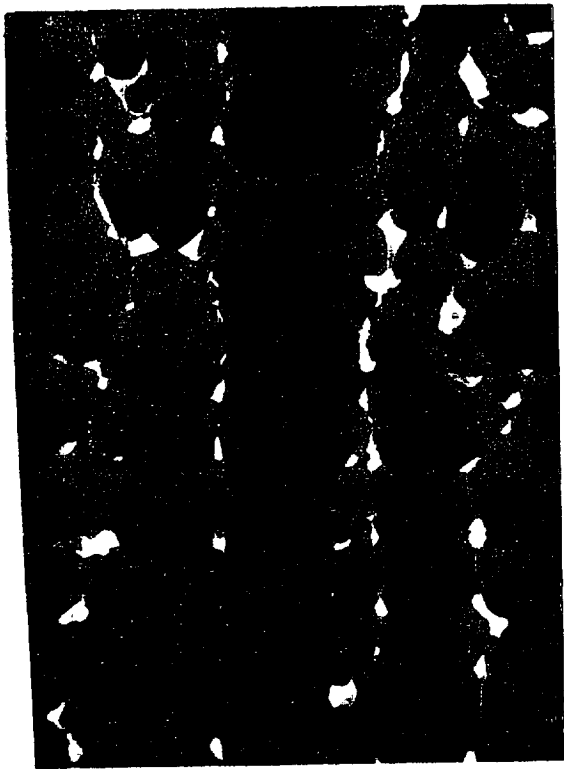
200X

HIP at 1274°C (2325°F)/103 MPa (15 ksi)/4 hr

+

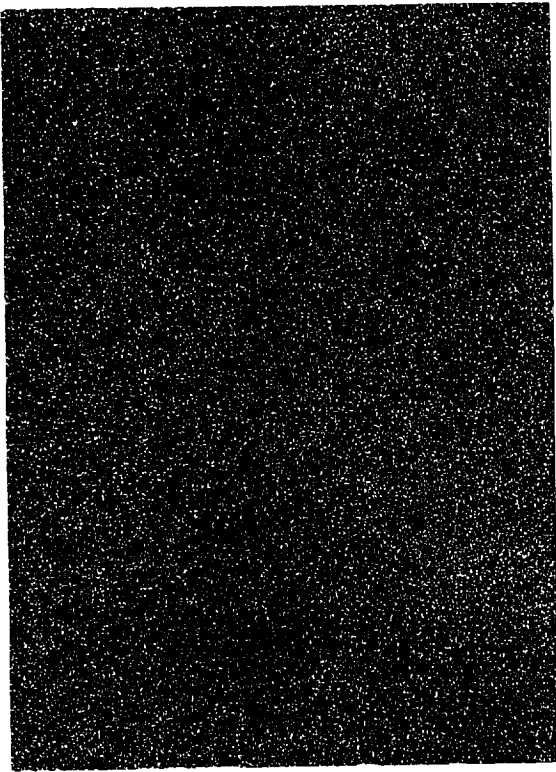
Solution Heat Treat at 1307°C (2385°F)/4 hr

Figure 8. Typical Microstructure of PWA 1482 Following HIP and Solution Heat Treatment (Etch: AG21)



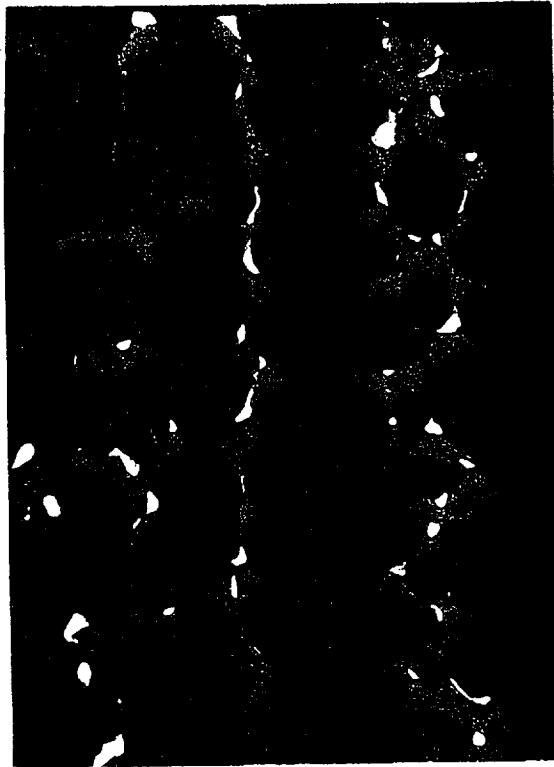
HIP at 1285°C (2345°F)/103 MPa (15 ksi)/4 hr

100X



200X

HIP at 1285°C (2345°F)/103 MPa (15 ksi)/4 hr  
+  
Solution Heat Treat at 1307°C (2385°F)/4 hr



HIP at 1296°C (2365°F)/103 MPa (15 ksi)/4 hr

100X



200X

HIP at 1296°C (2365°F)/103 MPa (15 ksi)/4 hr  
+  
Solution Heat Treat at 1307°C (2385°F)/4 hr

Figure 9. Typical Microstructure of PWA 1482 Following HIP and Solution Heat Treatment (Etch: AG21)



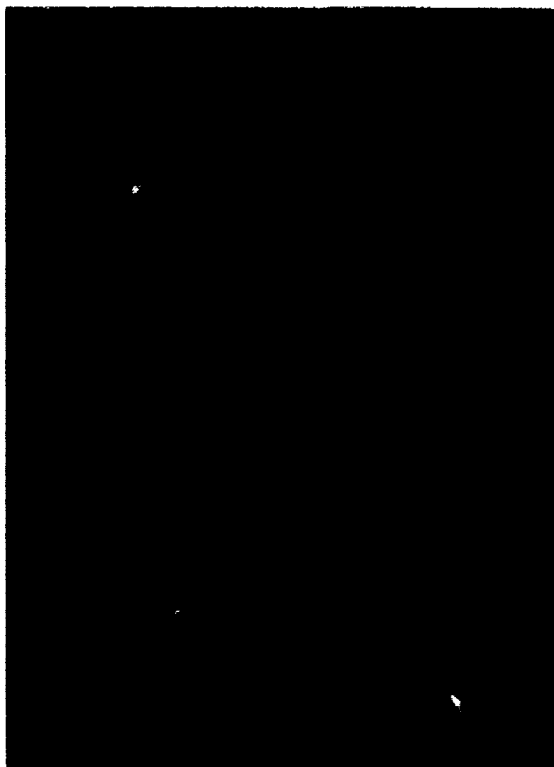
HIP at 1307°C (2385°F)/103 MPa (15 ksi)/4 hr

100X



HIP at 1307°C (2385°F)/103 MPa (15 ksi)/4 hr  
+  
Solution Heat Treat at 1307°C (2385°F)/4 hr

200X



HIP at 1318°C (2405°F)/103 MPa (15 ksi)/4 hr

100X



HIP at 1318°C (2405°F)/103 MPa (15 ksi)/4 hr  
+  
Solution Heat Treat at 1307°C (2385°F)/4 hr

200X

*Figure 10. Typical Microstructure of PWA 1482 Following HIP and Solution Heat Treatment (Etch: AG21)*

occurred during the HIP cycles. This metallography also indicates that no additional microporosity or RX was introduced into the microstructure following solution heat treatment. The desired pore-free, eutectic-free microstructure was achieved in each respective PWA 1482 sample.

A similar series of metallography was performed on PWA 1484 samples following the HIP cycles and solution heat treatment as shown in Figures 11 through 13. This metallography indicates that minimal eutectic  $\gamma/\gamma'$  solutioning occurs at HIP temperatures of 1307°C (2385°F) and below. The HIP cycles at temperatures of 1318°C (2405°F) and 1330°C (2425°F) produced appreciable amounts of eutectic solutioning. No evidence of incipient melting or RX was observed in any PWA 1484 samples.

Metallography from PWA 1484 samples following the HIP cycles and solution heat treatment indicated that complete eutectic solutioning was achieved in all samples regardless of the degree of eutectic solutioning that occurred during the HIP cycles. No additional microporosity or RX was introduced into the microstructure following solution heat treatment. The same pore-free, eutectic-free microstructure was achieved in all PWA 1484 samples.

Based on the metallographic results generated during the HIP optimization task, the following HIP cycles were recommended for each alloy:

- **PWA 1482** – HIP cycle at 1307°C (2385°F) for 4 hours/103 MPa (15 ksi)
- **PWA 1484** – HIP cycle at 1318°C (2405°F) for 4 hours/103 MPa (15 ksi).

The specific cycles for each respective alloy were selected based on the following criteria:

1. Temperature where full porosity closure was achieved during the HIP cycle.
2. Condition where appreciable  $\gamma/\gamma'$  eutectic solutioning occurs during the HIP cycle.
3. Condition where a documented processing window exists above and below the selected HIP temperature, where subsequent solution heat treatment produces the desired pore-free, eutectic-free microstructure.

The recommended HIP parameters were reviewed with the NASA technical monitor and approval was granted for processing of the remaining PWA 1482 and PWA 1484 test material.

A purchase order was subsequently placed with IMT requesting them to HIP the entire lot of PWA 1482 and PWA 1484 test material. IMT initially planned to HIP the as-cast test material in their 20.32-cm (8-in.) HIP furnace using alumina crucibles and foil wrap to protect the test bars from any potential carbon contamination during the HIP runs. A total of four HIP runs were planned (two for each alloy) to minimize the potential for complete material loss in the event of processing difficulties during HIP. A summary of the HIP results for each respective alloy is described as follows:

#### **PWA 1482**

All of the PWA 1482 test material was HIP'ed at IMT in two respective cycles in their 20.32-cm (8-in.) diameter furnace at 1307°C (2385°F)/103 MPa (15ksi)/4 hours. Following HIP, the PWA 1482 test material was shipped back to the RPCL for final grain and Laue' inspection. Visual inspection following grain etch revealed coarse grain RX on external surfaces of the majority of the 1.91-cm (0.75-in.) and 1.59-cm (0.625-in.) diameter test bars. Most of the RX appeared to be localized and associated with either the material feed runner at the tip of the bar or a 2.54-cm (1.0-in.) to 5.08-cm (2.0-in.) area near the bottom of the bar. However, some test bars showed RX over the entire length and were considered scrap for test purposes. Visual inspection of the PWA 1482 test slabs that were processed along with the test bars revealed no incidence of post-HIP RX.

The RX observed on this latest lot of test bars was in contrast to previous observations of PWA 1482 material that was processed during the HIP optimization matrix. Test bars included in each PWA 1482 HIP optimization trial were visually inspected in the grain etched condition following HIP and post-HIP solution heat treatment. No evidence of RX was observed on any test bars regardless of HIP parameters. Analysis of the pressure/temperature

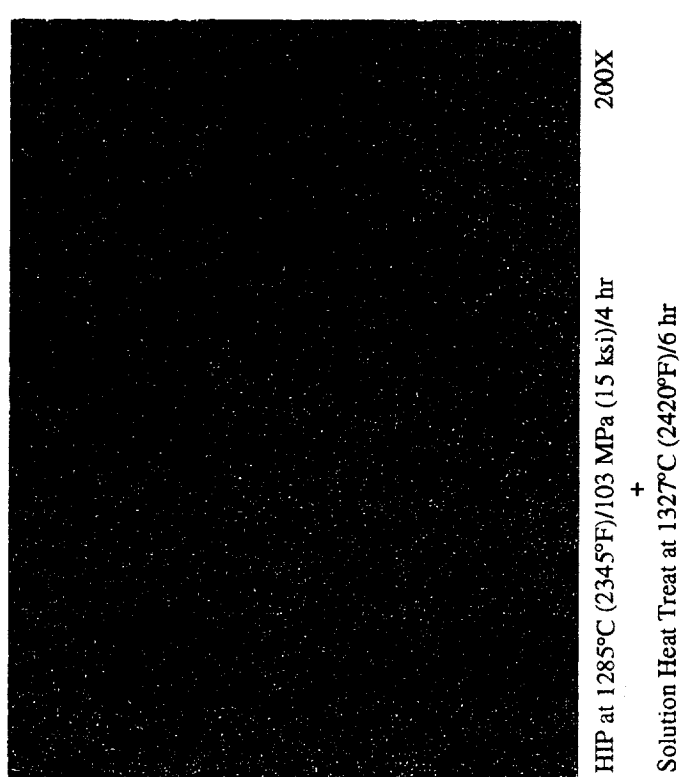
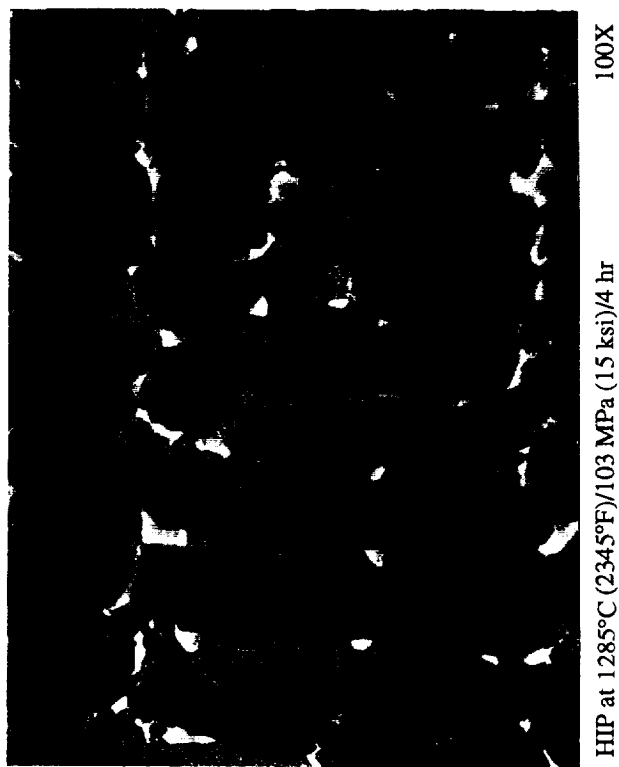
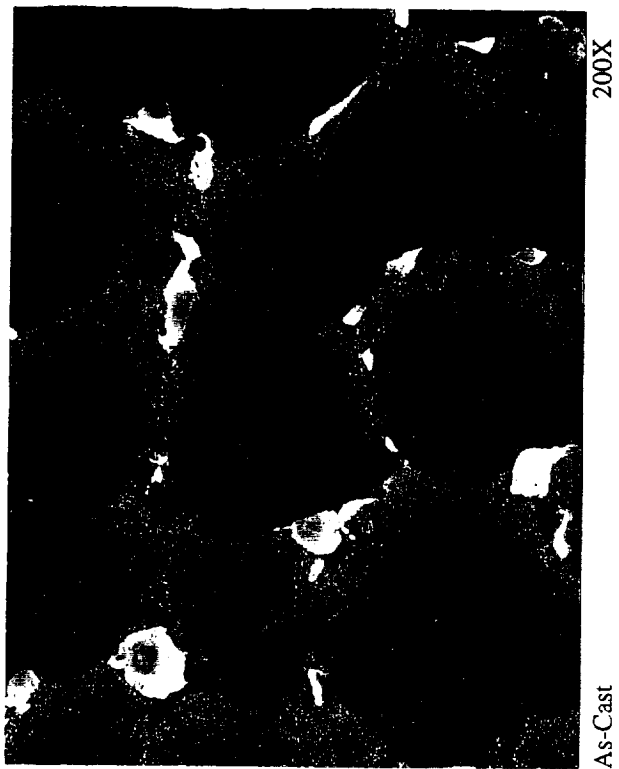
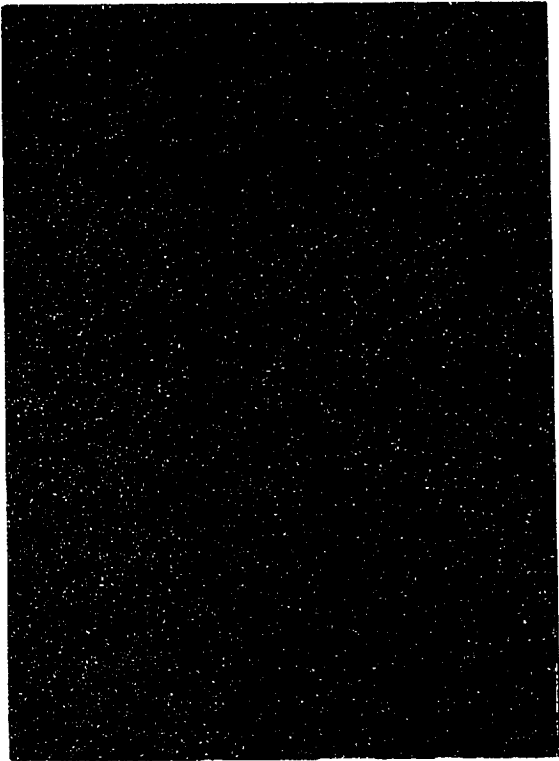


Figure 11. Typical Microstructure of PWA 1484 Following HIP and Solution Heat Treatment (Etch: AG21)



HIP at 1296°C (2365°F)/103 MPa (15 ksi)/4 hr

100X



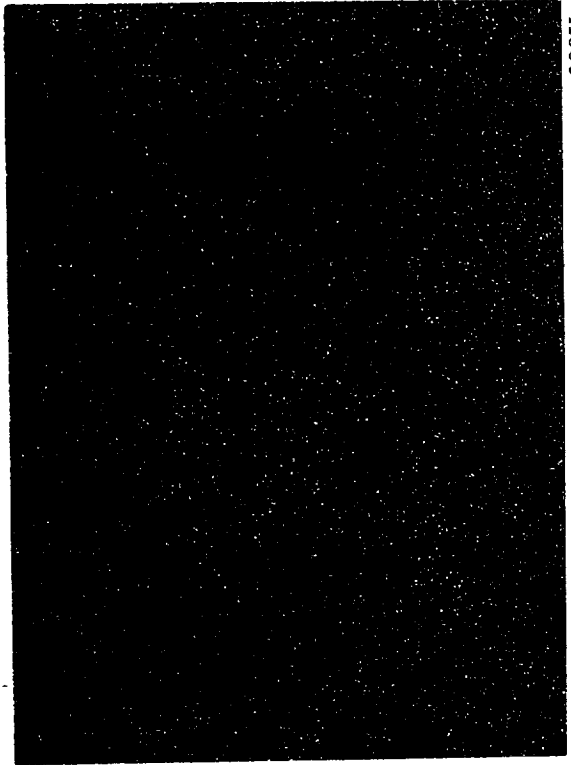
HIP at 1296°C (2365°F)/103 MPa (15 ksi)/4 hr  
+  
Solution Heat Treat at 1327°C (2420°F)/6 hr

200X



HIP at 1307°C (2385°F)/103 MPa (15 ksi)/4 hr

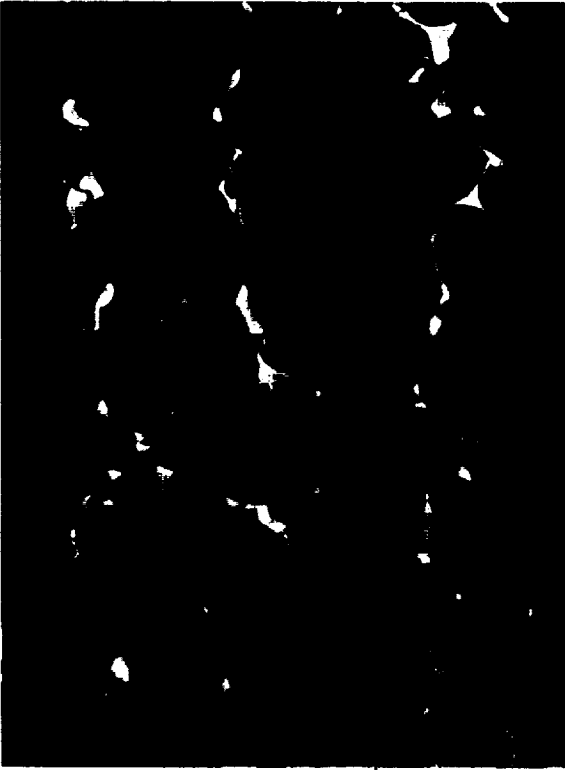
100X



HIP at 1307°C (2385°F)/103 MPa (15 ksi)/4 hr  
+  
Solution Heat Treat at 1327°C (2420°F)/6 hr

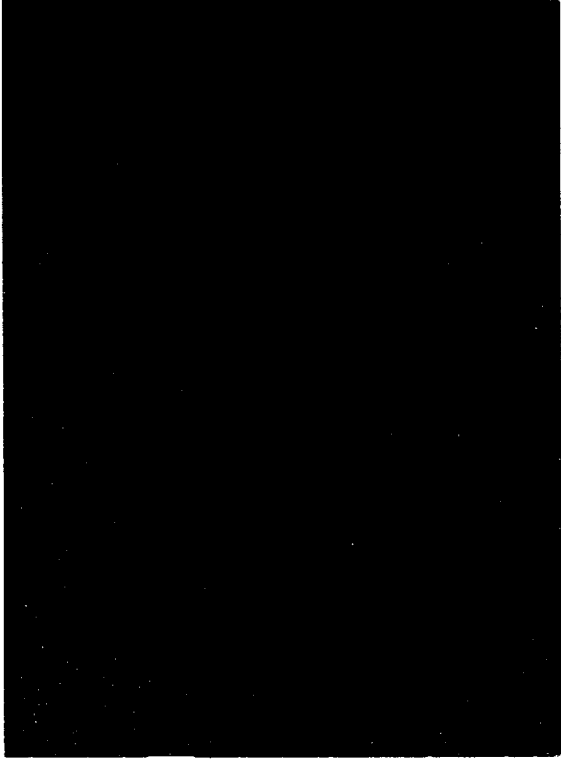
200X

Figure 12. Typical Microstructure of PWA 1484 Following HIP and Solution Heat Treatment (Etch: AG21)



HIP at 1318°C (2405°F)/103 MPa (15 ksi)/4 hr

100X



HIP at 1318°C (2405°F)/103 MPa (15 ksi)/4 hr  
+  
Solution Heat Treat at 1327°C (2420°F)/6 hr

200X



HIP at 1330°C (2425°F)/103 MPa (15 ksi)/4 hr

100X



HIP at 1330°C (2425°F)/103 MPa (15 ksi)/4 hr  
+  
Solution Heat Treat at 1327°C (2420°F)/6 hr

200X

Figure 13. Typical Microstructure of PWA 1484 Following HIP and Solution Heat Treatment (Etch: AG21)



plots from the 1307°C (2385°F) HIP trial run (Trial 4) and the latest production cycles at 1307°C (2385°F) indicate that the production cycles had a moderately slower temperature ramp cycle. This was most likely associated with the increased load size during the production runs, and the fact that the production cycles were run in IMT's 20.32-cm (8.0-in.) furnace versus the 15.24-cm (6.0-in.) furnace used for the HIP optimization trials. The slower temperature ramp cycle would allow application of argon gas pressure at a lower temperature during HIP, and this may have been a factor that contributed to the formation of RX grains in these samples.

These findings suggested that the PWA 1482 alloy may be sensitive to process variations during HIP, and that additional HIP parameter development would be required to define a production capable process for this alloy. It may also have suggested that the 1307°C (2385°F) HIP cycle was too high a temperature for this alloy and subsequent HIP trials should be conducted at lower temperature.

Cross-section metallography was performed on representative PWA 1482 test bars through specific areas with surface RX. This metallography indicated that most of the grains extend deep within the diameter of the bar, and RX of this nature is considered unacceptable for test material. Therefore, any test samples that could be machined from the remaining PWA 1482 test bars should be sectioned from areas along the length where no RX is visible. In most cases, this precludes the use of the entire bar length for machining of multiple test samples because most bars had some degree of surface RX. Based on the fact that the original material estimates were calculated with the intent of machining multiple specimens per bar, it was anticipated that additional PWA 1482 material would be required to complete the material screening and test matrix. A focused visual inspection was performed on the entire grain etched lot of PWA 1482 test material, and the results are seen in Table 5.

The current inventory of PWA 1482 (good) test material was insufficient to complete the program test matrix described in Paragraph 2.6 – *Program Test Matrix*. The RPCL performed an inventory of the existing PWA 1482 alloys and determined that 143 kg (65 lb) from the original master heats were available. This last 143 kg (65 lb) was cast into 4 new molds of 1.59-cm (0.625-in.) diameter test bars, which produced an additional 48 bars. However, additional PWA 1482 alloy was needed to cast the remaining 1.59-cm (0.625-in.) and 1.91-cm (0.75-in.) diameter test bars that was required to fulfill the original material order.

*Table 5. PWA 1482 Visual Inspection Results*

<i>Bars Description</i>	<i>Bars Hot Isostatic Processed</i>	<i>Bars Scraped for Recrystallization</i>	<i>Bars Acceptable</i>	<i>Additional Bars Required</i>
1.59-cm (0.625-in.) Diameter	99	40	59	80
1.91-cm (0.75-in.) Diameter	79	45	34	26
3.81-cm (1.5-in.) x 15.24-cm (6.0-in.) Slab	16	0	16	0

Pratt & Whitney determined that the quickest method to procure any additional alloy would be to revert melt the existing scrap test material at the RPCL and produce a subscale PWA 1482 heat for subsequent casting. Prior to commencing with any additional alloy procurement, P&W proposed the following recovery plan for NASA's approval:

- Process the recently cast 1.59-cm (0.625-in.) diameter test bars (48 bars) through a modified (lower temperature soak, modified temperature/pressurization ramp) PWA 1482 HIP cycle in IMT's 40.64-cm (16-in.) diameter production HIP furnace. Process all the 1.59-cm (0.625-in.) diameter bars using a pre-HIP stress relief grain etch to remove any surface residual stresses.
- Perform a post-HIP visual inspection on the newly processed PWA 1482 alloy and determine if RX is still

prevalent. The following actions were proposed based on the post-HIP visual inspections:

**If RX is observed:**

- Complete the Program Test Matrix with the current PWA 1482 alloy on hand.

**If no RX is observed:**

- Complete the Program Test Matrix with the PWA 1482 alloy currently on hand.
- Revert all the scrap PWA 1482 test material and produce a subscale master heat at the RPCL.
- Cast the additional PWA 1482 test bars from the revert alloy and use this test material along with residual material from the original heats to fulfill the original material order.

The HIP processing of the PWA 1484 alloy was put on hold at IMT until the proposed PWA 1482 process recovery plan was completed. The PWA 1484 alloy was shipped back to the RPCL to perform a pre-HIP stress relief grain etch to remove any surface residual stresses. The pre-HIP grain etch is not currently used in production for HIP processing of PWA 1484 castings; however, it is a precautionary process step that P&W felt was warranted based on the recent PWA 1482 results.

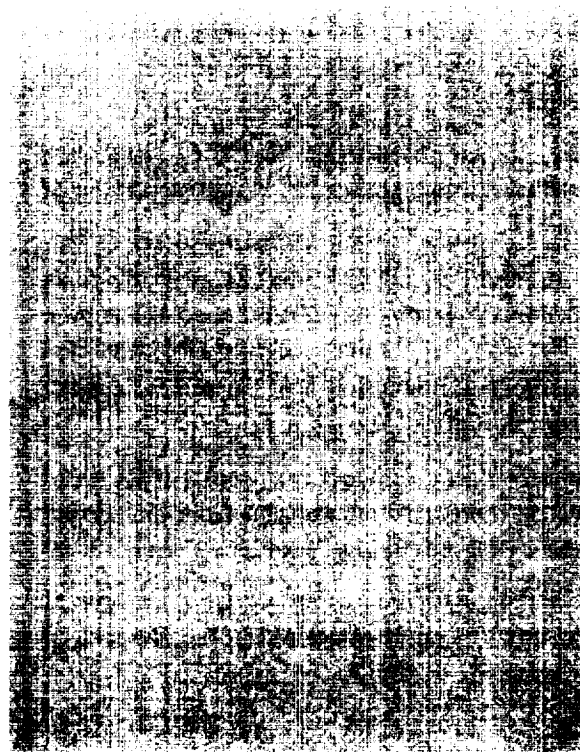
The proposed PWA 1482 material recovery plan was approved by the NASA contract monitor, and P&W proceeded with processing of the 48 1.59-cm (0.625-in.) diameter test bars as previously described. Each bar was processed through a pre-HIP stress relief etch at the RPCL and shipped to IMT for HIP cycling. The latest material was HIP cycled by IMT using their 40.64-cm (16-in.) diameter production furnace. The previous two production HIP runs, with the PWA 1482 test material, were conducted in IMT's smaller 20.32-cm (8-in.) diameter HIP furnace. IMT suggested running the latest material in their larger 40.64-cm (16-in.) furnace because HIP tooling was readily available and they were more confident in the thermocouple controls in this particular furnace.

Pratt & Whitney instructed IMT to run the latest PWA 1482 HIP run using a lower temperature soak with a modified pressurization/temperature cycle with respect to the baseline cycle. This HIP trial was conducted at 1285°C (2345°F)/4 hours/103 MPa (15 ksi), using a slower pressure and temperature ramp cycle during the HIP trial. Following the HIP run, the cast test bars were shipped back to the RPCL, where the material was grain etched. Visual inspection following grain etch did not reveal any evidence of surface RX.

Metallography conducted on two 1.59-cm (0.625-in.) diameter test bars that were included in this PWA 1482 trial indicated that complete pore closure was achieved. However, the proportion of eutectic solutioning was less than the level witnessed in samples HIP'ed at 1307°C (2385°F). Comparative microstructures from samples that were HIP'ed in each of the two runs are shown in Figure 14.

All the remaining eutectic phase islands were solutioned from the microstructure during the post-HIP solution heat treatment. This has been previously demonstrated with residual material from the HIP optimization test matrix, which was post-HIP solution heat treated and documented in Figures 8 through 10. This trial showed that PWA 1482 can be successfully processed without undesirable RX, using the modified HIP parameters demonstrated with the latest test bars.

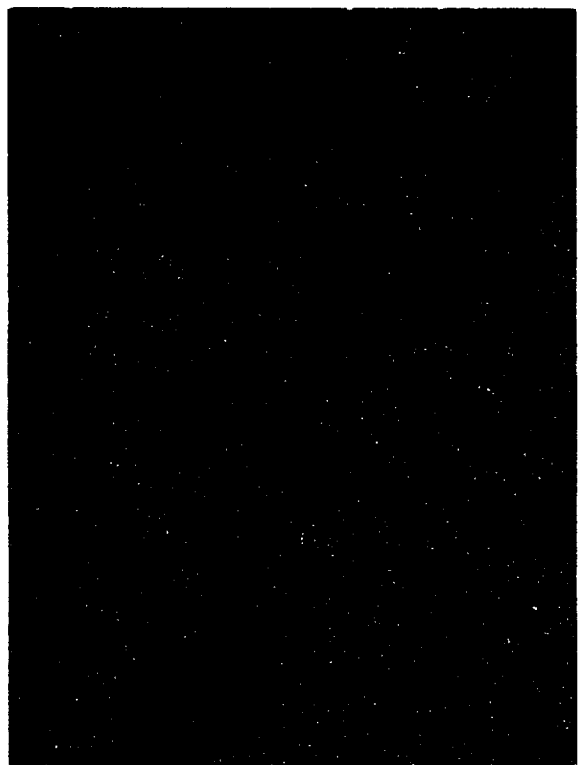
In keeping with the proposed material recovery plan, several additional molds of PWA 1482 test bars and slabs were cast from reverted PWA 1482 scrap test material at the RPCL. The additional test bars and slabs were used to replace the PWA 1482 material that was scrapped earlier in the program due to unacceptable levels of external RX. The scrap PWA 1482 test material was remelted at the RPCL in vacuum to produce a small 330 kg (150 lb) heat of alloy, which were subsequently poured into three 110 kg (50 lb) ingots. The heat code for the revert alloy produced at the RPCL was designated J203. Chemistry analysis performed on samples from the new ingots confirmed that the elemental compositions fall within PWA 1482 specification limits. Cast test bars from this alloy heat were submitted to the MCL in East Hartford for certification testing in accordance with the creep-stress rupture requirement previously described for PWA 1482. These tests were acceptable, and the revert heat was released by MCL for use in the NASA contract. The RPCL cast several molds of PWA 1482 test bars and slabs from the revert ingots as



As-Polished

S/N 156007

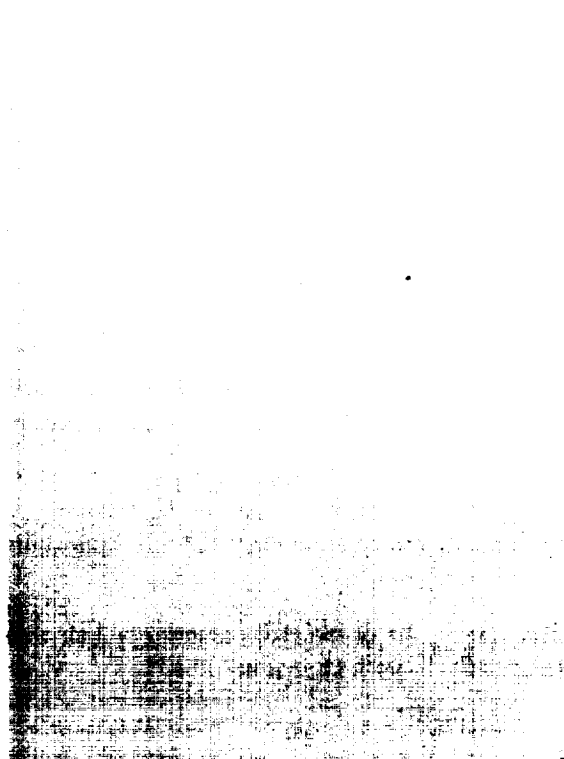
26X



Etch: AG21

S/N 156007

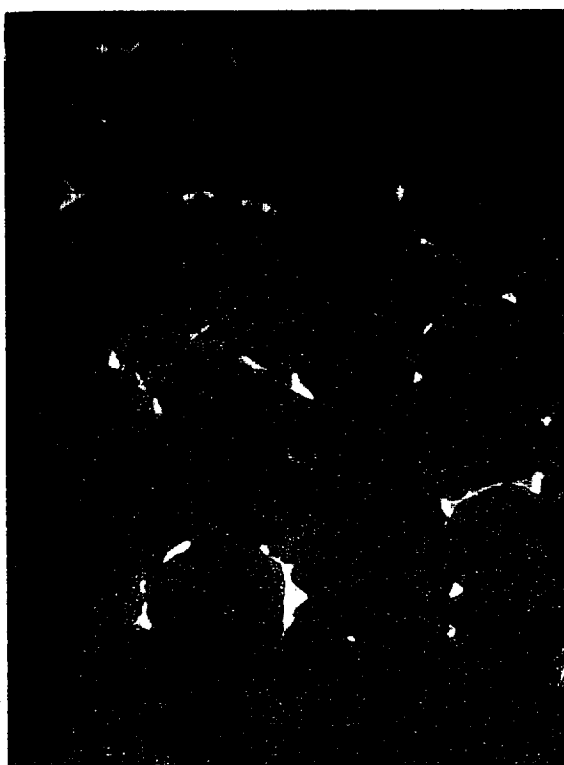
100X



As-Polished

S/N 769012

26X



Etch: AG21

S/N 769012

100X

Figure 14. Typical Microstructures from PWA 1482 Test Samples HIP Processed at 1307°C (2385°F)/103 MPa (15 ksi)/4 hr (Top) and 1285°C (2345°F)/103 MPa (15 ksi)/4 hr (Bottom)

described in Table 6. This revert PWA 1482 test material, along with the existing PWA 1482 material from the original heats, was sufficient to complete the testing outlined in the Program Test Matrix.

*Table 6. Revert PWA 1482 Test Material Procurement*

<i>Number of Molds</i>	<i>Specimen Type</i>	<i>Number of Specimens/ Molds</i>	<i>Total Number of Specimens</i>
3	1.59-cm (0.625-in.) Diameter	12	36
3	1.91-cm (0.75-in.) Diameter	8	24
1	Slabs	8	8

The RPCL processed the revert PWA 1482 test material through a pre-HIP stress relief etch and shipped the test bars and slabs to IMT for HIP processing. IMT processed this material through a HIP heat treatment in their 40.64-cm (16-in.) diameter furnace at 1285°C (2345°F)/4 hours/103 MPa (15 ksi), using the modified pressurization/temperature ramp cycle demonstrated on this alloy. Following the HIP cycle, the revert PWA 1482 test material lot was shipped back to the RPCL for grain etch processing. Visual inspection following grain etch did not reveal any evidence of surface RX. Metallography conducted on representative sample test bars that was included in this HIP run indicated that complete pore closure was achieved, and the level of eutectic  $\gamma/\gamma'$  solutioning was consistent with the microstructures from the last HIP run. All the revert PWA 1482 test material was subsequently shipped to the RPCL for final processing.

#### **PWA 1484:**

Two PWA 1484 HIP trials were performed in IMT's production 40.64-cm (16-in.) diameter furnace. These trials were conducted at 1307°C (2385°F)/4 hours/103 MPa (15 ksi) using a similar modified pressurization/temperature ramp cycle developed for this alloy. Pratt & Whitney selected a lower temperature HIP cycle for the PWA 1484 test material lot to minimize the potential for processing difficulties similar to those experienced with the PWA 1482 material lot. The PWA 1484 HIP trials were conducted in series, where the second trial was released to be run following metallographic review of test material from the first trial.

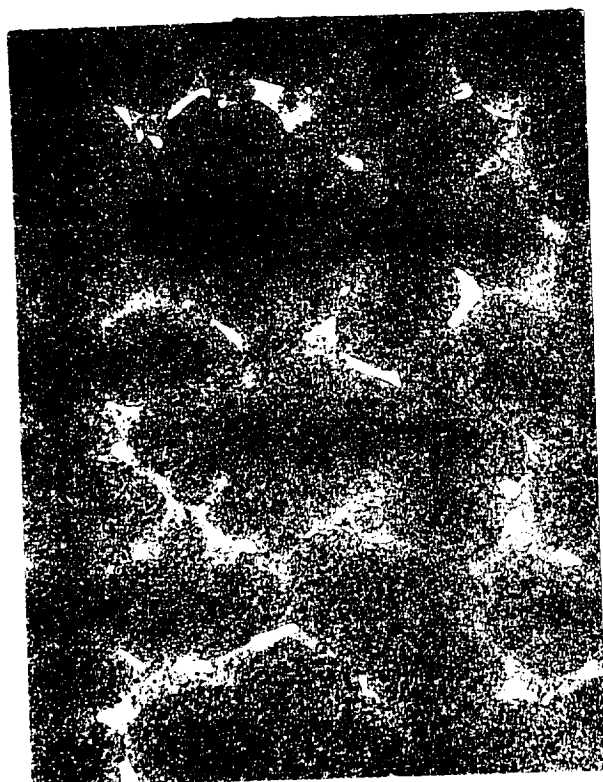
Following the HIP trials, the first PWA 1484 test material lot was shipped back to the RPCL for grain etch inspection and metallography. All of the test bars and slabs were processed through grain etch. Visual inspection of several grain etched test bars and slabs revealed no evidence of post-HIP RX.

Metallography was conducted on representative 1.59-cm (0.625-in.) and 1.91-cm (0.75-in.) diameter test bars to evaluate the microstructures for pore closure and  $\gamma'$  solutioning. This metallography indicated that complete pore closure was achieved at 1307°C (2385°F)/4 hours/103 MPa (15 ksi). The PWA 1484 microstructure also contained residual  $\gamma/\gamma'$  eutectic phase islands, which was solutioned during the post-HIP solution heat treatment. Typical microstructures from HIP'ed PWA 1484 test material samples are shown in Figure 15.

Based on the results of this metallography, IMT was given authorization to process the second PWA 1484 material lot using the same HIP parameters. Metallography conducted on representative samples from the second HIP run were considered acceptable, and no undesirable RX was observed during post grain etch visual inspections.

A final summary of the of the HIP parameters that were used to process the entire material test lots for each of the two single-crystal alloys is shown in Table 7.

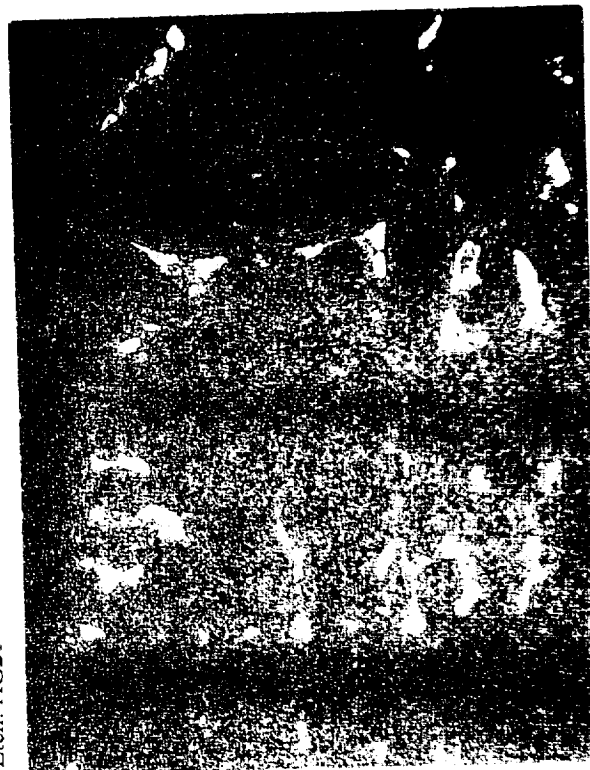
Following grain etch processing and visual inspection at the RPCL, each of the PWA 1482 and PWA 1484 test bars and slabs were Laue' x-rayed and the primary crystallographic orientations were recorded for each of the individual specimens. Secondary crystallographic orientations were also measured and recorded for each of the test



100X

S/N 1530407

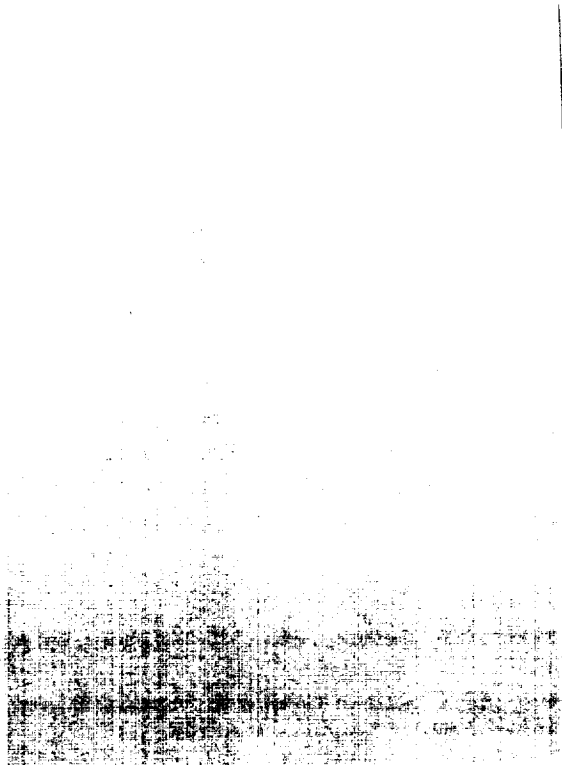
Etch: AG21



100X

S/N 155105

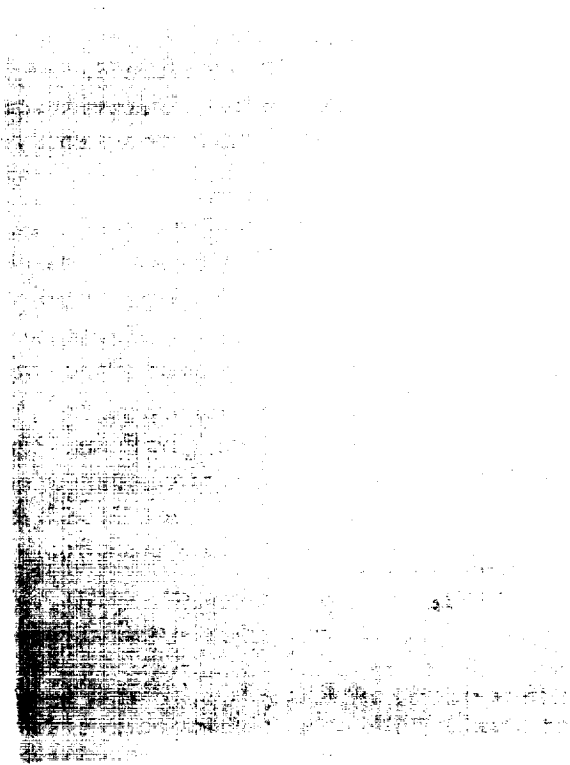
Etch: AG21



26X

S/N 1530407

As-Polished



26X

S/N 155105

As-Polished

*Figure 15. Typical Microstructures from PWA 1484 Test Samples HIP Processed at 1307°C (2385°F)/103MPa (15 ksi)/4 hr*

slabs. All the as HIP'ed test material was carefully boxed and shipped to the P&W MCL in Florida for alternate HT development studies and final processing.

Table 7. Summary of Final HIP Parameters Used on PWA 1482 and PWA 1484 Test Material

HIP Trial	Alloy	HIP Furnace Size (cm/in.)	HIP Parameters	Metallographic Results
1*	PWA 1482	20.32/8	1307°C (2385°F)/4 hr/103 MPa (15 ksi)	Complete Pore Closure, Surface RX
2**	PWA 1482	40.64/16	1285°C (2345°F)/4 hr/103 MPa (15 ksi)	Complete Pore Closure, No RX
3	PWA 1484	40.64/16	1307°C (2385°F)/4 hr/103 MPa (15 ksi)	Complete Pore Closure, No RX
4	PWA 1484	40.64/16	1307°C (2385°F)/4 hr/103 MPa (15 ksi)	Complete Pore Closure, No RX

Notes:

\* Initial PWA 1482 HIP trials.

\*\* Subsequent PWA 1482 HIP trials conducted with 48 cast 1.59-cm (0.625-in.) diameter test bars and revert PWA 1482 test material.

## 2.4 THERMAL TREATMENT OPTIMIZATION

Post-HIP alternate HT processes were developed for each respective single-crystal alloy. The goal of the thermal treatment optimization task was to develop and downselect an optimal PWA 1482 and PWA 1484 heat treatment that provided the best balance of mechanical properties for use in hydrogen environments. Selection of the optimized thermal treatment was based on the results of a series of mechanical property screening tests to be conducted on each of the modified HTs. Pratt & Whitney elected to perform screening characterization tests to evaluate the alternate HTs on PWA 1484. Trends in the single-crystal mechanical properties were expected to be applicable to PWA 1482. Two downselected heat treatments, for each respective alloy, were then applied to larger batches of test material for additional mechanical property characterization testing as outlined in Paragraph 2.6 – *Program Test Matrix*.

Pratt & Whitney's processing approach was to fully solution the eutectic  $\gamma/\gamma'$  phase islands from each alloy and develop a series of modified  $\gamma'$  morphologies for subsequent screening tests. This processing approach was based on observations by DeLuca *et. al.*,<sup>5,6</sup> where eutectic  $\gamma/\gamma'$  phase islands were identified as fatigue crack initiation sites in the microstructures of single-crystal LCF specimens tested at 20°C (68°F) in 34.5 MPa (5.0 ksi) gaseous hydrogen. Elimination of the eutectic  $\gamma/\gamma'$  phase islands from the microstructures of single-crystal test specimens has been shown to provide significant improvements in notch LCF lives. Additionally, DeLuca *et. al.*<sup>7,8</sup> have shown that substantial reductions in crack growth rates can be achieved by modifying the cuboidal  $\gamma'$  precipitate size and shape to make preferential crack propagation through the phase or along the  $\gamma/\gamma'$  interface more difficult. This can be accomplished by slow cooling down through the  $\gamma'$  solvus at controlled rates to precipitate out large  $\gamma'$  particles that act as barriers to the propagating crack front.

<sup>5</sup> SSME Alternate turbopump Development Program, NASA-MSFC Contract NAS8-36801.

<sup>6</sup> DeLuca, D.P. and Cowles, B.A.; *Hydrogen Effects on Material Behavior*; N.R. Moody, A.W. Thompson, eds.; TMS, Warrendale, PA; pp 603-613, 1989.

<sup>7</sup> DeLuca, D.P., Jones, H.B., Cowles, B.A., and Cobia, F.D.; *Second Workshop on Hydrogen Effects on Materials in Propulsion Systems*; Proceedings Conference at NASA-MSFC, Huntsville, AL; NASA CP-3182; 20-21 May 1992.

<sup>8</sup> *Investigation of Advanced Processed Single-Crystal Turbine Blade Alloys*; NASA-MSFC Contract NAS8-39050, 1989

Post-HIP alternate HT parameters were established for each alloy using residual material following HIP processing. All the alternate HT optimization trials were conducted in vacuum HT furnaces, which were manufactured by Vacuum Industries, in the materials laboratory at P&W. Two generic classes of microstructures were developed for each alloy:

- (1) Pore-Free, Eutectic-Free, Fine Cuboidal  $\gamma'$   
Precipitate Morphology
- (2) Pore-Free, Eutectic-Free, Bimodal  $\gamma'$   
Precipitate Morphology.

Microstructures from the PWA 1484 test samples, processed to develop the two generic microstructural classes, are seen in Figure 16. These microstructures were produced by processing PWA 1484 test material according to the schedule outlined in Table 8.

*Table 8. PWA 1484 Alternate HT Processing*

<i>Microstructure</i>	<i>Hot Isostatic Process</i>	<i>Heat Treatment</i>
Pore-Free, Eutectic-Free, Fine Cuboidal $\gamma'$	1307°C (2385°F)/103MPa (15 ksi)/4 hr	Solution at 1332°C (2430°F) 6 hr→Rapid Cool + 1079°C (1975°F)/4 hr + 704°C (1300°F)/24 hr
Pore-Free, Eutectic-Free, Bimodal $\gamma'$	1307°C (2385°F)/103 MPa (15 ksi)/4 hr	Solution at 1332°C (2430°F) 6 hr→Slow Cool* + 1079°C (1975°F)/4 hr + 704°C (1300°F)/24 hr
* Slow cool from 1332°C (2430°F) at 0.28°C/min to 1260°C (2300°F). Hold 2 hr→rapid vacuum cool to room temperature.		

The pore-free, eutectic-free, fine cuboidal  $\gamma'$  precipitate morphology was designed to evaluate the effect of eliminating microstructural defects without radically changing the typical  $\gamma'$  precipitate morphology. The pore-free, eutectic-free, bimodal  $\gamma'$  precipitate morphology microstructure evaluated the impact of defect elimination, coupled with radical changes to the  $\gamma'$  precipitate morphology and distribution.

In addition to the two microstructures produced using the HT cycles that were outlined in Table 8, several additional cycles were developed for subsequent mechanical property screening tests. The additional cycles, provided in Table 9, are variants based on the cycles described in Table 8, where slight modifications in thermal processing were introduced to produce differences in the size, shape, and distribution of the  $\gamma'$  precipitates for test screening purposes. Trial HTs 1 and 2 are cycles that produce pore-free, eutectic-free, fine cuboidal  $\gamma'$  precipitate morphologies that are similar to those observed in Figure 16. The remaining cycles were designed to produce pore-free, eutectic-free, bimodal precipitate morphologies. Heat treatments 2 and 5 are the same cycles previously described in Table 8.

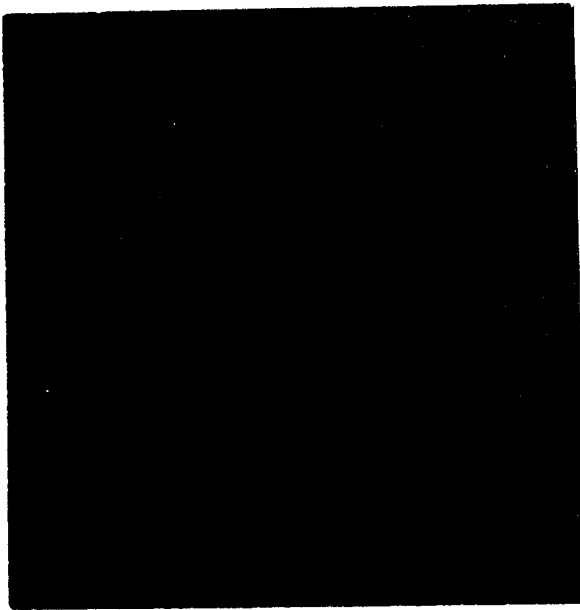
Metallography was performed in conjunction with each of the respective HT trials to document the resultant PWA 1484 microstructures. Typical microstructures for each of the seven alternate heat treatments produced in PWA 1484 are seen in Figures 17 through 23. These microstructures are a combination of optimal photomicrographs and high-magnification photomicrographs that were taken in the Transmission Electron Microscope (TEM) from replicas obtained from polished mounts for each sample. The high-magnification TEM micrographs were especially helpful in evaluating the effect of thermal processing on the size, morphology, and distribution of the  $\gamma'$  precipitates. Each of the seven PWA 1484 heat treatment microstructures are described more fully in Table 10.

Several PWA 1484 test bars and slabs were heat treated according to the respective thermal cycles outlined in Table 9. These test materials were subsequently sent to Metcut Research Associates and machined into mechanical property specimens for screening tests as outlined in Paragraph 2.5 – *Hydrogen Test – Alternate Microstructure Screening*. The results of the screening tests were then used to down select two heat treatments per alloy for further characterization testing as outlined in Paragraph 2.6 – *Program Text Matrix*.

*Table 9. PWA 1484 Alternate HTs for Screening Tests*

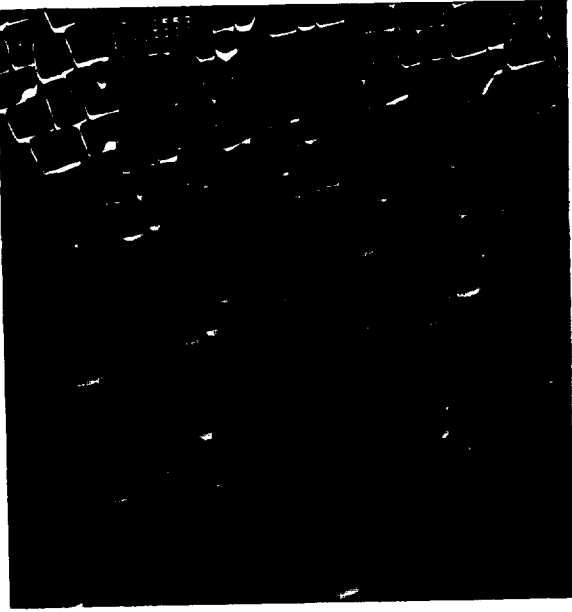
<i>Trial</i>	<i>Hot Isostatic Process</i>	<i>Heat Treatment</i>
1	1307°C (2385°F)/103 MPa (15 ksi)/4 hr	Solution at 1332°C (2430°F)/6 hr→Rapid Cool + 704°C (1300°F)/24 hr
2	1307°C (2385°F)/103 MPa (15 ksi)/4 hr	Solution at 1332°C (2430°F)/6 hr→Rapid Cool + 1079°C (1975°F)/4 hr + 704°C (1300°F)/24 hr
3	1307°C (2385°F)/103 MPa (15 ksi)/4 hr	Solution at 1332°C (2430°F)/6 hr→Rapid Cool + 1079°C (1975°F)/4 hr + 704°C (1300°F)/24 hr
4	1307°C (2385°F)/103 MPa (15 ksi)/4 hr	Solution at 1332°C (2430°F)/6 hr→Rapid Cool* + 704°C (1300°F)/24 hr
5	1307°C (2385°F)/103 MPa (15 ksi)/4 hr	Solution at 1332°C (2430°F)/6 hr→Rapid Cool* + 1079°C (1975°F)/4 hr + 704°C (1300°F)/24 hr
6	1307°C (2385°F)/103 MPa (15 ksi)/4 hr	Solution at 1332°C (2430°F)/6 hr→Rapid Cool** + 704°C (1300°F)/24 hr
7	1307°C (2385°F)/103 MPa (15 ksi)/4 hr	Solution at 1332°C (2430°F)/6 hr→Rapid Cool** + 1079°C (1975°F)/4 hr + 704°C (1300°F)/24 hr
<p>* Slow cool from 1332°C (2430°F) at 0.28°C/min to 1260°C (2300°F). Hold for 2 hr→rapid vacuum cool to room temperature.</p> <p>** Slow cool from 1332°C (2430°F) at 0.56°C/min to 1204°C (2200°F)→rapid vacuum cool to room temperature.</p>		



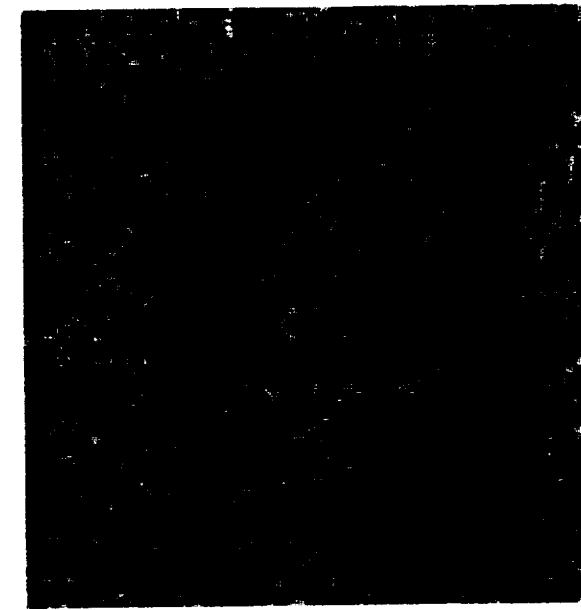


500X

Pore-Free, Eutectic-Free, Fine Cuboidal  $\gamma$



10,000X



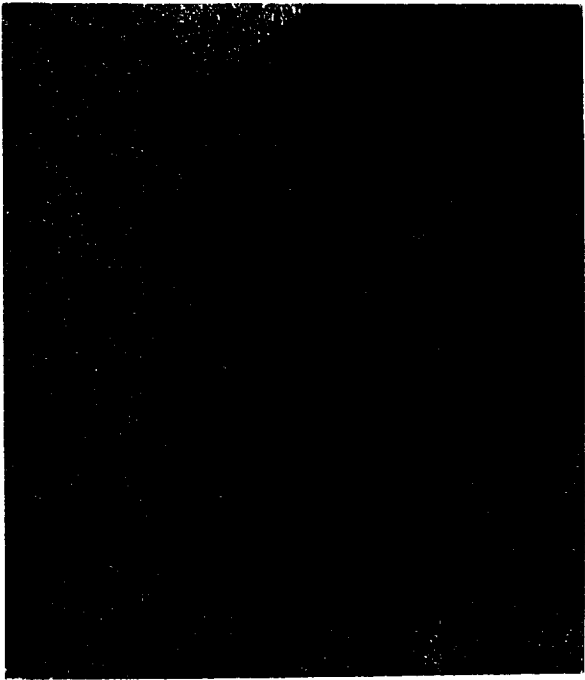
500X

Pore-Free, Eutectic-Free, Bimodal  $\gamma$



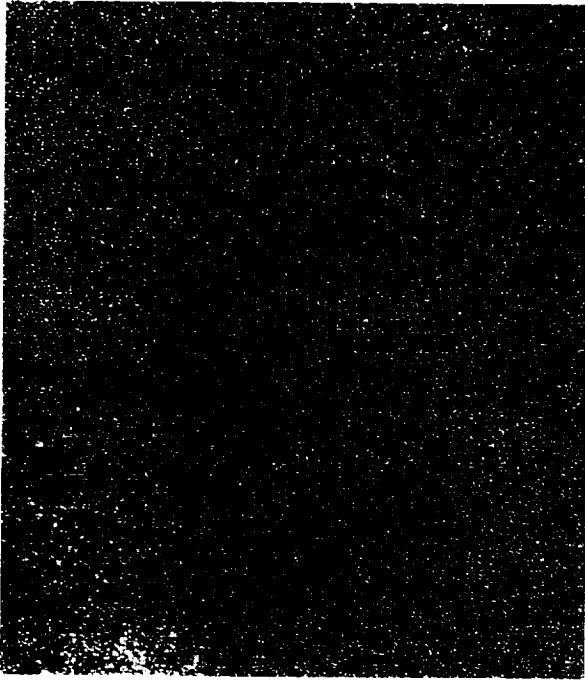
10,000X

Figure 16. PWA 1484 Alternate HT Microstructures

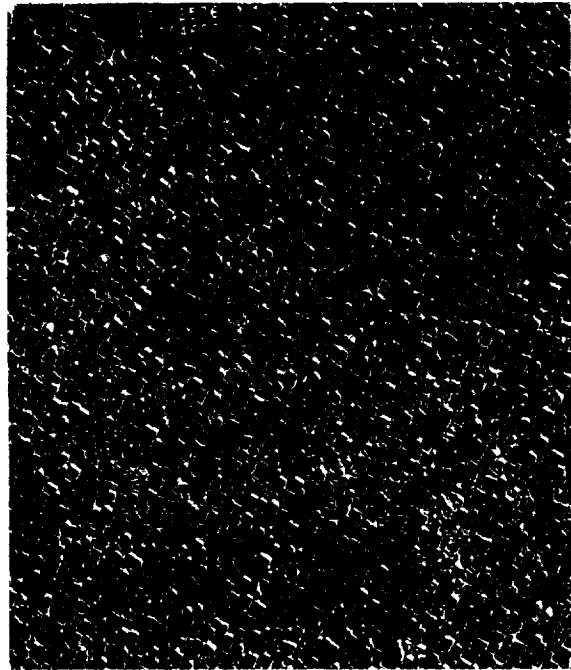


Heat Treat 1

200X

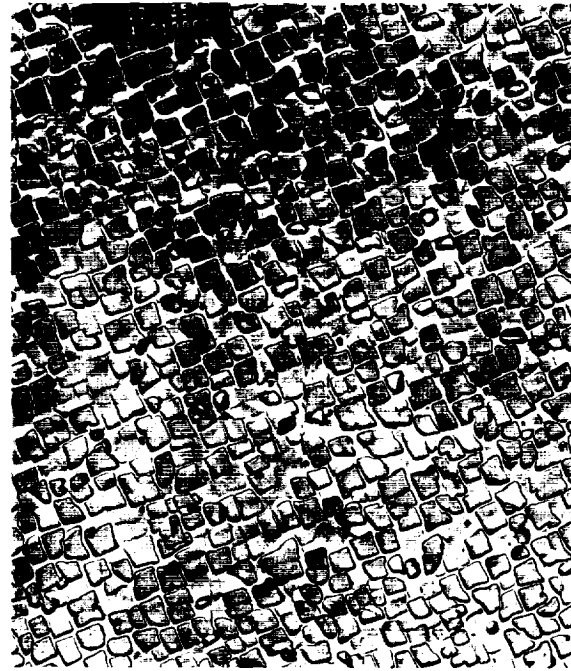


500X



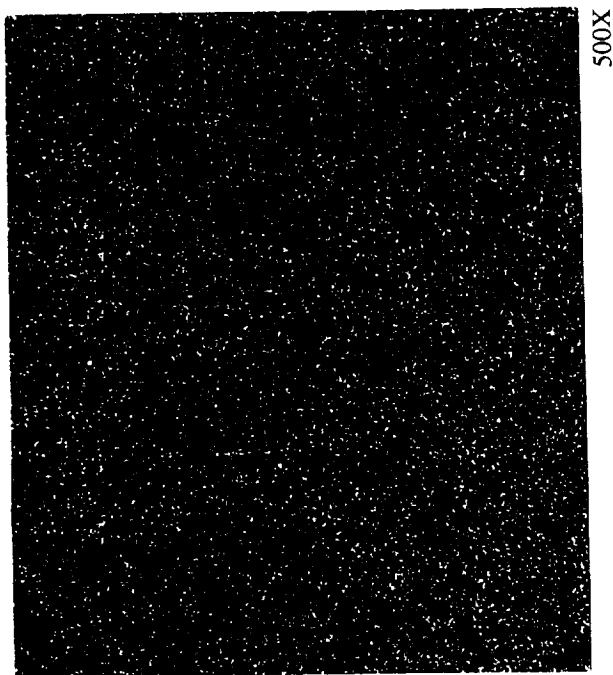
Heat Treat 1

4600X



10,000X

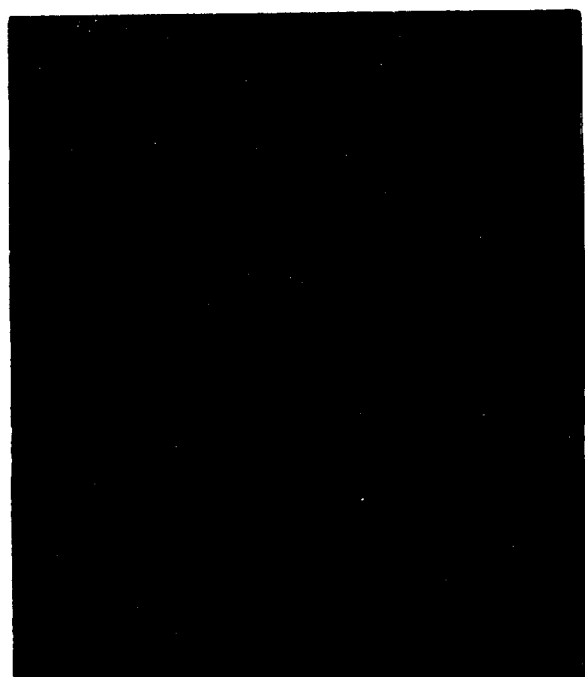
*Figure 17. PWA 1484 Microstructure Produced in Thermal Treatment Optimization Studies*



500X

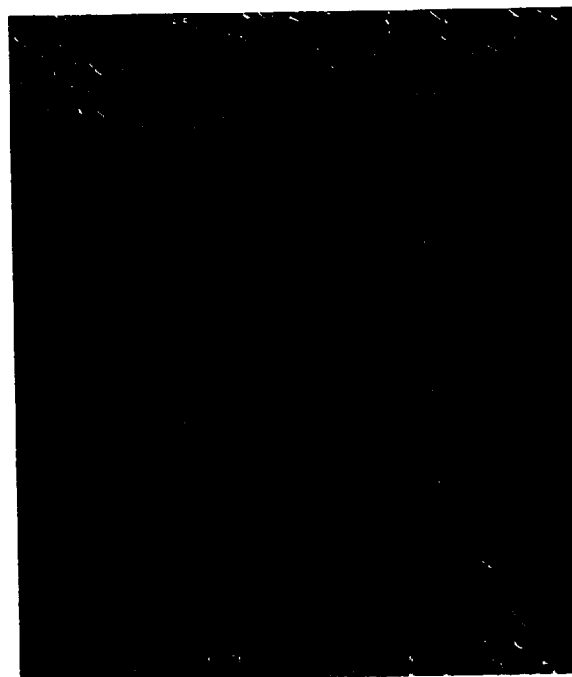


10,000X



200X

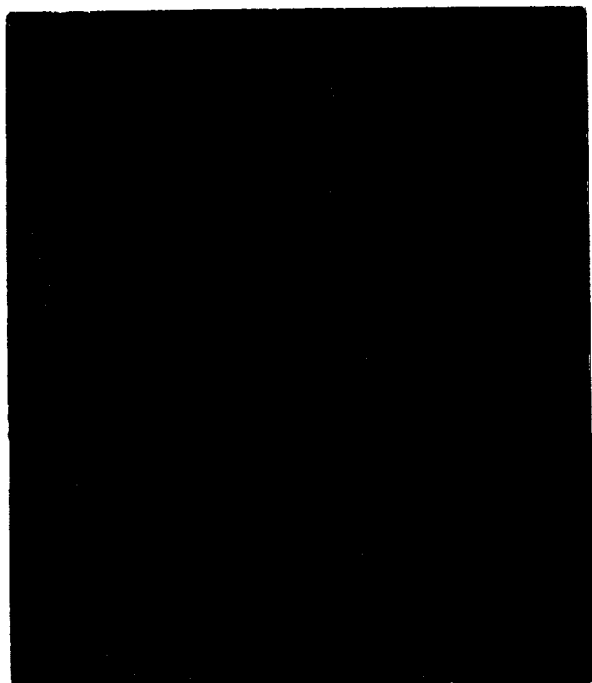
Heat Treat 2



4600X

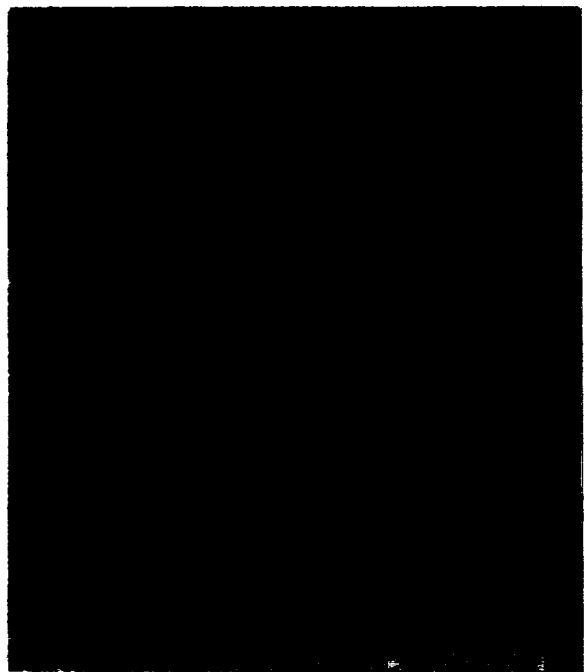
Heat Treat 2

*Figure 18. PWA 1484 Microstructure Produced in Thermal Treatment Optimization Studies*



Heat Treat 3

200X

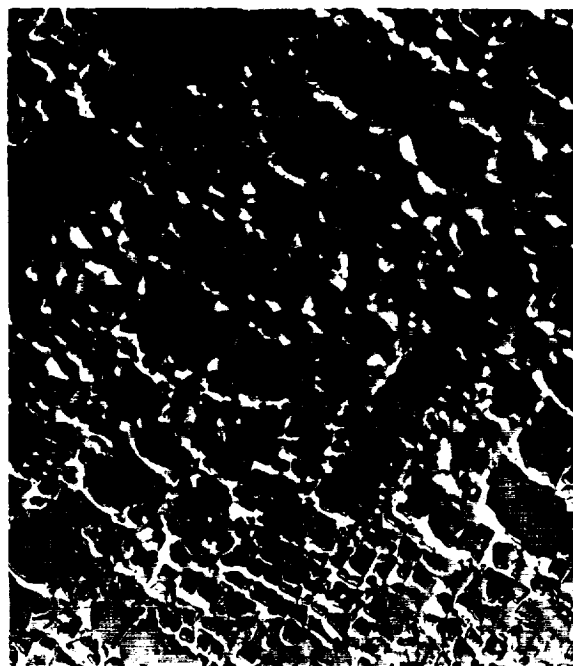


500X



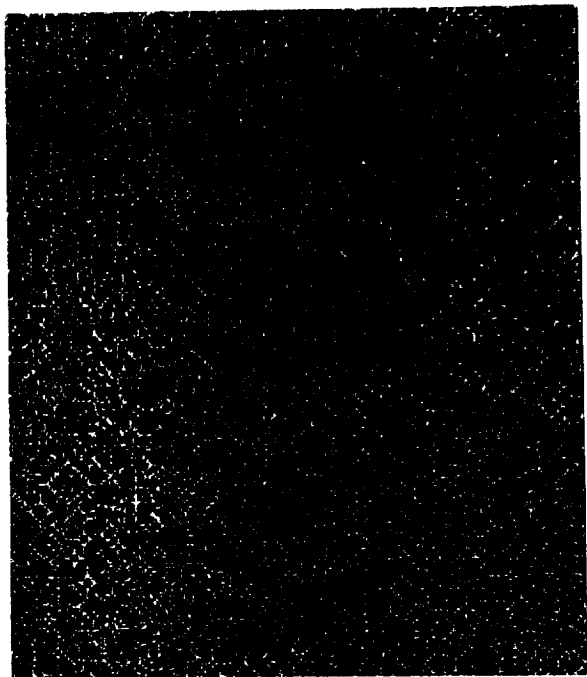
Heat Treat 3

4600X



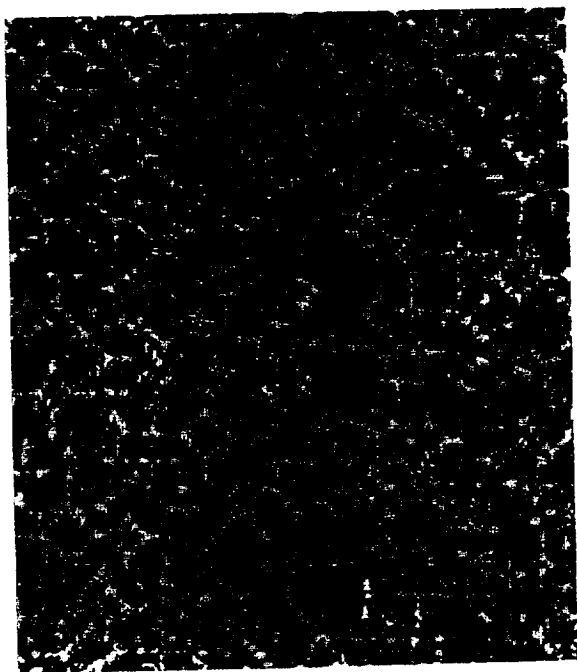
10,000X

*Figure 19. PWA 1484 Microstructure Produced in Thermal Treatment Optimization Studies*

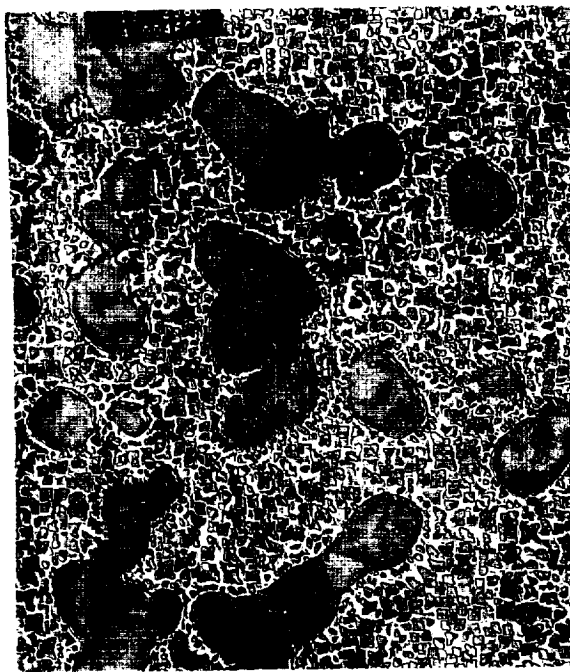


Heat Treat 4

200X



500X



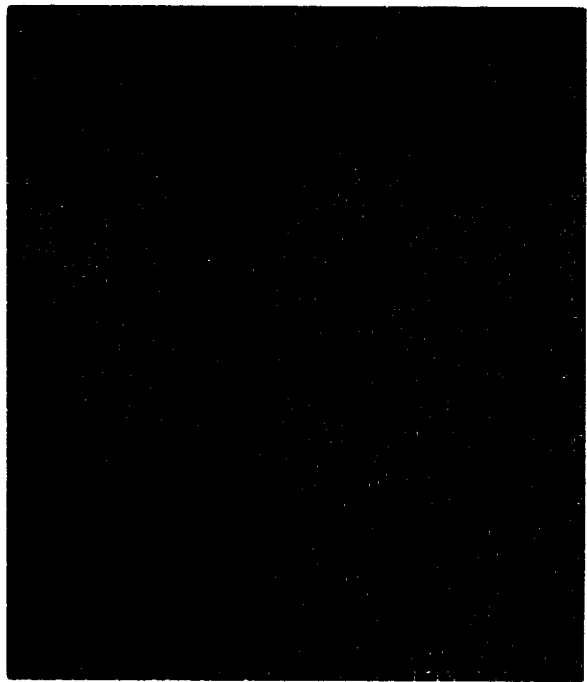
Heat Treat 4

4600X



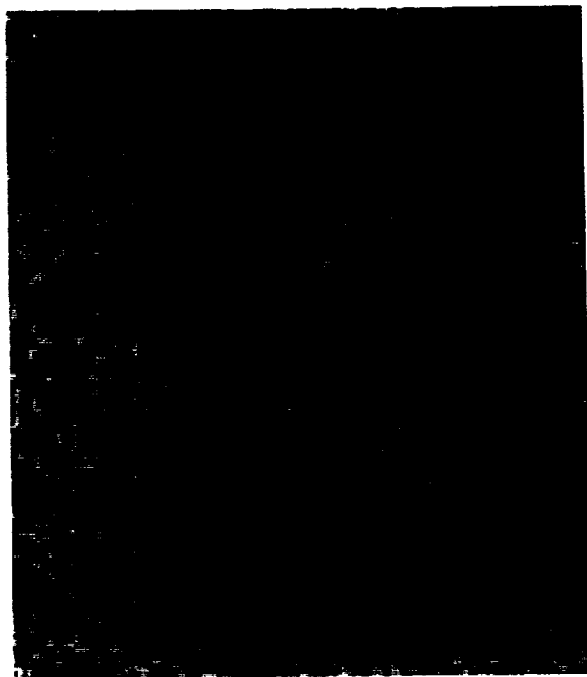
10,000X

*Figure 20. PWA 1484 Microstructure Produced in Thermal Treatment Optimization Studies*



Heat Treat 5

200X



500X



Heat Treat 5

4600X



10,000X

*Figure 21. PWA 1484 Microstructure Produced in Thermal Treatment Optimization Studies*



Heat Treat 6

200X



500X



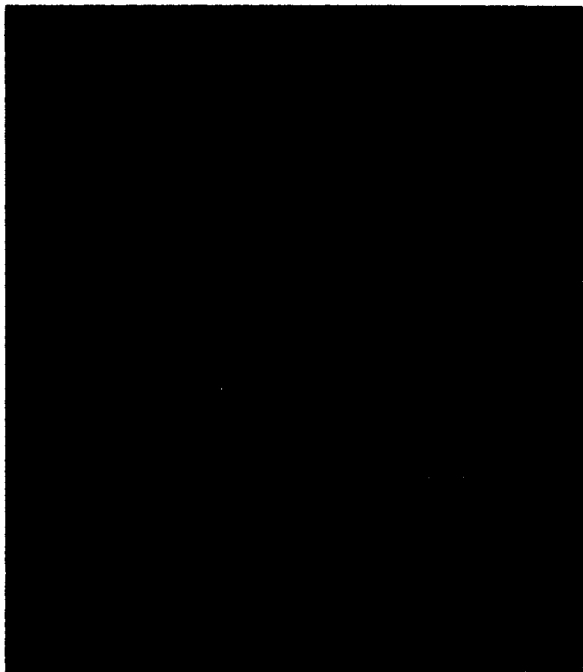
Heat Treat 6

4600X



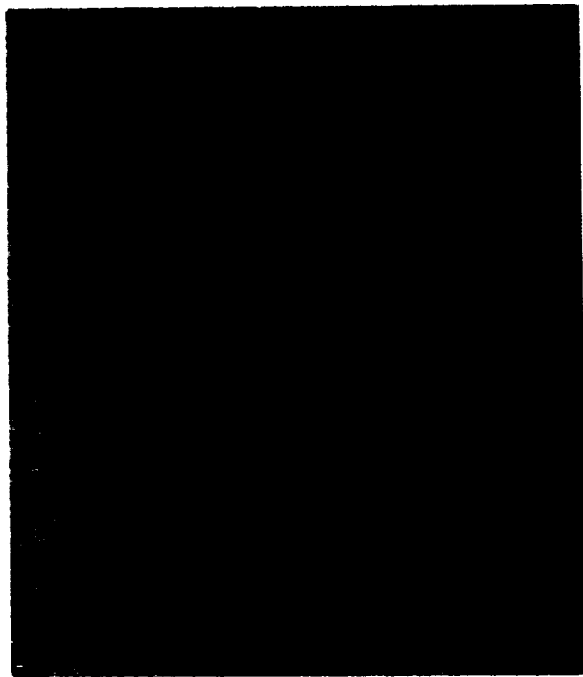
10,000X

*Figure 22. PWA 1484 Microstructure Produced in Thermal Treatment Optimization Studies*

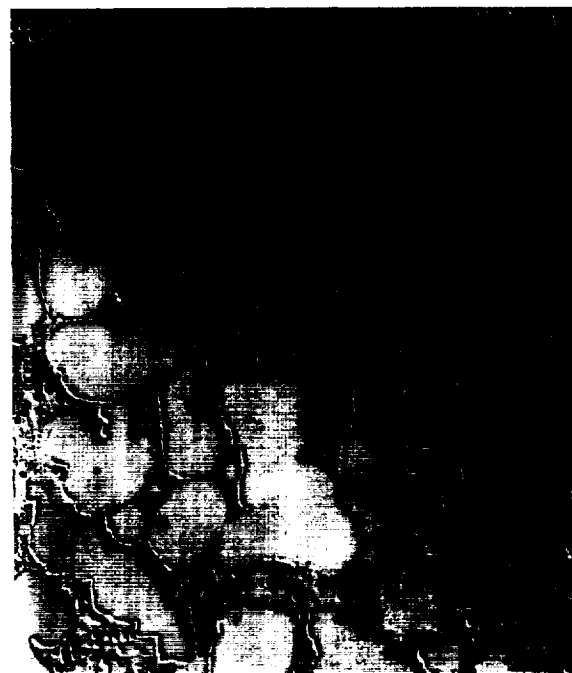


Heat Treat 7

200X

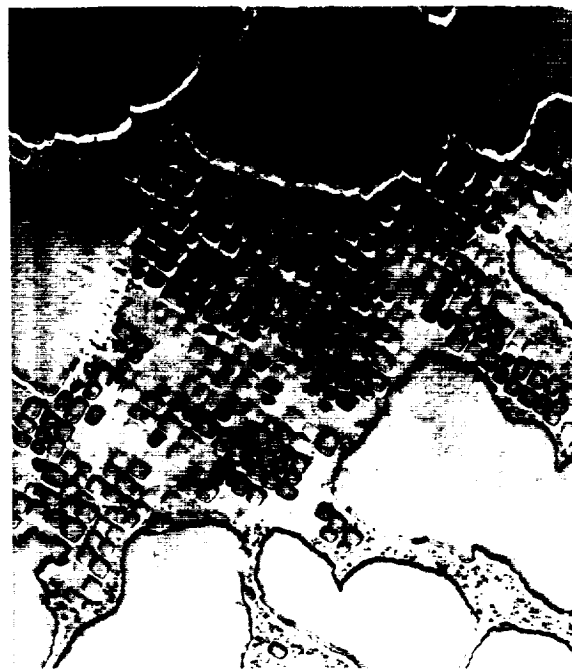


500X



Heat Treat 7

4600X



10,000X

Figure 23. PWA 1484 Microstructure Produced in Thermal Treatment Optimization Studies



Table 10. Microstructural Summary of PWA 1484 Alternate HT

Heat Treat Number	Microstructural Class	Microstructural Description
1	Pore-Free, Eutectic-Free, Fine Cuboidal $\gamma'$	Fine Cuboidal $\gamma'$ (0.3 - 0.4 $\mu$ ), Noncoherent $\gamma'$ Arrays, Irregular Shape to Particular Edges
2	Pore-Free, Eutectic-Free, Fine Cuboidal $\gamma'$	Fine Cuboidal $\gamma'$ (0.4 - 0.5 $\mu$ ), Very Coherent $\gamma'$ Arrays, Rounded Edges on Particles
3	Pore-Free, Eutectic-Free, Bimodal $\gamma'$	Irregularly Shaped Large Barrier $\gamma'$ Precipitates (1 - 3 $\mu$ ), Fine Cuboidal $\gamma'$ (0.1 - 0.3 $\mu$ ), Noncoherent $\gamma'$ Arrays, Irregular Shape to Particular Edges
4	Pore-Free, Eutectic-Free, Bimodal $\gamma'$	27 Volume Percent Large Barrier $\gamma'$ Precipitates (20 $\mu$ ), Fine Cuboidal $\gamma'$ (0.3 - 0.4 $\mu$ ), Noncoherent $\gamma'$ Arrays, Irregular Shape to Particular Edges
5	Pore-Free, Eutectic-Free, Bimodal $\gamma'$	27 Volume Percent Large Barrier $\gamma'$ Precipitates (20 $\mu$ ), Fine Cuboidal $\gamma'$ (0.4 - 0.5 $\mu$ ), Very Coherent $\gamma'$ Arrays, Rounded Edges on Particles
6	Pore-Free, Eutectic-Free, Bimodal $\gamma'$	45 Volume Percent Large Barrier $\gamma'$ Precipitates (15 $\mu$ ), Fine Cuboidal $\gamma'$ (0.2 $\mu$ ), Noncoherent $\gamma'$ Arrays, Irregular Shape to Particular Edges
7	Pore-Free, Eutectic-Free, Bimodal $\gamma'$	45 Volume Percent Large Barrier $\gamma'$ Precipitates (15 $\mu$ ), Fine Cuboidal $\gamma'$ (0.2 $\mu$ ), Very Coherent $\gamma'$ Arrays, Round Edges on Particles

#### PWA 1482 Thermal Treatment Optimization

Based on the selection of HT 4 and 6 as the optimal thermal processing parameters for further characterization testing in Paragraph 2.6 – *Program Text Matrix*, a series of heat treatments were performed using as-HIP PWA 1482 test material samples to develop similar microstructures in this alloy that resembled the PWA 1484 HT 4 and 6 microstructures. The maximum solution HT processing temperature was lowered to account for the differences in  $\gamma'$  solvus temperature between the two alloys. The established PWA 1482 HT 4 and 6 thermal processing parameters are seen in Table 11. Typical microstructures from test samples heat treated according to the HT cycles defined in Table 11 are shown in Figures 24 and 25.

The PWA 1482 microstructures contain very similar size and volume fractions of the large barrier  $\gamma'$  previously seen in the PWA 1484 alloy. The microstructures also display similar characteristics with respect to the finer  $\gamma'$  precipitates.

Table 11. PWA 1482 Alternate HT Processing Parameters

Heat Treat	Hot Isostatic Pressing	Heat Treatment
4	1285°C (2345°F)/103 MPa 15 ksi/4 hr	Solution at 1307°C (2385°F)/6 hr→Slow Cool*+871°C (1600°F)/32 hr
6	1285°C (2345°F)/103 MPa 15 ksi/4 hr	Solution at 1307°C (2385°F)/6 hr→Slow Cool**+871°C (1600°F)/32 hr

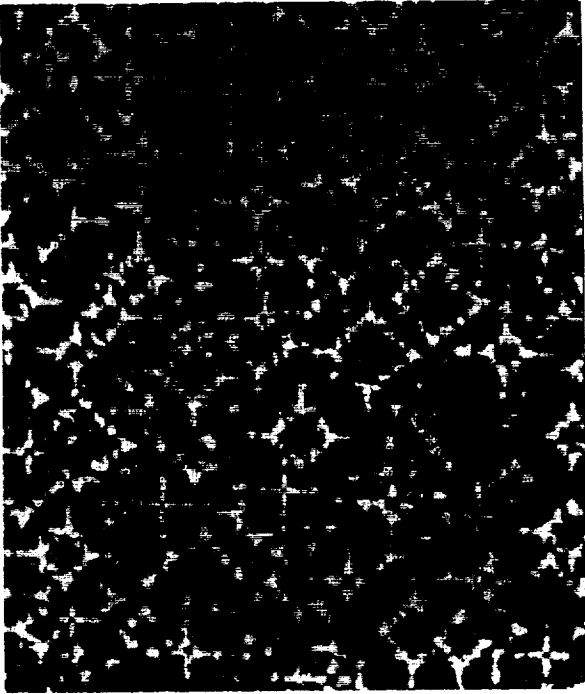
\* – Slow cool from 1307°C (2385°F) at 0.28°C/min to 1232°C (2250°F). Hold for 2 hr→rapid vacuum cool to RT.

\*\* – Slow cool from 1307°C (2385°F) at 0.56°C/min to 1177°C (2150°F)→rapid cool to RT.



Heat Treat 4

200X

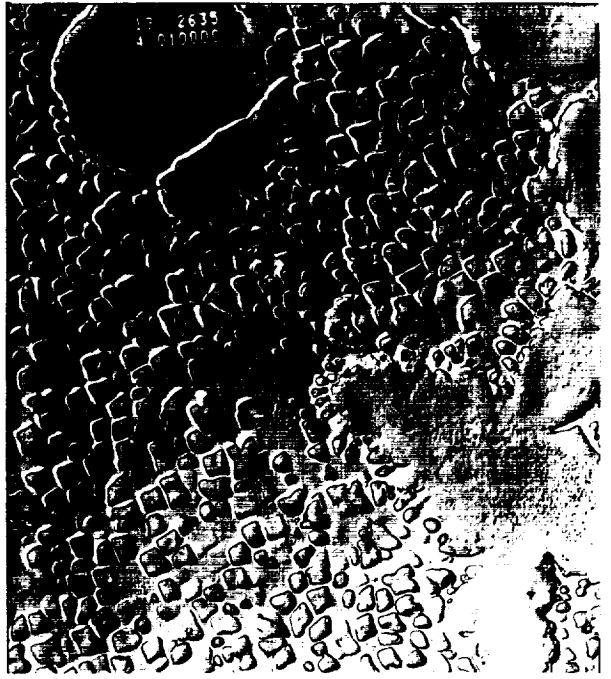


500X



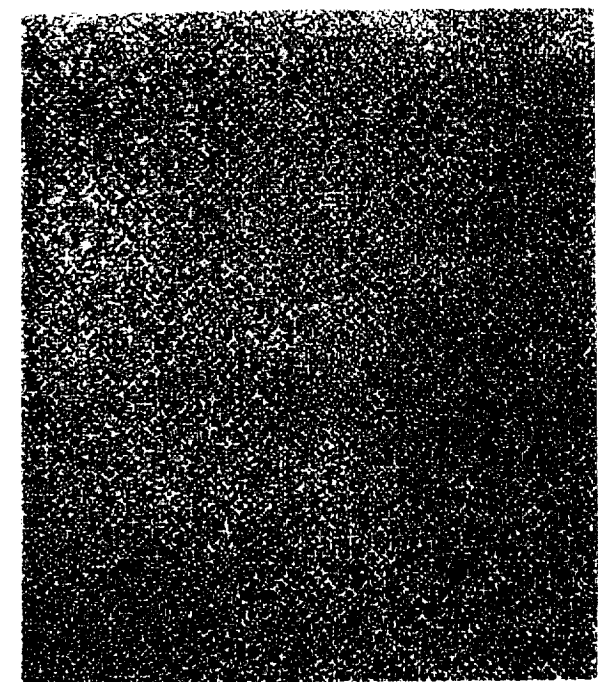
Heat Treat 4

4600X



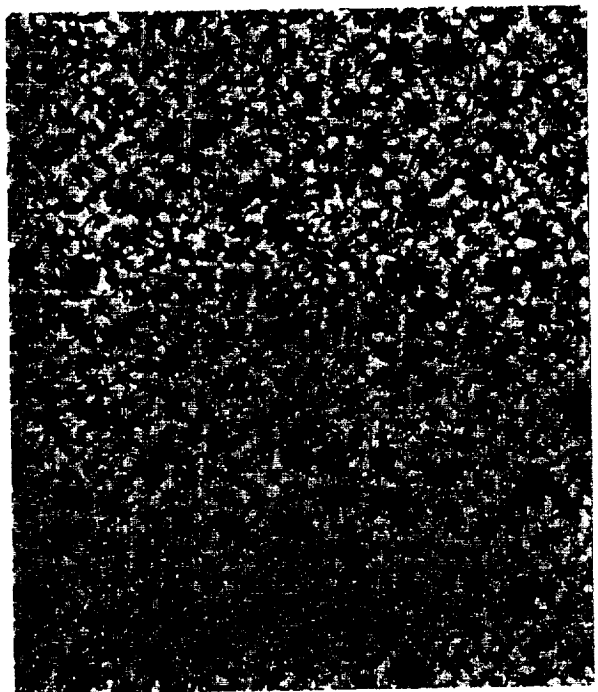
10,000X

Figure 24. PWA 1482 Alternate HT 4

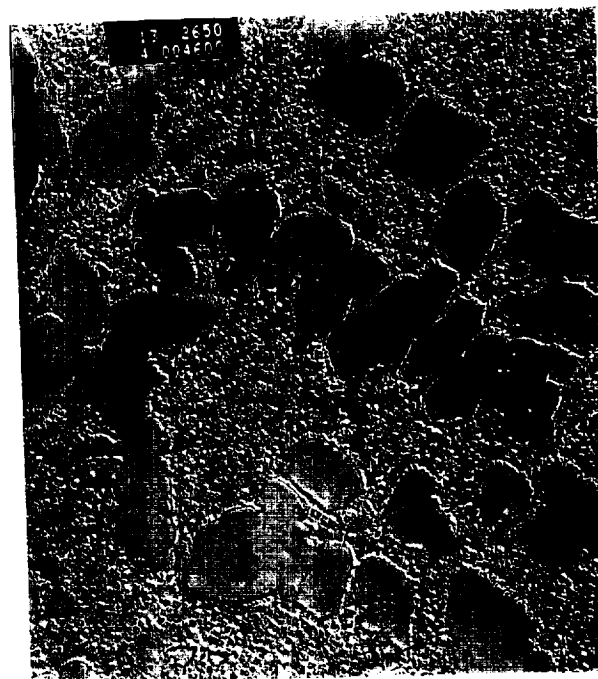


Heat Treat 6

200X

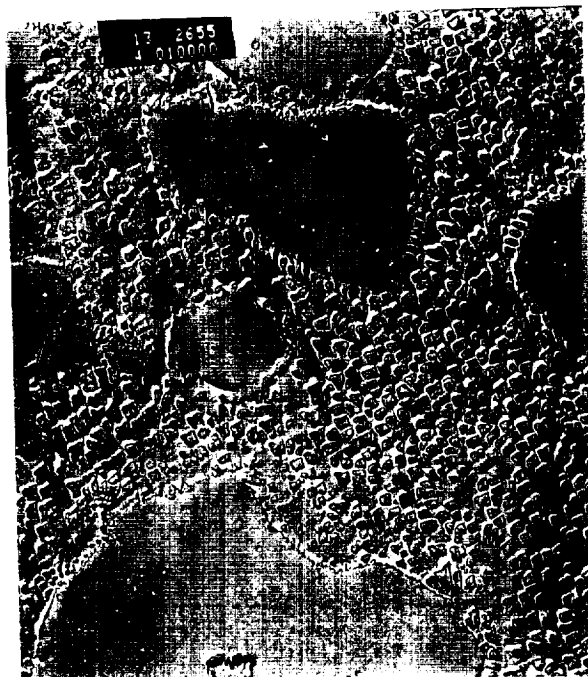


500X



Heat Treat 6

4600X



10,000X

Figure 25. PWA 1482 Alternate HT 6

## 2.5 HYDROGEN TEST – ALTERNATE MICROSTRUCTURE SCREENING

### 2.5.1 Approach

#### 2.5.1.1 Hydrogen Test Facilities

Pratt & Whitney (P&W) has upgraded its advanced environmental test facilities for evaluating materials in extreme environments. These facilities include four environmental test stands that are fully capable of performing all standard materials testing in extreme environments, including high-pressure gaseous hydrogen to pressures of 55 MPa (8 ksi) and at temperatures to 980°C (1796°F). Test capabilities include standard tensile, creep, stress rupture, strain- and load-controlled low-cycle fatigue (LCF) and high-cycle fatigue (HCF), and cyclic crack growth.

Four servohydraulic test machines are located in individual remote blast cells (Figure 26) equipped with high-pressure, high-volume gas supplies. Gaseous hydrogen is supplied directly from liquid boil-off. The pressure vessel and seal designs, which have been in use for this type of testing at P&W for over 20 years, permit rapid test turnaround and efficiency, while maintaining an ultra-pure gas environment and the utmost in safety. The vessels were designed and developed by P&W to permit testing in high-pressure hydrogen environments using, for the most part, ASTM standard specimens and test procedures. Each system is equipped with remotely operated gas sample bottles for sampling gas in the pressure vessel either before or after testing.

Test system electronics are located in a blast protected, pressurized control room, which are equipped for automated, unattended operation. To coordinate control room and test stand activities, each test cell is monitored by a remote closed circuit television and intercom during test setup. The gas control console (Figure 27), located in the control room, enables the operator to control pressurization through remotely operated valves (ROVs).

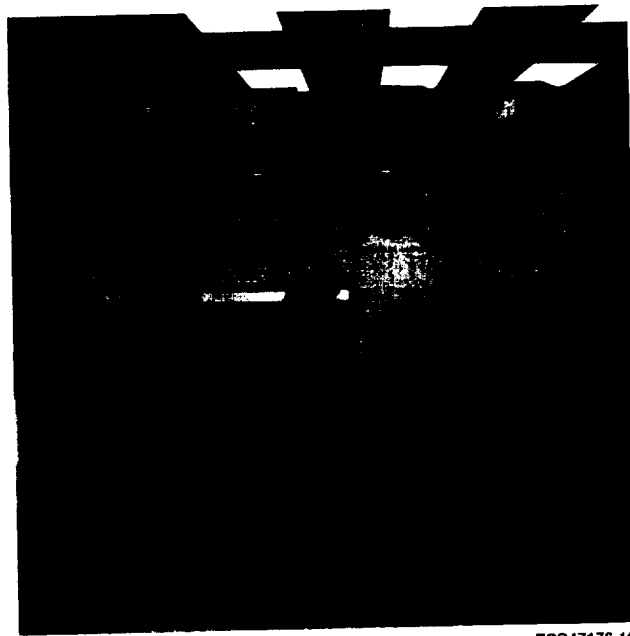
The overall facility provides a comprehensive capability for evaluating material behavior in representative service environments that permits direct comparison with ambient atmospheric data.

Both commercially available and specially developed capabilities and equipment used on this program are detailed in the following paragraphs.



FCD47178-12

*Figure 26. Remote Blast Cells Housing High-Pressure Environment Test Machines*



FCD47176-16

*Figure 27. Gas Control Console and Television Monitors*

#### • *Low- and High-Cycle Fatigue Testing Equipment*

All high-pressure environmental LCF and HCF tests are conducted in a closed-loop type, hydraulically actuated test machine capable of operating in both the strain- and load-controlled modes at pressures of up to 55 MPa (8 ksi). The test machine, shown in Figure 28, is located in an isolated, blast-proof test cell, with all controls and instrumentation located in a protected control room. A pressure transducer provides a feedback signal, proportional to chamber pressure, to the servocontroller to counteract pressure loads through the servosystem. This signal is used to control a mean load applied to the fixturing, so that zero strain in the specimen gage is maintained when the vessel assembly is pressurized. This same load is then superimposed on the cyclic load during testing.

The closed-loop servohydraulic machine is capable of conducting strain- and/or load-controlled fatigue tests. The maximum load capacity is 44.5 kN (10 kip) tension or compression. Tests can be run at frequencies from 0 to 30 Hz. The servohydraulic feature of the equipment can provide triangular and sine loading waveforms, thus making it extremely versatile for testing. The machine can be run to a mission cycle, since any supplied analog signal can be used to provide a loading waveform of virtually any shape or frequency, with the response time of the hydraulic system being the only limiting factor.

An external load cell is used to obtain cyclic load data. The effect of friction at the load rod seals has been determined and accounted for. Electrical connections to the extensometer system (for strain control tests), furnace (for elevated temperature tests), and thermocouples are made through the pressure vessel by high-pressure bulk-head connectors. Strain measurements are made using averaging-type linear variable differential transformer (LVDT) extensometers. A closeup view of a typical specimen and extensometer is shown in Figure 29.

For elevated temperature testing, a two-zone resistance furnace with separate control systems for each zone is used to achieve a maximum temperature of 980°C. The furnace surrounds the specimen and fits within the frame of



FCD47177-3

*Figure 28. High-Pressure Environmental LCF/HCF Test Machine; Pressure Vessel Open*



FED266920

*Figure 29. View of Typical LCF Specimen Installed in Extensometer*

the pressure vessel. Thermocouples, looped around the specimen gage section, are used to monitor and control temperature during testing. Thermal exposures in high-pressure hydrogen at zero load are possible for internal hydrogen embrittlement (IHE) tests.

Test control is performed with Interlaken's computer-operated Universal Test Program (UTP) and a specially configured Interlaken 3100 controller that is capable of meeting the special needs of high-pressure environmental testing at elevated temperatures. The UTP provides data acquisition for strain (sensed by the extensometer system) and load (sensed by the external load cell); thereby providing hysteresis loop data, as desired, during the cyclic life of the tests. Hysteresis loops are also recorded on an X-Y plotter; and test pressure, specimen temperature, load, and strain signals are recorded on a strip chart recorder.

#### • ***Crack Growth Test Equipment***

High-pressure environmental crack growth tests are conducted on equipment, almost identical to the LCF/HCF test system, which consists of a closed-loop, hydraulically actuated test machine with a pressure vessel. The test machine is located in an isolated, blast proof test cell with all controls and instrumentation located in a protected control room. Elevated temperature tests are performed using the same furnace system described for the LCF/HCF test machine. The test machine compensates for internal gas pressure loading of the test specimen through a pressure transducer feedback signal to the servosystem. The signal is used to control a steady force to the fixturing that is equal and opposite to the internal hydrogen pressure load against the load rod.

Specimen crack mouth opening displacement (CMOD) is measured and recorded throughout the test duration, using a capacitance probe attached to the front of the specimen. The CMOD is monitored on the X-axis of an X-Y recorder, while load is recorded on the Y-axis of the recorder. Load is sensed by the external load cell or internal load cell for low load testing, to eliminate the effects of friction. Test pressure, specimen temperature, load, and CMOD signals are also recorded on a stripchart recorder. The CMOD instrumentation and internal load cell were added during this program and represent a significant upgrade in high-pressure hydrogen crack growth testing capability. Combined with the temperatures and pressures discussed earlier, the upgrades have produced one of the most advanced hydrogen fatigue crack growth systems available.

All tests are computer controlled, with continuous computer monitoring and data acquisition (Figure 30). Test signals, which include test cycle count, load, and CMOD, pass through an analog-to-digital interface. Recorded data is analyzed in real time to determine crack length, stress intensity, and crack growth rate. The computer also monitors the test to provide for test shutdown and visual inspection of the specimen at either a desired crack length or a desired cycle count.

#### • ***Tensile and Creep Testing Equipment***

All high-pressure environmental tensile and creep tests are conducted in a closed-loop, hydraulically actuated test machine with an 89 kN (20 kip) maximum load capacity. The test machine is located in an isolated, blast-proof test cell with all controls and instrumentation located in a protected control room. A pressure vessel that is similar to the one used for fatigue testing is made of AISI 304 stainless steel and incorporates a high-pressure GrayLoc connector. The vessel is mounted on the upper platen of the test machine. A compensating device built into the base of the vessel eliminates the effect of loads, resulting from differential pressure, on the load fixturing.

An averaging-type LVDT extensometer system is used to measure specimen strain for both room temperature and elevated temperature tests. Specimen load is determined by both external and internal load cells; therefore, absolute specimen load is known, and friction at the pressure vessel seals is of no consequence. Electrical connections to the internal load cell, extensometer, thermocouples, and furnace are made through the pressure vessel by high-pressure bulkhead connectors.

To conduct elevated temperature tests, at up to 980°C (1796°F) at 55 MPa (8 ksi) hydrogen, a two-zone furnace with separate control systems for each zone is used, minimizing any heat gradient due to high thermal conductivity of the gases. Thermocouples, looped around the specimen gage section, are used to control and monitor specimen



Figure 30. Automated Crack Growth Rate Control and Data Acquisition System

temperature during each test. Temperature variation over the gage length of smooth specimens is minimal, less than approximately  $\pm 3^{\circ}\text{C}$  ( $\pm 5^{\circ}\text{F}$ ).

For all tensile tests, load and strain are recorded using computer data acquisition and an X-Y recorder. For creep and tensile tests, test pressure, specimen temperature, load, and strain signals are also recorded on a strip chart recorder.

#### 2.5.1.2 Test Methods

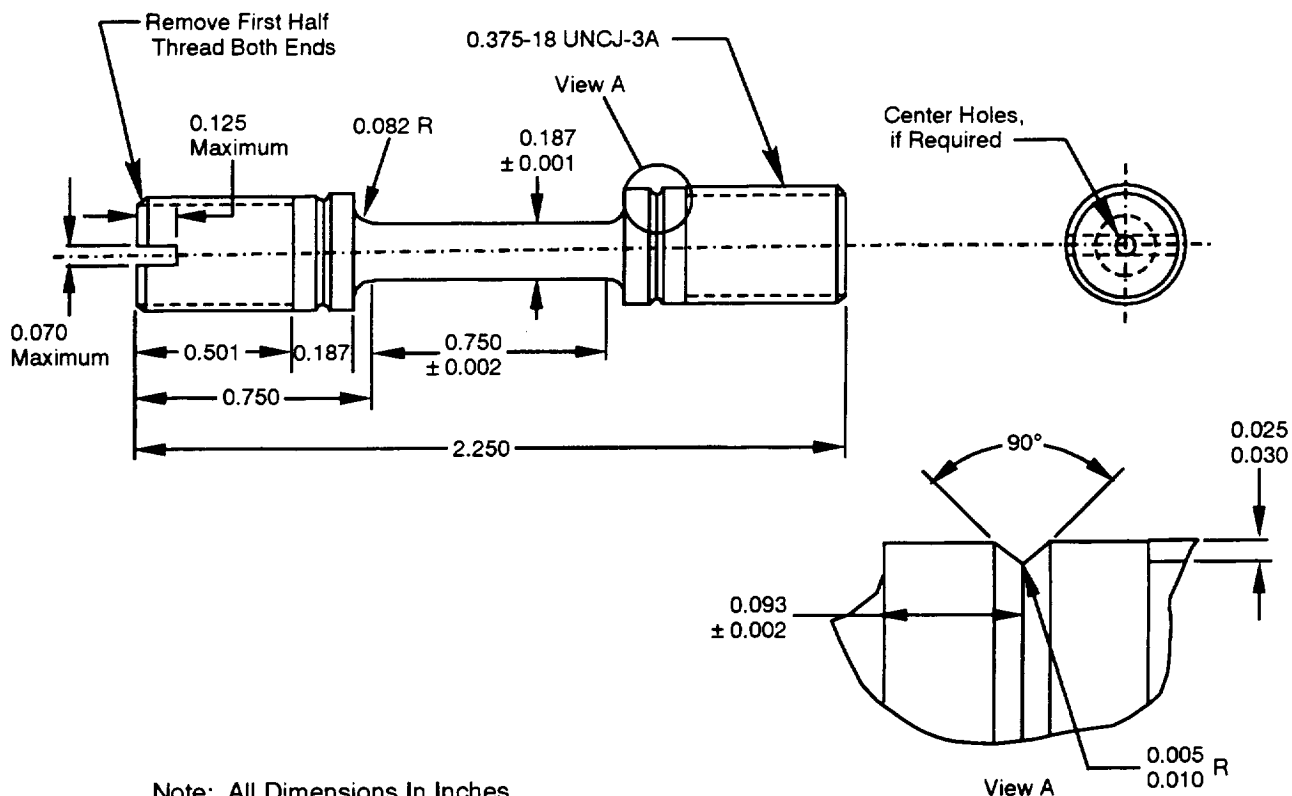
##### • Tensile Testing

Tensile tests are conducted in accordance with ASTM E8-95a – *Tension Testing of Metallic Materials* and ASTM E-21 – *Tension Testing of Metallic Materials at Elevated Temperatures*, using the smooth specimens shown in Figure 31. Air tests are performed on commercially available test equipment, and the hydrogen tests are performed on the test system described previously in Paragraph 2.5.1.1 – *Hydrogen Test Facilities*.

Established test procedures are in place covering the various aspects of materials characterization, which include raw material documentation (composition, heat-treat, processing, crystallographic orientation, etc.), machining, inspection, specimen handling, testing, post-test examination, and data analysis. These procedures, which have been developed over the past 20 years of testing in high-pressure hydrogen and elevated-temperature air environments, are briefly highlighted in the following paragraphs.

After crystallographic inspection, round bar castings are machined to blueprint by outside vendors (e.g., Met-cut Research Associates) or at P&W. Once the specimens are received from the manufacturer, they are logged into P&W's records for continued documentation and traceability. Specimens are then visually inspected at 10-30X magnification and measured to verify that they conform to blueprint. Following inspection the specimens are





72886.cdr

Figure 31. Tensile Stress-Strain Specimen

cleaned to remove grease and other foreign matter. Specimens are handled with white gloves from this point through installation in the test machine.

To perform a specific tensile test, a cleaned and measured specimen is placed in the test machine. Multiple thermocouples are attached around the test specimen gage section for temperature monitoring and control. Temperature gradients along the gage length are maintained at  $\pm 3^{\circ}\text{C}$  ( $\pm 5^{\circ}\text{F}$ ) or less. An averaging-type LVDT extensometer, or a commercially available extensometer for air tests, is attached to the specimen for specimen axial strain measurement and control.

For the high-pressure hydrogen environment tests, the pressure vessel is closed and purged. Following the purge cycle, the vessel is pressurized with hydrogen to 34.5 MPa (5 ksi). After the specimen has been installed for elevated temperature tests, the furnace is turned on and the temperature allowed to stabilize. When the temperature has stabilized for approximately 30 minutes, the test is started. Smooth specimens are tested at a strain rate of 0.005/min to yield, and the equivalent crosshead speed is maintained throughout the test.

Tensile data reported include ultimate strength, yield strength, modulus of elasticity, stress-strain parameters, percent elongation, and reduction in area, with data plots where applicable. The following comparisons are made where data permits:

- Air-to-hydrogen data to determine the effects of hydrogen
- Alloy-to-alloy
- Temperature effects.

These comparisons help direct material selection and processing for future turbopump applications.

### • Creep-Rupture Testing

Creep-rupture tests are conducted in accordance with ASTM E139 – *Conducting Creep, Creep-Rupture, and Stress Rupture Tests of Metallic Materials*. Air tests are performed on commercially available test equipment, and hydrogen tests are performed on the test system previously described in Paragraph 2.5.1.1 – *Hydrogen Test Facilities*.

Creep-rupture test specimens are manufactured per requirements shown in Figure 32. Specimen handling and test setup procedures are similar to those described for tensile testing. After the testing and data analysis, creep versus time and stress level versus rupture life are reported. Comparisons similar to those described under tensile testing are made where data permits.

### • Low-Cycle Fatigue Testing

Uniaxial LCF testing is performed generally in conformance to ASTM E606-92 – *Standard Recommended Practice for Constant Amplitude Low-Cycle Fatigue Testing*. Tests are performed at a cyclic test frequency between 0.167 and 0.33 Hz. Air tests are performed on commercially available test equipment, and the hydrogen tests are performed on the test system described previously in Paragraph 2.5.1.1 – *Hydrogen Test Facilities*. For rocket applications, high stress and strain levels are chosen, whenever possible, to produce lives that fall between the range of 50 to 1000 cycles.

Double notch LCF specimens (Figure 33) are used for load-controlled LCF tests in both air and hydrogen. The notches in the specimen are representative of notches and holes that are found in engine hardware. Smooth, cylindrical specimens (Figure 34) are used for the strain-controlled LCF tests to be conducted in air, while collared specimens (Figure 35) are used for the strain-controlled LCF tests in the high-pressure hydrogen environment. The

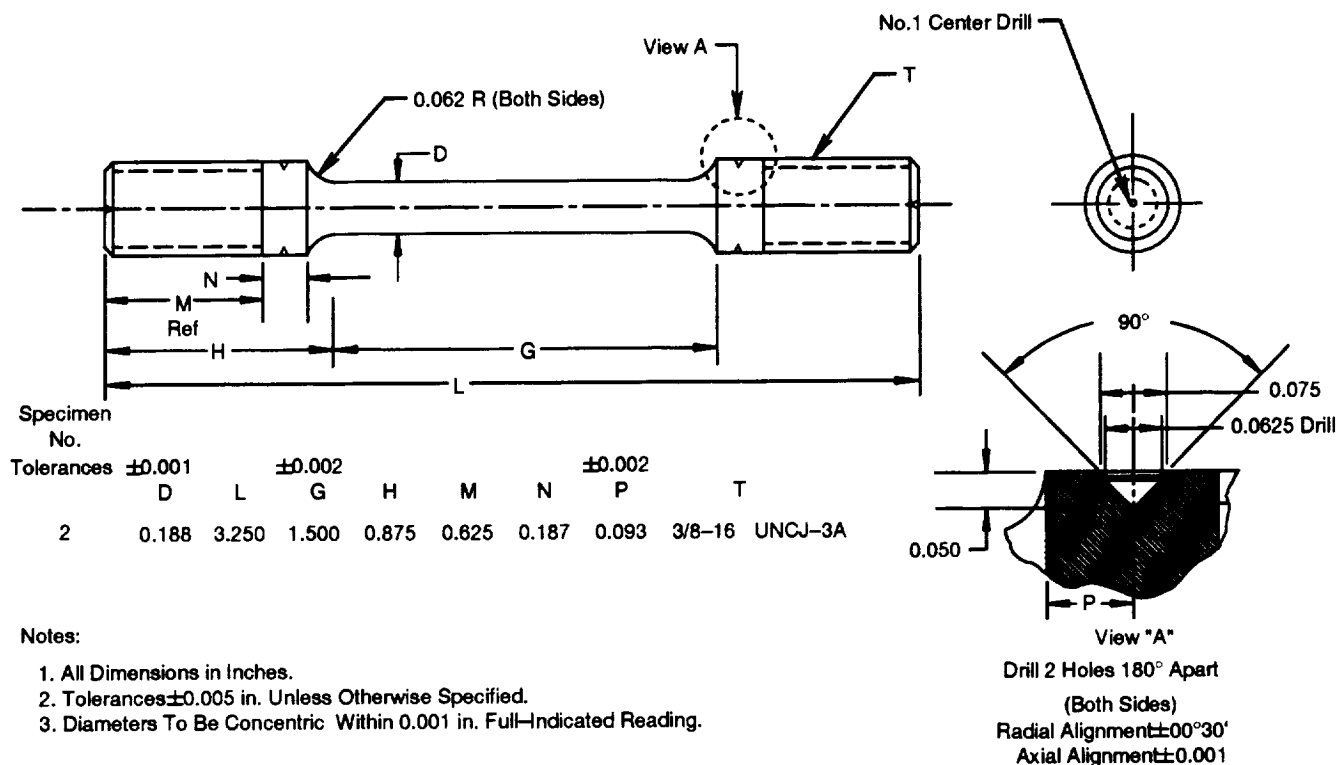


Figure 32. Creep Rupture Specimen

high-pressure environment specimen incorporates integral machined extensometer collars to provide increased strain measurement stability that is necessary for material testing in the 34.5 MPa (5 ksi) environments. Although the integral specimen extensometer collars are not specifically recommended by ASTM E606-80, this modification is necessary for the extreme-environment testing required in this program. A calibration procedure has been established to relate the maximum strain-to-collar deflection during both the elastic and plastic portions of the strain cycle. All other specifications of ASTM E606 are adhered to.

Specimen handling and test setup procedures are similar to those described for tensile testing. Double notch LCF specimens are run with an all tensile stress cycle (stress ratio = 0.05), and strain-controlled LCF tests are typically run with a fully-reversed strain cycle (mean strain = 0). A typical strain-controlled test cycle is shown in Figure 36. Stress/strain hysteresis loops are monitored and recorded periodically throughout the duration of the test. The test machines are automated and are programmed to shut down the test and turn off the furnace when the specimen fails.

In a high-pressure environment materials test, after the specimen has failed, the actuator can be cycled to determine the effects of friction. The frictional loading is then taken into account during the data analysis. After the specimen fails, it is removed from the test machine and inspected optically (and metallurgically for some of the tests) to determine the origin and mechanisms of failure.

After analysis, data reported include total strain range, inelastic strain range, total stress range, mean stress, cycles-to-failure, and appropriate plots of cycles-to-failure versus strain range for strain-controlled tests.

For load-controlled testing of double notch specimens the data report includes maximum stress and cycles to failure. Plots of LCF data obtained from tests run in both air and hydrogen show the embrittling effects of hydrogen on-the material. Comparisons similar to those described under tensile testing are made where data permits.

A least squares statistical regression of the data is performed using a typical fatigue life model such as:

$$\text{Log } N = A + B/X,$$

where:

N = cycles to failure

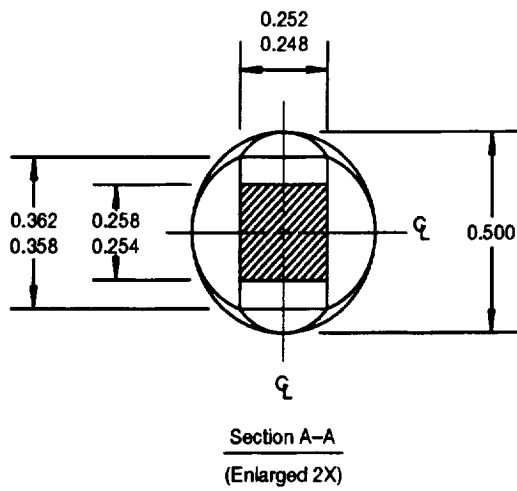
X = total strain range or maximum stress

A and B are regression constants.

- **High-Cycle Fatigue Testing**

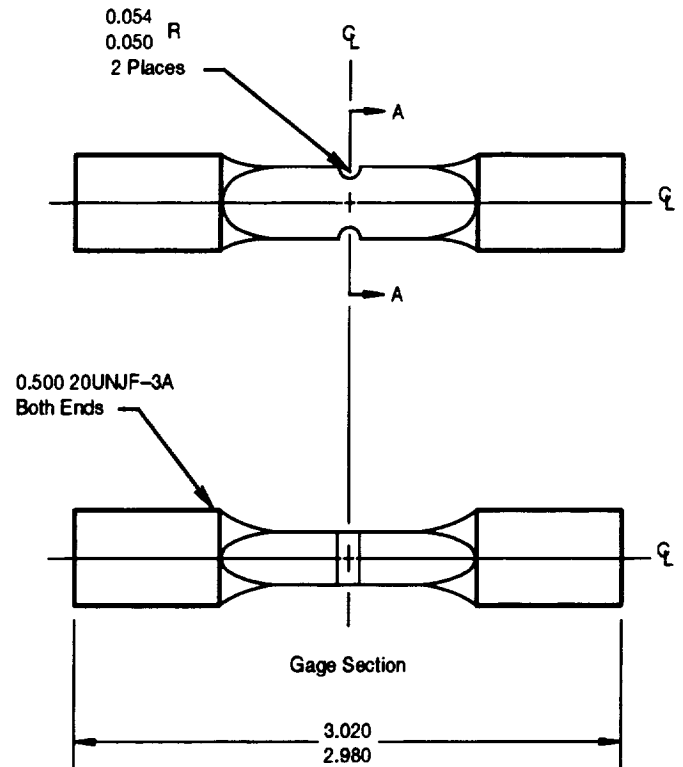
Uniaxial HCF testing is performed in conformance to ASTM E466-82 – *Standard Practice for Conducting Constant Amplitude Axial Fatigue Tests of Metallic Materials*. Air tests are performed on commercially available test equipment, and the hydrogen tests are performed on the test system described previously in Paragraph 2.5.1.1 – *Hydrogen Test Facilities*. The cyclic test frequency ranges from 20 to 30 Hz, and stress ranges are chosen to span a cyclic life range from  $10^3$  to  $10^7$  cycles. Smooth HCF specimens (Figure 37) are used for the HCF tests to be conducted in both air and high-pressure hydrogen environments. Specimen handling and test setup procedures are similar to those described for tensile testing.

Testing is performed under load control and is commonly run with a fully-reversed stress cycle ( $R = -1$  with mean stress = 0), and alternate stress ratios (e.g.,  $R = 0.05$  for an all-tensile cycle) can also be run. The test machines are automated and are programmed to shut down the test and turn off the furnace when the specimen fails. In a high-pressure environment materials test, after the specimen has failed, the actuator can be cycled to determine the effects of friction. The frictional loading is then taken into account during the data analysis. After the specimen fails it is removed from the test machine and inspected optically (and metallurgically, for some of the tests) to determine the origin and mechanisms of failure.



Notes:

1.  $K_t = 2.18$ .
2. Double Notch LCF Specimen.
3. All dimensions Are in Inches.



72894

Figure 33. Double Notch LCF Specimen

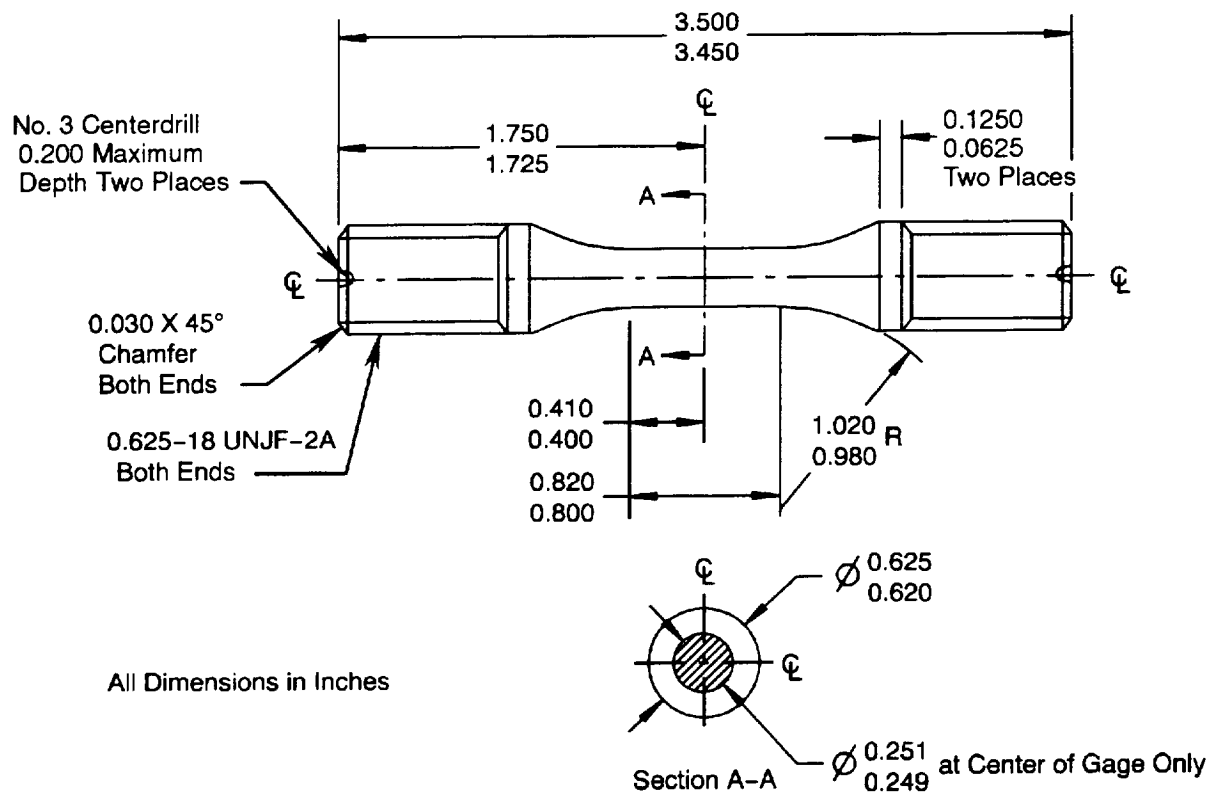
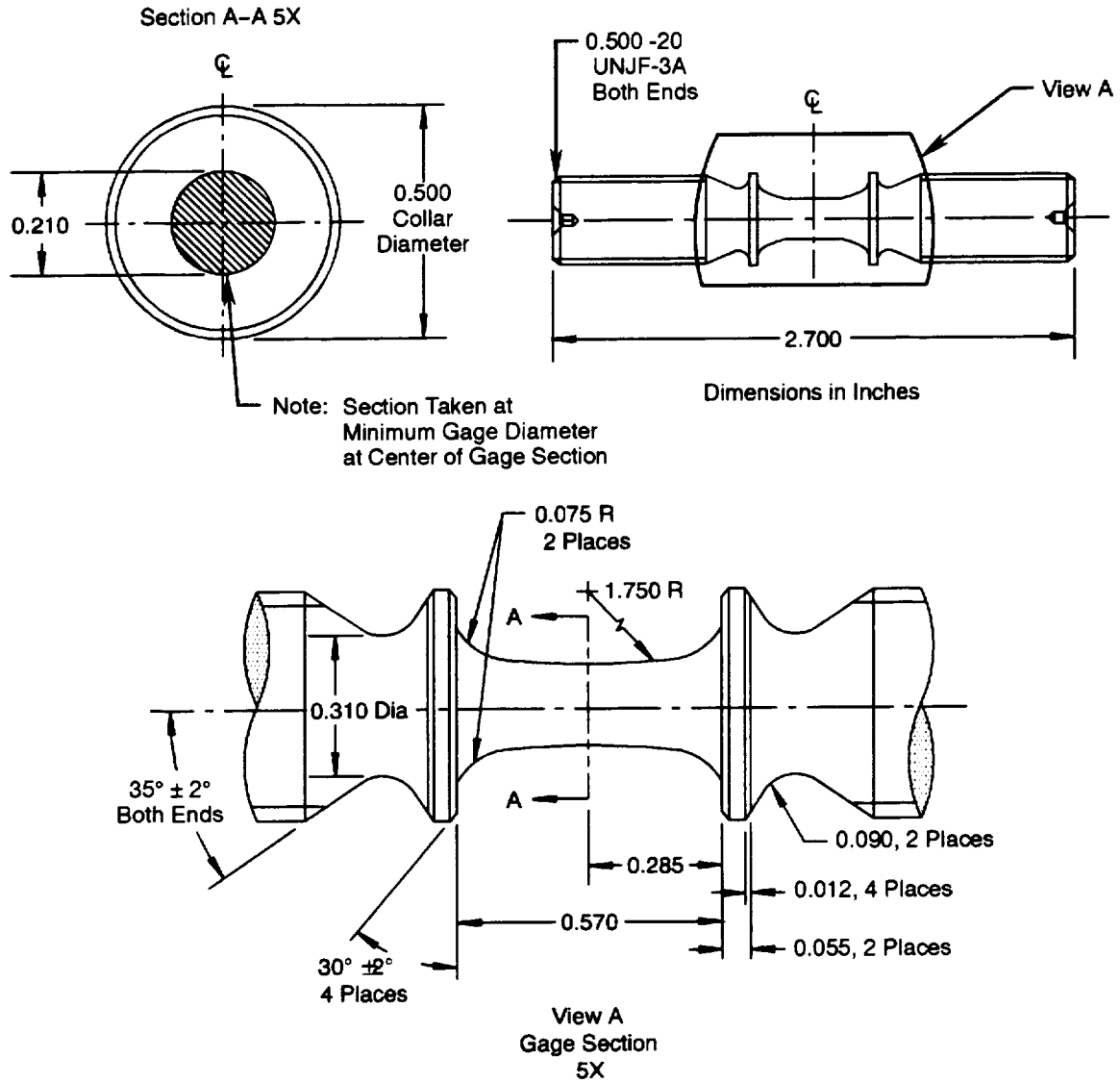
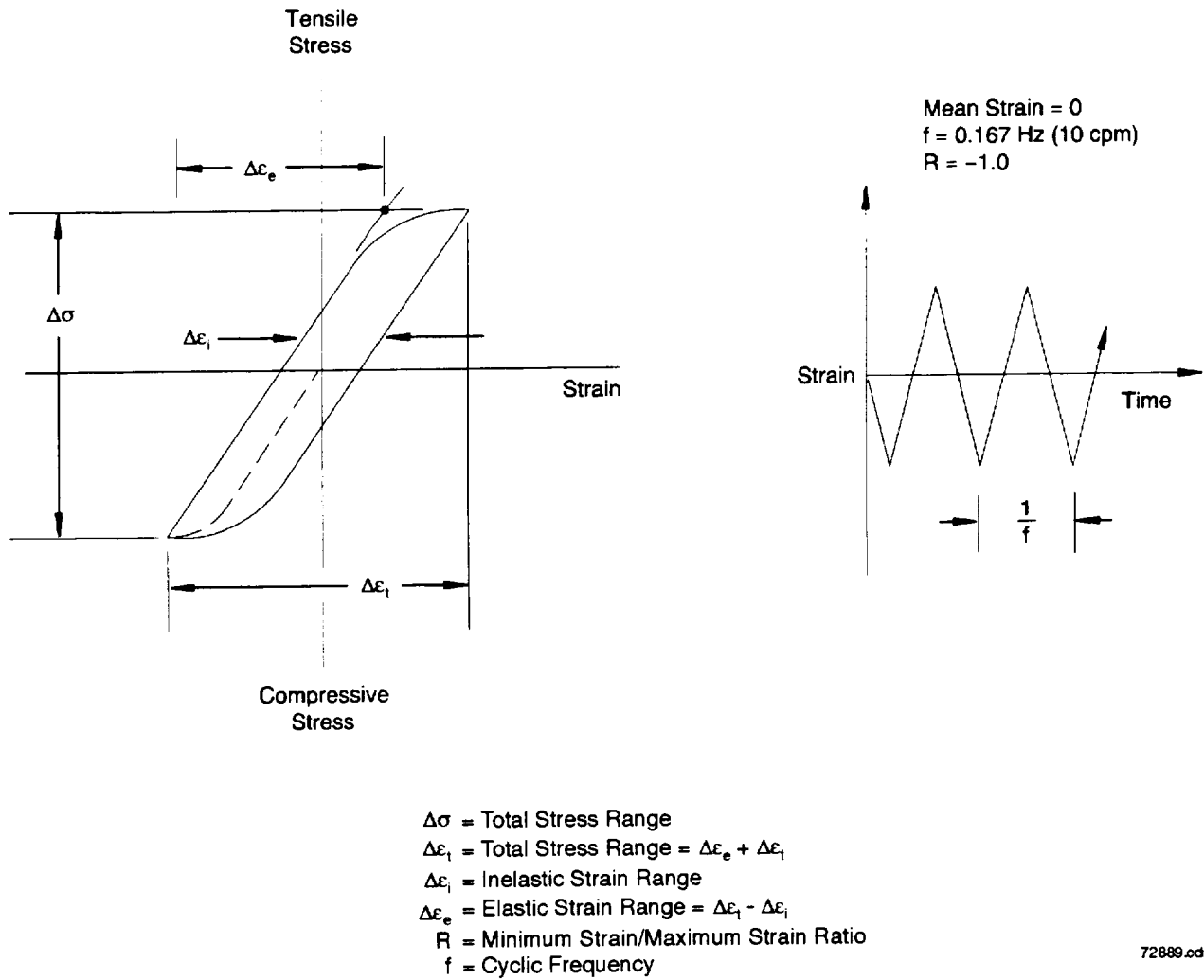


Figure 34. Low-Cycle Fatigue Specimen for Air Testing



72888.cdr

Figure 35. High-Pressure Environment LCF Specimen



72889.cdr

Figure 36. Typical LCF Test With Mean Strain of Zero

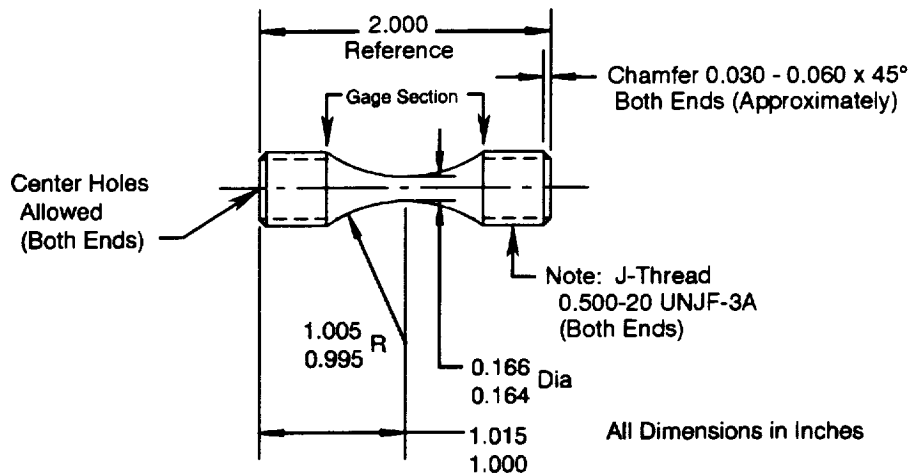


Figure 37. High-Cycle Fatigue Specimen (Smooth  $K_t = 1.0$ )

Maximum likelihood techniques are used in the statistical analyses of the test results. High-cycle fatigue data often include run-outs – specimens that do not fail, even after millions of loading cycles. Treating these observations as specimen failures can result in underestimation of the material's true HCF capability at low stresses and overestimation at high stresses. To ignore run-outs is to discard valuable information, obtained at great cost, since the specimens were under test for so long.

Maximum likelihood estimation is a statistically rigorous method for analyzing fatigue data with suspended observations (run-outs). The method gives identical estimates for fatigue model parameters as least-squares procedures when there are no run-outs; in addition, it provides parameter estimates that are statistically correct and physically reasonable when run-outs make least-squares unusable. The procedure, based on the method of maximum likelihood, does not depend on replacing run-outs with pseudo failures and can be used with any appropriate fatigue model.

After analysis, the data reported include alternating stress, cycles-to-failure, and appropriate plots of cycles to failure versus alternating stress. Plots of HCF data that were obtained from tests run in both air and hydrogen show the embrittling effects of hydrogen on the material. Comparisons similar to those described under tensile testing are made where data permits.

#### • Crack Growth Rate Testing

Crack growth rate testing in air and 34.5 MPa (5 ksi) hydrogen is performed in conformance to ASTM E647-95 – *Standard Test Method for Measurement of Fatigue Crack Growth Rates*. Air tests are performed on commercially available test equipment, and the hydrogen tests are performed on the test system described previously in Paragraph 2.5.1.1 – *Hydrogen Test Facilities*.

The specimen configuration used for crack growth testing is the compact-type (CT) specimen shown in Figure 38. This specimen incorporates a chevron-type crack-starter notch and integrally machined knife edges for crack opening displacement (COD) extensometry attachment as recommended by ASTM E399-90 – *Plane-Strain Fracture Toughness of Metallic Materials*. Specimen thickness is 9.5 mm (0.37 in.). The notch is oriented to obtain crack growth properties across the grain or solidification direction (i.e., loading direction in [001] direction, with crack path in the [010] direction)

Specimen handling and test setup procedures are similar to those described for tensile testing. To perform a specific crack growth test, a cleaned and measured specimen is typically precracked initially in air at room temperature (427°C [800°F] for some single-crystal alloys, including PWA 1484, to prevent octahedral crack growth) at a cyclic frequency between 20 and 50 Hz. Final precracking is performed at the test temperature and environment.



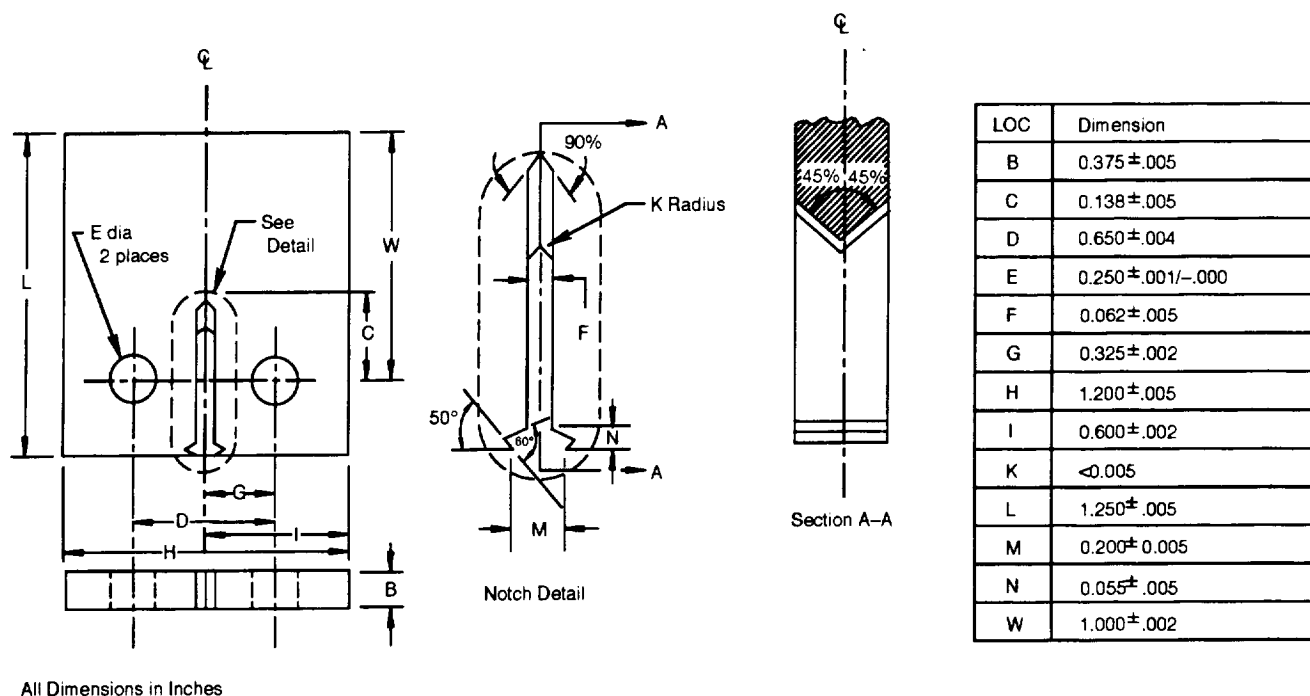


Figure 38. Crack Growth Rate Specimen

72AR3

Following precracking, the specimen is placed in the crack growth rate test machine. Multiple thermocouples are attached to the specimen for temperature monitoring and control. Temperature gradients on the specimen are maintained at  $\pm 3^{\circ}\text{C}$  ( $\pm 5^{\circ}\text{F}$ ) or less. The test consists of cyclically loading the specimen between the minimum and maximum load until complete fracture or a maximum crack length is attained. The loading cycle is all tensile, and specimens are typically tested at a stress ratio  $R = 0.1$ .

A capacitance probe is attached to the specimen for specimen crack mouth opening displacement (CMOD) measurement during high-pressure hydrogen tests. The CMOD signal from the extensometer is correlated directly to average crack length, while the test is in progress, through appropriate signal conditioning and computer software. Air tests can be performed using either a compliance method similar to that described for hydrogen testing or electric potential drop (EPD).

All tests are computer controlled using a Fracture Technologies Associates (FTA) crack growth system, which includes a computer, analog-to-digital interface, and software. This system is capable of test control, data acquisition, and data analysis. The recorded data are analyzed in real time to determine crack length, stress intensity, and crack growth rate. The computer also monitors the test to provide for shutdown for visual inspection of the specimen at either a desired crack length or a desired cycle count. Visual inspections are made periodically for calibration to relate the CMOD or EPD measurement to the test specimen crack length.

Just before the specimen fails, the test is stopped and the specimen tensiled. After the specimen has been tensiled, it is removed from the test machine and inspected optically to determine the final crack length using a 5-point averaging technique.

Data to be reported include crack growth rates, cycles, stress intensity range ( $\Delta K$ ), and other pertinent data required to develop plots of stress intensity range versus crack growth rate,  $da/dN$ . Plots of crack growth rate data obtained from tests run in both air and hydrogen show the embrittling effects of hydrogen on the material. Comparisons similar to those described under tensile testing are made where data permits.

### 2.5.1.3 Test Plan

Pratt & Whitney selected a total of seven alternate heat treat (HT) cycles to screen based on the metallography results that were discussed in Paragraph 2.4 – *Thermal Treatment Optimization*. Sufficient PWA 1484 was heat treated to allow for machining of three smooth tensile specimens (Figure 31), three double notch LCF specimens (Figure 33), and one compact tension specimen (Figure 38) for each of the seven HTs. The specimens were machined at Metcut Research Associates with the loading direction aligned along the [001] crystallographic direction. Specimens were tested in 34.5 MPa (5 ksi) hydrogen at 20°C (68°F) according to the matrix shown in Table 12.

### 2.5.2 Results

The tensile results of testing in 34.5 MPa (5 ksi) hydrogen at 20°C (68°F) from the alternate microstructure screening tests are shown in Table 13 and in Figures 39 and 40. Yield strengths provided for HTs 1 and 2 are based on the peak of the stress-strain curve, which is the maximum stress achieved on loading before the stress dropped and the specimen started deforming plastically. Reduction in area data is not provided for specimens that had radius failures. The tensile data showed that HTs 1 and 2 produced good strength with medium ductility. Heat treat 3 produced average strength, but had poor ductility. Heat treats 4 and 5 produced average strength with good ductility, and HTs 6 and 7 yielded lower strengths and average ductility.

Fatigue results are shown in Table 14 and Figure 41. The data showed that HTs 3, 4, and 5 offered the best fatigue properties in 34.5 MPa (5 ksi) hydrogen at 20°C (68°F), and the remaining HTs had good fatigue properties even though they were slightly lower. All the HTs produced lives in excess of 30,000 cycles. This is a substantial improvement over standard PWA 1484, as shown in Figure 42, which compares HT 4 to typical PWA 1484 and HIP, eutectic free PWA 1484. These fatigue lives represent more than an order-of-magnitude improvement in LCF capability, as compared to PWA 1480,<sup>9</sup> and three orders of magnitude improvement, as compared to directionally-solidified (DS) columnar-grained MAR-M-246+Hf.

Table 12. Alternate Microstructure Screening Test Matrix Performed on PWA 1484 in 34.5 MPa Hydrogen at 20°C (68°F) Number of Tests

Heat Treat Trial Number	Number of Tests		
	Tensile	Double Notch LCF	Crack Growth
1	2	2	1
2	2	2	1
3	2	3	1
4	3	3	1
5	3	3	–
6	3	2	1
7	3	2	1

<sup>9</sup> Because the program alloys are potential candidates for SSME advanced turbopump applications, comparisons have been made throughout this report to other turbopump blade/vane alloys. To provide this relevant basis for comparison, data obtained in the NASA/P&W SSME ATD Material Characterization Program from PWA 1489, PWA 1480, and DS MAR-M-246-Hf testing have been shown.

Table 13. Summary of Tensile Data for PWA 1484 Alternate Microstructure Screening Studies With Testing in 34.5 MPa (5 ksi) Hydrogen at 20°C (68°F)

Heat Treat Trial Number	Specimen Sample Number	<u>Yield Strength</u>		<u>Tensile Strength</u>		Elongation (%)	Reduction in Area (%)
		(MPa)	(ksi)	(MPa)	(ksi)		
1	704-1	895.0	129.8*	895.0	129.8	2.6	9.4
1	705-1	942.5	136.7*	942.5	136.7	2.0	10.9
2	802-1	962.5	139.6*	962.5	139.6	2.0	11.4
2	804-1	982.5	142.5*	982.5	142.5	1.7	10.4
3	701-1	889.5	129.0	895.0	129.8	1.6	8.9
3	702-1	927.4	134.5	942.5	136.7	1.2	3.2
4	712-1	848.1	123.0	953.6	138.3	4.0	**
4	810-1	832.9	120.8	859.8	124.7	3.0	10.8
4	811-1	815.7	118.3	895.7	129.9	4.4	9.9
5	710-1	843.3	122.3	912.9	132.4	3.6	11.9
5	711-1	837.1	121.4	932.9	135.3	3.5	**
5	809-1	846.7	122.8	909.5	131.9	4.4	**
6	709-1	775.0	112.4	834.3	121.0	2.7	6.6
6	807-1	776.4	112.6	915.0	132.7	2.9	**
6	808-1	761.7	110.4	860.5	124.8	2.9	**
7	706-1	768.1	111.4	863.9	125.3	4.2	**
7	707-1	764.7	110.9	812.2	117.8	3.8	9.4
7	806-1	780.5	113.2	874.3	126.8	2.5	7.1

Notes:

\* Peak of Curve.

\*\* Failed in radius.

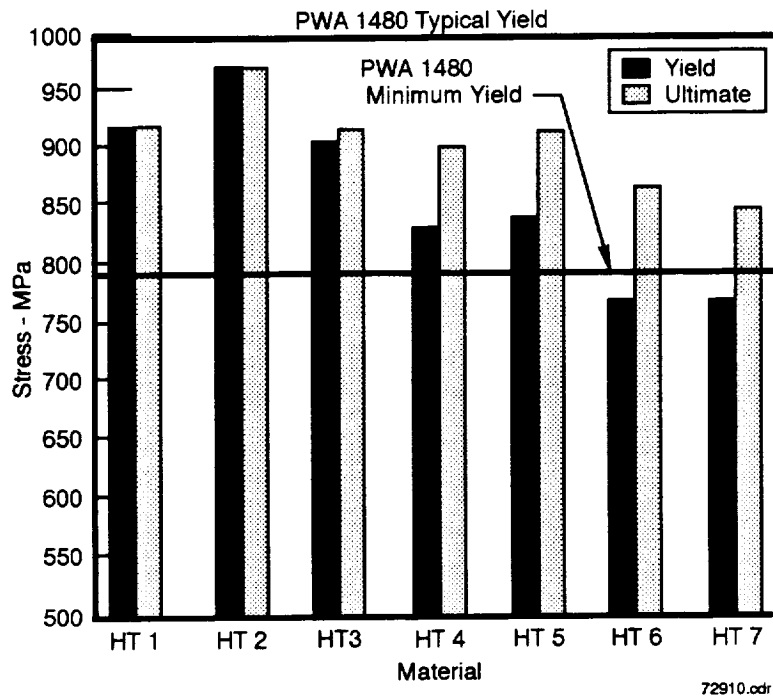


*Figure 39. Tensile Yield and Ultimate Data for PWA 1484 HT Trials, Tested at 20°C (68°F) in 34.5 MPa (5 ksi) Hydrogen With Comparison to PWA 1480 Yield Data for Same Condition*

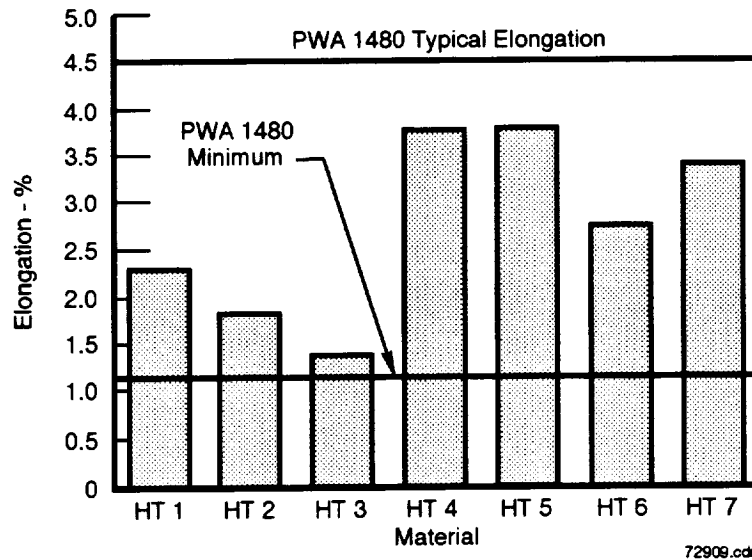


*Figure 40. Tensile Ductility Data for PWA 1484 HT Trials Tested at 20°C (68°F) in 34.5 MPa (5 ksi) Hydrogen With Comparison to PWA 1480 Ductility Data for Same Condition*

**Table 14. Load Controlled LCF Alternate Microstructure Screening Results for [001] Oriented PWA 1484 Double Notch Specimens Tested in 34.5 MPa (5 ksi) Hydrogen at 0.167 Hz, 20°C (68°F),  $R = 0.05$ ,  $K_t = 2.18$**

Specimen Sample Number)	Heat Treat Number	<u>Maximum Stress</u>		Cycles to Failure	Comments
		(MPa)	(ksi)		
704-2	1	620.55	90.0	37,148	
803-2	1	620.55	90.0	42,605	
802-2	2	620.55	90.0	30,066	Thread Failure
703-2	2	620.55	90.0	33,253	
701-2	3	620.55	90.0	36,170	
702-2	3	620.55	90.0	52,275	
801-2	3	620.55	90.0	59,409	Thread Failure
712-2	4	620.55	90.0	55,556	
811-2	4	620.55	90.0	71,102	Thread Failure
810-2	4	620.55	90.0	85,645	
711-2	5	620.55	90.0	50,112	
809-2	5	620.55	90.0	52,563	
710-2	5	620.55	90.0	53,126	
807-2	6	620.55	90.0	27,406	
709-2	6	620.55	90.0	33,230	
707-2	7	620.55	90.0	32,512	
706-2	7	620.55	90.0	53,081	

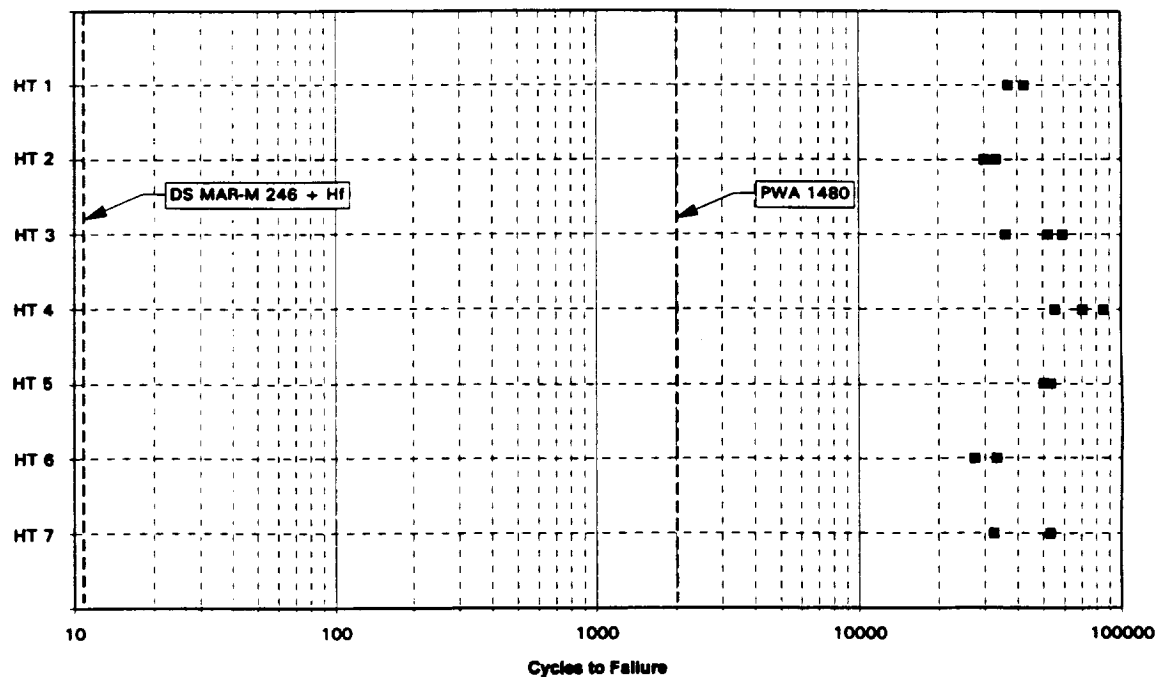
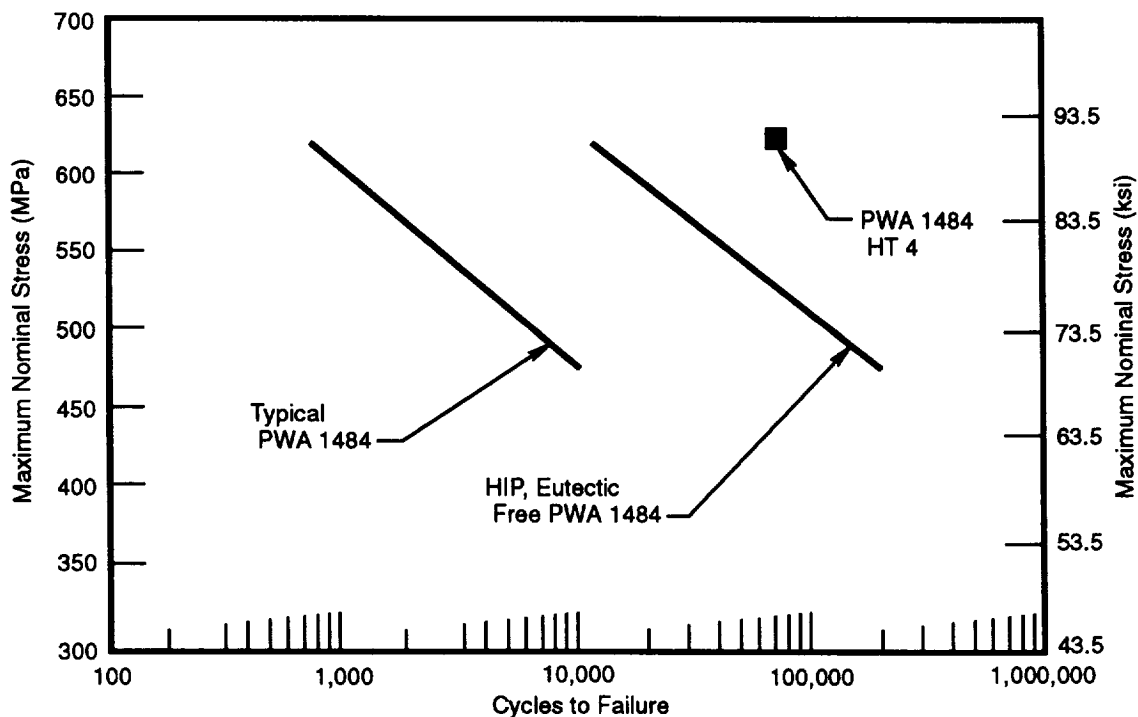


Figure 41. Load Controlled LCF Screening Results for [001] Oriented PWA 1484 Double Notch specimens Tested in 34.5 MPa (5 ksi) Hydrogen at 0.167 Hz, 20°C (68°F),  $R = 0.05$ , 620.55 MPa (90 ksi),  $K_t = 2.18$ ; Comparison to the Means of DS MAR-M-246+Hf and PWA 1480 Tested Under the Same Condition



72912.odr

Figure 42. Comparison of Double Notch LCF Data for Different HTs of PWA 1484, Tested at Room Temperature in 34.5 MPa (5 ksi) Hydrogen,  $R = 0.05$

Crack Growth tests in 34.5 MPa (5 ksi) hydrogen at 20°C (68°F) were attempted on most of the HTs with limited success, as shown in Table 15, due to the difficulty in performing crack growth tests on single-crystal materials in high-pressure hydrogen. Data were obtained for HTs 4 and 6, which is shown compared to PWA 1480 data in Figure 43. Heat treat 4 and 6 data were used for relative comparison study only. The data should not be used as characterization data, because the tests were run prior to the installation of an internal load cell, and the friction component in the load (due to seal friction) cannot be easily removed from the data. Also, the data showed that HT 6 has a significantly slower growth rate than HT 4 and is also slower than PWA 1480 for  $\Delta K$  less than 20 MPa $\sqrt{\text{m}}$ . Heat treat 4 has the more rapid crack growth rate shown in the comparison; however, it was slower than the limited data obtained for the other HTs without the duplex microstructure. For the other materials, crack growth was too rapid to obtain adequate data for comparison here, or they were difficult to control during testing.

*Table 15. Crack Growth Alternate Microstructure Screening Results for [001] Oriented PWA 1484 Compact Tension Specimens Tested in 34.5 MPa (5 ksi) Hydrogen at 0.167 Hz, 20°C (68°F), R = -1*

<i>Heat Treat Number</i>	<i>Specimen Sample Number</i>	<i>Comments</i>
1	55A	Specimen failed during test startup; no data acquired
2	44A	Crack grew out of plane; invalid test
3	44B	Difficulty precracking specimen in hydrogen; test data not valid, crack beyond valid $\Delta K$ solution
4	44D	Test data that are shown in Figure 18 were used to select HTs
6	55B	Test data that are shown in Figure 18 were used to select HTs
7	44C	Difficult precracking specimen in hydrogen; test data not valid, excessive scatter

### 2.5.3 Summary

Heat treats 3, 4, and 5 offer the best fatigue properties in 34.5 MPa (5 ksi) hydrogen with similar strengths; however, HT 3 has lower ductility, while HTs 4 and 5 have the best ductility. Heat treats 1, 2, 6, and 7 have good fatigue properties, with HTs 1 and 2 having good strength and medium ductility and HTs 6 and 7 having good ductility, but lower strength. All the HTs produce fatigue lives in excess of 30,000 cycles, which is a substantial improvement over standard PWA 1484 that is shown in Figure 42.

Heat treat 4 has good fatigue and tensile properties; however, the crack growth properties are not as good as HT 6. Heat treat 6 has the best crack growth properties; however, its tensile and fatigue properties are lower than HT 4.

Based on the screening tests performed under this task, HT 4 was selected for further characterization based on its fatigue and tensile properties. Additionally, HT 6 was selected for further characterization based on its superior crack growth properties. Both advanced processed alloys demonstrated superior notched LCF capabilities compared to any turbopump blade alloy currently available. The additional characterization is discussed in the following section.

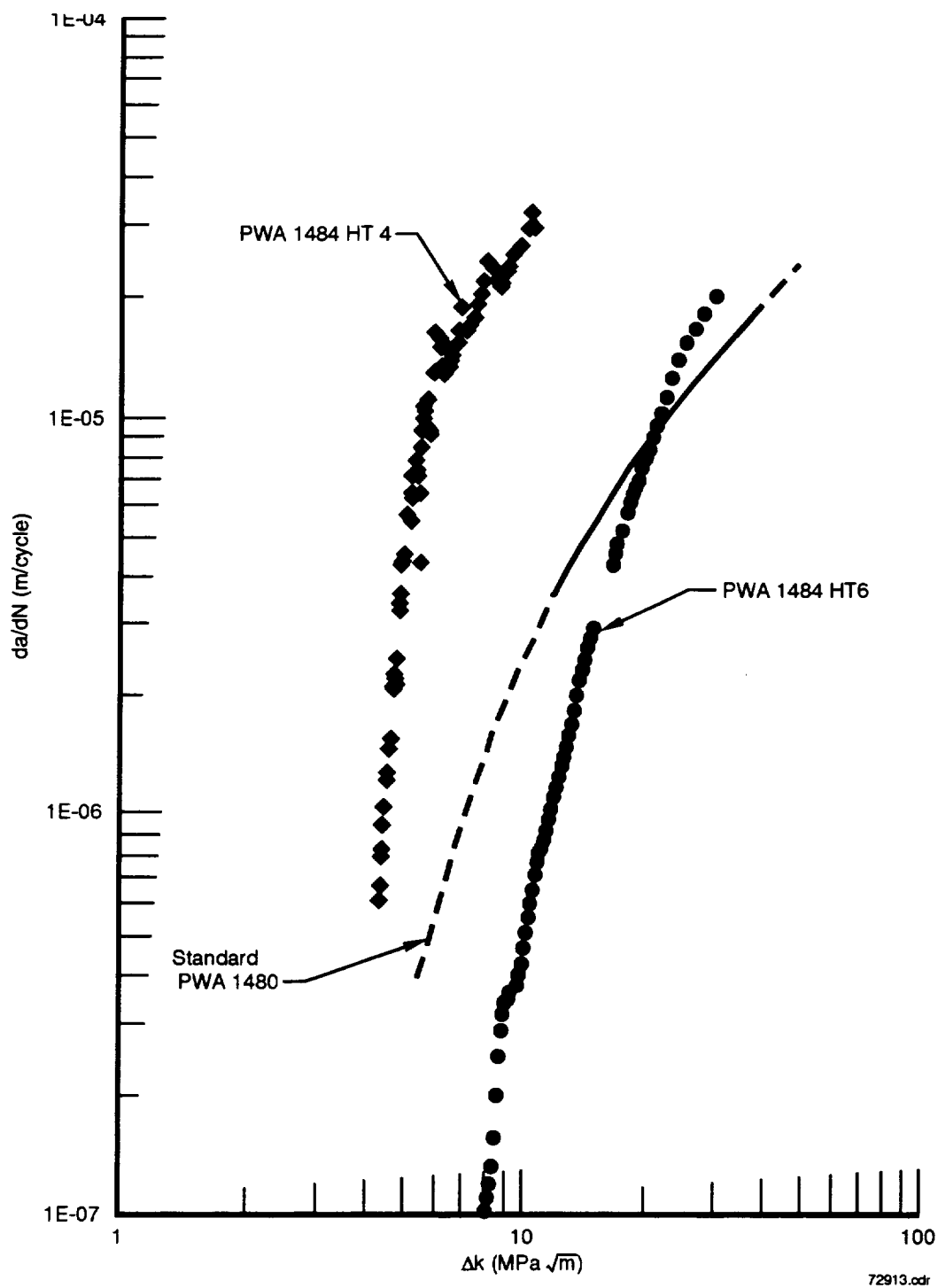


Figure 43. Crack Growth Screening Results for [001] Oriented PWA 1484 Specimens Tested in 34.5 MPa (5 ksi) Hydrogen at 0.167 Hz, 20°C (68°F),  $R = 0.05$ ,  $K_I = 2.18$ ; Comparison of PWA 1484, HTs 4 and 6 with PWA 1480



## 2.6 PROGRAM TEST MATRIX

### 2.6.1 Test Matrix and Description

Testing in this section was performed to obtain comparisons between the two heat treats (HTs 4 and 6) selected from the alternate microstructure screening. The test matrix for this program is shown in Table 16; the discretionary tests listed at the bottom of the matrix were used in the alternate microstructure screening to assist in selecting the HTs to be studied. Sufficient PWA 1482 and PWA 1484 were heat treated to each condition (HTs 4 and 6) to make tensile, creep/rupture, smooth LCF, notched LCF, HCF and fatigue crack growth specimens to perform the testing outlined in Table 16.

Heat treating of the test specimen blanks was performed in multiple batches using vacuum furnaces in the P&W Materials Laboratory. Heat Treating was performed in accordance with the PWA 1482 and PWA 1484 thermal processing cycles described in Paragraph 2.4 – *Thermal Treatment Optimization*. Following HT, each of the test specimen blanks were grain etched, visually inspected, and metallographically examined. Visual inspection did not reveal any evidence of coarse grain recrystallization on the specimen blanks to be used for testing purposes. Metallography confirmed that the proper HT microstructures were achieved in each of the two alloy systems. Based on the results of these inspections, all the test material was released for specimen machining. A list of specimens machined for this matrix, with corresponding heats and bar identifications, is provided in Appendix B – *Test Matrix Specimens*.

The tensile, fatigue, and fatigue crack growth tests were performed at P&W, and the creep rupture tests were performed at Metcut Research Associates. The air tests were performed in atmospheric air, and the hydrogen (H<sub>2</sub>) tests were performed in 34.5 MPa (5 ksi) hydrogen with less than 1 ppm of oxygen. The tensile tests were performed in hydrogen and in air at 649°C (1200°F) and the creep tests at 871°C (1600°F), based on critical temperatures for these properties expected in rocket engine hardware. The fatigue and crack growth tests were performed at 20°C (68°F) because this is the most severe condition for hydrogen embrittlement and would provide the clearest indication of improved hydrogen resistance. The results of the testing for this program are discussed in the Paragraph 2.6.2 – *Results*.

### 2.6.2 Results

#### 2.6.2.1 Tensile

The tensile results for [001] oriented PWA 1482 and PWA 1484, HTs 4 and 6 are shown in Tables 17 and 18 and in Figures 44 through 54. The tests were performed in atmospheric air at 649°C (1200°F) and in 34.5 MPa (5 ksi) hydrogen at 20°C (68°F) and 649°C (1200°F).

Mean tensile engineering stress/strain results comparing PWA 1482 and PWA 1484, combining HTs 4 and 6, are plotted in Figures 44 through 46. The 20°C (68°F)/34.5 MPa (5 ksi) hydrogen stress/strain curves in Figure 44 show that the two alloys have similar behavior up to yield, but the engineering stress for PWA 1484 drops off more rapidly after yield. At 649°C (1200°F), the behavior is similar for both alloys and shows no hydrogen degradation (Figure 45). Engineering stress/strain behavior for PWA 1484 at three elevated temperatures (649°C [1200°F], 760°C [1400°F] and 871°C [1600°F]) is shown in Figure 46. The data at 649°C (1200°F) were obtained under this program, but the data at the other two temperatures are from another program and are shown here for comparison. These data indicate that the strength of PWA 1484 peaked at approximately 760°C (1400°F) and dropped at 871°C (1600°F).

Tensile property versus temperature plots are shown in Figures 47 through 54. Yield strength properties, shown in Figures 47 and 48, for PWA 1482 and PWA 1484 at elevated temperature fall in between the properties for PWA 1480 and PWA 1489 in both air and hydrogen. The room temperature hydrogen data show that HT 4 produces better yield strengths than PWA 1489; however, yield strengths for HT 6 are lower than PWA 1489. Ultimate strengths of PWA 1482 are slightly better or comparable to the strengths of PWA 1484, where comparisons can be made as shown Figures 49 and 50. The strengths tend to fall between PWA 1480 and PWA 1489, except in air at 760°C (1400°F), where PWA 1484 has the highest strength. Hydrogen room temperature strengths of PWA 1482 and

PWA 1484 are close to the strength of PWA 1489. Figures 51 through 54 show that PWA 1484 tends to have the highest ductility at elevated temperatures, and that PWA 1482 has ductility similar to PWA 1480 and PWA 1489. Room temperature hydrogen ductilities for PWA 1482 and PWA 1489 are slightly below those of PWA 1480 and PWA 1484.

Table 16. Program Test Matrix

Material	Condition	Temp. (°C)	Env <sup>1</sup>	Tens.	LCF		da/dN	HCF	Rupt.
					S	N			
PWA 1482	Process #1 (HIP + HT 4)	20	AIR		4	4			
		649	AIR	3					
		871	AIR						2
		20	H <sub>2</sub>	2	3	4	1	4	
		649	H <sub>2</sub>	2					
	Process #2 (HIP + HT 6)	20	AIR		4	4			
		649	AIR	3					
		871	AIR						2
		20	H <sub>2</sub>	2	3	4	1	4	
		649	H <sub>2</sub>	2					
PWA 1484	Process #1 (HIP + HT 4)	20	AIR		4	4			
		649	AIR	3					
		871	AIR						2
		20	H <sub>2</sub>	2	3	4	1	4-	
		649	H <sub>2</sub>	2					
	Process #2 (HIP + HT 6)	20	AIR		4	4			
		649	AIR	3					
		871	AIR						2
		20	H <sub>2</sub>	2	3	4	1	4	
		649	H <sub>2</sub>	2					
TOTAL 121 Tests			AIR	12	16	16			8
			H <sub>2</sub>	16	12	16	2	16	

Discretionary Tests - 24

S - Smooth specimens  
N - Notched specimens  
HIP - Hot Isostatic Pressed  
HT - Heat Treatment

<sup>1</sup> -Hydrogen (H<sub>2</sub>) environments are at 34.5 MPa (5000 psig) with less than 1 ppm.  
of oxygen, air environments are at ambient pressure.

Table 17. Tensile Results for [001] Oriented PWA 1482

Specimen S/N *	Environment **	Test Temp		Proportional Limit		0.2% Yield Strength		Ultimate Tensile Strength		% Elongation	% Reduction of Area	Elastic Modulus	
		(°C)	(°F)	MPa	ksi	MPa	ksi	MPa	ksi			GPa	msi
4-4	Hydrogen	20	68	660.5	95.8	858.8	124.6	922.3	133.8	3.1	5.7	128.2	18.6
4-5	Hydrogen	20	68	660.5	95.8	891.6	129.3	943.2	136.8	2.9	9.0	131.7	19.1
6-4	Hydrogen	20	68	660.5	95.8	762.9	110.6	884.4	128.3	2.8	4.9	134.5	19.5
6-5	Hydrogen	20	68	660.5	95.8	751.3	109.0	874.0	126.8	2.6	5.9	134.5	19.5
4-1	Air	650	1200	673.0	97.6	910.5	132.1	1050.9	152.4	8.5	10.0	100.7	14.6
4-2	Air	650	1200	673.0	97.6	920.3	133.5	1147.4	166.4	8.1	10.3	107.6	15.6
4-3	Air	650	1200	673.0	97.6	928.2	134.6	1286.1	186.5	6.9	7.3	107.6	15.6
4-8	Hydrogen	650	1200	766.0	111.1	887.3	128.7	1031.6	149.6	4.8	5.4	115.8	16.8
4-9	Hydrogen	650	1200	766.0	111.1	916.9	133.0	1054.3	152.9	3.8	2.8	113.8	16.5
6-1	Air	650	1200	673.0	97.6	915.4	132.8	1158.0	167.9	6.1	11.0	111.0	16.1
6-2	Air	650	1200	673.0	97.6	903.3	131.0	1132.5	164.2	7.8	11.5	105.5	15.3
6-3	Air	650	1200	673.0	97.6	881.5	127.8	1045.4	151.6	11.3	20.7	105.5	15.3
6-8	Hydrogen	650	1200	766.0	111.1	946.7	137.3	1114.9	161.7	3.8	5.9	113.8	16.5
6-9	Hydrogen	650	1200	766.0	111.1	896.4	130.0	1039.2	150.7	4.0	3.8	113.1	16.4

\* 4-: heat treat 4; 6-: heat treat 6

\*\* Air: ambient pressure air; Hydrogen: 34.5 MPa hydrogen with less than 1 ppm of oxygen

Table 18. Tensile Results for [001] Oriented PWA 1484

Specimen S/N *	Environment **	Test Temp		Proportional Limit		0.2% Yield Strength		Ultimate Tensile Strength		% Elongation	% Reduction of Area	Elastic Modulus	
		(°C)	(°F)	MPa	ksi	MPa	ksi	MPa	ksi			GPa	msi
4-4	Hydrogen	20	68	744.0	107.9	833.5	120.9	882.1	127.9	1.9	4.9	132.4	19.2
4-5	Hydrogen	20	68	744.0	107.9	835.8	121.2	896.6	130.0	2.0	7.8	132.4	19.2
6-4	Hydrogen	20	68	744.0	107.9	761.4	110.4	877.0	127.2	2.6	5.4	133.8	19.4
6-5	Hydrogen	20	68	744.0	107.9	770.3	111.7	830.9	120.5	2.4	5.2	134.5	19.5
4-1	Air	650	1200	718.5	104.2	947.9	137.5	1095.5	158.9	12.4	22.6	115.1	16.7
4-2	Air	650	1200	718.5	104.2	886.0	128.5	1027.1	149.0	16.2	21.5	109.6	15.9
4-3	Air	650	1200	718.5	104.2	918.6	133.2	1047.1	151.9	15.2	20.5	113.8	16.5
4-8	Hydrogen	650	1200	780.5	113.2	922.9	133.8	1012.4	146.8	7.3	6.9	115.8	16.8
4-9	Hydrogen	650	1200	780.5	113.2	960.3	139.3	1040.2	150.9	4.8	5.4	117.2	17
6-1	Air	650	1200	718.5	104.2	916.2	132.9	1114.7	161.7	10.7	16.3	107.6	15.6
6-2	Air	650	1200	718.5	104.2	935.4	135.7	1078.2	156.4	10.3	9.8	111.7	16.2
6-3	Air	650	1200	718.5	104.2	923.3	133.9	1117.3	162.0	10.5	16.2	108.9	15.8
6-8	Hydrogen	650	1200	780.5	113.2	928.6	134.7	1015.9	147.3	6.0	11.0	111.7	16.2
6-9	Hydrogen	650	1200	780.5	113.2	898.6	130.3	1000.0	145.0	7.8	9.0	113.1	16.4
4-10	Air	760	1400	605.4	87.8	967.5	140.3	1320.5	191.5	12.4	18.4	100.7	14.6
4-11	Air	871	1600	523.3	75.9	1402.3	110.1	959.3	139.1	30.8	46.2	95.8	13.9

\* 4-: heat treat 4; 6-: heat treat 6

\*\* Air: ambient pressure air; Hydrogen: 34.5 MPa hydrogen with less than 1 ppm of oxygen

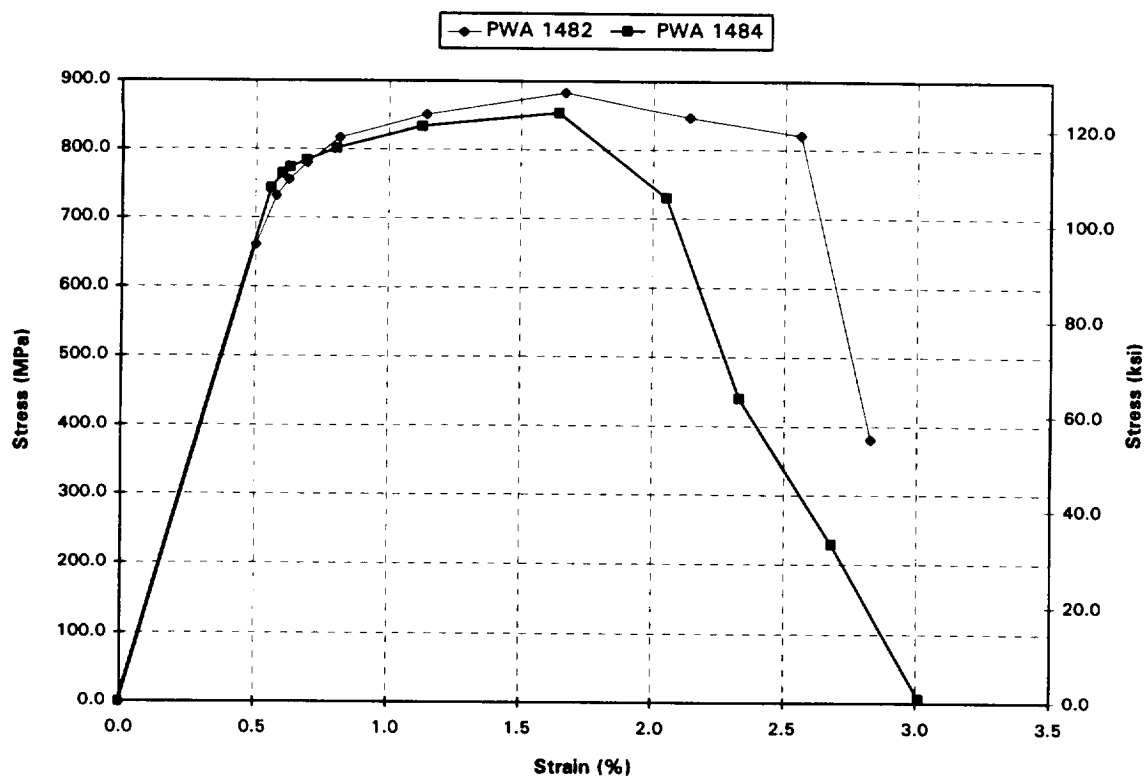


Figure 44. Tensile Engineering Stress/Strain Results for [001] Oriented PWA 1482 and PWA 1484 Tested in 34.5 MPa (5 ksi) Hydrogen at 20°C (68°F)

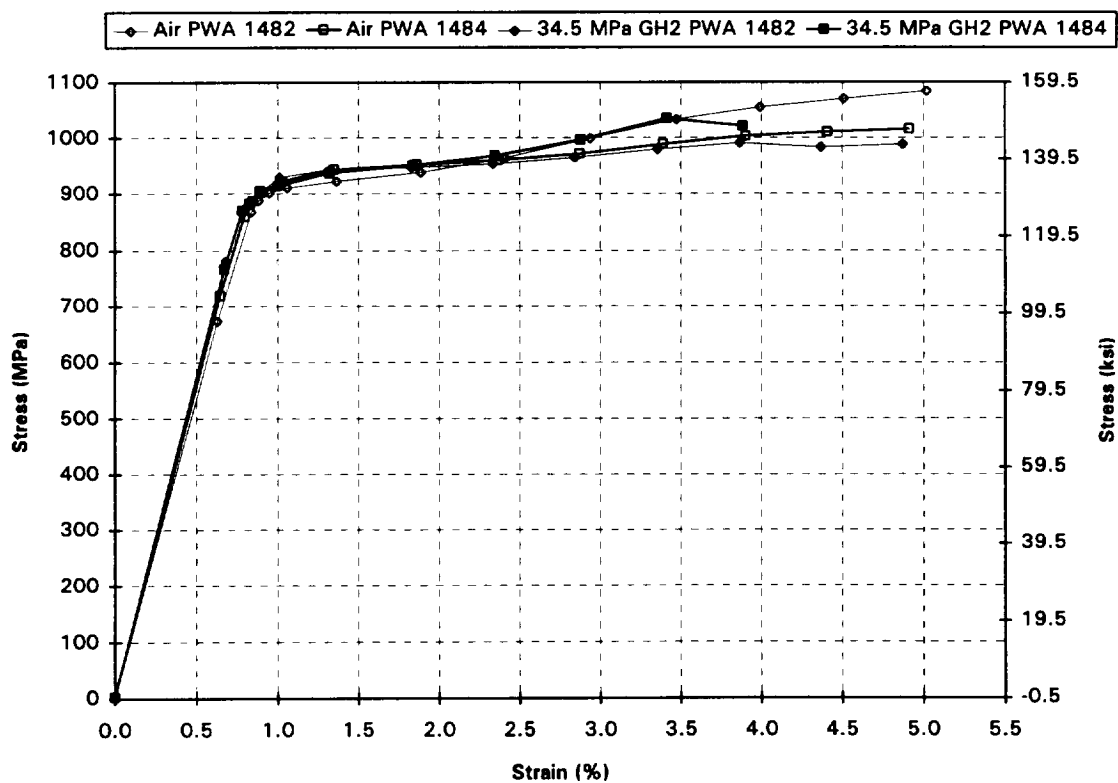


Figure 45. Tensile Engineering Stress/Strain Results for [001] Oriented PWA 1482 and PWA 1484 Tested in Air and 34.5 MPa (5 ksi) Hydrogen at 649°C (1200°F)

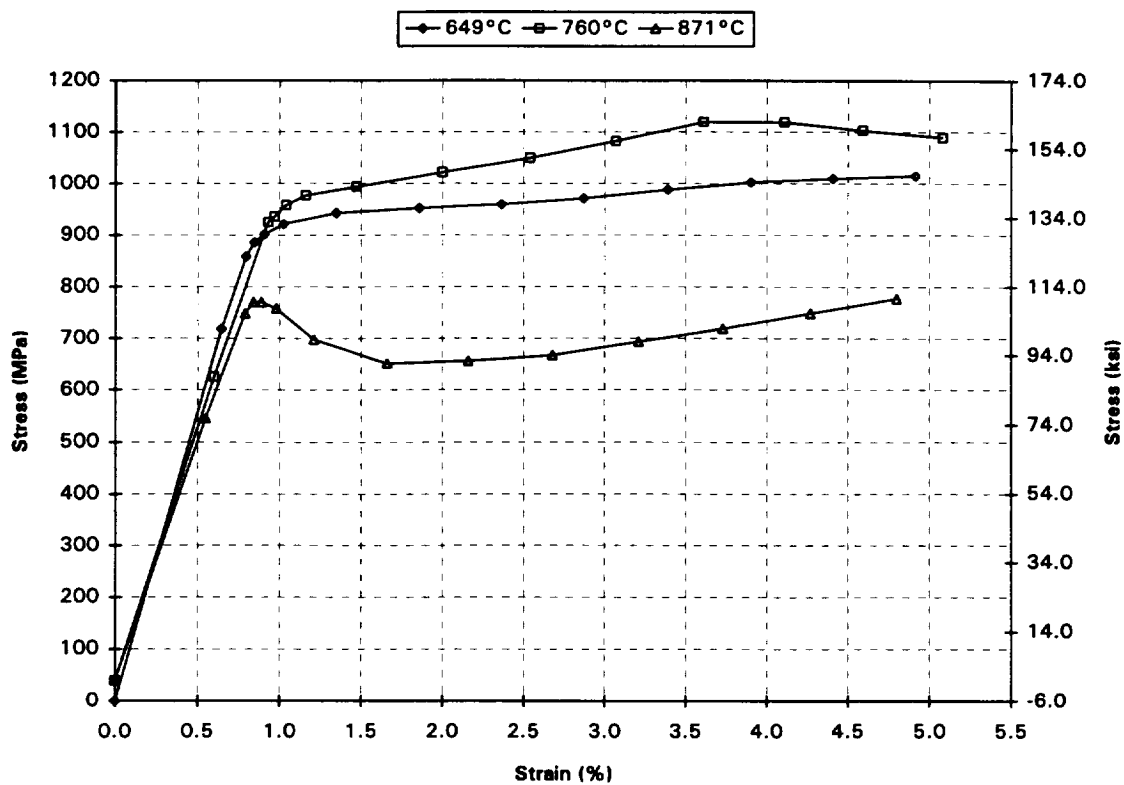


Figure 46. Tensile Engineering Stress/Strain Results for [001] Oriented PWA 1484 Tested in Air at 649°C (1200°F), 760°C (1400°F), and 871°C (1600°F)

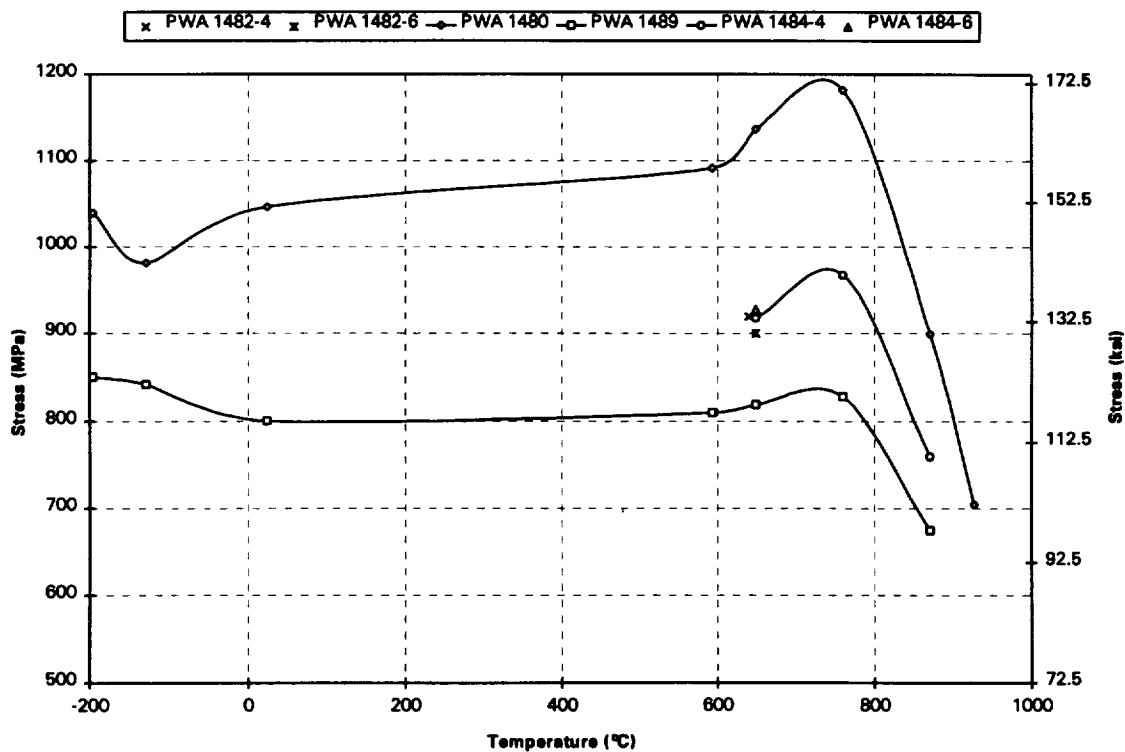


Figure 47. Air 0.2 percent Yield Properties Versus Temperature for PWA 1489 and [001] Oriented PWA 1480, PWA 1482, and PWA 1484

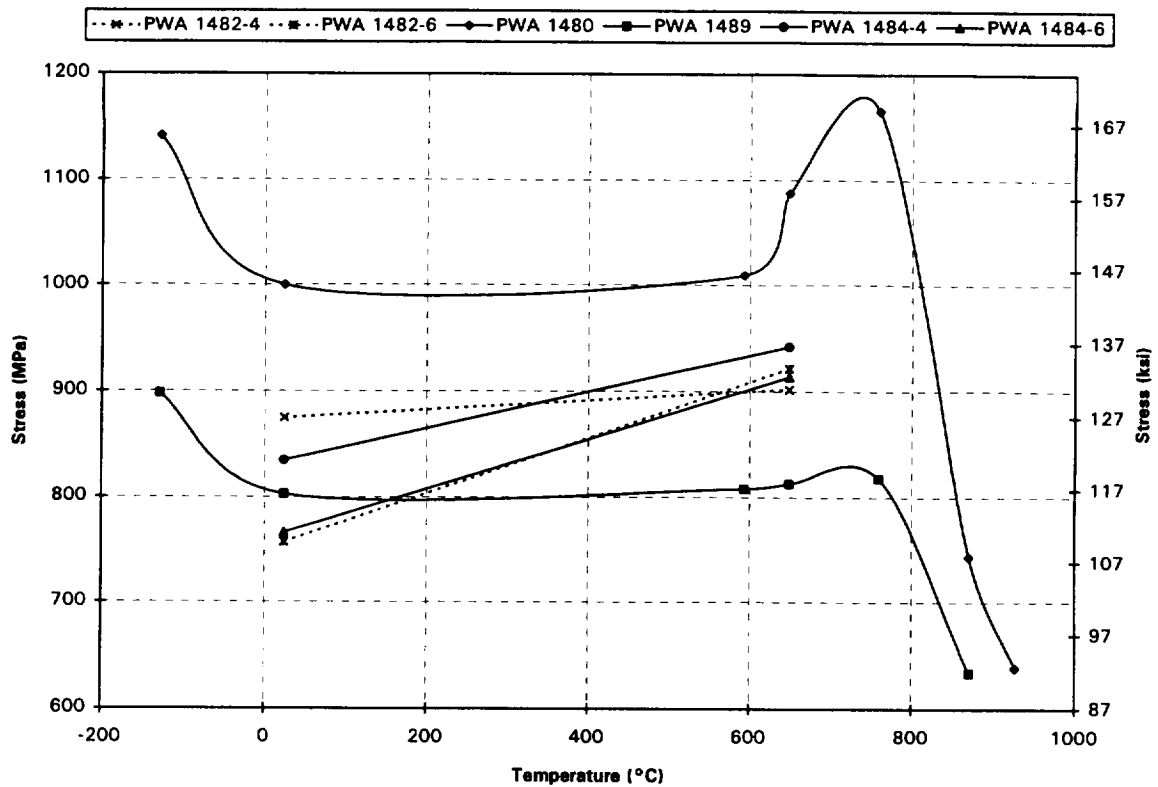


Figure 48. 34.5 MPa (5 ksi) Hydrogen 0.2 percent Yield Properties Versus Temperature for PWA 1489 and [001] Oriented PWA 1480, PWA 1482, and PWA 1484

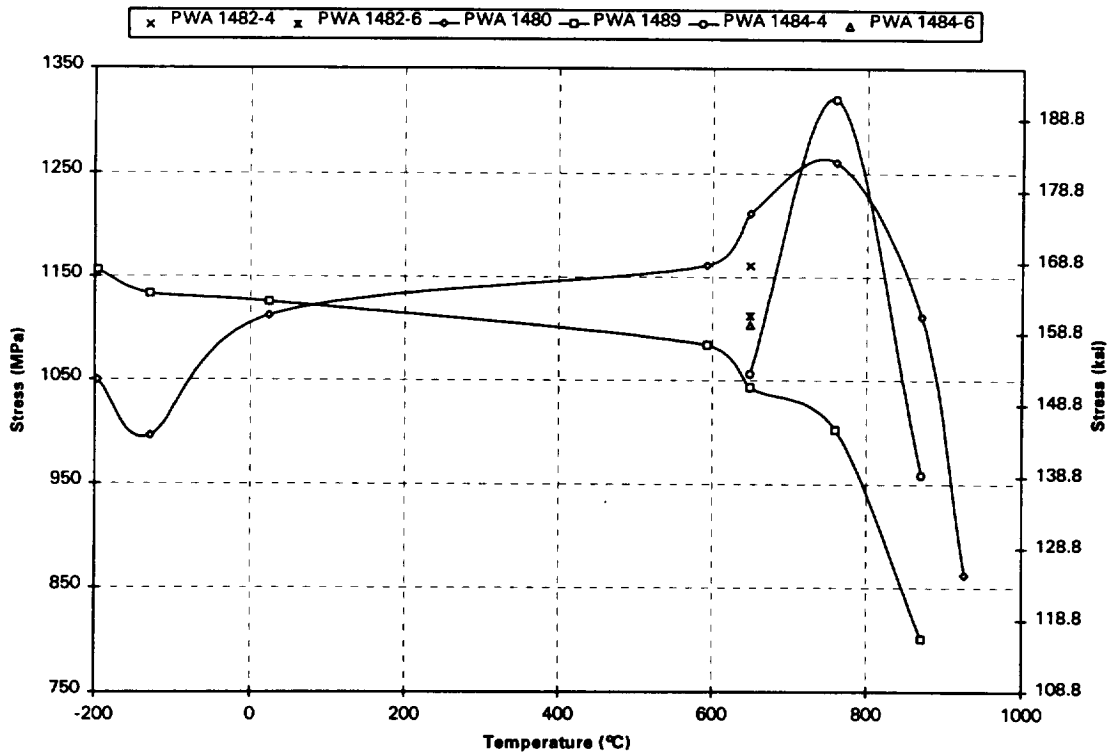


Figure 49. Air Ultimate Strength Properties Versus Temperature for PWA 1489 and [001] Oriented PWA 1480, PWA 1482, and PWA 1484

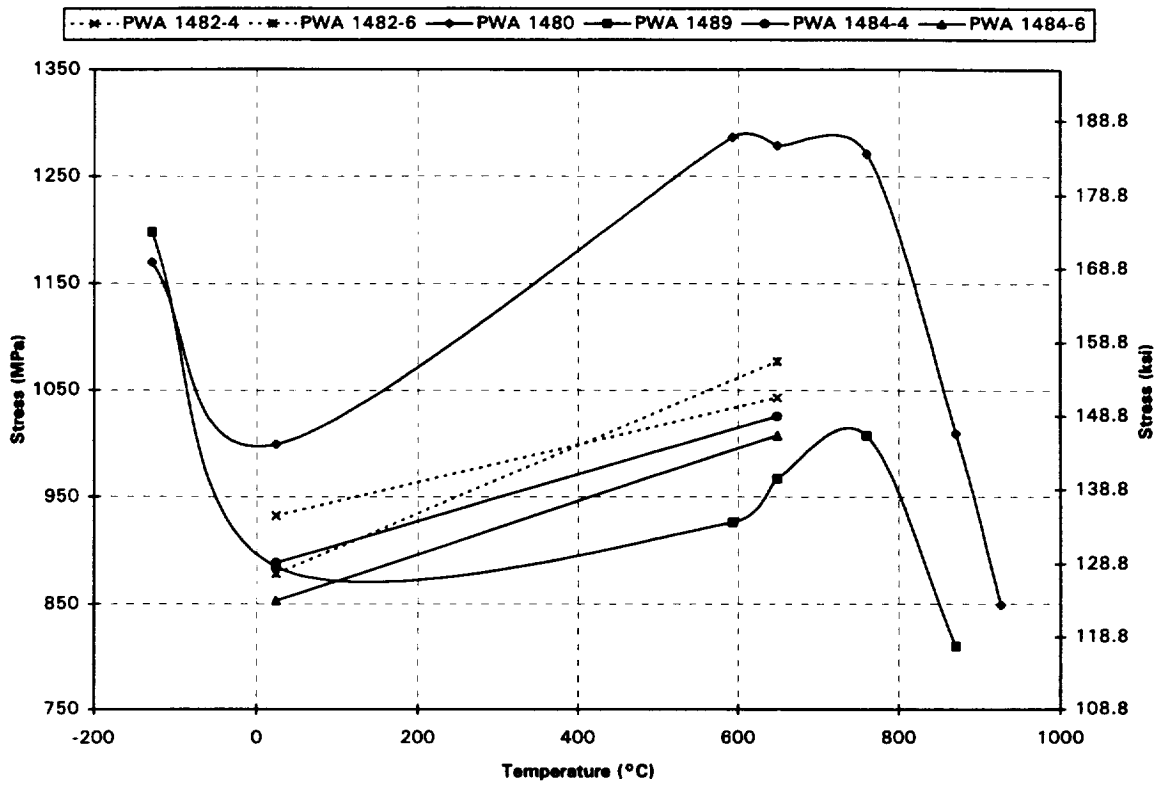


Figure 50. 34.5 MPa (5 ksi) Hydrogen Ultimate Strength Properties Versus Temperature for PWA 1489 and [001]

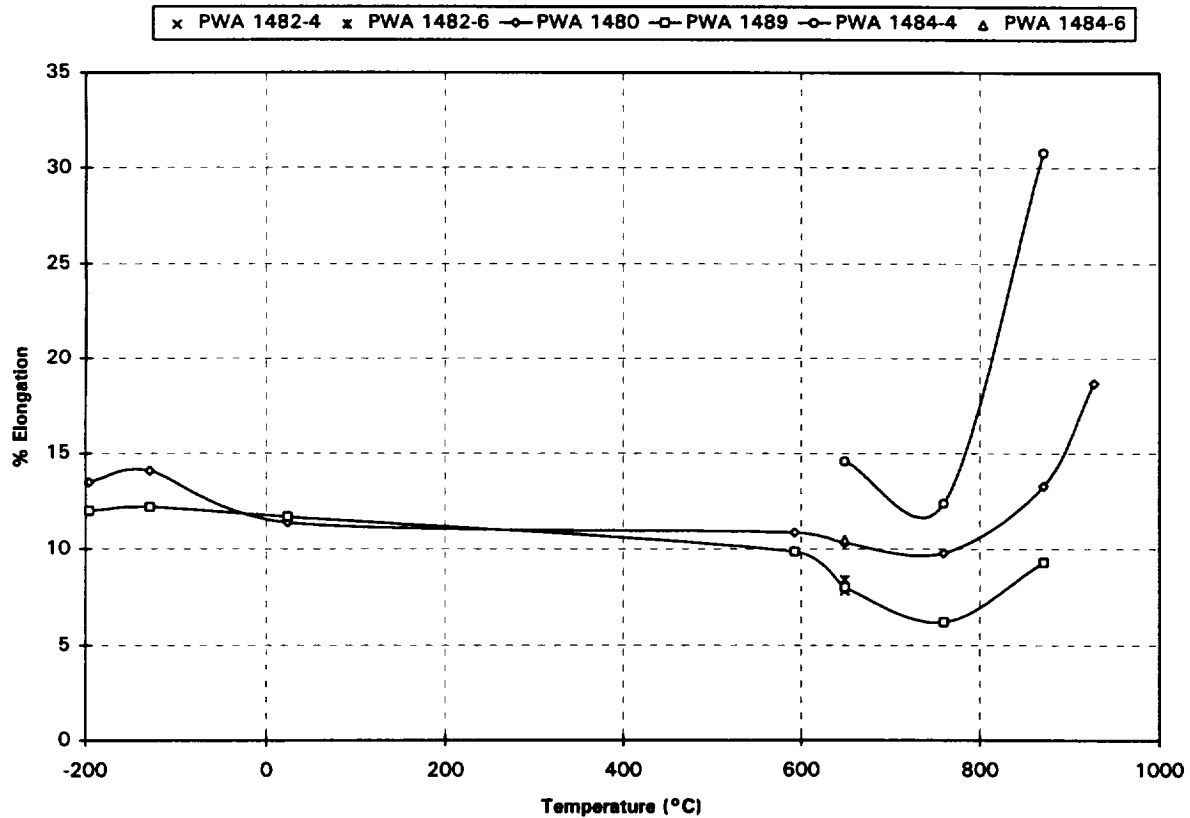


Figure 51. Air Percent Elongation Versus Temperature for PWA 1489 and [001] Oriented PWA 1480, PWA 1482, and PWA 1484



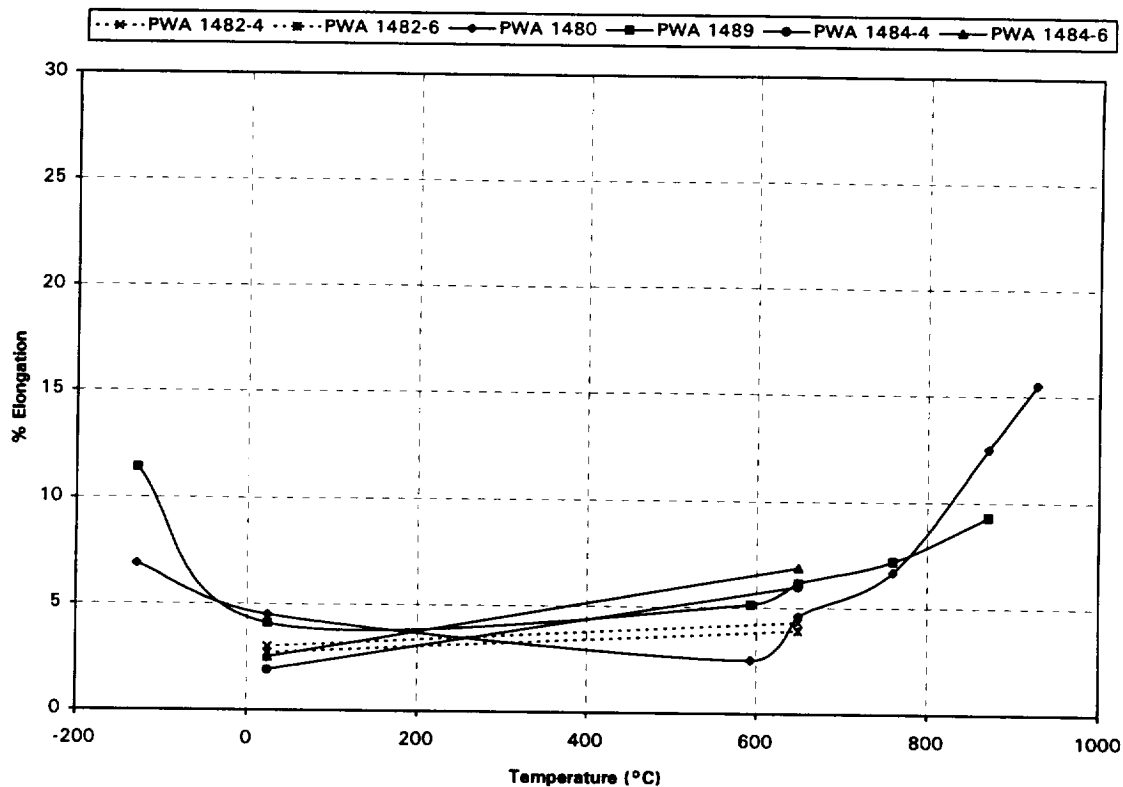


Figure 52. 34.5 MPa (5 ksi) Hydrogen Percent Elongation Versus Temperature for PWA 1489 and [001] Oriented PWA 1480, PWA 1482, and PWA 1484

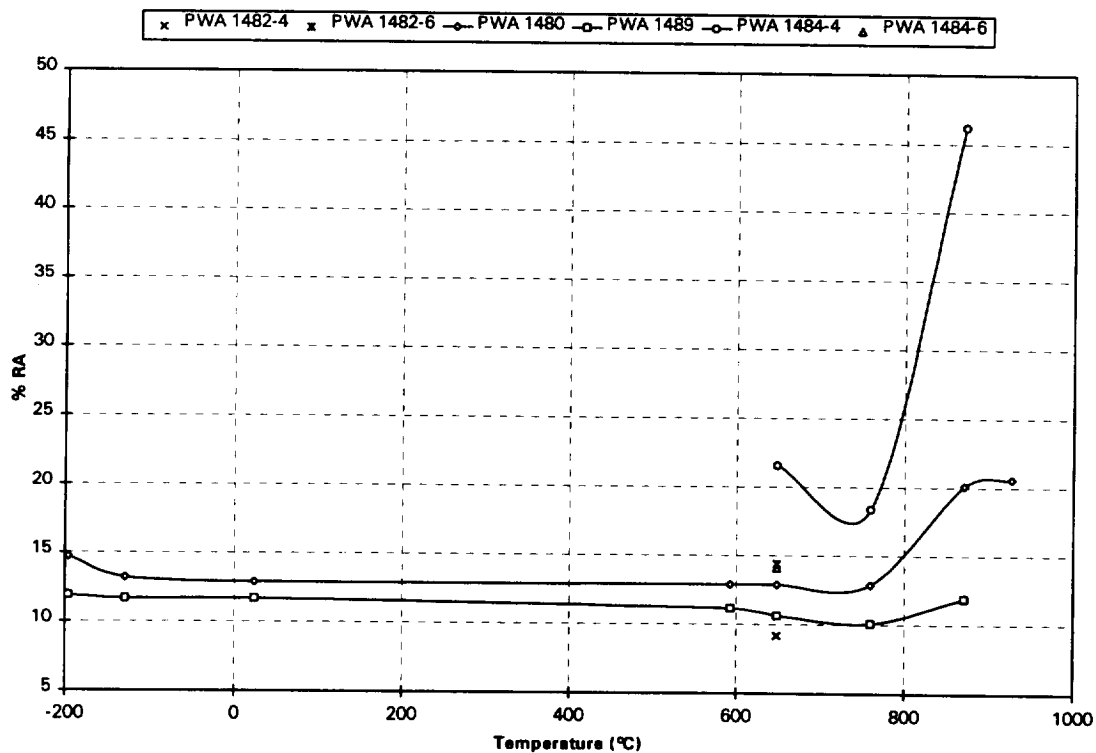


Figure 53. Air Percent Reduction in Area Versus Temperature for PWA 1489 and [001] Oriented PWA 1480, PWA 1482, and PWA 1484

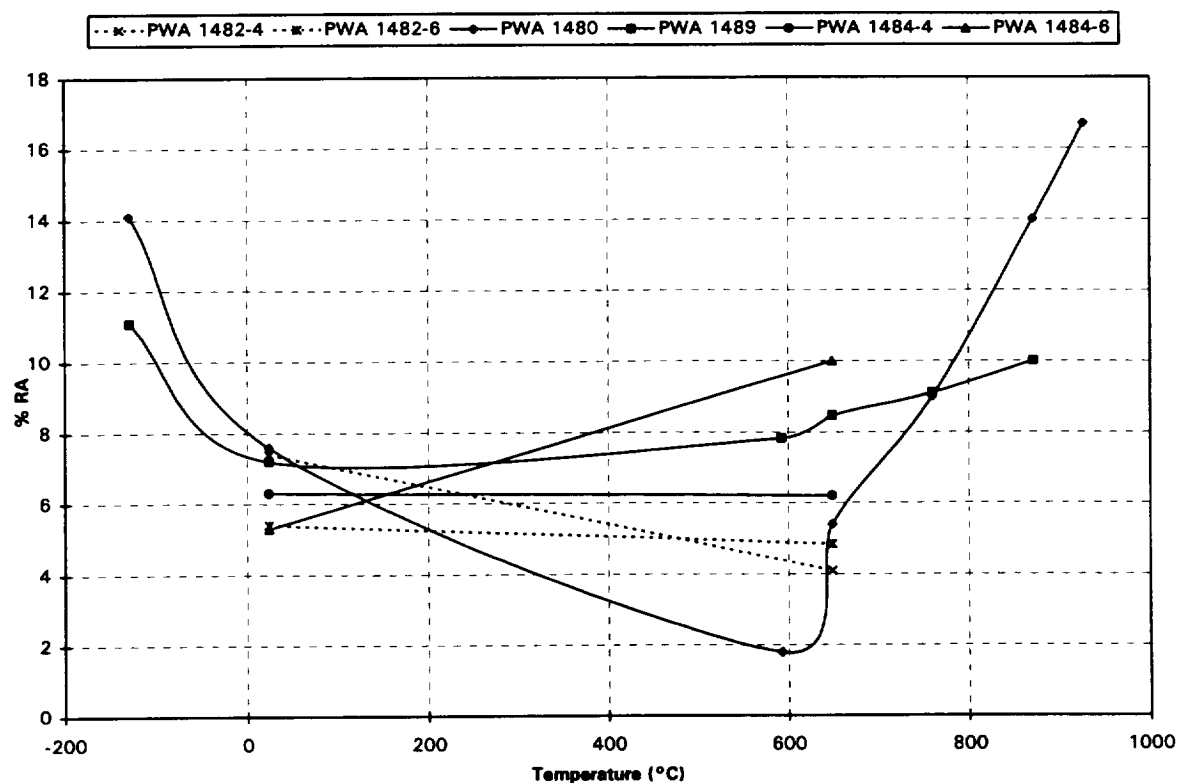


Figure 54. 34.5 MPa (5 ksi) Hydrogen Percent Reduction in Area Versus Temperature for PWA 1489 and [001] Oriented PWA 1480, PWA 1482, and PWA 1484

### 2.6.2.2 Creep Rupture

The creep results for [001] oriented PWA 1482 and PWA 1484, HTs 4 and 6 are shown in Tables 19 and 20. The tests were performed in atmospheric air with a stress of 413.7 MPa (60 ksi) at 871°C (1600°F). A comparison of mean creep behavior for turbine blade alloys under these conditions is shown in Figure 55. This comparison shows that PWA 1482 has the lowest creep capability under these test conditions and PWA 1484 HT 4 has the best creep capability. PWA 1480 falls in between PWA 1482 and PWA 1484.

### 2.6.2.3 High-Cycle Fatigue

The HCF results for [001] oriented PWA 1482 and PWA 1484, HTs 4 and 6 are shown in Tables 21 and 22 and in Figures 56 through 58. The tests were performed in 34.5 MPa (5 ksi) hydrogen at 20°C (68°F) with a fully reversed stress cycle ( $R = -1$ ) at a frequency of 30 Hz. The PWA 1482 and PWA 1484 data with mean curves regressed through both HTs are shown plotted in Figures 56 and 57, respectively. There was no significant difference in the HCF properties of HT 4 or 6, so the mean curves were regressed through the combined data for each alloy using maximum likelihood techniques. Tests, which were discontinued due to run-out, thread failure, etc., are marked with arrows on the plots to indicate possible longer lives. These data were treated as run-outs in the regression. Thread failures, although not desirable, occur in most alloys and are not exclusive to PWA 1482 and PWA 1484.<sup>10</sup>

A comparison of HCF mean curves for turbine blade alloys is shown in Figure 58. This plot shows that PWA 1482 has the highest endurance limit, and that both PWA 1484 and PWA 1482 have better properties than either PWA 1480 or PWA 1489. The air data for PWA 1480 are also included on this plot and show that PWA 1482 and PWA 1484 in 34.5 MPa (5 ksi) hydrogen have significantly better properties than PWA 1480 tested in air.

### 2.6.2.4 Low-Cycle Fatigue

Low-cycle fatigue results for [001] oriented PWA 1482 and PWA 1484 double notch specimens, HTs 4 and 6 are shown in Tables 23 and 24 and in Figures 59 through 62. The tests were performed in atmospheric pressure air and 34.5 MPa (5 ksi) hydrogen at 20°C (68°F) with an all tensile stress cycle ( $R = 0.05$ ) at a frequency of 0.167 Hz. The PWA 1482 and PWA 1484 data with mean curves regressed through both HTs are shown plotted in Figures 59 and 60, respectively. There was no significant difference in the notched low-cycle fatigue properties of HTs 4 and 6, so mean curves were regressed through the combined HT data making distinctions only between alloy and test environment. Comparison of air and hydrogen data shows that hydrogen debits fatigue properties approximately one order of magnitude for each alloy.

A comparison of notched specimen LCF air mean curves for turbine blade alloys in Figure 61 shows that PWA 1482 and PWA 1484 have similar fatigue capabilities that are slightly lower than PWA 1480 and PWA 1489. However, the hydrogen comparison in Figure 62 shows that PWA 1482 and PWA 1484 again have similar fatigue capabilities, but show a significant improvement (approximately 8X) over PWA 1480 and PWA 1489.

---

<sup>10</sup> The DS MAR-M-246-Hf fracture is shown in Figure 77 of Paragraph 2.7 – *Microstructural and Fractographic Analysis* is an example.

Table 19. Creep Rupture Results for [001] Oriented PWA 1482 Tested at 413.7 MPa (60 ksi)

Specimen S/N *	Environment	Test Temp (°C)	Test Temp (°F)	Time (hrs) to % Creep of								Plastic			Comments
				0.1	0.2	0.5	1.0	2.0	Strain on Loading %	Duration (Hours)	% Elongation	% Reduction of Area			
4-1	Air	871	1600	0.2	1.0	6.4	17.0	33.0	0	152.2	45.0	55.0	failed in the threads		
4-2	Air	871	1600	0.05	--	--	--	--	0.0327	0.5	1.6	--			
4-3	Air	871	1600	0.4	2.7	9.7	20.0	39.0	0	133.6	33.0	59.0	failed in the threads		
6-1	Air	871	1600	0.2	0.8	6.4	13.5	24.0	0	68.3	--	--			
6-2	Air	871	1600	0.4	1.7	8.2	15.5	26.0	0	85.6	28.0	55.0			
6-3	Air	871	1600	0.3	1.8	8.2	15.1	25.0	0	95.5	39.0	52.0			

\* 4-: heat treat 4; 6-: heat treat 6

Table 20. Creep Rupture Results for [001] Oriented PWA 1484 Tested at 413.7 MPa (60 ksi)

Specimen S/N *	Environment	Test Temp (°C)	Time (hrs) to % Creep of	Time (hrs) to % Creep of								Plastic			Comments
				0.1	0.2	0.5	1.0	2.0	5.0	10.0	Strain on Loading %	Duration (Hours)	% Elongation	% Reduction of Area	
4-1	Air	871	1600	16.0	41.00	97.0	160.0	260.0	0	814.2	0	814.2	33.0	59.0	
4-2	Air	871	1600	14.2	41.00	87.0	142.0	226.0	0	807.1	0	807.1	54.0	55.0	
4-3	Air	871	1600	13.0	33.00	73.0	122.0	204.0	0	722.1	0	722.1	39.0	52.0	
6-1	Air	871	1600	2.4	28.00	76.0	116.0	177.0	0.078	561.1	0.078	561.1	38.0	54.0	
6-2	Air	871	1600	--	17.80	78.0	128.0	192.0	0.125	606.3	0.125	606.3	37.0	53.0	
6-3	Air	871	1600	37.0	55.00	93.0	133.0	195.0	0	617.0	0	617.0	36.0	47.0	failed at extensometer

\* 4-: heat treat 4; 6-: heat treat 6

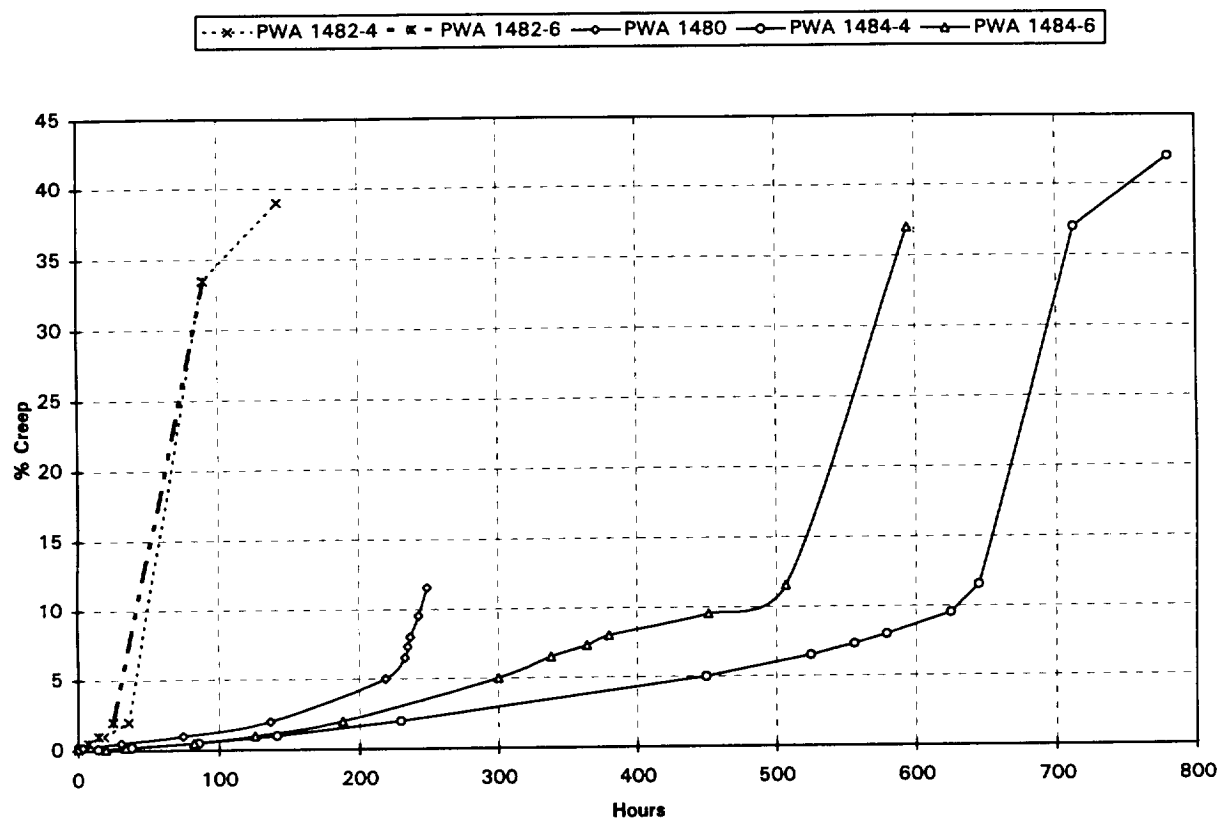


Figure 55. Air 871°C (1600°F) Creep Properties at 413.7 MPa (60 ksi) for [001] Oriented PWA 1480, PWA 1482, and PWA 1484

*Table 21. Load Controlled HCF Results for [001] Oriented PWA 1482 Specimens Tested in 34.5 MPa (5 ksi)  
Hydrogen at 30 Hz, 20°C (68°F), R = -1*

Specimen S/N *	Heat Code	Alternating Stress (MPa)	Stress (ksi)	Cycles to Failure	Comments
4-2	J203	621	90	638,500	
4-1	J203	552	80	5,673,500	Tensiled due to power failure
4-3	J203	552	80	2,056,050	
4-5	P1030	483	70	8,020,000	Thread failure
6-1	J203	621	90	49,586	
6-4	P1030	552	80	7,480,350	Uploaded after run-out at 414 MPa
6-2	J203	483	70	2,894,430	Thread failure
6-4	J203	414	60	+10,000,000	Did not fail

\* 4-: heat treat 4; 6-: heat treat 6

*Table 22. Load Controlled HCF Results for [001] Oriented PWA 1484 Specimens Tested in 34.5 MPa (5 ksi)  
Hydrogen at 30 Hz, 20°C (68°F), R = -1*

Specimen S/N *	Heat Code	Alternating Stress (MPa)	Stress (ksi)	Cycles to Failure	Comments
4-2	1033	621	90	487,315	
4-4	1034	552	80	1,700,200	
4-5	1034	552	80	2,295,600	
4-1	1033	483	70	7,386,500	Thread failure
6-2	1033	621	90	295,145	
6-3	1033	621	90	907,500	
6-5	1034	621	90	133,505	Uploaded after run-out at 483 MPa
6-1	1033	552	80	6,856,000	
6-4	1034	552	80	1,650,350	
6-5	1034	483	70	+10,000,000	Did not fail

\* 4-: heat treat 4; 6-: heat treat 6

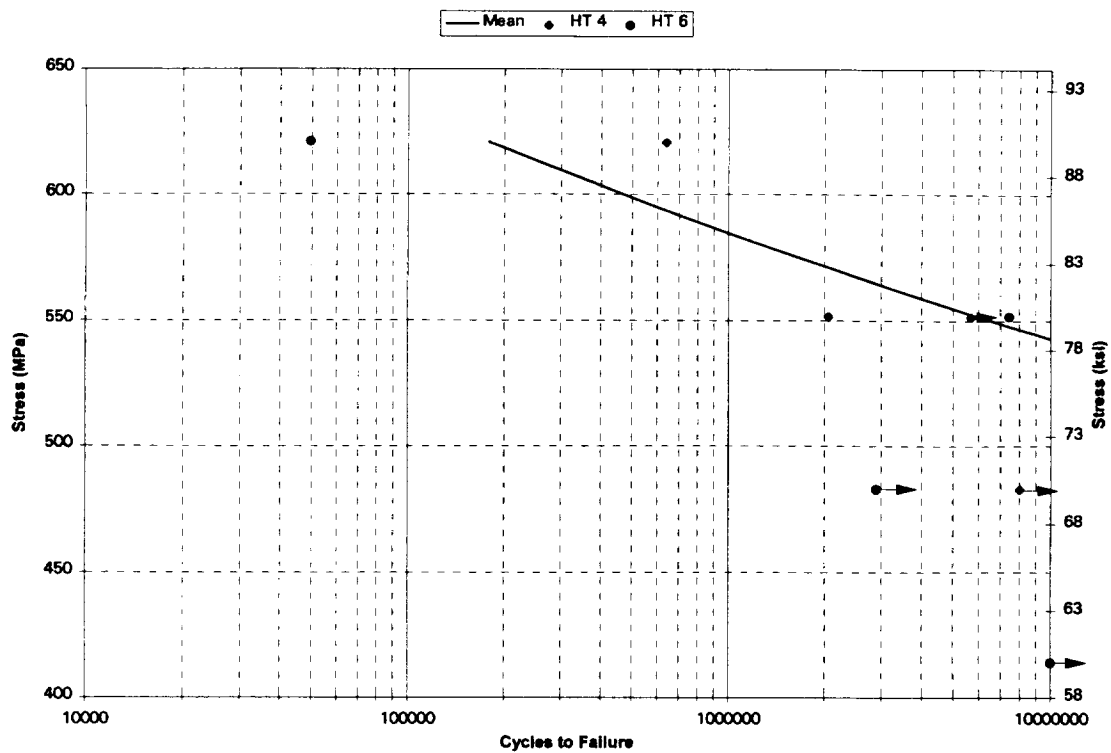


Figure 56. Load Controlled HCF Results for [001] Oriented PWA 1482 Specimens Tested in 34.5 MPa (5 ksi) Hydrogen at 0.167 Hz, 20°C (68°F),  $R = -1$

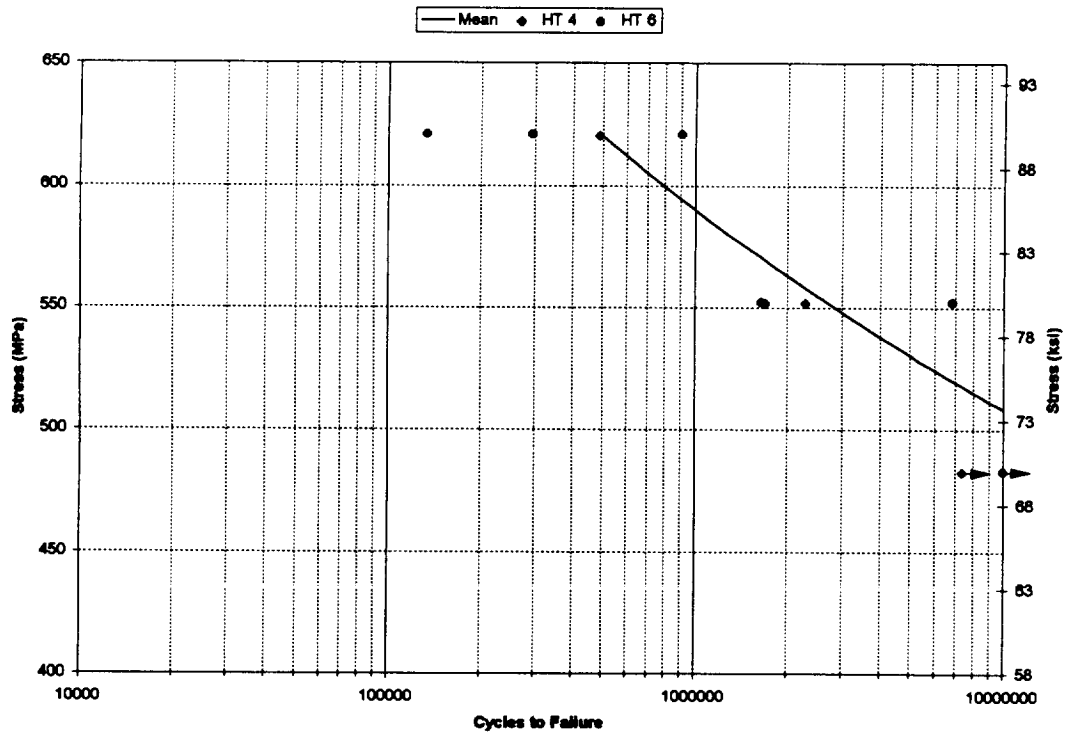


Figure 57. Load Controlled HCF Results for [001] Oriented PWA 1484 Specimens Tested in 34.5 MPa (5 ksi) Hydrogen at 0.167 Hz, 20°C (68°F),  $R = -1$

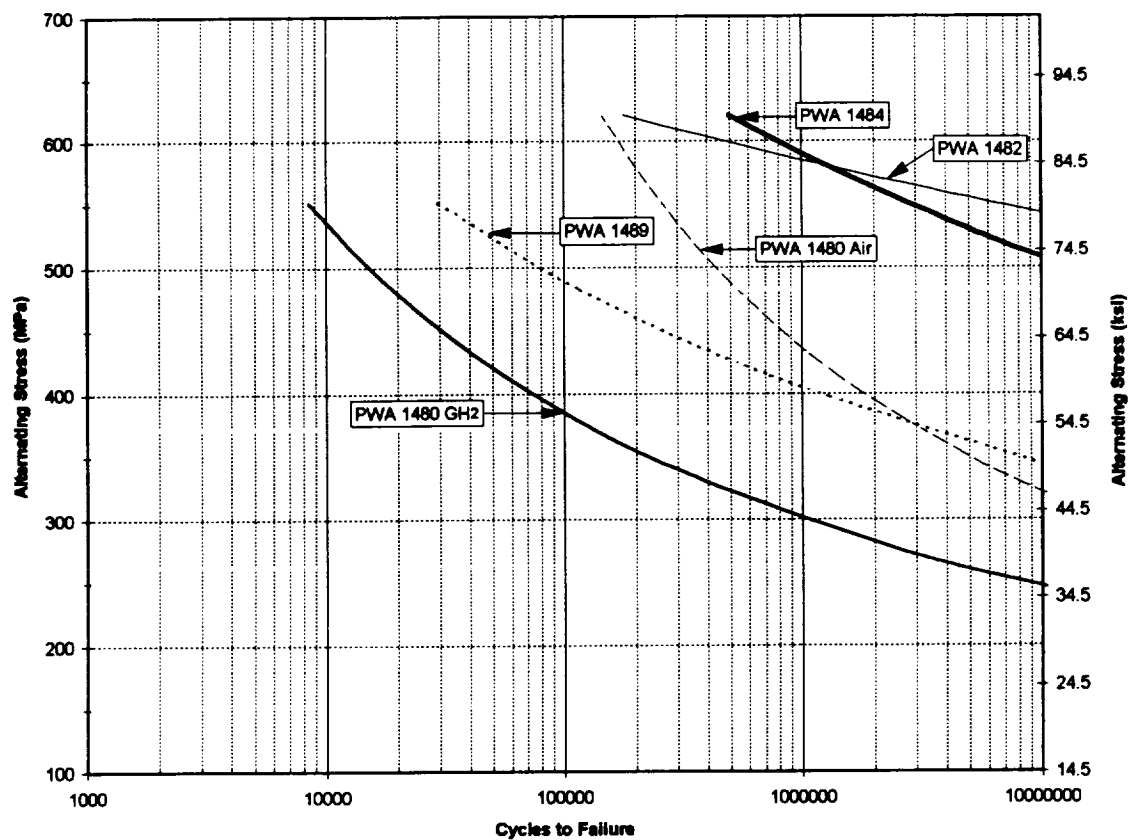


Figure 58. Alloy Comparison of Mean Curves 34.5 MPa (5 ksi) Hydrogen HCF Results Smooth Specimens Tested at 20/30 Hz, 20°C (68°F), R = -1



Table 23. Load Controlled LCF Results for [001] Oriented PWA 1482 Double Notch Specimens Tested at 0.167 Hz, 20°C (68°F),  $R = 0.05$ ,  $K_t = 2.18$

Specimen S/N *	Environ- ment **	Max Stress		Cycles to Failure
		(MPa)	(ksi)	
4-1	Air	896.35	130.0	8,900
4-3	Air	896.35	130.0	7,960
4-2	Air	758.45	110.0	16,809
4-4	Air	758.45	110.0	17,151
4-7	Hydrogen	758.45	110.0	675
4-8	Hydrogen	689.5	100.0	7,288
4-6	Hydrogen	620.55	90.0	156,038
4-9	Hydrogen	620.55	90.0	52,063
6-2	Air	896.35	130.0	5,410
6-4	Air	896.35	130.0	8,196
6-1	Air	758.45	110.0	26,389
6-3	Air	758.45	110.0	17,035
6-7	Hydrogen	758.45	110.0	2,792
6-9	Hydrogen	758.45	110.0	2,717
6-6	Hydrogen	620.55	90.0	7,907
6-8	Hydrogen	620.55	90.0	18,096

\* 4- : heat treat number 4; 6- : heat treat number 6

\*\* Air : atmospheric air; Hydrogen 34.5 MPa hydrogen with less than 1 ppm of oxygen

Table 24. Load Controlled LCF Results for [001] Oriented PWA 1484 Double Notch Specimens Tested at 0.167 Hz, 20°C (68°F),  $R = 0.05$ ,  $K_t = 2.18$

Specimen S/N *	Environ- ment **	Max Stress		Cycles to Failure
		(MPa)	(ksi)	
4-6	Air	896.4	130.0	7,895
4-8	Air	896.4	130.0	7,639
4-7	Air	758.5	110.0	17,694
4-10	Air	758.5	110.0	21,929
4-1	Hydrogen	827.4	120.0	411
4-3	Hydrogen	758.5	110.0	3,586
4-4	Hydrogen	689.5	100.0	9,329
4-2	Hydrogen	620.6	90.0	19,549
6-6	Air	896.4	130.0	5,589
6-7	Air	896.4	130.0	5,106
6-8	Air	758.5	110.0	17,664
6-9	Air	758.5	110.0	16,869
6-1	Hydrogen	758.5	110.0	851
6-3	Hydrogen	758.5	110.0	989
6-4	Hydrogen	689.5	100.0	7,268
6-2	Hydrogen	620.6	90.0	11,821
6-5	Hydrogen	620.6	90.0	11,219

\* 4- : heat treat number 4; 6- : heat treat number 6

\*\* Air : atmospheric air; Hydrogen 34.5 MPa hydrogen with less than 1 ppm of oxygen

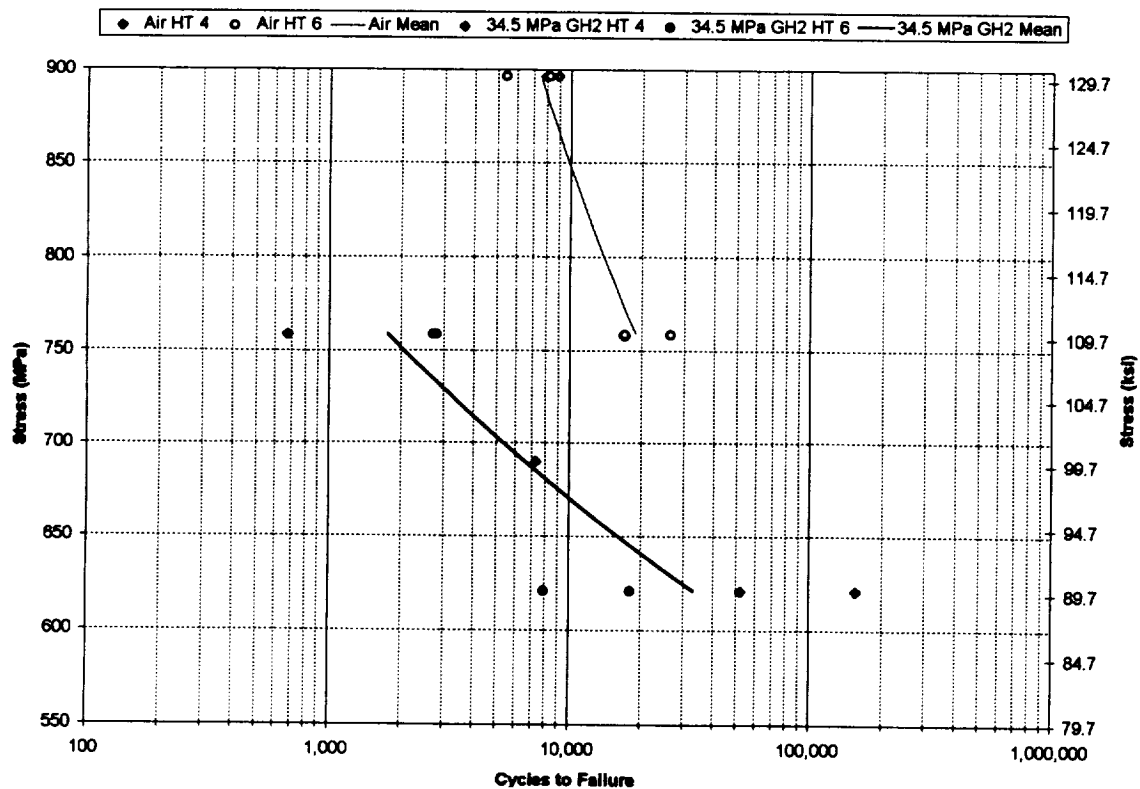


Figure 59. Load Controlled LCF Results for [001] Oriented PWA 1482 Double Notch Specimens Tested at 0.167 Hz, 20°C (68°F),  $R = 0.05$ ,  $K_t = 2.18$

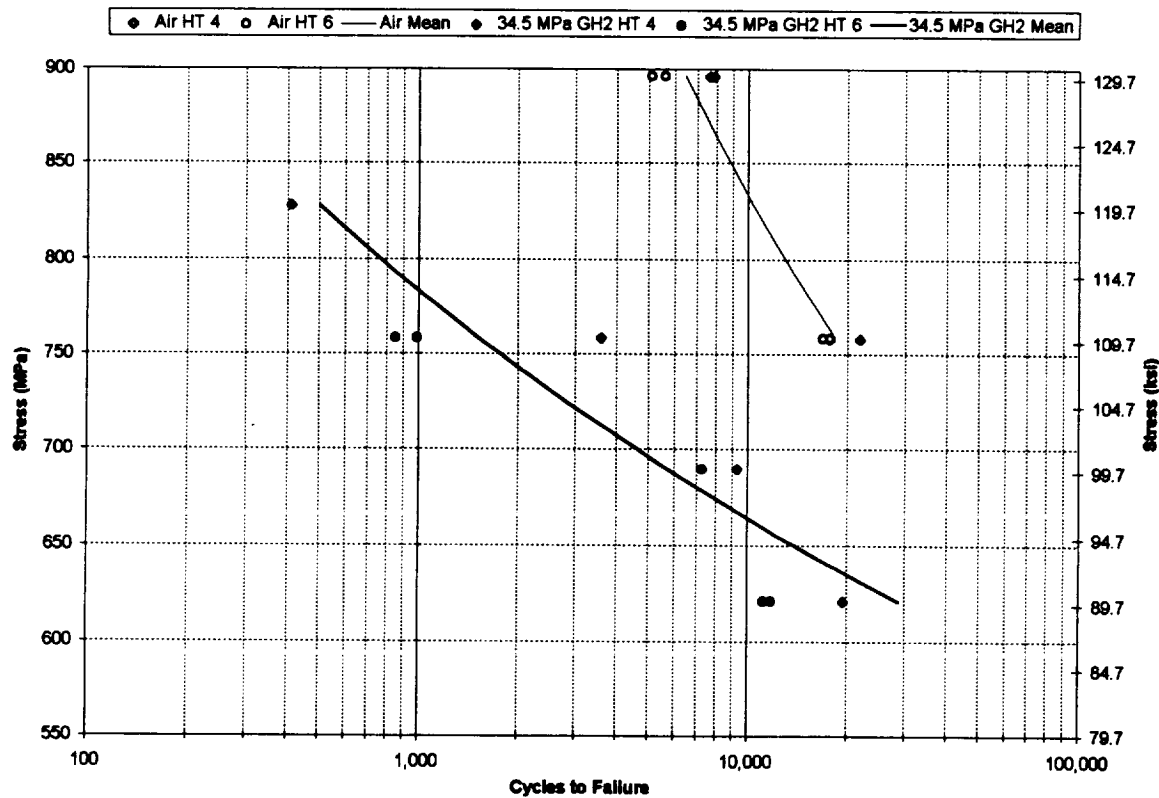


Figure 60. Load Controlled LCF Results for [001] Oriented PWA 1484 Double Notch Specimens Tested at 0.167 Hz, 20°C (68°F),  $R = 0.05$ ,  $K_t = 2.18$

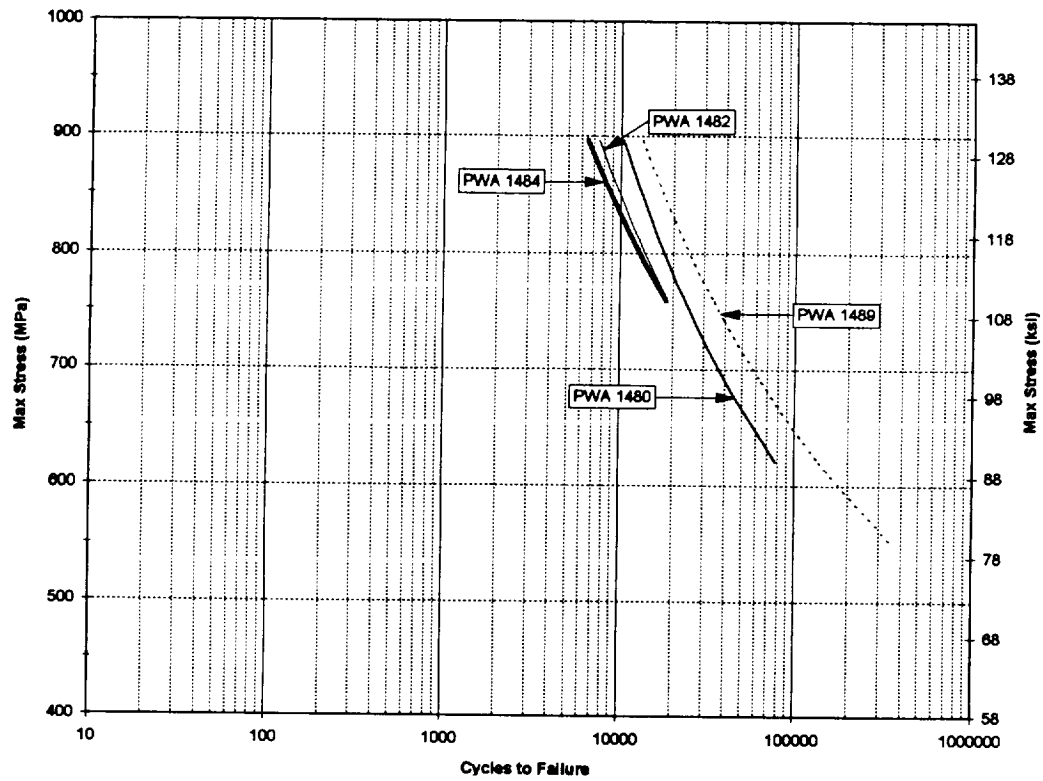


Figure 61. Alloy Comparison of Mean Curves Air Load Controlled LCF Results Double Notch Specimens Tested at 0.167 Hz, 20°C (68°F),  $R = 0.05$ ,  $K_t = 2.18$

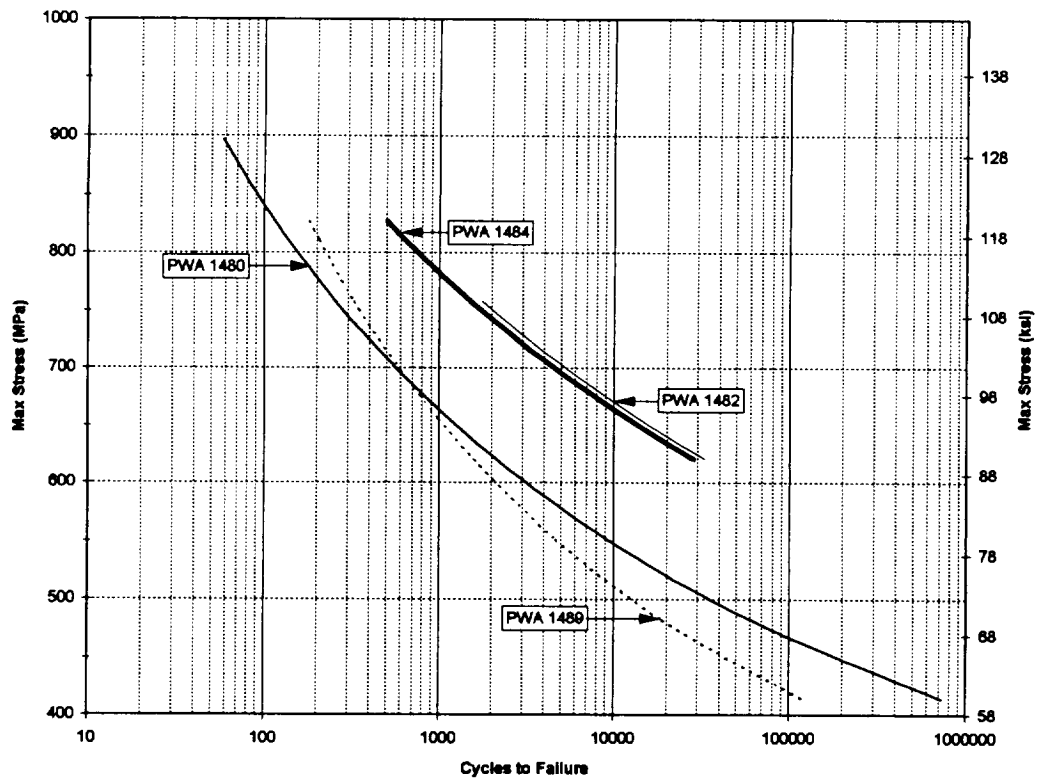


Figure 62. Alloy Comparison of Mean Curves 34.5 MPa (5 ksi) Hydrogen Load Controlled LCF Results Double Notch Specimens Tested at 0.167 Hz, 20°C (68°F),  $R = 0.05$ ,  $K_t = 2.18$

Low-cycle fatigue results for [001] oriented PWA 1482 and PWA 1484 smooth specimens, HTs 4 and 6 are shown in Tables 25 and 26 and in Figures 63 through 66. The tests were performed in atmospheric pressure air and 34.5 MPa (5 ksi) hydrogen at 20°C (68°F) with a fully reversed strain cycle ( $R = -1$ ) at a frequency of 0.167 Hz. The PWA 1482 and PWA 1484 data with mean curves regressed through both HTs are shown plotted in Figures 63 and 64, respectively. There was no significant difference in the smooth LCF properties of HTs 4 and 6, so the mean curves were regressed through the combined HT data to make distinctions only between alloy and test environment. Comparison of air and hydrogen data shows that hydrogen debits smooth fatigue properties of PWA 1482 slightly (approximately 1.5X) over the range of hydrogen data as shown in Figure 63. Air and hydrogen comparisons for PWA 1484 in Figure 64 show that the hydrogen debit is greatest at high strains and decreases for lower strain ranges (approximately 2X at 1.2 percent).

A comparison of smooth specimen LCF air mean curves for turbine blade alloys in Figure 65 shows that PWA 1484 has the best fatigue properties at 20°C (68°F), with PWA 1482 having slightly lower fatigue capabilities. Both alloys have better fatigue capability than PWA 1480 and PWA 1489 at strain ranges below 1.5 percent, but PWA 1480 starts to have better properties than PWA 1482 above 1.5 percent. In hydrogen, both PWA 1482 and PWA 1484 have significantly better fatigue capabilities than either PWA 1480 or PWA 1489 (Figure 66), but PWA 1482 has the best fatigue properties above 1.3 percent strain range.

#### **2.6.2.5 Fatigue Crack Growth**

Fatigue crack growth tests were performed on two [001] oriented PWA 1484 compact tension specimens (HTs 4 and 6). Two tests were performed on PWA 1484, rather than PWA 1482, because the matrix required a total of two crack growth tests to be performed, and PWA 1484 is being investigated as a vane material in the SSME-ATD. The tests were performed in 34.5 MPa (5 ksi) hydrogen at 20°C (68°F), with an all tensile stress cycle ( $R = 0.1$ ) at a frequency of 0.167 Hz. The test on the HT 4 specimen had to be stopped several times, which resulted in a plastic zone at the crack tip that influenced the crack growth behavior and invalidated the data. The test on HT 6 produced valid data, which is shown in Figure 67.

Data on HTs 4 and 6, generated under the SSME-ATD Program, are also included in this report for comparison. Test results are provided in Table 27 and shown in Figure 67. The PWA 1480 data and model, generated under the SSME-ATD Program, are included in Figure 67 for comparison and show that HT 6 has similar crack growth properties to PWA 1480. Heat treat 4 has significantly faster crack growth rates than HT 6 for the data shown, but starts approaching HT 6 growth rates at  $\Delta K = 4 \text{ MPa} \sqrt{\text{m}}$ , which indicates that the threshold values should be similar for the two HTs.

Table 25. Strain Controlled Results for [001] Oriented PWA 1482 Tested at 0.167 Hz, 20°C (68°F), R = -1

Specimen SN *	Environ- ment **	Strain Range (%)	Modulus		Initial				Half Life								Cycles to Failure	Comments						
			(GPa)	(msi)	Inelastic Strain (%)	Max Stress (MPa)	Min Stress (MPa)	Mean Stress (MPa)	Stress Range (MPa)	Inelastic Strain (%)	Max Stress (MPa)	Min Stress (MPa)	Mean Stress (MPa)	Stress Range (MPa)										
															(ksi)	(ksi)			(ksi)	(ksi)	(ksi)	(ksi)	(ksi)	(ksi)
4-8	Air	1.6	129	18.7	0.315	848	123	-855	-124	-3	-1	1703	247	0.078	972	141	-958	-139	7	1	1931	280	408	
4-1	Air	1.5	127	18.4	0.185	841	122	-827	-120	7	1	1669	242	0.022	924	134	-896	-130	14	2	1820	264	4,952	
4-3	Air	1.4	128	18.6	0.135	834	121	-800	-116	17	3	1634	237	0.009	910	132	-883	-128	14	2	1793	260	6,373	
4-5	Air	1.2	128	18.6	0.077	752	109	-738	-107	7	1	1489	216	0.005	758	110	-779	-113	-10	-2	1538	223	12,062	
4-2	Air	1.2	128	18.5	0.067	738	107	-717	-104	10	2	1455	211	0.007	772	112	-758	-110	7	1	1531	222	6,854	Radius failure
4-7	Air	1.1	128	18.6	0.006	710	103	-703	-102	3	1	1413	205	0.007	703	102	-710	-103	-3	-1	1413	205	54,963	
4-3	Hydrogen	1.5	131	19.0	0.073	913	132	-898	-130	8	1	1811	263	0.010	979	142	-967	-140	6	1	1946	282	1,698	Radius failure
4-1	Hydrogen	1.2	132	19.2	0.010	786	114	-725	-105	31	4	1511	219	0.003	807	117	-780	-113	13	2	1587	230	11,189	
4-5	Hydrogen	1.2	133	19.3	0.019	796	115	-778	-113	9	1	1573	228	0.010	785	114	-795	-115	-5	-1	1580	229	8,678	
6-3	Air	1.8	123	17.8	0.360	931	135	-869	-126	31	5	1800	261	0.037	1117	162	-1034	-150	41	6	2151	312	1,951	
6-8	Air	1.6	119	17.2	0.321	793	115	-772	-112	10	2	1565	227	0.033	972	141	-924	-134	24	4	1896	275	4,040	
6-6	Air	1.6	125	18.2	0.346	821	119	-800	-116	10	2	1620	235	0.104	924	134	-889	-129	17	3	1813	263	591	
6-5	Air	1.4	125	18.2	0.240	731	106	-703	-102	14	2	1434	208	0.030	876	127	-869	-126	3	1	1744	253	5,121	
6-1	Air	1.4	124	18.0	0.168	793	115	-752	-109	21	3	1544	224	0.008	889	129	-848	-123	21	3	1738	252	6,406	
6-7	Air	1.1	125	18.1	0.023	690	100	-655	-95	17	3	1345	195	0.006	696	101	-669	-97	14	2	1365	198	75,835	
6-2	Hydrogen	1.5	130	18.8	0.155	843	122	-850	-123	-4	-1	1693	246	0.009	955	139	-979	-142	-12	-2	1934	281	2,158	
6-1	Hydrogen	1.2	132	19.2	0.053	767	111	-761	-110	3	0	1528	222	0.008	784	114	-798	-115.8	-7	-1	1582	230	15,805	Radius failure
6-3	Hydrogen	1.2	133	19.3	0.059	761	110	-763	-111	-1	0	1524	221	0.008	787	114	-791	-114.7	-2	0	1578	229	12,274	

\* 4- : heat treat number 4; 6- : heat treat number 6

\*\* Air : atmospheric air; Hydrogen 34.5 MPa hydrogen with less than 1 ppm of oxygen

Table 26. Strain Controlled Results for [001] Oriented PWA 1484 Tested at 0.167 Hz, 20°C (68°F), R = -1

Specimen S/N *	Environ-ment **	Strain Range (%)	Modulus		Initial					Half Life										Cycles to Failure	Comments			
			(GPa)	(msi)	Inelastic Strain (%)	Max Stress (MPa)	(ksi)	Min Stress (MPa)	(ksi)	Mean Stress (MPa)	(ksi)	Stress Range (MPa)	(ksi)	Inelastic Strain (%)	Max Stress (MPa)	(ksi)	Min Stress (MPa)	(ksi)	Mean Stress (MPa)			(ksi)	Stress Range	
																							(MPa)	(ksi)
4-3	Air	1.6	126	18.3	0.247	889	129	-834	-121	28	4	1724	250	0.033	945	137	-821	-119	62	9	1765	256	2,003	
4-6	Air	1.6	128	18.6	0.192	910	132	-896	-130	7	1	1806	262	0.010	1034	150	-993	-144	21	3	2027	294	6,472	
4-7	Air	1.4	129	18.7	0.149	814	118	-793	-115	10	2	1607	233	0.008	910	132	-889	-129	10	2	1800	261	9,439	
4-8	Air	1.2	129	18.7	0.017	779	113	-752	-109	14	2	1531	222	0.007	793	115	-752	-109	21	3	1544	224	37,881	
4-1	Air	1.0	126	18.3	0.000	634	92	-634	-92	0	0	1269	184	0.000	648	94	-634	-92	7	1	1282	186	158,480	
4-3	Hydrogen	1.5	137	19.8	0.080	923	134	-810	-132	6	1	1833	266	0.010	969	141	-1011	-147	-21	-3	1980	287	229	
4-4	Hydrogen	1.2	136	19.7	0.017	814	118	-752	-109	31	5	1566	227	0.004	820	119	-794	-115	13	2	1613	234	5,402	
4-5	Hydrogen	1.2	138	20.0	0.015	807	117	-784	-114	11	2	1591	231	0.003	818	119	-814	-118	2	0	1631	237	25,258	Radius failure
6-7	Air	1.6	128	18.5	0.279	889	129	-841	-122	24	4	1731	251	0.009	1034	150	-993	-144	21	3	2027	284	6,492	
6-4	Air	1.5	129	18.7	0.279	821	119	-793	-115	14	2	1613	234	0.013	965	140	-945	-137	10	2	1910	277	2,771	
6-3	Air	1.4	128	18.6	0.060	752	109	-717	-104	17	3	1469	213	0.008	952	138	-841	-122	55	8	1793	260	11,767	
6-5	Air	1.3	128	18.6	0.114	779	113	-745	-108	17	3	1524	221	0.007	848	123	-814	-118	17	3	1662	241	23,411	
6-8	Air	1.3	128	18.6	0.131	765	111	-745	-108	10	2	1510	219	0.008	855	124	-807	-117	24	4	1662	241	22,880	
6-6	Air	1.2	128	18.6	0.064	752	109	-710	-103	21	3	1462	212	0.007	779	113	-752	-109	14	2	1531	222	55,561	
6-4	Hydrogen	1.5	136	19.7	0.100	827	120	-821	-119	3	1	1648	239	0.000	965	140	-986	-143	-10	-2	1951	283	273	
6-5	Hydrogen	1.2	137	19.9	0.027	767	111	-767	-111	0	0	1533	222	0.002	810	118	-818	-119	-4	-1	1628	236	32,539	Radius failure
6-6	Hydrogen	1.2	137	19.9	0.041	798	116	-785	-114	7	1	1582	230	0.002	827	120	-812	-118	8	1	1640	238	25,542	

\* 4- : heat treat number 4; 6- : heat treat number 6

\*\* Air : atmospheric air; Hydrogen 34.5 MPa hydrogen with less than 1 ppm of oxygen

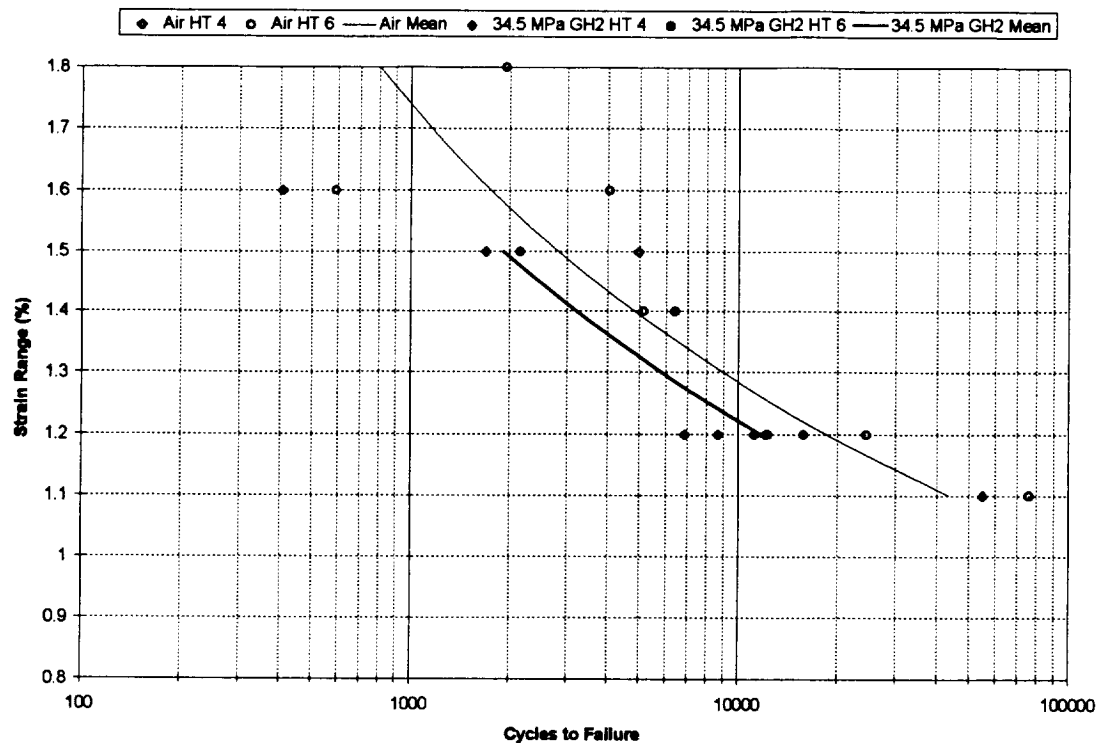


Figure 63. Strain Controlled LCF Results for [001] Oriented PWA 1482 Specimens Tested at 0.167 Hz, 20°C (68°F),  $R = -1$

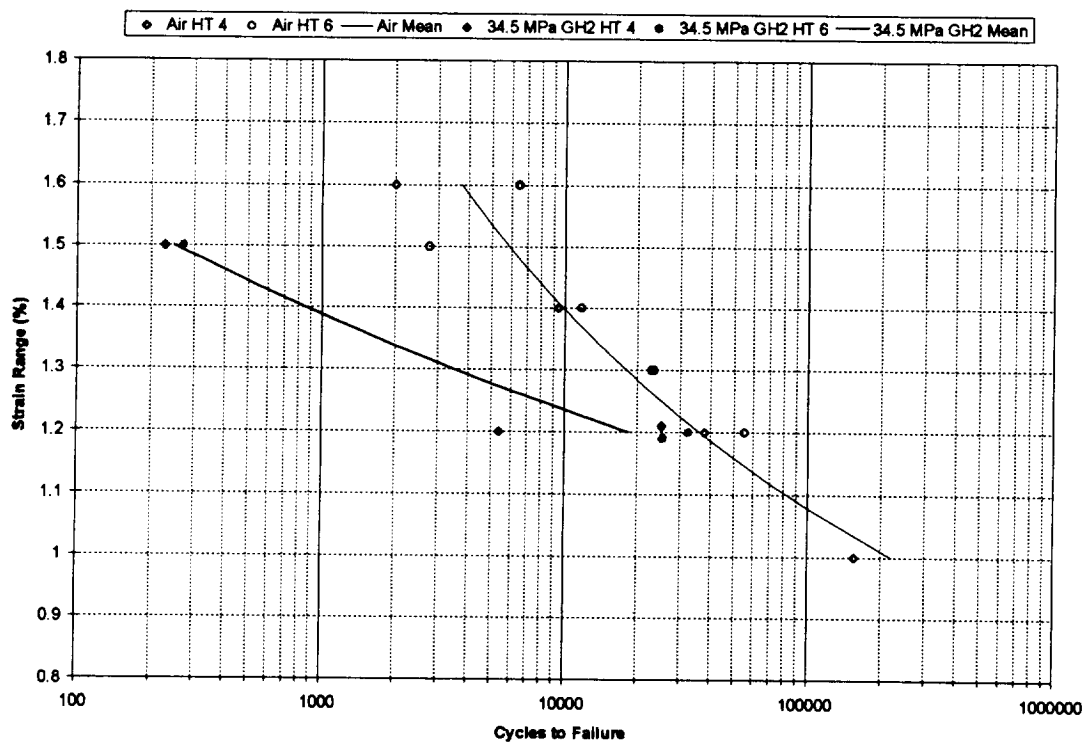


Figure 64. Strain Controlled LCF Results for [001] Oriented PWA 1484 Specimens Tested at 0.167 Hz, 20°C (68°F),  $R = -1$

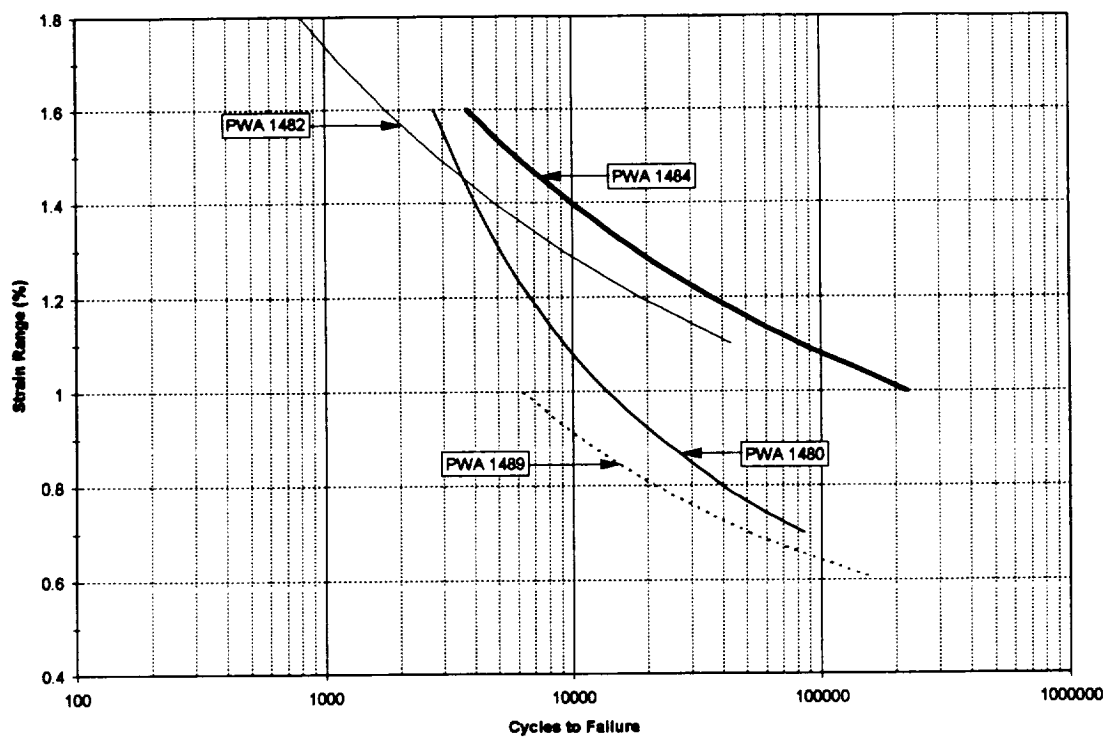


Figure 65. Alloy Comparison of Mean Curves Air Strain Control LCF Results Smooth Specimens Tested at 0.167 Hz, 20°C (68°F),  $R = -1$

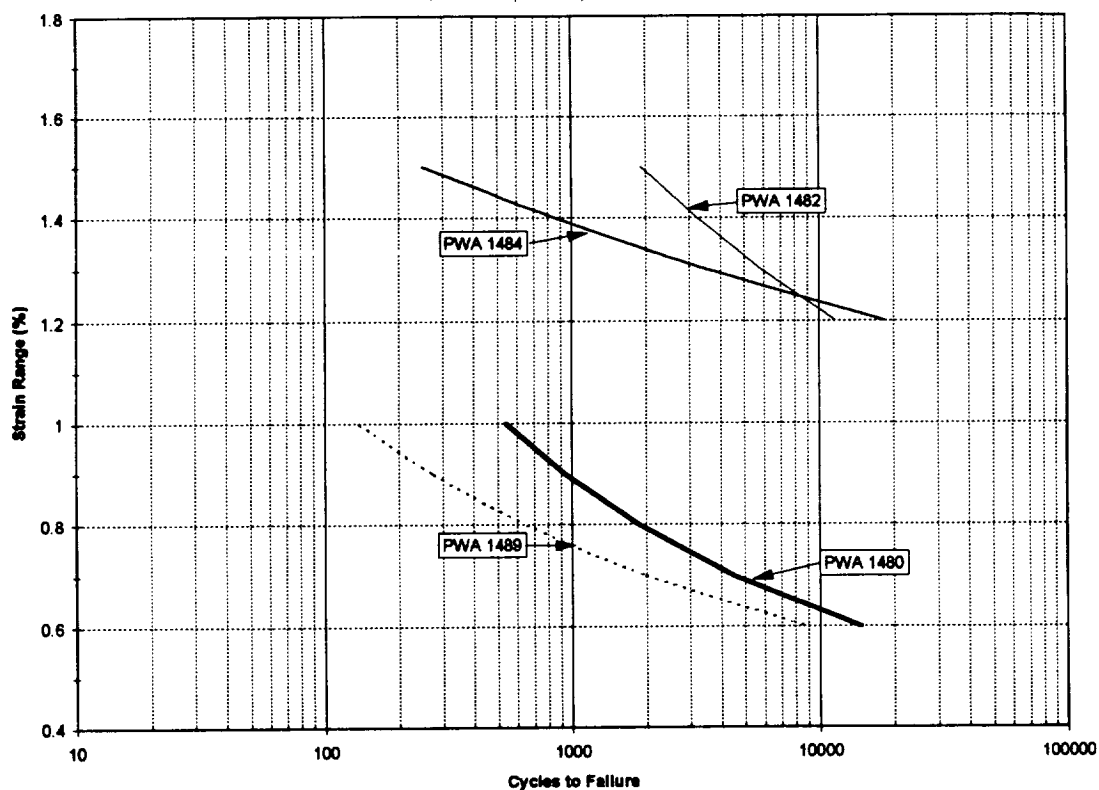


Figure 66. Alloy Comparison of Mean Curves 34.5 MPa (5 ksi) Hydrogen Strain Control LCF Results Smooth Specimens Tested at 0.167 Hz, 20°C (68°F),  $R = -1$



Table 27. Fatigue Crack Growth Testing of [001] Oriented PWA 1484 Compact Tension Specimens Tested in 34.5 MPa (5 ksi) Hydrogen at 0.167 Hz, 20°C (68°F),  $R = -1$

Specimen S/N	Heat Treat Number	Comments
4-1	4	Test shutdown resulted in invalid data due to plastic zone effects.
7253	4	Valid data generated under another program shown in Figure 67 for comparison.
6-1	6	Valid data.
7254	6	Valid data generated under another program shown in Figure 67 for comparison.
7255	6	Valid data generated under another program shown in Figure 67 for comparison.

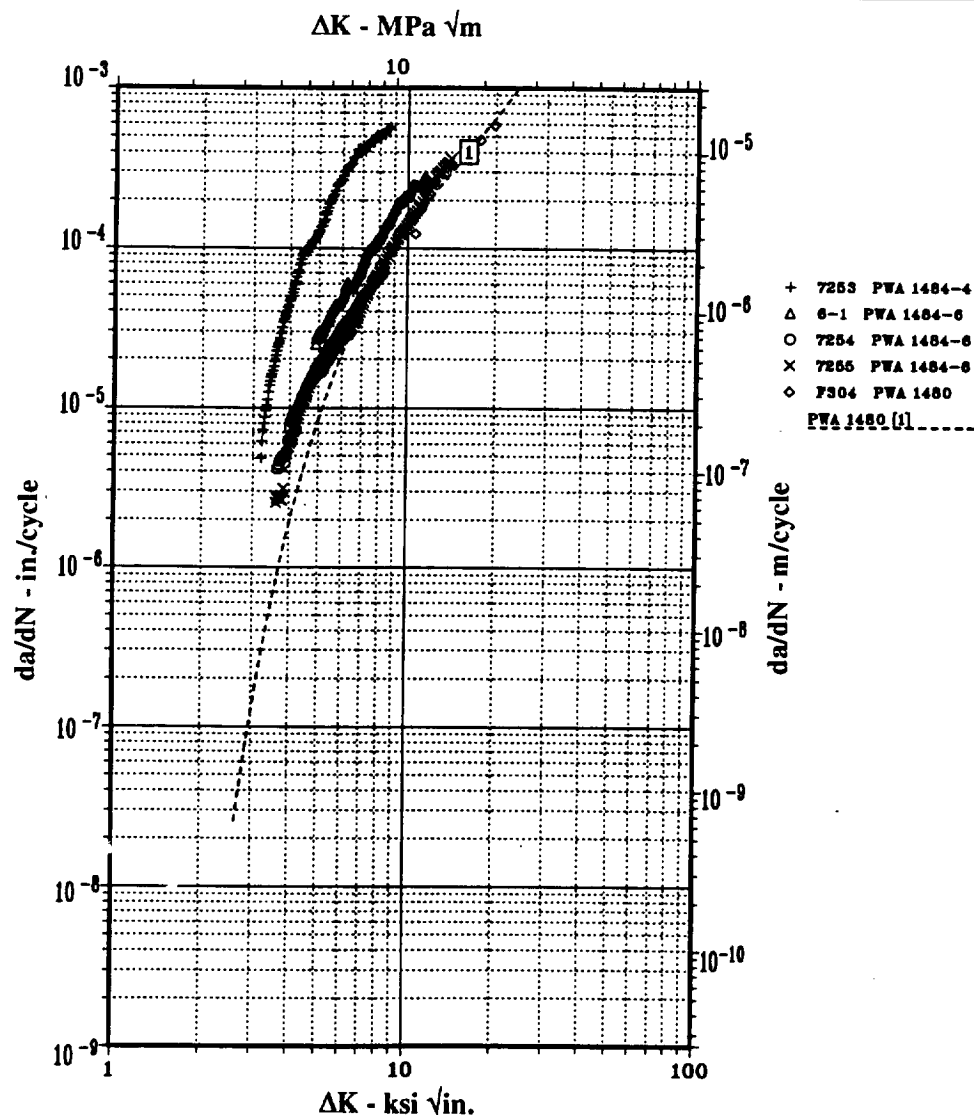


Figure 67. Fatigue Crack Growth Results for [001] Oriented PWA 1484 Tested in 34.5 MPa (5 ksi) Hydrogen at 0.167 Hz, 20°C (68°F),  $R = 0.1$  Compared to PWA 1480 Data and Model for Same Condition

## 2.6.3 Summary

Tensile properties for PWA 1482 and PWA 1484 tend to be similar to each other and are generally lower than PWA 1480 and higher than PWA 1489. At 649°C (1200°F), hydrogen did not debit the strength of the two alloys, although the ductility was reduced slightly. Creep results show that PWA 1484 has creep properties that are significantly better than PWA 1480 at 871°C (1600°F), with HT 4 exhibiting the best creep behavior. However, PWA 1482 did not have good creep properties at 871°C (1600°F), and is not recommended for applications where creep would be a concern at this temperature.

Fatigue properties were not significantly affected by HT conditions studied in this contract, so HTs 4 and 6 data were combined for analysis. High-cycle fatigue properties for both PWA 1484 and PWA 1482 in hydrogen are significantly better than properties for either PWA 1480 or PWA 1489 under the same conditions, and are even better than PWA 1480 in air. Low-cycle fatigue properties for both alloys studied in this contract are debited by hydrogen, but hydrogen LCF properties are still significantly better than PWA 1480 and PWA 1489.

Fatigue crack growth data from testing in high-pressure hydrogen show a significant difference between HT conditions in PWA 1484. The coarser microstructural morphology of HT 6 is designed to improve crack growth properties, and HT 6 is significantly better than HT 4 with the finer microstructure. In comparison to PWA 1480, PWA 1484, HT 6 has similar crack growth properties to PWA 1480 at 20°C (68°F).

## 2.7 MICROSTRUCTURAL AND FRACTOGRAPHIC ANALYSIS

### 2.7.1 Introduction and background

Fundamental aspects of alloy structure play an important role when considering hydrogen embrittlement mechanisms. Cast  $\gamma'$  strengthened alloys, such as single-crystal PWA 1480 and directionally solidified (DS) MAR-M-246+Hf, are currently used in turbopump hot section applications, where hydrogen embrittlement is a problem. The  $\gamma'$  strengthening precipitate in these alloys is composed of alloyed  $\text{Ni}_3\text{Al}$  with  $\text{L}_{12}$  order, assuming a cuboidal morphology geometrically ordered in the matrix. The cube edges are aligned with the  $\langle 001 \rangle$  directions.

The effects of hydrogen on the fatigue and fracture characteristics of cast Ni based superalloys have been the subject of intensive research for decades. The mechanisms of hydrogen degradation vary depending on, among other things, the alloy class ( $\gamma, \gamma'$ ), casting form, DS, single-crystal, equiaxed, and the particular mechanical property in question (fatigue, crack growth).

Frequently, degradation is the result of a microscopic fracture mode transition (e.g., transgranular to intergranular), resulting from perhaps hydrogen induced changes in dislocation mobility.<sup>11</sup>

Recent studies<sup>12</sup> conducted by P&W examined hydrogen degradation mechanisms in several cast  $\gamma'$  strengthened alloys. One of these investigations focused on PWA 1480 and DS MAR-M-246+Hf. Low-cycle fatigue (LCF) and fatigue crack growth (FCG) specimens that were tested in a high-pressure (34.5 MPa [5 ksi]) hydrogen environment were compared to specimen fractures produced in air. Test results indicated that the maximum hydrogen-to-air debit for both alloys occurs at 20°C (68°F). Notched LCF tests were the most sensitive indicator of degradation, so these specimens were chosen for review to obviate any differences between air and hydrogen fracture details.

Both alloys showed fatigue crack initiations at the normally benign eutectic  $\gamma/\gamma'$ , and both alloys also experience a hydrogen induced fracture mode transition from microscopic (111) fracture on the  $\gamma'$  precipitate level in air to localized fracture substantially confined to the  $\gamma$  matrix or the  $\gamma/\gamma'$  interface in hydrogen.

Matrix failure also occurs in the near threshold region of FCG when testing PWA 1480 in room temperature air.<sup>13</sup> This fracture mode remains operative at much higher stress intensities in the presence of high-pressure hydro-

<sup>11</sup> DeLuca, D.P. and Cowles, B.A.; *Fatigue and Fracture of Single-Crystal Nickel in High-Pressure Hydrogen*; Hydrogen Effects on Material Behavior; Moody, N.R. and Thompson, A.W., eds., TMS, Warrendale, Pa, 1989, pp 703-716.

<sup>12</sup> *SSME Alternate Turbopump Development Program*, NASA-MSFC Contract NAS8-36801.

gen,<sup>14</sup> resulting in more than an order of magnitude increase in FCG rate. Extrapolating the near threshold FCG air behavior to 20 MPa  $\sqrt{\text{m}}$  will accurately predict the hydrogen growth rate because the microscopic fracture mode operative in hydrogen is the same (Figure 68).

Crack growth rate was significantly reduced in PWA 1480 with the development of bimodal  $\gamma'$  structures in 1991<sup>15</sup> (Figure 69).

Fatigue capability was restored, once the source of LCF and HCF degradation in hydrogen was recognized. A solution was readily apparent (full  $\gamma'$  solutioning), and the effect on fatigue through the elimination of the eutectic  $\gamma/\gamma'$  was demonstrated with PWA 1482 in 1988.<sup>16</sup>

The eutectic-free bimodal  $\gamma'$  microstructures evaluated in this program were an outgrowth of that research.

The mechanisms by which fracture resistance is achieved is important, since the effects of hydrogen were reversed by a partial restoration of the normal air fracture mode. Several possible explanations exist, and microstructural/fractographic analysis has concentrated on understanding how this change has occurred in order to extend this approach to other alloy systems.

Consequently, this section on fractographic and microstructural analysis has, in addition to documenting test specimen failure modes, focussed on collecting information relating macroscopic behavior to microstructure and micromechanisms.

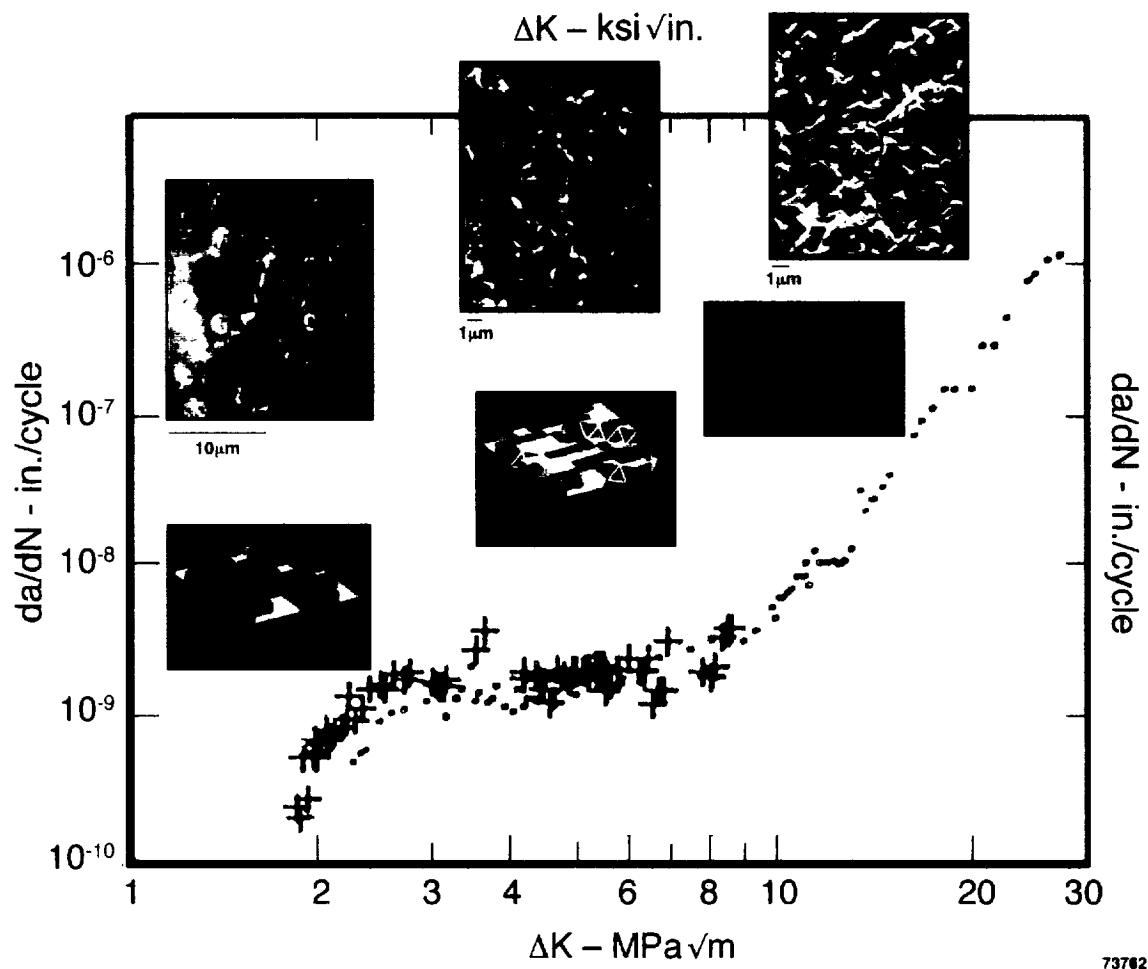
---

<sup>13</sup> Telesman, J. and Ghosn, L.J.; *Accelerated Fatigue Crack Growth Behavior of PWA 1480 Single-Crystal Alloy and Its Dependence on the Deformation Mode*; NASA LeRC, Cleveland, OH; NASA TM 100943; June 1988.

<sup>14</sup> Telesman, J., Ghosn, L.J., and DeLuca, D.P.; *Influence of the Failure Mode on Fatigue Crack Growth Behavior in Single Crystal Alloys*, Hydrogen Effects on Material Behavior; Moody, N.R. and Thompson, A.W., eds.; TMS., Warrendale, Pa, 1994 (To Be Published).

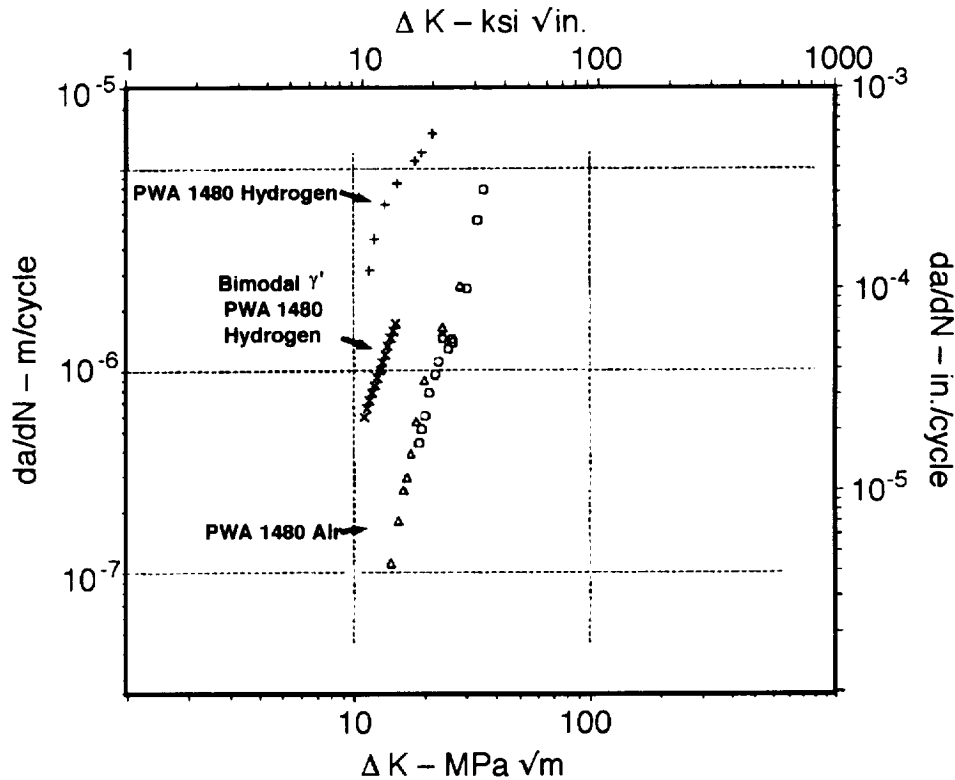
<sup>15</sup> DeLuca, D.P., Jones, H.B., Cowles, B.A., and Cobia, F.D.; *Second Workshop on Hydrogen Effects on Materials in Propulsion Systems*; Proceedings of a Conference Held at NASA-MSFC, Huntsville Alabama, 20-21 May 1992; NASA CP-3182.

<sup>16</sup> DeLuca, D.P. and Cowles, B.A.; *Hydrogen Degradation Mechanisms in Single Crystal Nickel*; Hydrogen Effects on Material Behavior, Moody, N.R. and Thompson, A.W., eds., TMS., Warrendale, Pa, 1994, (To be published).



73762

Figure 68. Microscopic Fracture Modes Dictate Crack Growth Behavior in Single-Crystals; Matrix Failure Prevails in Near Threshold Region (Left) and Is Shown Idealized and Fractographically Above the Data; In Region II, Propagation Is by Microscopic (111) Failure On the Size Order of the  $\gamma'$  Precipitate



73763

Figure 69. Partially Restoring Normal Air Fracture Mode in PWA 1480 Under Hydrogen Embrittlement Conditions Has a Pronounced Effect on Crack Growth Rate in Hydrogen

### 2.7.2 PWA 1484 Tensile Fractures

The alternate microstructure screening task included tensile tests on one of the two program alloys (PWA 1484) with seven variations in  $\gamma$  morphology applied to the basic HIP eutectic-free microstructure. Limited room temperature testing was conducted in high-pressure hydrogen. Post-test examination of these tensile fractures produced with HTs 1 through 7 are summarized below:

- *Heat Treatment 1* – Both specimens exhibited classic matrix failure (Figure 70), highly reflective, appearing as does standard PWA 1484. Matrix failure appears macroscopically parallel to (001), but has been shown by Bernstein<sup>17</sup> *et. al.* to be microscopic (111) failure confined to the  $\gamma$  matrix. Areas of microscopic (111) fracture were also present. Significant plastic deformation on the gage section outside diameter adjacent to fracture is consistent with good ductility.
- *Heat Treatment 2* – Tensile fractures (Figure 71) were similar to HT 1, but for a less ductile appearance at the gage section outside diameter.
- *Heat Treatment 3* – Failure in both specimens originated at the surface intersection of prominent (111) crystallographic plane. Propagation continued along (111). The outside diameter of the gage section surface adjacent to the fracture showed some plastic deformation.

<sup>17</sup> Bernstein, I.M. and Dollar, M.; *Hydrogen Effects on Material Behavior*; Moody, N.R. and Thompson, A.W., eds.; TMS, Warrendale, PA, 1989, pp 603-613.

- *Heat Treatment 4* – Both specimens showed macroscopic/noncrystallographic failure origins at reflective areas consisting of microscopic (111) failure of the cuboidal  $\gamma'$  and of the failure parallel to (001) in primary  $\gamma$  (Figure 72 through 75). This becomes less coherent transitioning to more (111) crystallographic fracture as stress intensity increases. On the fracture surface, lenticular cracks (secondary cracks parallel to the loading axis) were noted. Lenticular cracking is typical of hydrogen fractures in single-crystal, columnar grain, and equiaxed cuboidal  $\gamma'$  strengthened cast Ni base superalloys. These cracks occur parallel to (001) crystallographic planes, preferentially in the matrix phase. Examples of this type of cracking in the equiaxed alloy HIP Microcast Mar-M-247 and DS MAR-M-246+Hf are shown in Figures 76 and 77.
- *Heat Treatment 5* – Both tensile fractures showed noncrystallographic origins similar to Heat Treatment 4.
- *Heat Treatment 6* – Both specimens showed macroscopic/noncrystallographic failure origins at reflective areas consisting of submicroscopic (111) failure of the cuboidal  $\gamma'$  and of the failure parallel to (001) in primary  $\gamma$  (Figure 78 and 79). This becomes less coherent, but not macroscopic/crystallographic, as in HT 4. Lenticular cracks were present in the high-stress intensity areas of the fractures.
- *Heat Treatment 7* – These fractures showed noncrystallographic origin at matrix failure transitioning to (111) fracture.

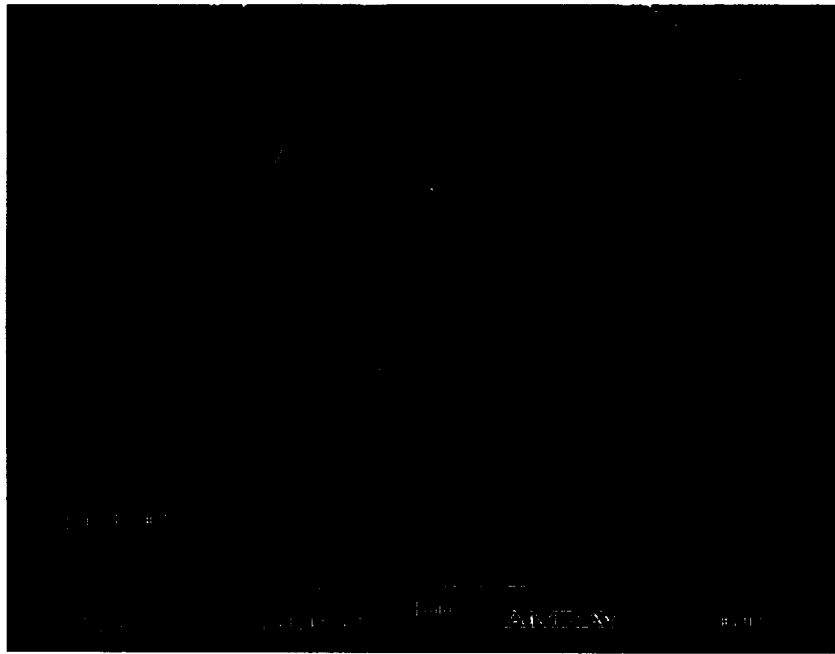


*Figure 70. Overall View of PWA 1484 HT 1; Fracture Origin (Center of Photo) Is Matrix Failure; Conditions – PWA 1484 HT 1, 20°C (68°F), 34.5 MPa (5 ksi), Hydrogen, Tensile*



Figure 71. Overall View of PWA 1484 HT 2; Fracture Origin Is at Streaks of Matrix Failure;  
Conditions – PWA 1484 HT 2, 20°C (68°F), 34.5 MPa (5 ksi), Hydrogen, Tensile

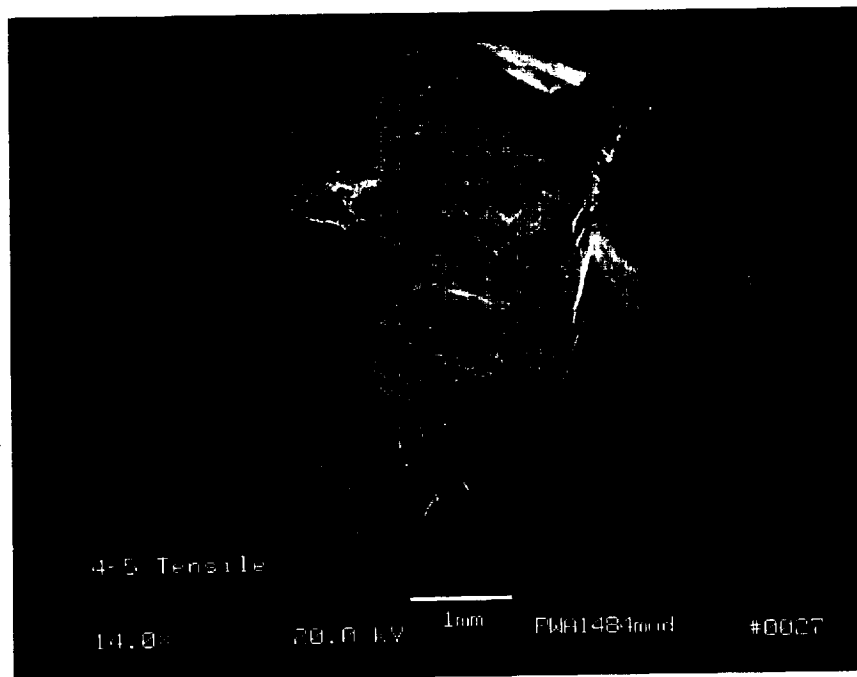
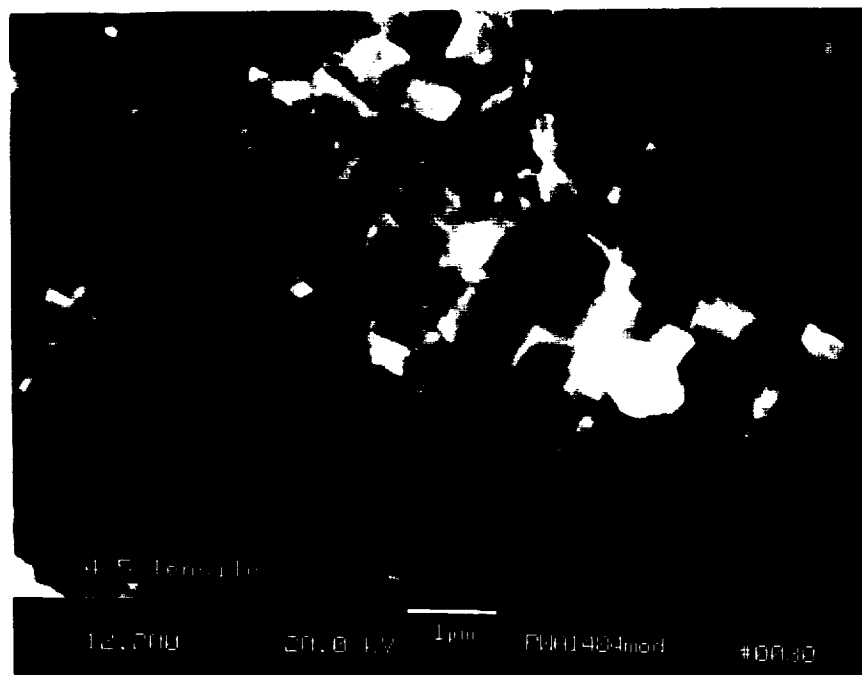
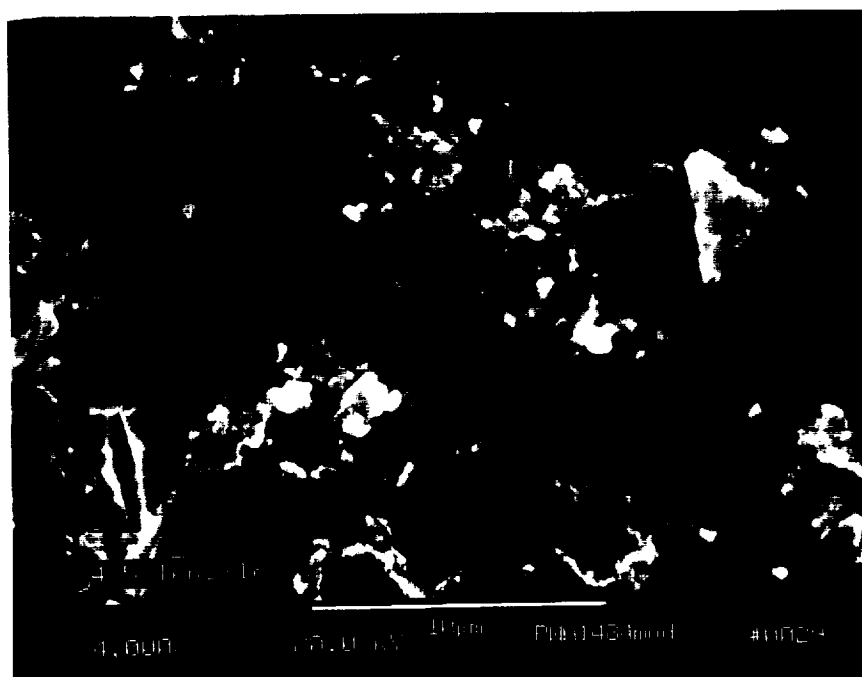


Figure 72. Overall View of PWA 1484 HT 4; Fracture Is Noncrystallographic (Macroscopically) (Note Lenticular Crack at Upper Right); Conditions – PWA 1484 HT 4, 20°C (68°F), 34.5 MPa (5 ksi) Hydrogen, Tensile



*Figure 73. Flat Fracture Nominally Parallel to (001) Occurs in Primary  $\gamma'$  Microscopic (111) Fracture Occurs in Surrounding Cuboidal  $\gamma'$ ; Conditions – PWA 1484 HT 4, 20°C (68°F), 34.5 MPa (5 ksi) Hydrogen, Tensile*



*Figure 74. Fine Lenticular Cracking in Same Specimen Is Nominally Parallel To (001) and in Some Cases Can Be Resolved as Interprecipitate; Conditions – PWA 1484 HT 4, 20°C (68°F), 34.5 MPa (5 ksi) Hydrogen, Tensile*



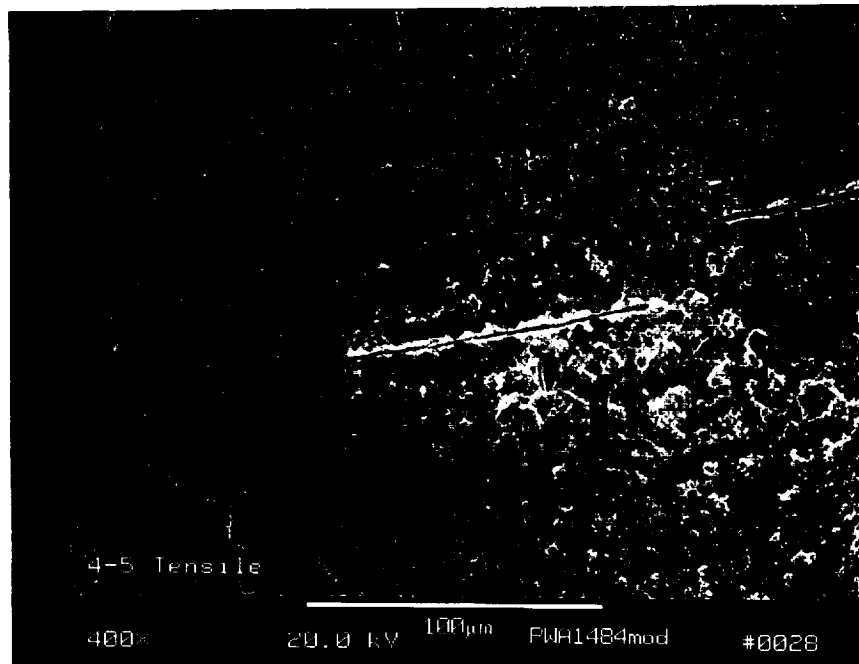


*Figure 75. Larger Cracks in Same Specimen; Onset of this Form of Cracking Appears To Be Stress Intensity Dependent; Conditions – PWA 1484 HT 4, 20°C (68°F), 34.5 MPa (5 ksi) Hydrogen, Tensile*

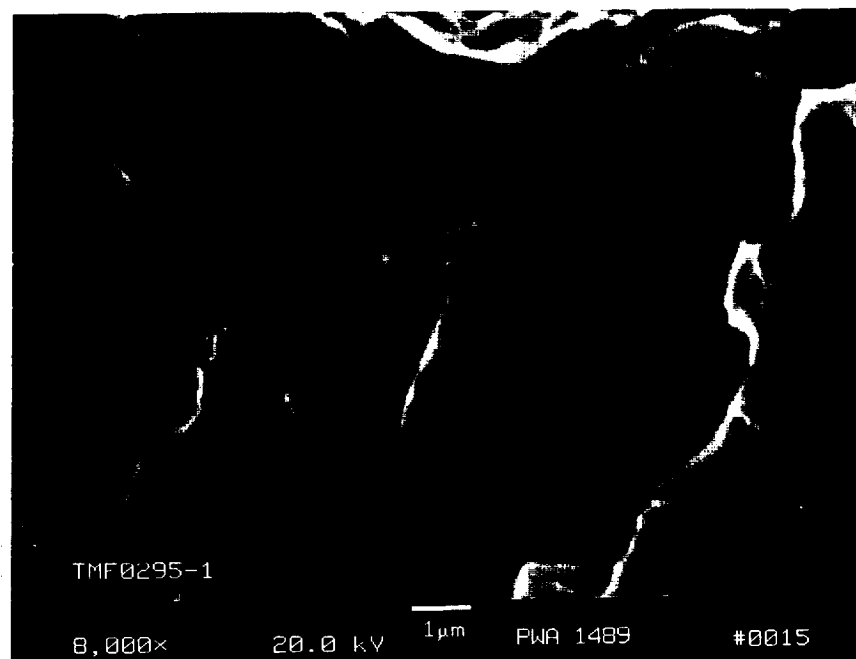


*Figure 76. Lenticular Cracking in Cast  $\gamma'$  Superalloys in Hydrogen; This Example is Equiaxed Alloy, HIP Microcast MAR-M-247 (Notched LCF in 34.5 MPa (5 ksi) Hydrogen, 20°C (68°F))*

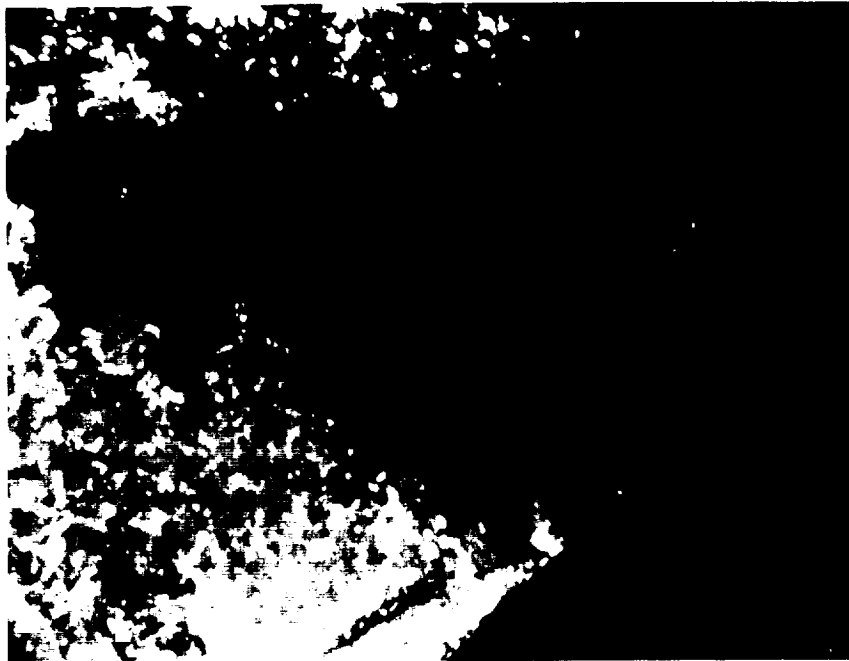


*Figure 77. Lenticular Cracking in DS MAR-M-246+Hf (Notched LCF in 34.5 MPa [5 ksi] Hydrogen, 20°C [68°F]) Showing Prominent Lenticular Cracks*

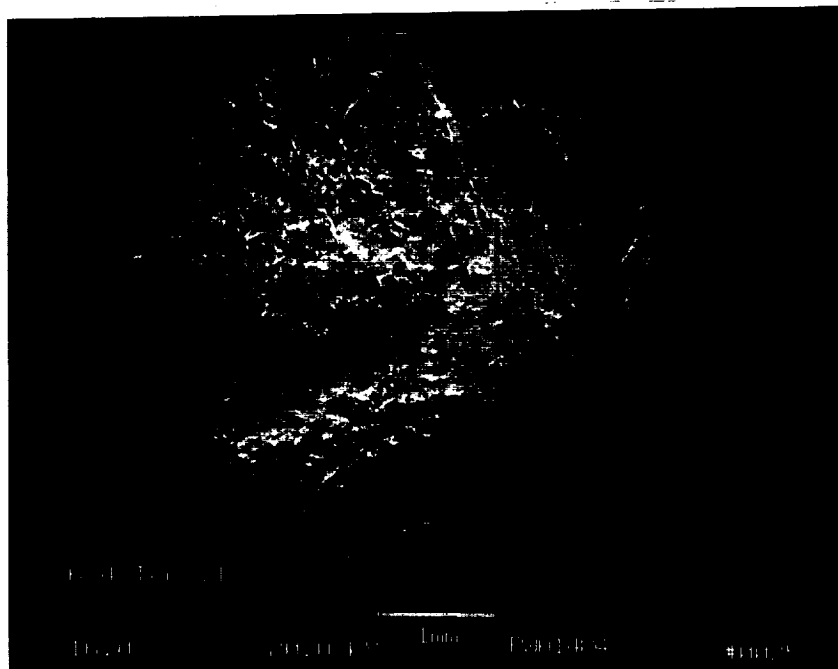


*Figure 78. Overall View of PWA 1484 HT 6; Fracture Is Noncrystallographic (Macroscopically); Conditions – PWA 1484 HT 6, 20°C (68°F), 34.5 MPa (5 ksi) Hydrogen, Tensile*

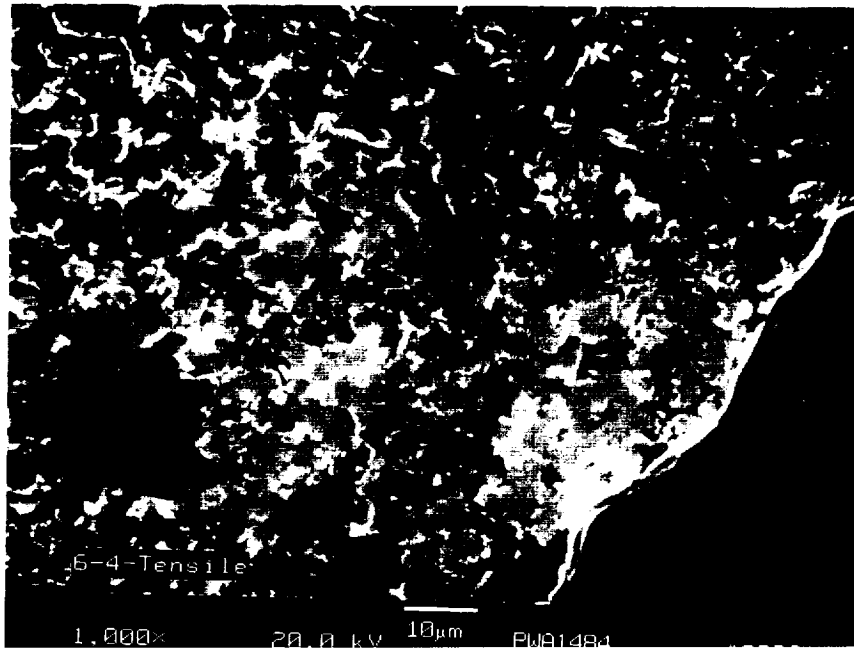


*Figure 79. Detail of  $\gamma'$  Fracture Nominally Parallel to (001), But Decidedly Rough (Increased Crack Path Tortuosity), Microscopic (111) Fracture Outlines Primary  $\gamma'$ ; Conditions – PWA 1484 HT 6, 20°C (68°F), 34.5 MPa (5 ksi) Hydrogen, Tensile*

Examinations of room temperature air tensile fractures from PWA 1484 HTs 4 and 6 are shown in Figures 80 through 84.

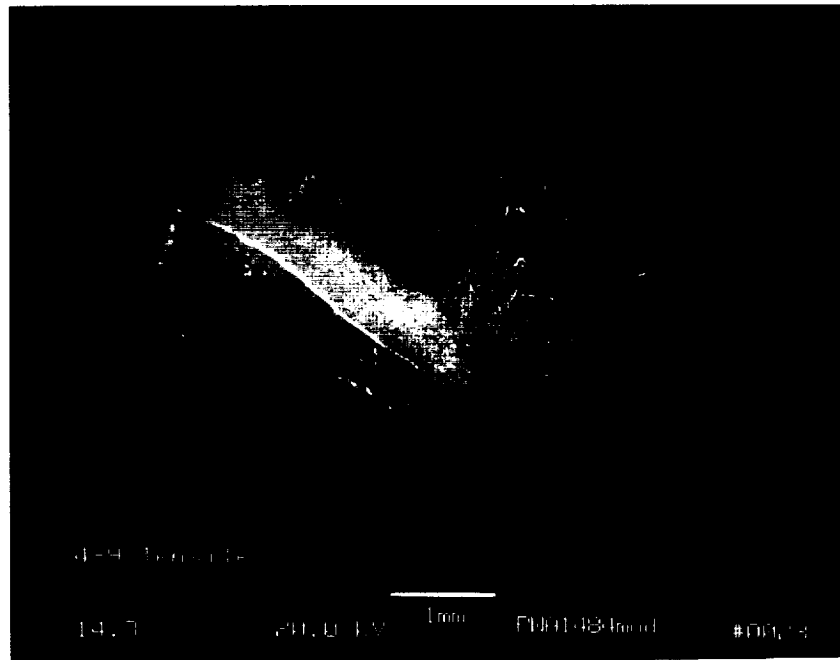


*Figure 80. Overall View of PWA 1484 HT 4 Tested in Air at Room Temperature Showing Prominent Macroscopic (111) Planes; Conditions – PWA 1484 HT 4, 20°C (68°F), Air, Tensile*

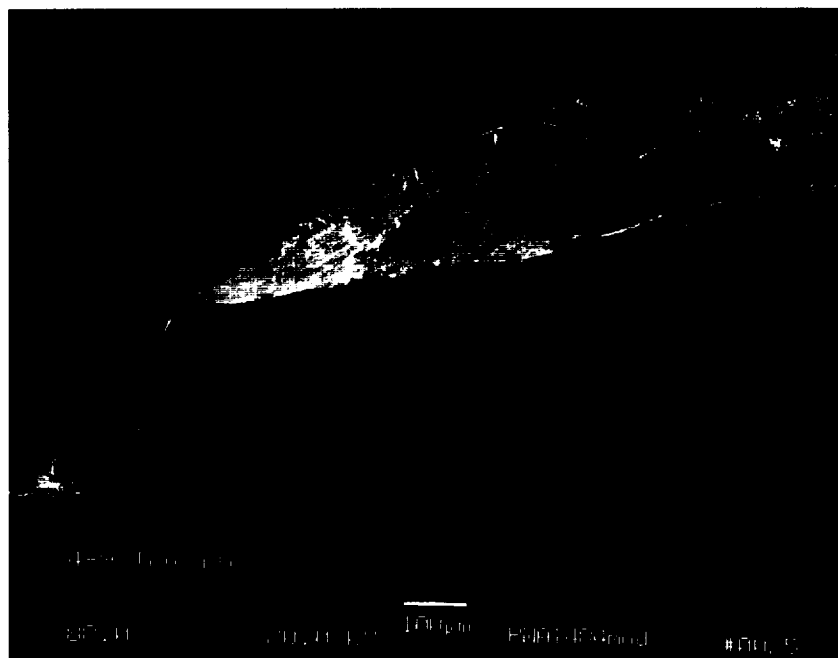


*Figure 81. Detail of Crystallographic Fracture Plane From Previous Fracture, Nominally Parallel to (111); Conditions – PWA 1484 HT 4, 20°C (68°F), Air, Tensile*

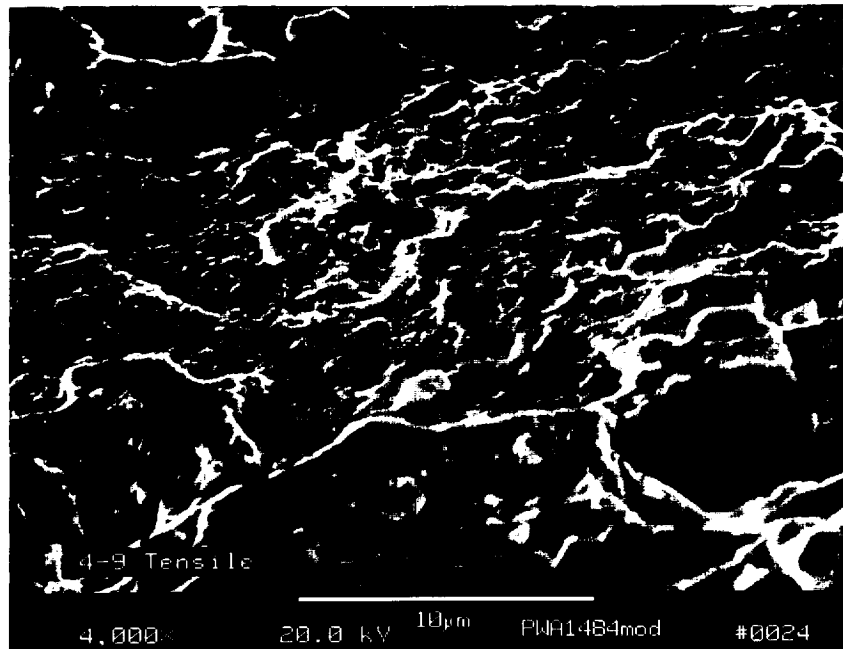


*Figure 82. High-Magnification View of (111) Fracture Surface Shows More Roughness Than Conventional Microstructures Exhibit; Conditions – PWA 1484 HT 4, 20°C (68°F), Air, Tensile*

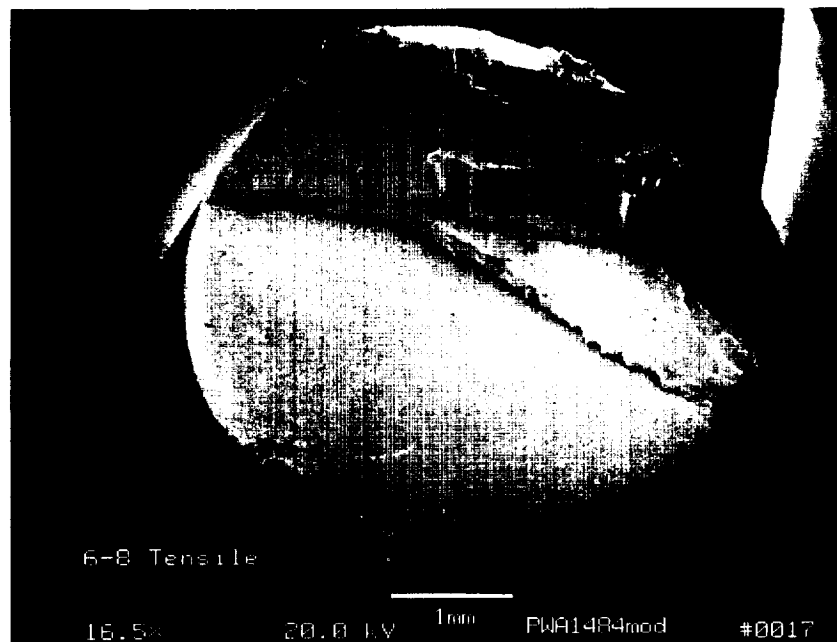


*Figure 83. Overall View of PWA 1484 HT 6 Tested in Air at Room Temperature Showing Prominent Macroscopic (111) Planes; Conditions – PWA 1484 HT 6, 20°C (68°F), Air, Tensile*

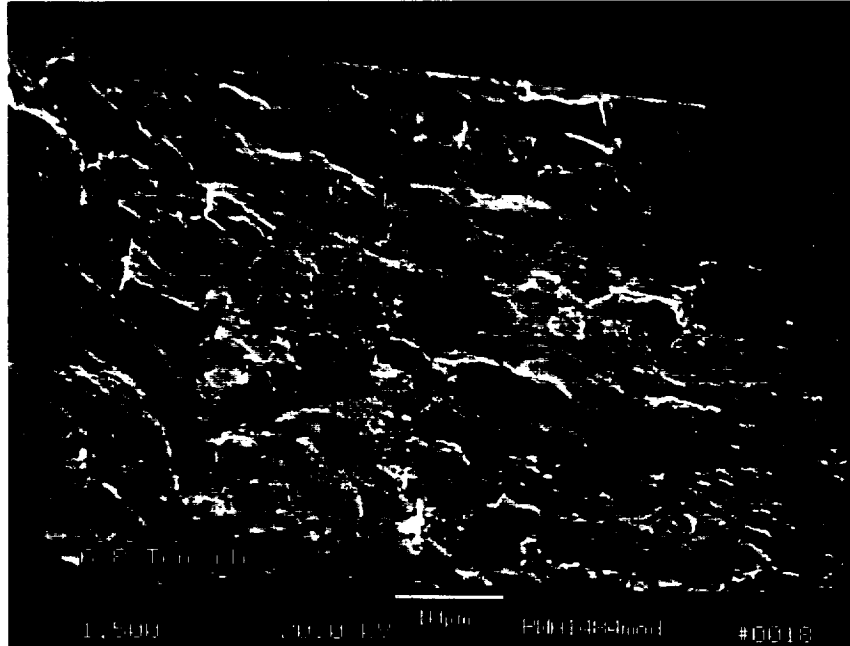


*Figure 84. High-Magnification View of (111) Fracture Surface Shows High Degree of Roughness Versus Conventional Microstructures; Conditions – PWA 1484 HT 6, 20°C (68°F), Air, Tensile*

Elevated temperature (871°C [1600°F]) tensile fractures produced in air for PWA 1484 HTs 4 and 6 are shown in Figures 85 through 89.

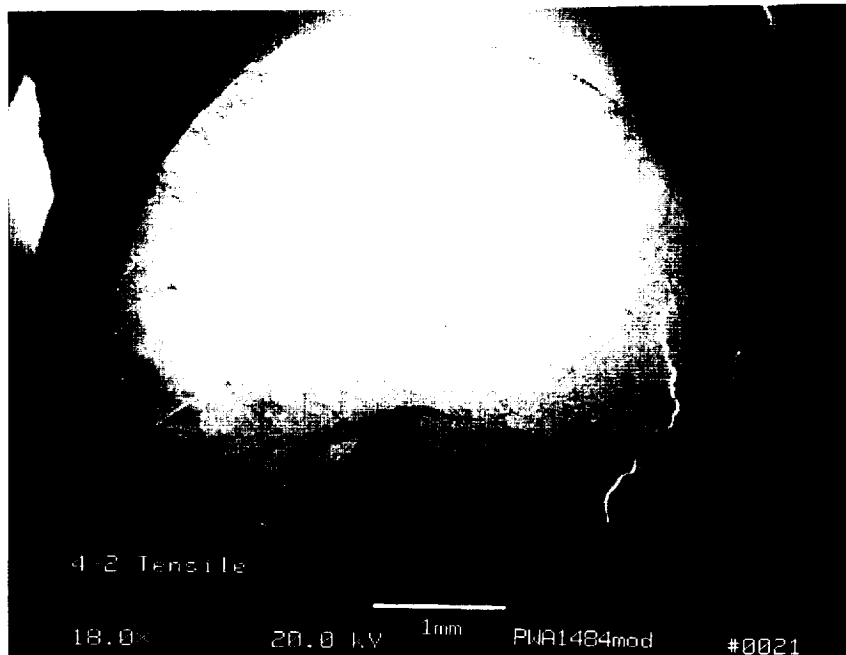


Figure 85. Overall View of PWA 1484 HT 4 Tested in Air at Room Temperature Showing Single (111) Planar Fracture; Conditions – PWA 1484 HT 4, 650°C (1200°F), Air, Tensile

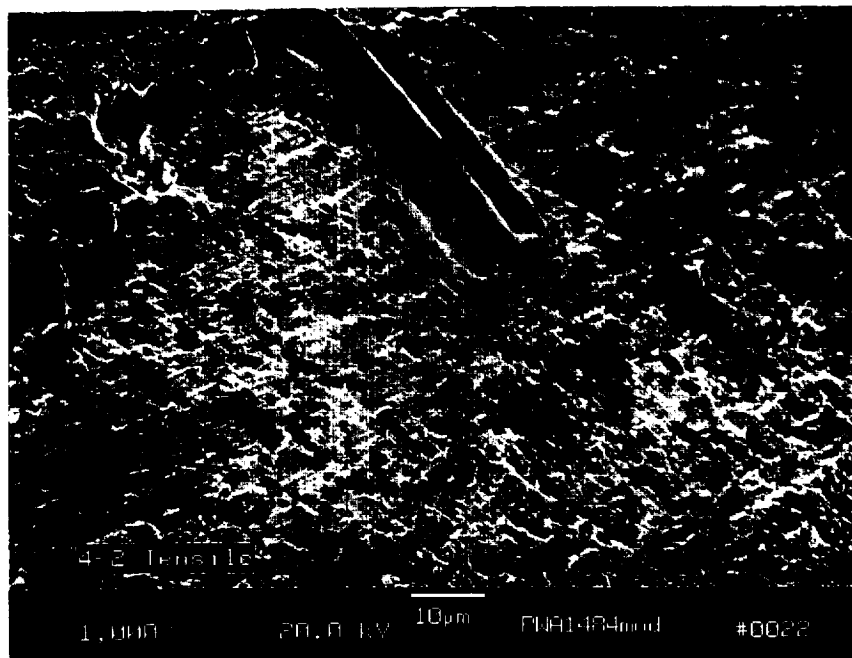
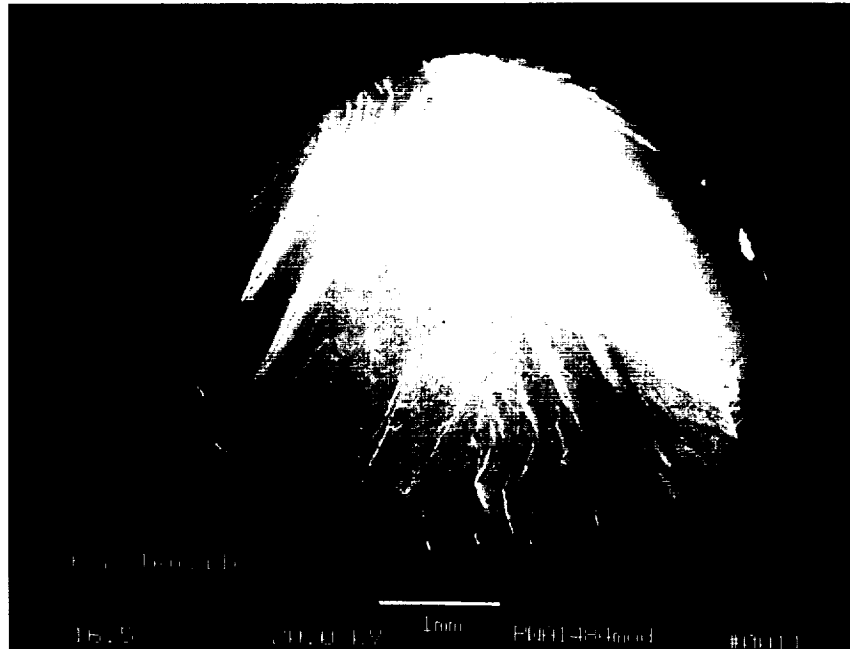
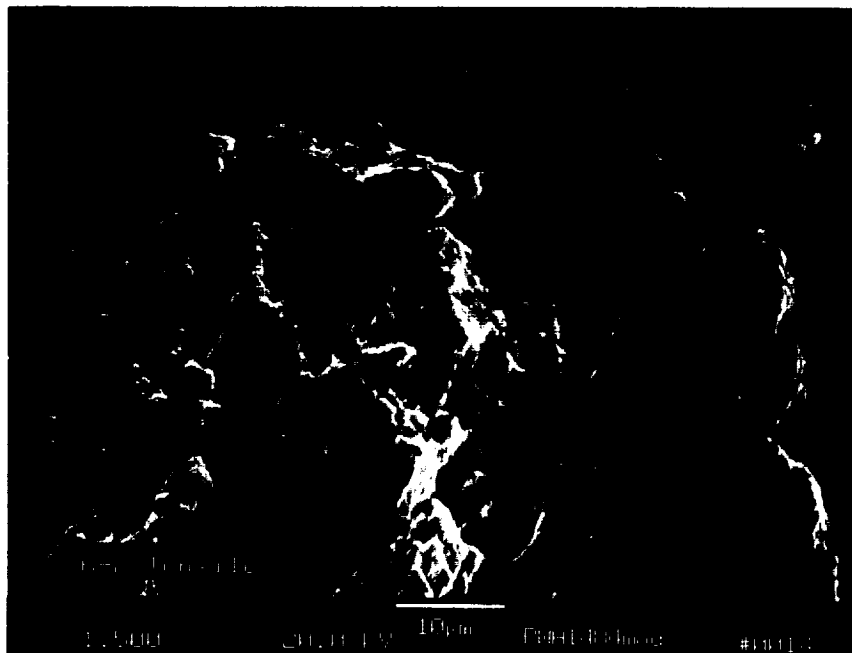


Figure 86. High-Magnification View of (111) Fracture Surface Shows Oxidized  $\gamma$  Phase and Roughness Associated With Bimodal  $\gamma'$ ; Conditions – PWA 1484 HT 4, 650°C (1200°F), Air, Tensile



*Figure 87. Overall View of PWA 1484 HT 6 Tested in Air at 650°C (1200°F) Showing Two Intersecting (111) Fracture Planes (Typical of Elevated Single-Crystal Tensile Failures); Conditions – PWA 1484 Microstructure HT 6, 650°C (1200°F), Air, Tensile*



*Figure 88. Detail of (111) Fracture Surface Shows Oxidized  $\gamma$  Phase and Marked Roughness; Conditions – PWA 1484 HT 6, 650°C (1200°F), Air, Tensile*



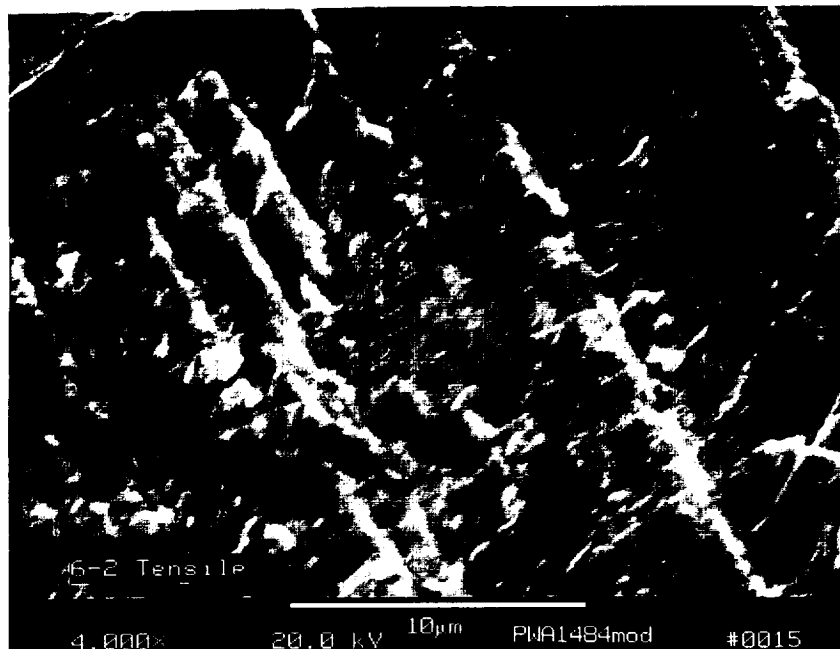


*Figure 89. High-Magnification Study of (III) Fracture Surface Shows Unoxidized Primary  $\gamma'$  and Marked Roughness; Conditions – PWA 1484 HT 6, 650°C (1200°F), Air, Tensile*

Examinations of 650°C (1200°F) hydrogen tensile fractures from PWA 1484 HTs 4 and 6 are shown in Figures 90 through 94.



*Figure 90. Overall View of PWA 1484 HT 6 Tested in 650°C (1200°F) Hydrogen Showing Prominent Macroscopic (111) Planes Intersecting at Center of Specimen; Overall Appearance Does Not Differ From 650°C (1200°F) Air Fracture; Conditions – PWA 1484 HT 6, 650°C (1200°F), Hydrogen, Tensile*

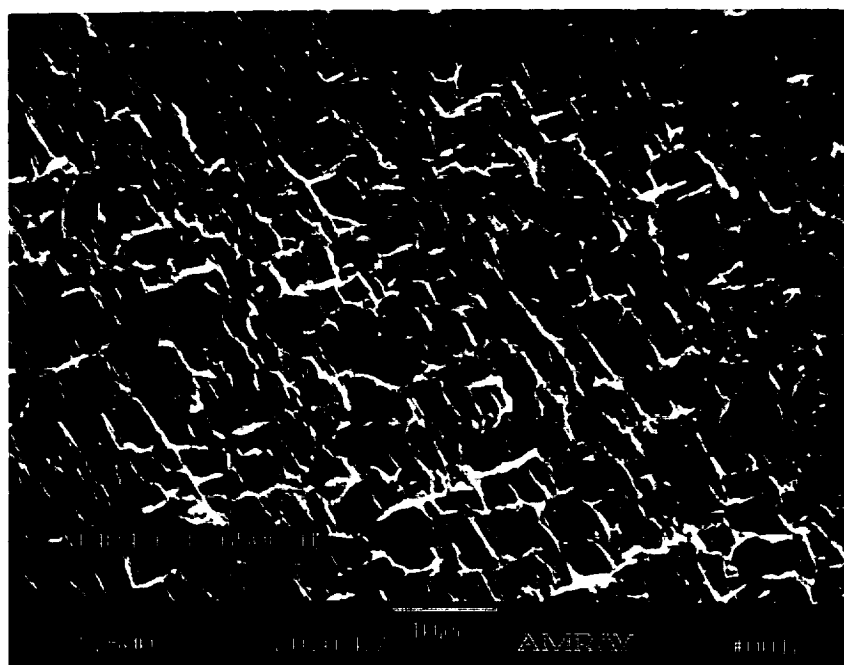


*Figure 91. High-Magnification View of (111) Fracture Surface Shows High Degree of Ductility in  $\gamma$  Phase Versus 650°C (1200°F) Air Tests; Conditions – PWA 1484 HT 6, 650°C (1200°F) Hydrogen, Tensile*

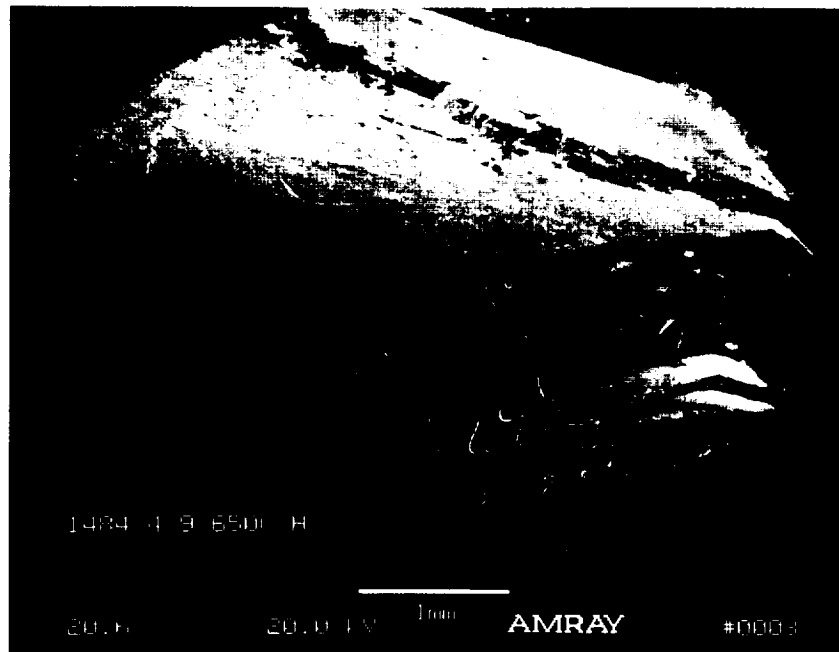


*Figure 92. Overall View of PWA 1484 HT 4 Tested in 650°C (1200°F) Hydrogen Showing Prominent Macroscopic (111) Planes and Steps (Detailed in Subsequent Figures; Conditions – PWA 1484 HT 4, 650°C (1200°F), Hydrogen, Tensile*

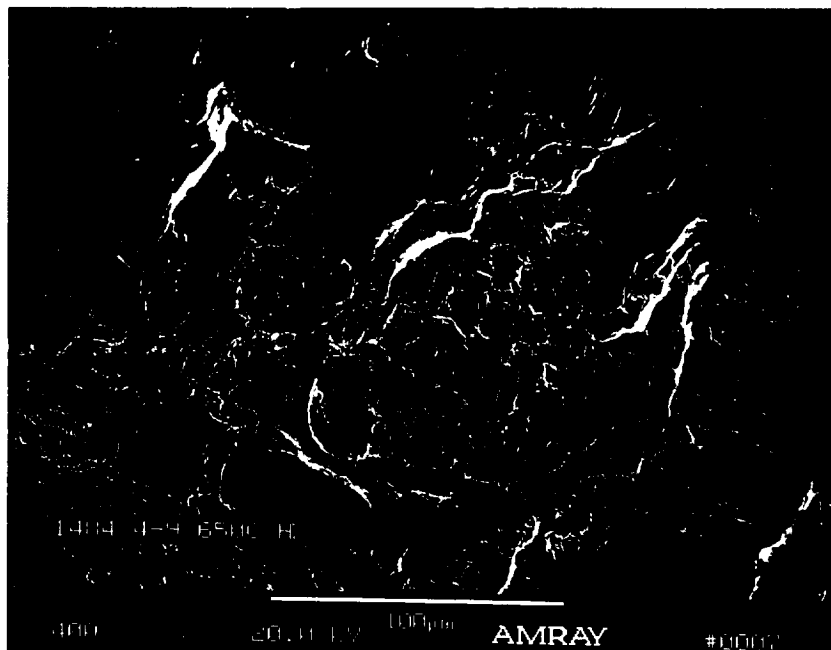


*Figure 93. High-Magnification View of Step on (111) Fracture Surface; Dark Area at Center Is Analyzed in Figure 94; Conditions – PWA 1484 HT 4, 650°C (1200°F), Hydrogen, Tensile*



*Figure 94. Back Scattered Electron Image of Field Shown Figure 93 Shows Localized Area of Precipitated Carbide; Conditions – PWA 1484 HT 4, 650°C (1200°C), Hydrogen, Tensile*

#### ***PWA 1482 Tensile Fractures***

Examinations of room temperature hydrogen tensile fractures from PWA 1482 HTs 4 and 6 are shown in Figures 95 through 98.

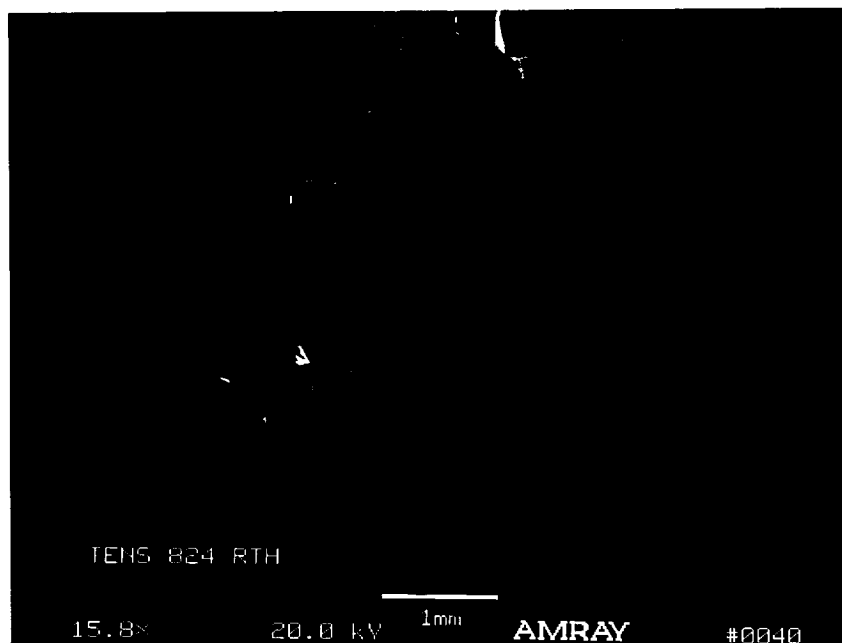


*Figure 95. Overall View of Tensile Failure Shows Localized Areas of Hydrogen Affected Fracture in the Form of Flat Feathery Areas at Perimeter (Detailed in Subsequent Figures); Condition – PWA 1482 HT 4, 20°C (68°F), Hydrogen Tensile*

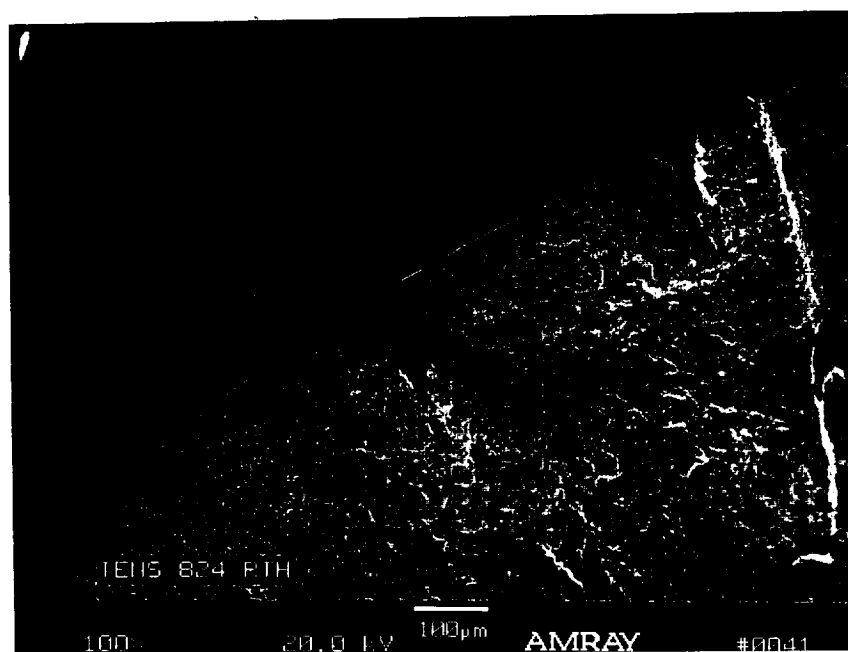


*Figure 96. Closeup View of Localized Areas of Hydrogen Affected Fracture from Figure 95; This Is Typical Hydrogen Tensile Fractures; Conditions – PWA 1482 HT 4, 20°C (68°F), Hydrogen, Tensile*

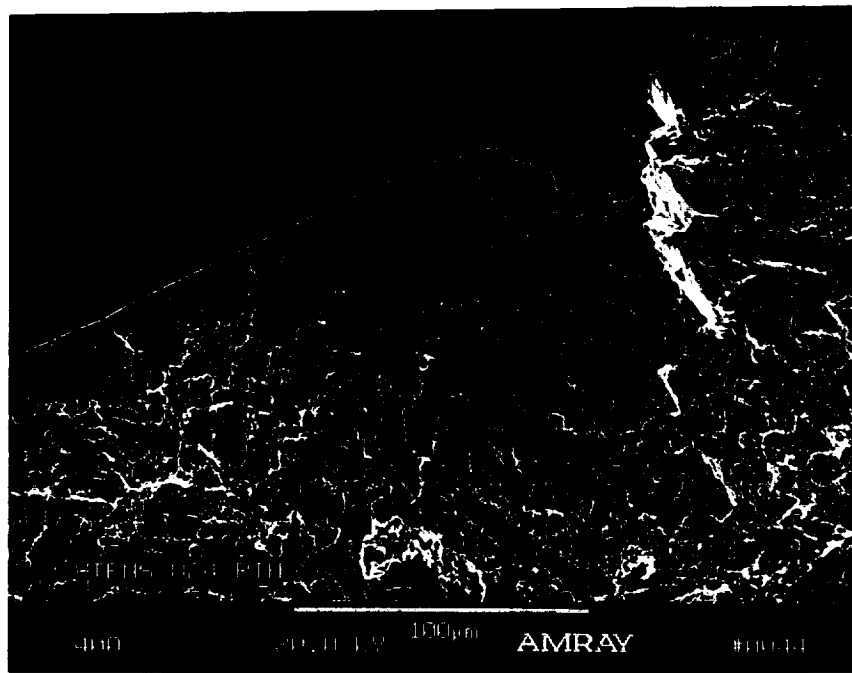


*Figure 97. At 400X, Microstructure Can Be Discerned Because of Differential Fracture Modes in Primary Versus Fine Cuboidal  $\gamma'$ ; At low stress intensity ( $\Delta K$ ), Fracture Is Nearly All Nominally (001); As  $\Delta K$  Increases, Fine Cuboidal Precipitates Begin To Fracture Along (111) Planes Delineating Larger Primary  $\gamma'$ ; Conditions – PWA 1482 HT 4, 20°C (68°F), Hydrogen, Tensile.*

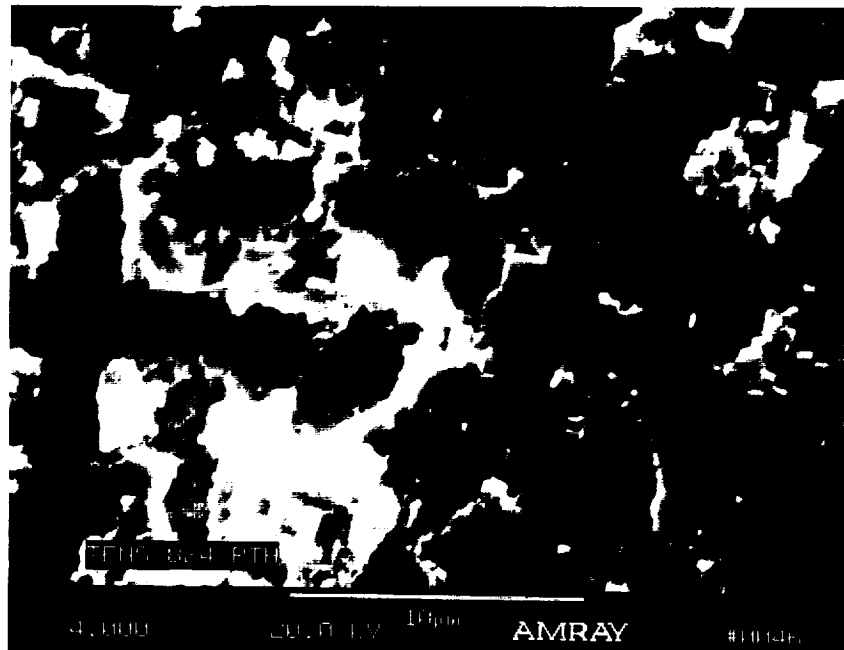


*Figure 98. At 4000X, Behavior Described in Figure 97 Can Be Discerned; Fine Cuboidal  $\gamma'$  Appears White and Larger Primary  $\gamma'$  is dark; Conditions – PWA 1482 HT 4, 20°C (68°F), Hydrogen, Tensile*

Elevated temperature (650°C [1200°F]) tensile fractures produced in air for PWA 1482 HTs 4 and 6 are shown in Figures 99 and 100. Elevated temperature (650°C [1200°F]) tensile fractures produced in hydrogen for PWA 1482 HT 4 are shown in Figures 101 and 102.

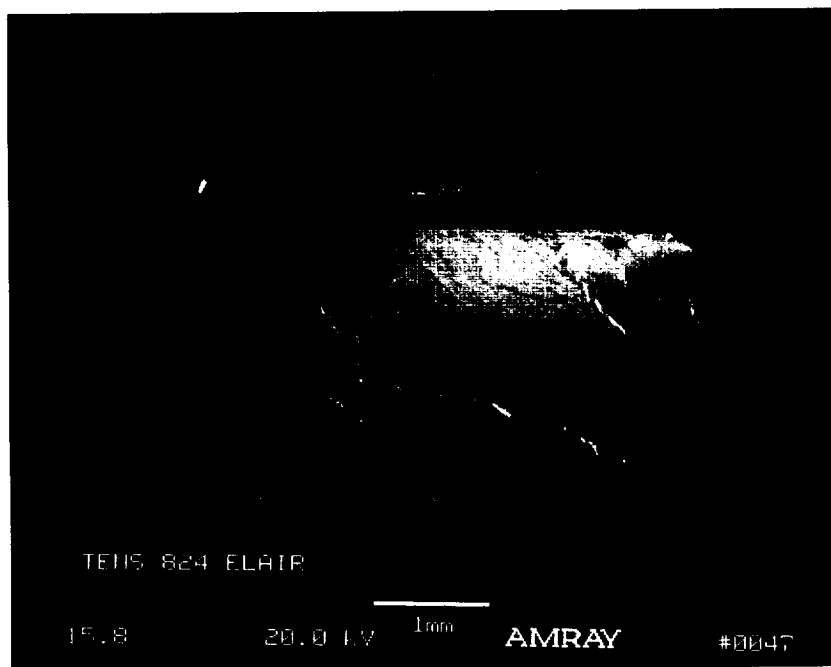


*Figure 99. Overall View of Tensile Failure Produced in 650°C (1200°F) Air Shows Typical Prominent (111) Intersecting Crystallographic Planes; Conditions – PWA 1482 HT 4, 650°C (1200°F), Air, Tensile*

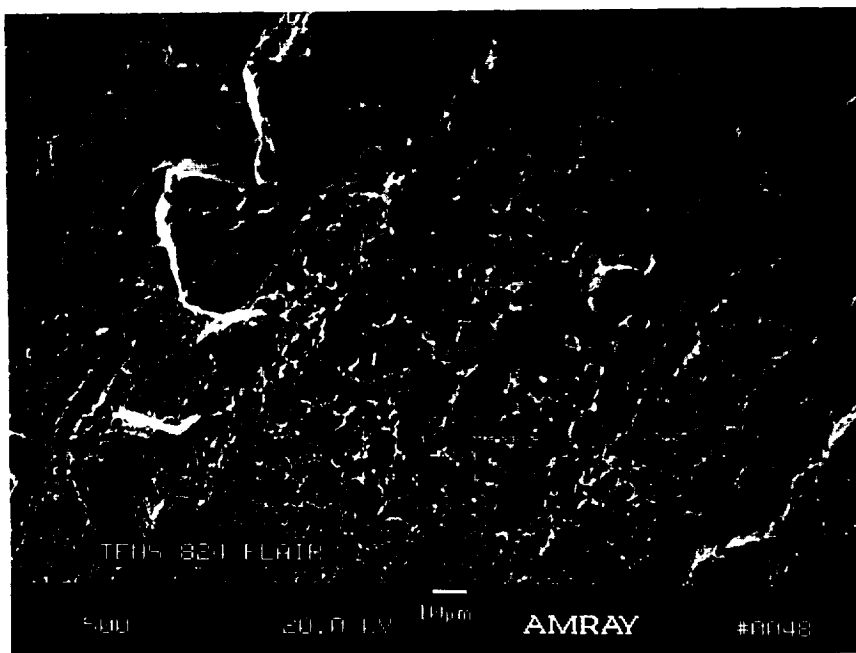


*Figure 100. Cellular Appearance of (111) Fracture Plane Is a Result of Microstructure and Appears To Be Associated With Unusual Roughness (Presumed Beneficial Under Conditions Where Octahedral Crack Initiation Is a Concern); Conditions – PWA 1482 HT 4, 650°C (1200°F), Air, Tensile*

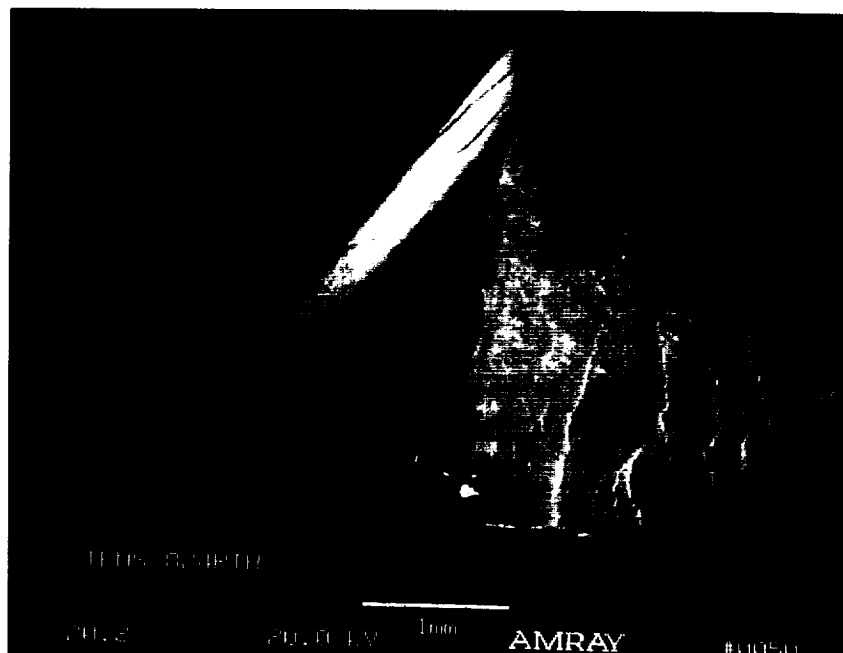


*Figure 101. Overall View of 650°C (1200°F) Tensile Fracture Produced in 34.5 MPa (5 ksi) Hydrogen Showing Typical (111) Crystallographic Fracture; Conditions – PWA 1482 HT 4, 650°C (1200°F), Hydrogen, Tensile*

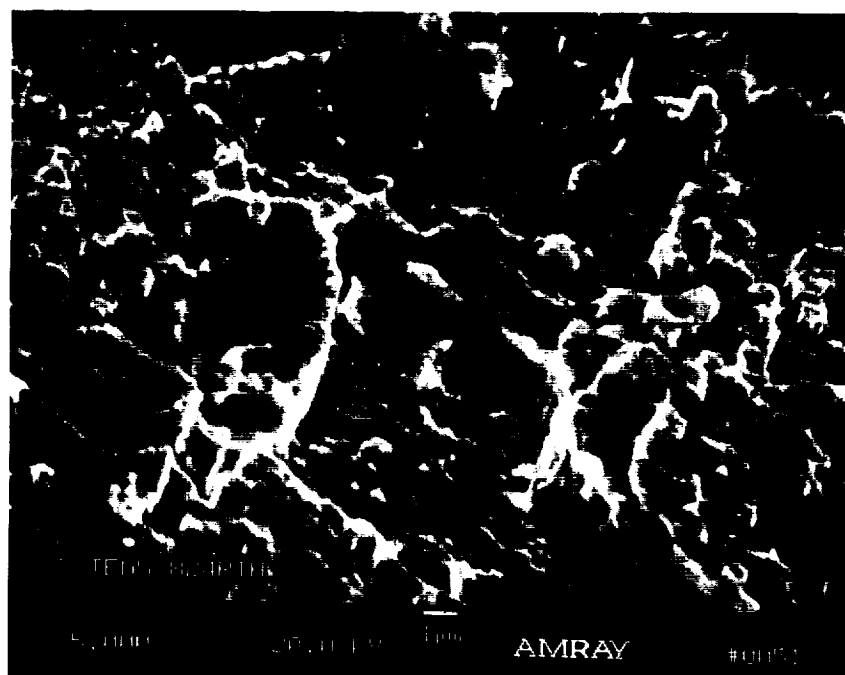


*Figure 102. High-Magnification View of (111) Fracture Suggests Some Structure Within Primary  $\gamma'$ ; Conditions – PWA 1482 HT 4, 650°C (1200°F), Hydrogen, Tensile*



### 2.7.3 Creep Fractures

Examinations of creep fractures produced in 871°C (1600°F) air from PWA 1482 and PWA 1484 HTs 4 and 6 are summarized Figures 103 through 106.

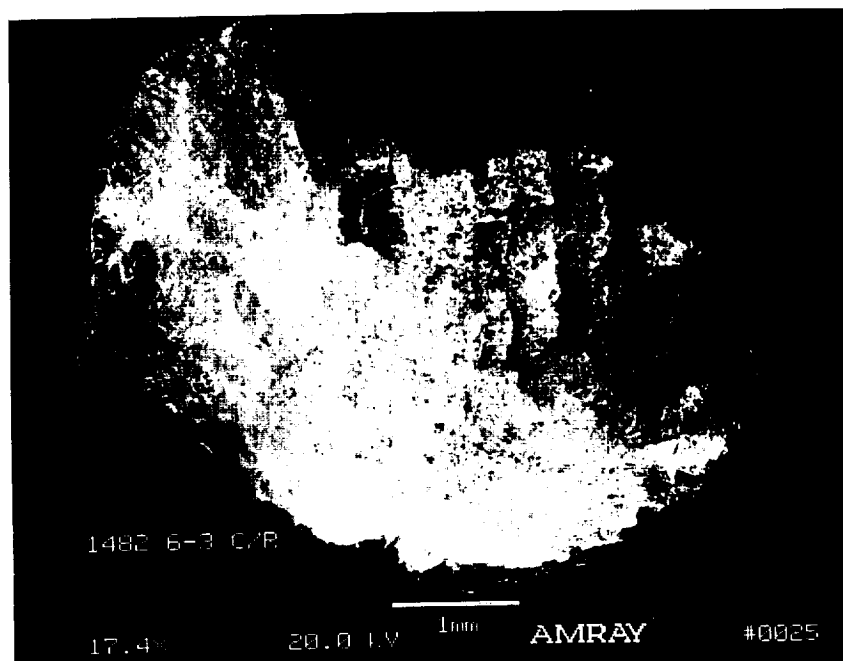


*Figure 103. Overall View of Creep/Stress Rupture Fracture Produced in Air Showing Mixed Noncrystallographic and (111) Crystallographic Fracture; Conditions – PWA 1482 HT 6, 871°C (1600°F), Air, Creep/Stress Rupture*

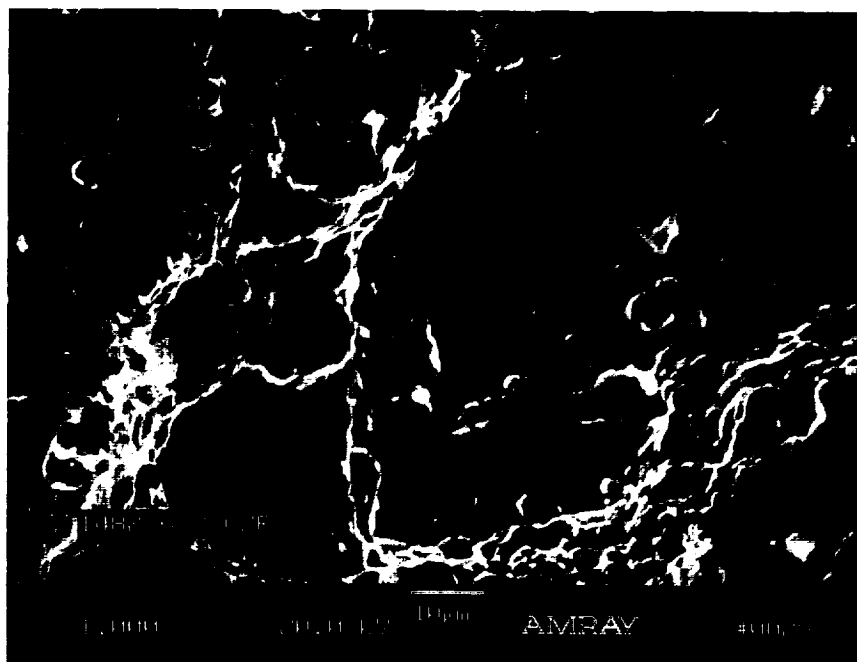


*Figure 104. High-Magnification View of Stress Rupture Fracture Details; Conditions – PWA 1482 HT 6, 871°C (1600°F), Air, Creep/Stress Rupture*

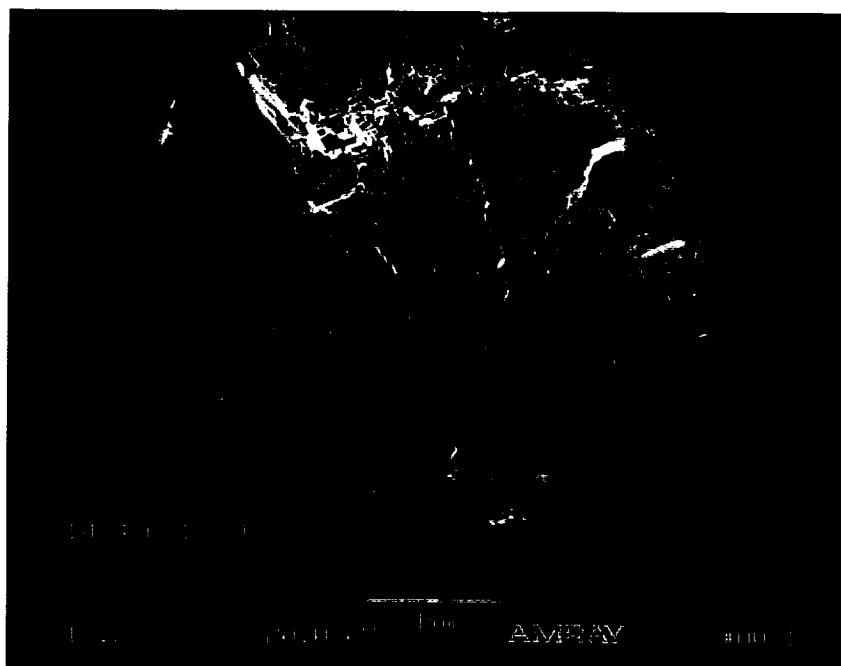


*Figure 105. Overall View of Creep/Stress Rupture Fracture Produced in Air Shows Noncrystallographic Macroscopically and (111) Crystallographic Fracture Microscopically in Figure 106; Conditions – PWA 1484 HT 6, 871°C (1600°F), Air, Creep/Stress Rupture*

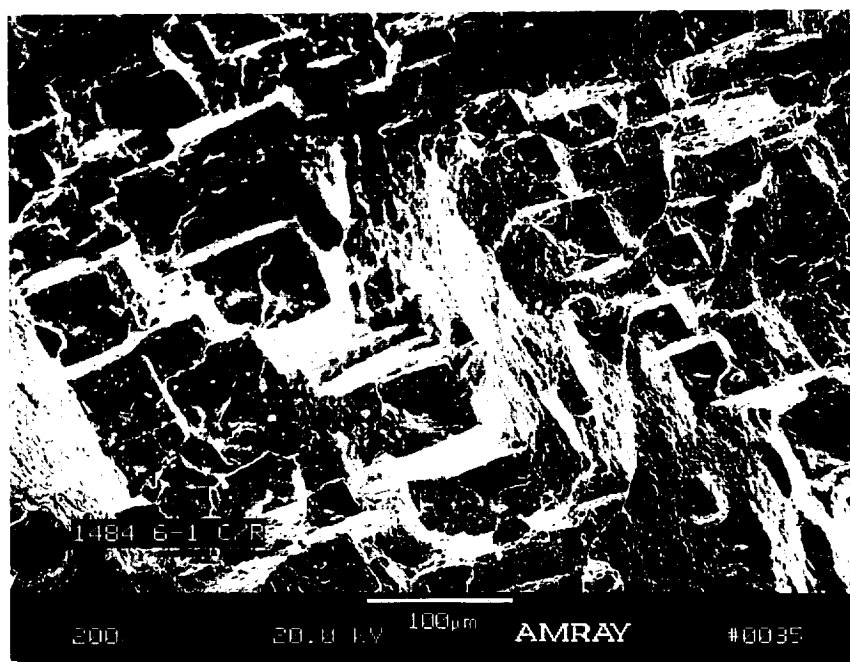


*Figure 106. High-Magnification View of Stress Rupture Fracture Details Shows Large Area of (111) Fracture; Conditions – PWA 1484 HT 6, 871°C (1600°F), Air, Creep/stress Rupture*

## 2.7.4 Fatigue Fractures

### *Notched Low-Cycle Fatigue*

Examination results of representative notched fatigue fractures from PWA 1484 and PWA 1482 tests conducted in hydrogen at room temperature are summarized in the following paragraphs.

Fractures from both alloys and heat treatments exhibited what is now recognized as the typical fatigue crack origin in HIP eutectic-free, low-carbon, single crystals, namely Stage I crack initiation at a discrete (111) crystallographic facet (10 x 30 micron in the case illustrated) and immediately transitioning to Stage II crack propagation by failure nominally parallel to (001) as shown in Figure 107. Matrix failure is probable in this case (PWA 1484 HT 2) because of the non-bimodal  $\gamma'$  structure.

High-magnification study (Figure 108) of the fracture shows isolated microscopic (111)  $\gamma'$  fracture. Although this fatigue crack propagation mode associated with the fine uniform cuboidal  $\gamma'$  structure of HT 1 was extremely rapid in FCG tests, the time to initiate the crack (LCF life) was much greater than conventional blade alloys with eutectic  $\gamma/\gamma'$ . This is exemplified in hydrogen notched LCF results for HTs 1 through 7 (shown previously in Figure 41).

PWA 1482 HTs 4 and 6 also showed crystallographic fatigue crack origins (Figure 109) and microscopic (111) fracture in the fine cuboidal  $\gamma'$  surrounding the large primary  $\gamma'$  and lenticular (001) cracking cutting the large primary  $\gamma'$  (Figure 110). In some areas of the fracture, secondary cracks appeared to be skirting the primary  $\gamma'$  (Figure 111), which was confirmed by replica TEM analysis. By relating microstructural features (Figure 112) to fractographic features (Figure 113), the cracks can be shown to be interprecipitate.

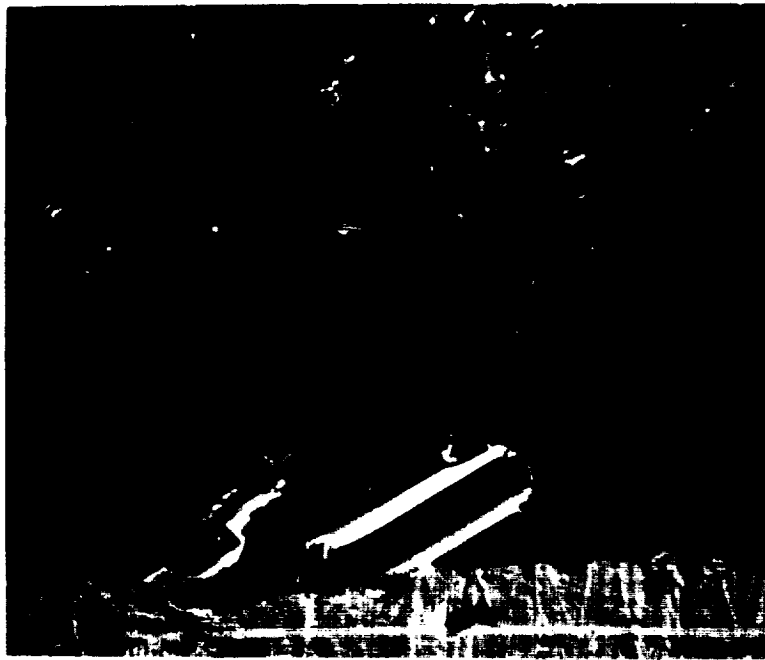


*Figure 107. Stage I Crack Initiation at Discrete (111) Crystallographic Facet (10 x 30 micron);  
Conditions – PWA 1484 HT 2, Notched LCF, 20°C (68°F), 34.5 MPa (5 ksi) Hydrogen, Magnification 1000X*



*Figure 108. Isolated Microscopic (111) γ' Fracture Among Predominantly Matrix Failure;  
Conditions – PWA 1484 HT 2, Notched LCF, 20°C (68°F), 34.5 MPa (5 ksi) Hydrogen, Magnification 10,000X*

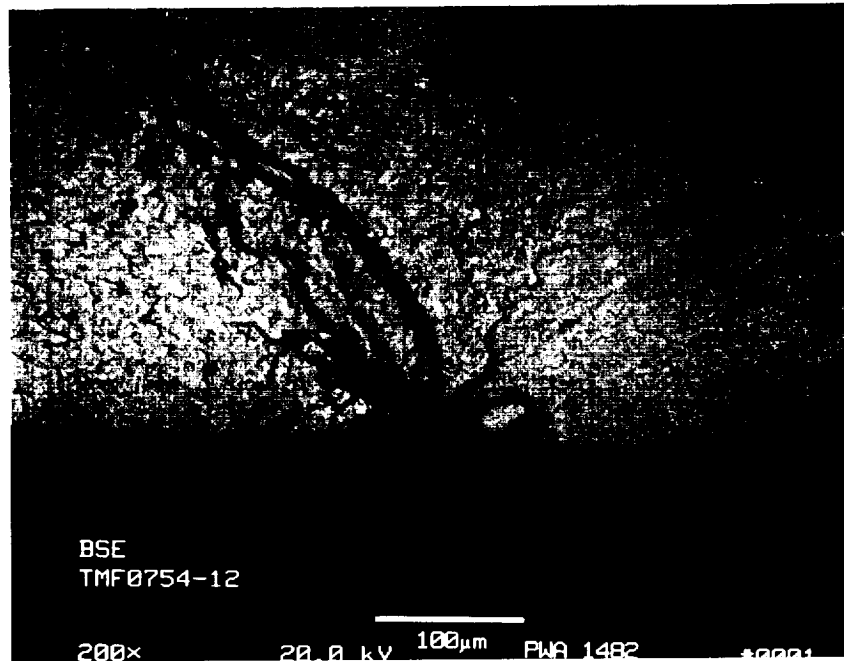


Figure 109. Crystallographic Fatigue Crack Origins and Microscopic (111) Fracture in Fine Cuboidal  $\gamma$ ; Conditions – PWA 1482 HT 4, Notched LCF, 20°C (68°F), 34.5 MPa (5 ksi) Hydrogen

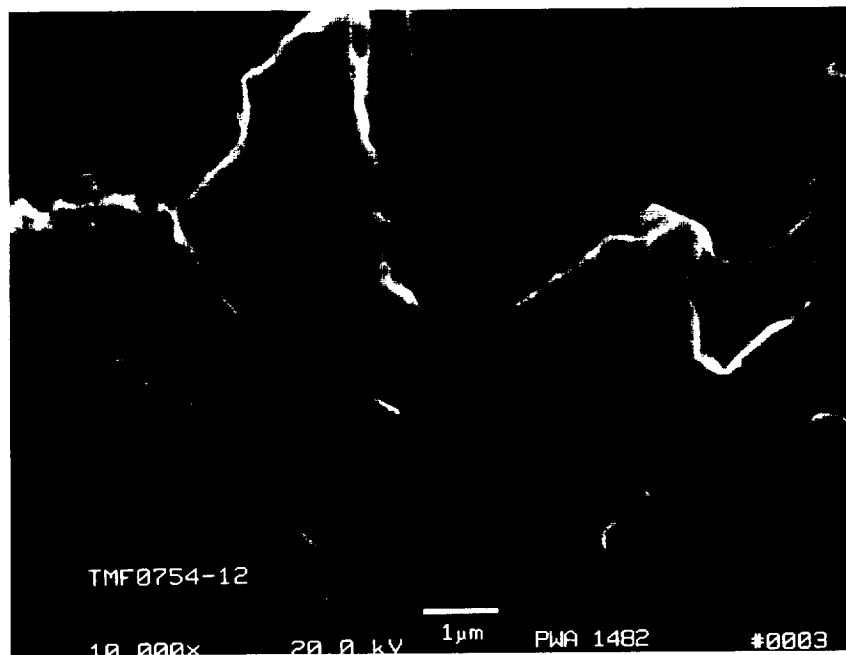
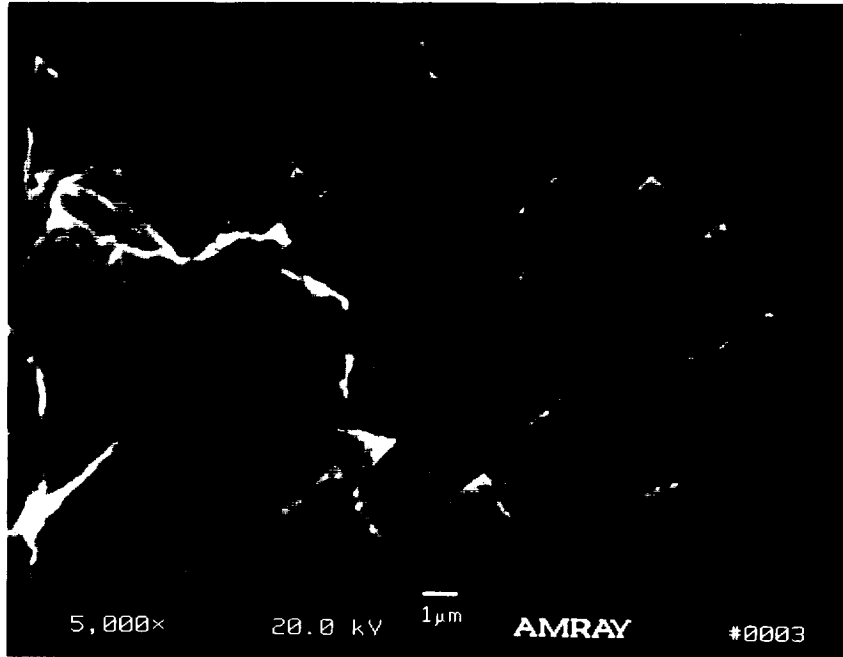
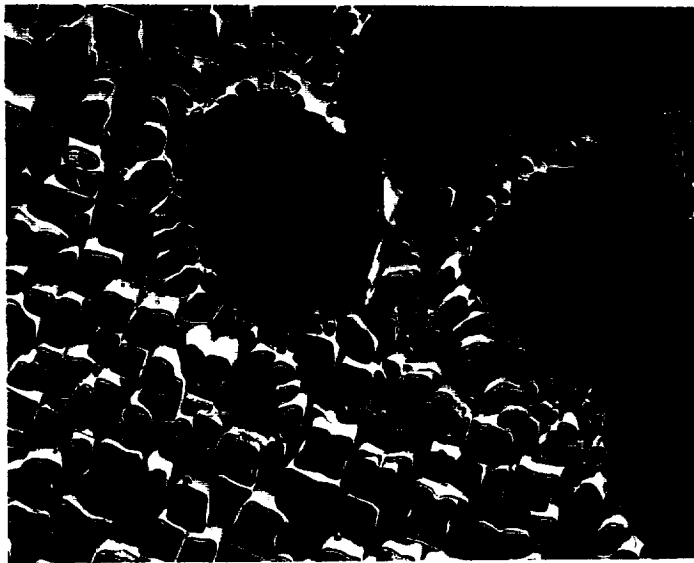


Figure 110. Lenticular (001) Cracking Cutting Large Primary  $\gamma$ ; Conditions – PWA 1482 HT 4, Notched LCF, 20°C (68°F), 34.5 MPa (5 ksi) Hydrogen



*Figure 111. In Some Cases Secondary Cracks Appeared To Be Skirting Primary  $\gamma'$ ; Conditions – PWA 1482 HT 6, Notched LCF, 20°C (68°F), 34.5 MPa (5 ksi) Hydrogen*



*Figure 112. Replica TEM of PWA 1482 HT 6 Was Compared to Previous Fracture in Figure 111 and Subsequent Figure 113 To Confirm Cracks Skirting Primary  $\gamma'$ ; Magnification Is 22,000X*



*Figure 113. Replica TEM of Primary  $\gamma'$  Fracture Features Show Interprecipitate Cracking;  
Conditions – PWA 1482 HT 6, Notched LCF, 20°C (68F), 34.5 MPa (5 ksi) Hydrogen; Magnification Is 22,000X*

In cases where the large primary  $\gamma'$  are being cut, the fracture surface of that microconstituent are of particular interest. A comparison of replica TEM and SEM is shown in Figures 114 and 115. Both perspectives suggest mixed (111) and Mode I fracture, (001) cannot be confirmed. The SEM imagery suggests structure within the large primary  $\gamma'$  (possibly reprecipitated  $\gamma$  phase<sup>18</sup>); however,  $\gamma$  phase was not evident in subsequent thin foil analytical TEM analysis (Figure 116), nor does it appear in high-magnification field emission electron microscopy (FEM) images that were taken from etched metallographic sections (Figure 117).

<sup>18</sup> Oblak, J.M., Doherty, J.E., Giamei, A.F., and Kear, B.H.; *Metallurgical Transactions*, Vol 5, pp 1275, May 1974.



*Figure 114. Replica TEM of Primary  $\gamma'$  Fracture Surface Suggests Microscopic (111) Fracture and Perhaps Some Type of Structure Within Precipitate; Conditions – PWA 1482 HT 6, Notched LCF, 20°C (68°F), 34.5 MPa (5 ksi) Hydrogen; Magnification Is 22,000X*

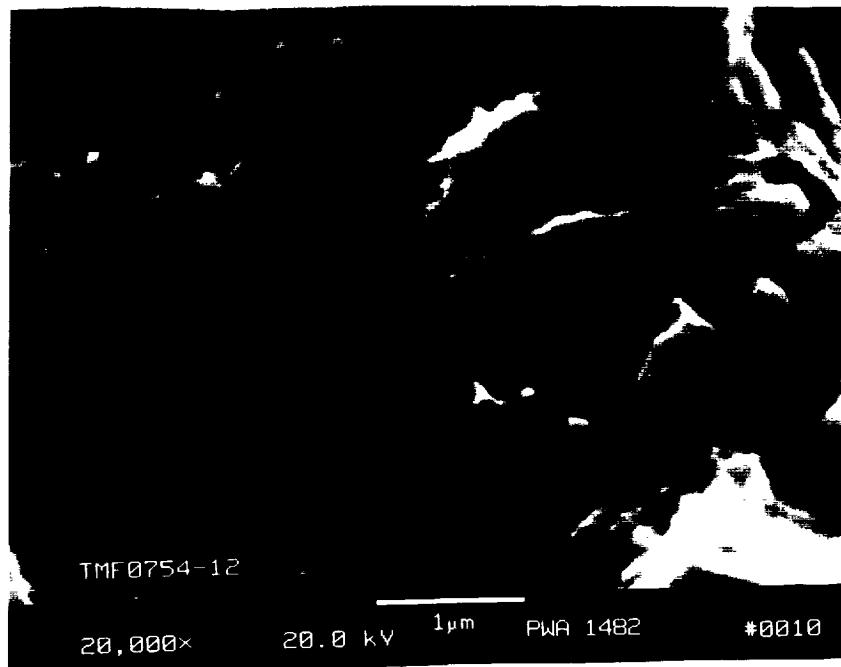


*Figure 115. SEM Imagery of Primary  $\gamma'$  Fracture Surfaces Suggests Structure Within Large Primary  $\gamma'$  (Possibly  $\gamma$  Phase Retrograde Solubility)*



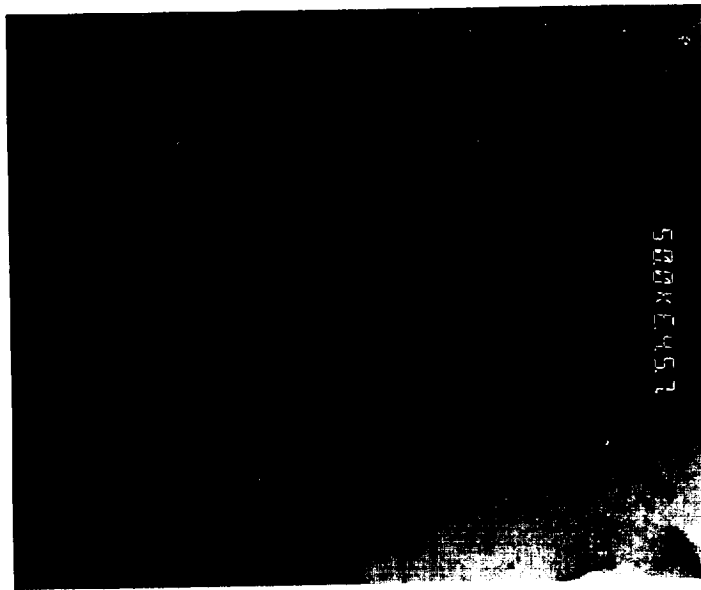


*Figure 116. Thin Foil TEM Shows No Presence of  $\gamma$  Within Primary  $\gamma'$ ; Fine Cuboidal Precipitates Are at the Upper Left; Interfacial Dislocations Outline Primary  $\gamma'$  and Appear Tangled; Arrangement of Dislocations Within Primary  $\gamma'$  Show Some Correlation With Fractographic Structures Shown in Figure 111; PWA 1484 HT 3; Magnification is 50,000X*

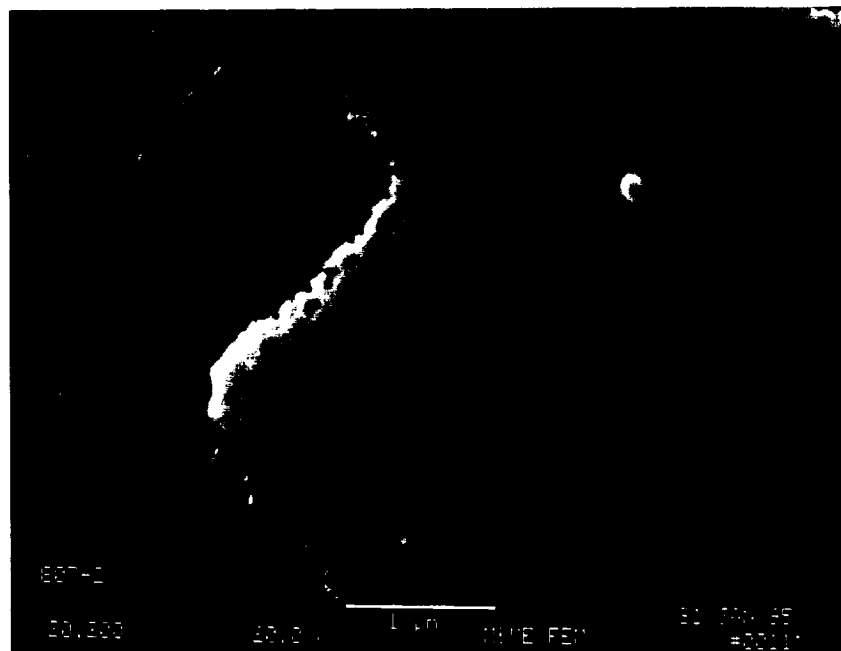


*Figure 117. High-Magnification FEM Images Taken From Etched Metallographic Sections Show No Reprecipitated  $\gamma$  Within Primary  $\gamma'$ ; PWA 1484 HT 3*

Notched LCF fractures produced in air at room temperature (Figures 118 through 121) were macroscopically similar to conventional single-crystals showing prominent (111) planar fracture at fatigue origins. No point source defects were observed. Microscopically, the bimodal structures could be discerned by the dissimilar fracture modes exhibited by the two precipitate distributions.



*Figure 118. Overall View of Notched LCF Air Fracture (20°C [68°F]) Shows Typical (111) Fracture;  
Conditions – PWA 1484 HT 4, Notched LCF, 20°C (68°F), Air*

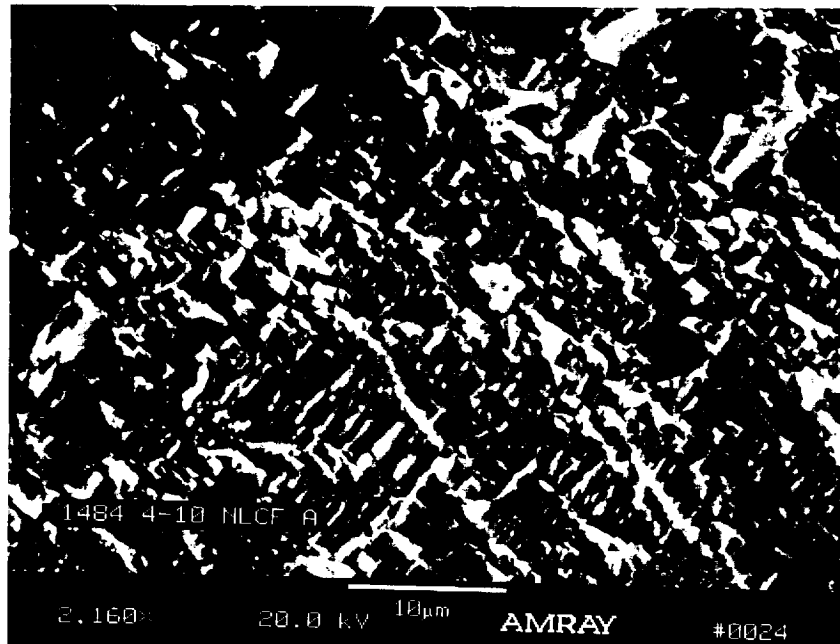


*Figure 119. High-Magnification View of Microscopic (111) Fracture in Areas That Macroscopically Appear Noncrystallographic; Conditions – PWA 1484 HT 4, Notched LCF, 20°C (68°F), air*

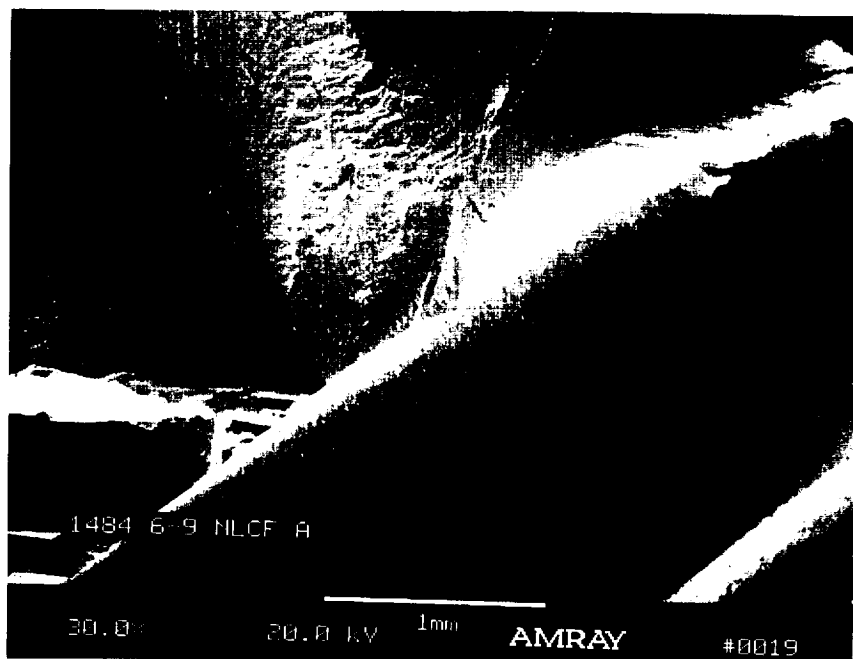


*Figure 120. Similar to Previous Fracture in Figure 115; Overall View of Notched LCF Air Fracture Shows Typical (111) Fracture; Conditions – PWA 1484 HT 6, Notched LCF, 20°C (68°F), Air*

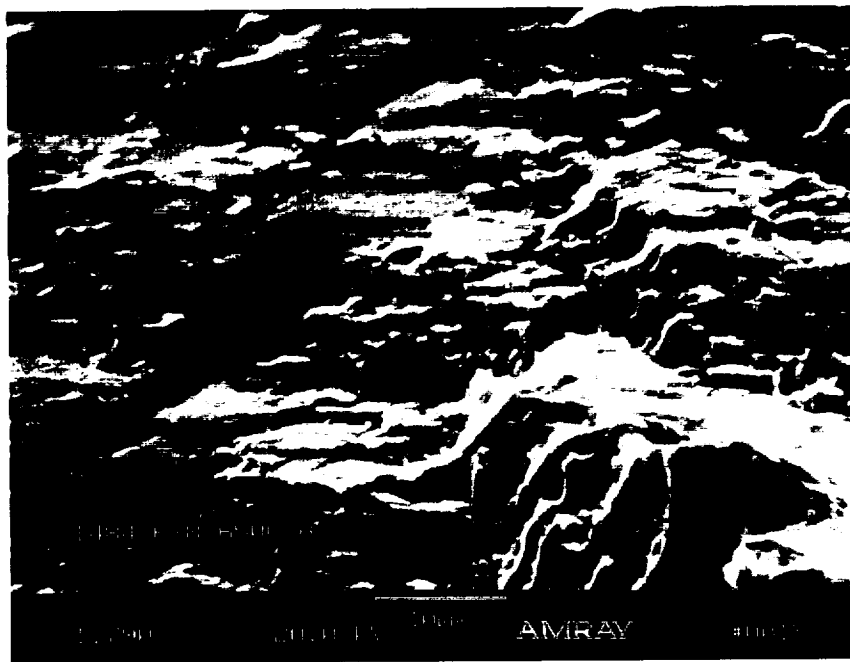


*Figure 121. Primary and Fine Precipitates Show Differential Fracture in This High-magnification View of Microscopic (111) Fracture; These Areas Macroscopically Appear Noncrystallographic; Conditions – PWA 1484 HT 6, Notched LCF, 20°C (68°F), Air*

#### *Strain Smooth Low-Cycle Fatigue*

Examination of representative controlled strain fatigue fractures from PWA 1482 and PWA 1484 produced in room temperature air and hydrogen for HTs 4 and 6 are summarized in Figures 122 through 137. The specimen in Figures 124 shows large (111) fracture surfaces and no specific point source origin. One of the (111) planes is shown enlarged in Figure 125. The specimen in Figure 126 shows the hexagonal crack sometimes present on (111) fractures initiated internally. The pattern is the result of intersecting slip systems.<sup>19</sup> Microscopic details of the fracture are shown in Figure 127.

<sup>19</sup> DeLuca, D.P. and Annis, C.G., Jr., *Fatigue in Single Crystal Nickel Superalloys*, 1995, U.S. Navy/ONR Contract N00014-91-C-0124.



*Figure 122. (111) Fracture Planes Typical of 20°C (68°F) Single-Crystal Fractures Produced in Air; Conditions – PWA 1484 HT 4, 20°C (68°F), Air, Controlled Strain LCF*

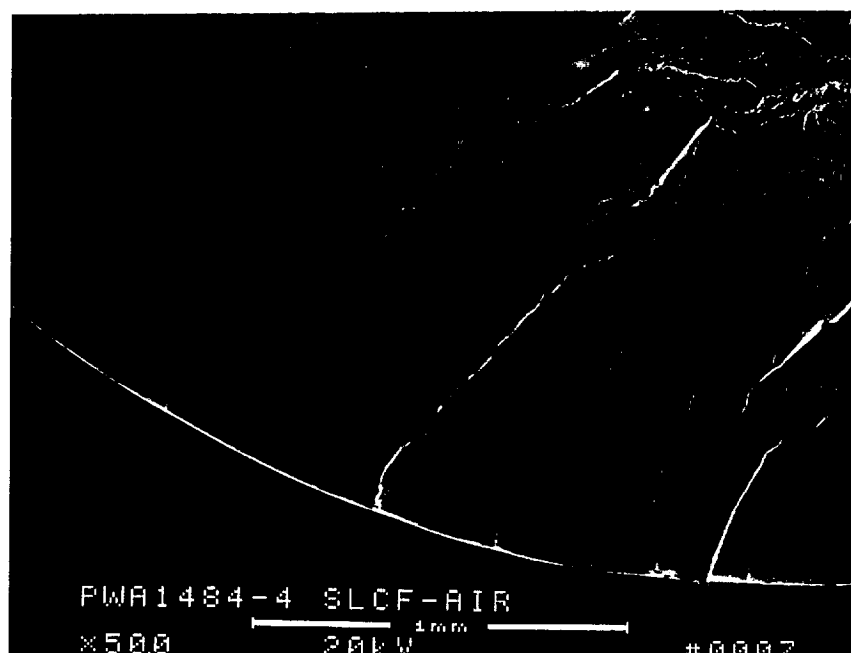


*Figure 123. Detail of Origin Area From Figure 122; Conditions – PWA 1484 HT 4, 20°C (68°F), Air, Controlled Strain LCF*

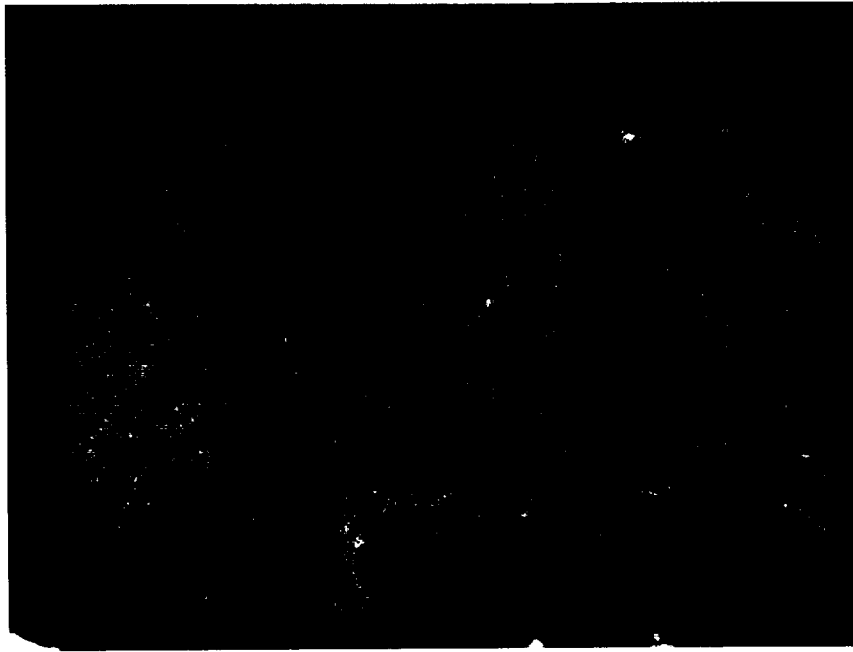


*Figure 124. Hexagonal Crack Front on Large (111) Plane Results From  $\langle 110 \rangle$  Slip Directions Intersecting (111) Plane; No Point Source Was Detected at Origin; Conditions – PWA 1484 HT 6, 20°C (68°F), Air, Controlled Strain LCF, Magnification 10X*



*Figure 125. Microscopic Appearance of (111) Fracture Planes; Conditions – PWA 1484 HT 6, 20°C (68°F), Air, Controlled Strain LCF*

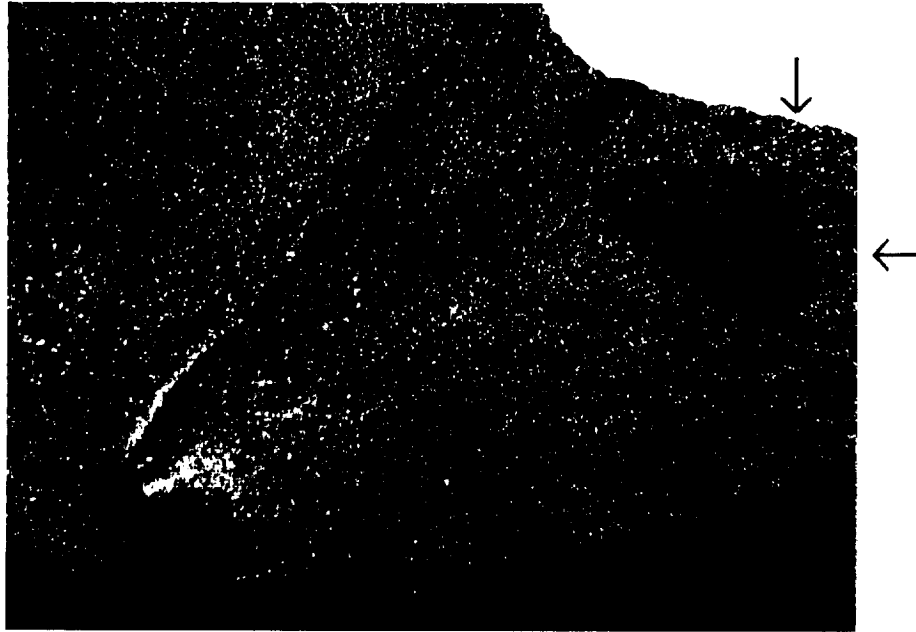


*Figure 126. Overall of Strain Control LCF Fracture Produced in Room Temperature Hydrogen; Fatigue Origin Is at Stage I Crystallographic Facet; Enlarged in Figure 127; Dark Oval Shape at Right Is Secondary Grain; Conditions – PWA 1482 HT 4, 20°C (68°F), 34.5 MPa (5 ksi) Hydrogen, Controlled Strain LCF, Magnification 30X*

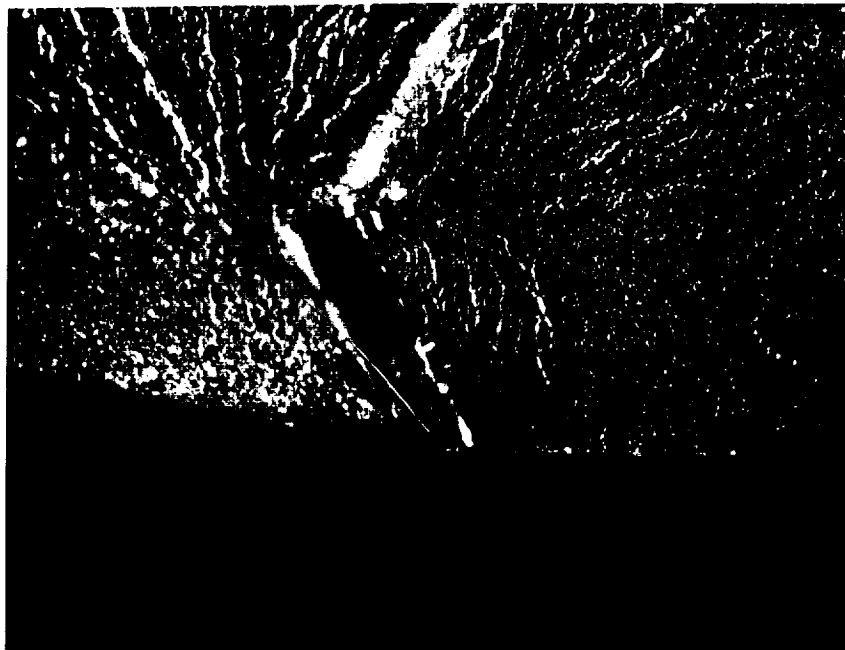


*Figure 127. Microscopic (111) Facet Initiated Crack in Figure 126; Note Fatigue “Thumbprint” Crack Front Radiating From (111) Face; Conditions – PWA 1482 HT 6, 20°C (68°F), 34.5 MPa (5 ksi) hydrogen, Controlled Strain LCF, Magnification 50X*



*Figure 128. Transverse Metallographic Section Through Specimen Gage Shown in Figure 127 Reveals Secondary Grain; Conditions – PWA 1482 HT 6, 20°C (68°F), 34.5 MPa (5 ksi) Hydrogen, Controlled Strain LCF, Magnification 60X*



*Figure 129. Longitudinal Metallographic Section Through Specimen Gage Shown in Figure 128 Reveals Secondary Grain; Conditions – PWA 1482 HT 6, 20°C (68°F), 34.5 MPa (5 ksi) Hydrogen, Controlled Strain LCF, Magnification 12X*





*Figure 130. Overall View of Strain Control LCF Fracture Produced in Room Temperature Hydrogen; Conditions – PWA 1482 HT 4, 20°C (68°F), 34.5 MPa (5 ksi) Hydrogen, Controlled Strain LCF, Magnification 10X*

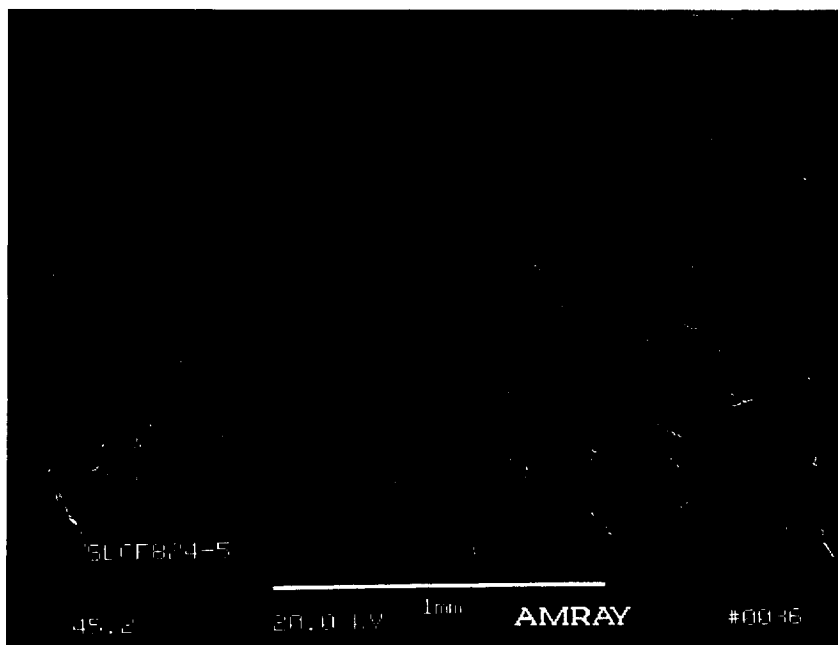


*Figure 131. Enlargement of Origin Area From Figure 130 Shows Increasing Roughness as Stress Intensity Increases; Conditions – PWA 1482 HT 4, 20°C (68°F), 34.5 MPa (5 ksi) Hydrogen, Controlled Strain LCF*

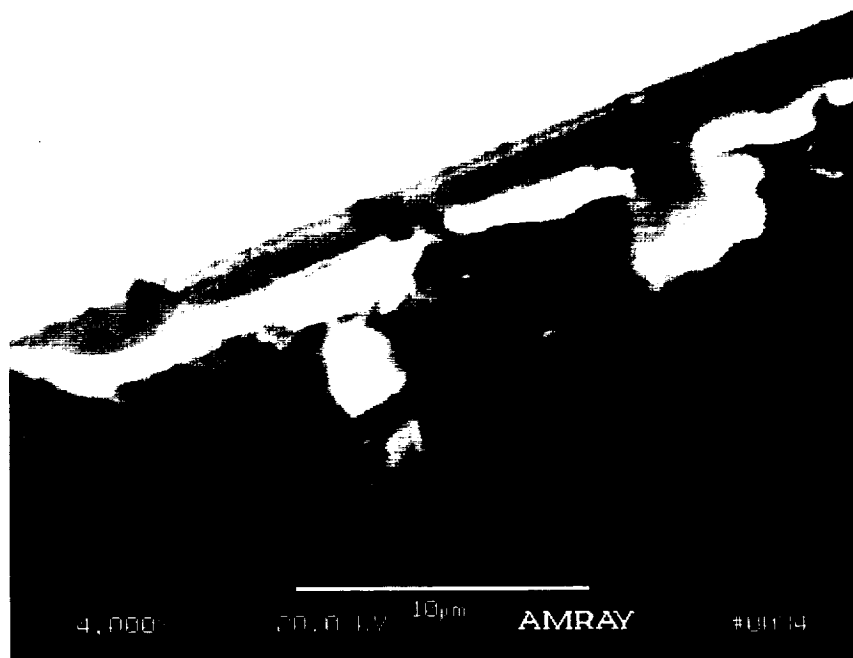


*Figure 132. Fatigue Crack Origin From Figure 131 Shows Extremely Flat Fracture and Apparent Machining Marks at Specimen Edge; Conditions – PWA 1482 HT 4, 20°C (68°F), 34.5 MPa (5 ksi) Hydrogen, Controlled Strain LCF*



*Figure 133. Overall View of Strain Control LCF Fracture Produced in Room Temperature Hydrogen; Fatigue Origin Was Nonspecific (No Point Source Present); Flat Smooth Surface Characteristic of Hydrogen Fractures Is Absent; Conditions – PWA 1482 HT 6, 20°C (68°F), 34.5 MPa (5 ksi) Hydrogen, Controlled Strain LCF*

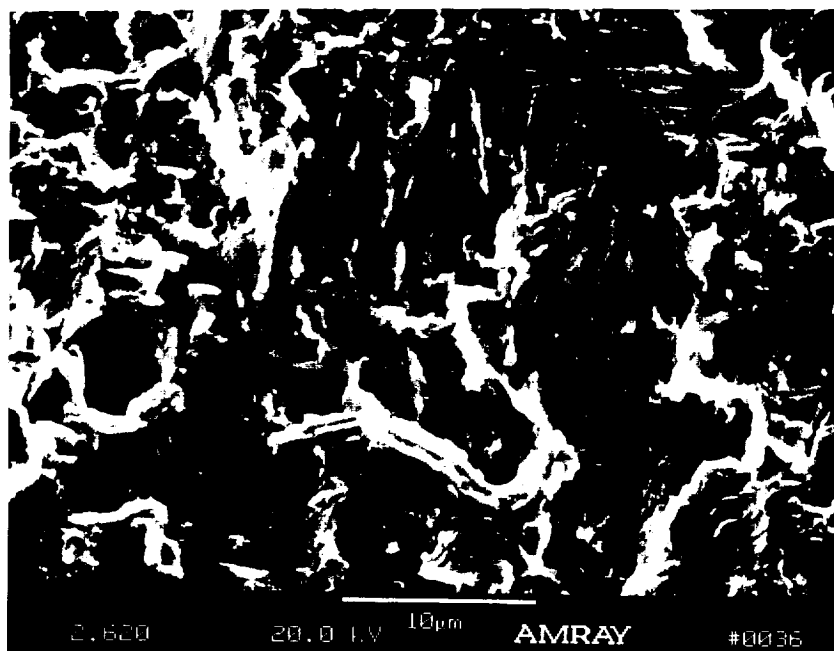


*Figure 134. High-Magnification Details of  $\gamma'$  Fracture Modes Near Suspected Origin in Figure 133; Dark Shape at Lower Left and Right Are Primary  $\gamma'$ ; Note High Degree of Roughness Surrounding These Features; Conditions – PWA 1482 HT 6, 20°C (68°F), 34.5 MPa (5 ksi) Hydrogen, Controlled Strain LCF*

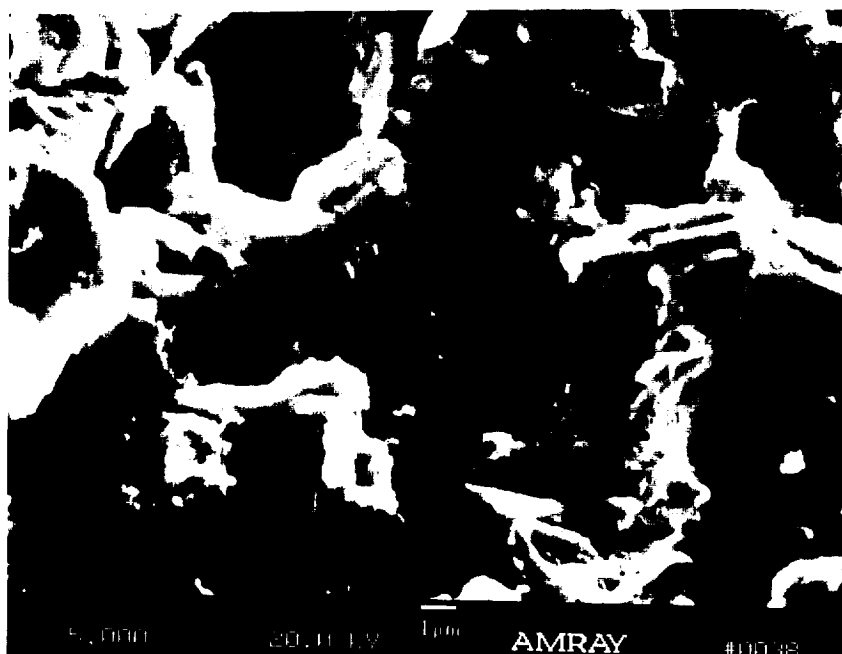


*Figure 135. Further Study of Primary  $\gamma'$  From Figure 134 Shows Pronounced Ridges and (111) Facets Covering Areas Where Fine Cuboidal  $\gamma'$  Reside; Conditions – PWA 1482 HT 6, 20°C (68°F), 34.5 MPa (5 ksi) Hydrogen, Controlled Strain LCF*

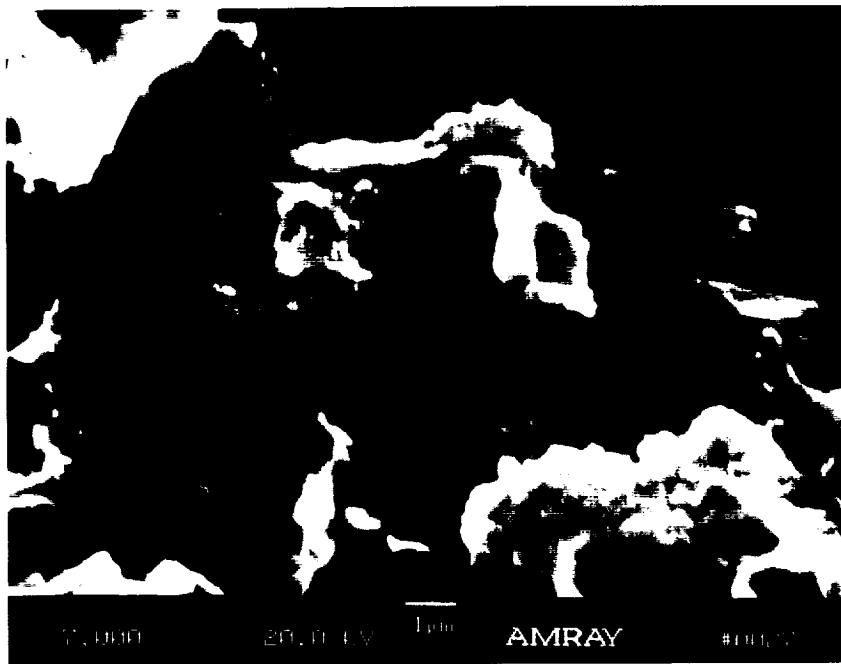


*Figure 136. Detail From Lower Right of Figure 134; Interprecipitate (Primary  $\gamma'$ ) (111) Fracture Mode Is Not Well Resolved and Appears Distorted; Regardless, This Topography Represents More Tortuous Crack Path Than That Offered by Conventional Fine Uniform Cuboidal  $\gamma'$  Structure; Conditions – PWA 1482 HT 6, 20°C (68°F), 34.5 MPa (5 ksi) Hydrogen, Controlled Strain LCF*

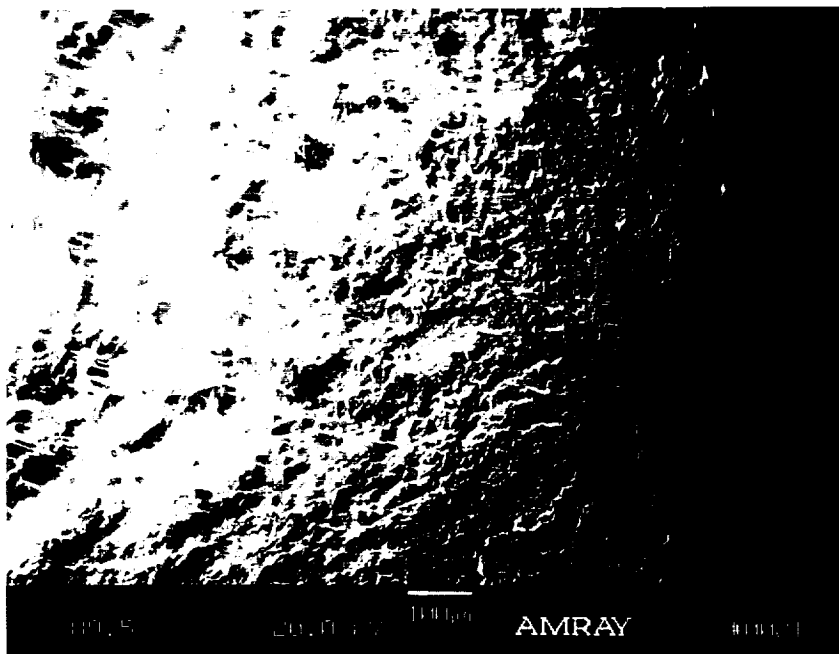


*Figure 137. PWA 1484 HT 4 Controlled Strain LCF Crack Origin Area Shows Relatively Flat Fracture; Stress Intensity (K) Dependent Increasing Roughness Is Clearly Seen; Conditions – PWA 1484 HT 4, 20°C (68°F), 34.5 MPa (5 ksi) Hydrogen, Controlled Strain LCF*

### *High Cycle Fatigue*

Examination of HCF fatigue fractures from PWA 1482 and PWA 1484 HTs 4 and 6 are summarized in Figures 138 through 143.

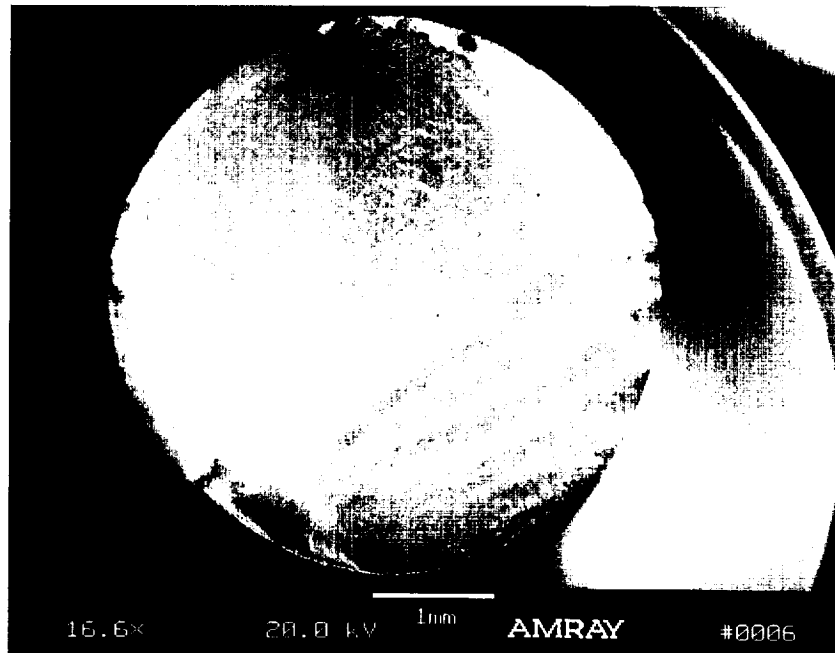


*Figure 138. PWA 1484 HT 4 HCF Overall View; Crack Origin Area (At Top) Shows Relatively Flat Fracture; Conditions – PWA 1484 HT 4, 20°C (68°F), 34.5 MPa (5 ksi) Hydrogen, R = -1.0 HCF*

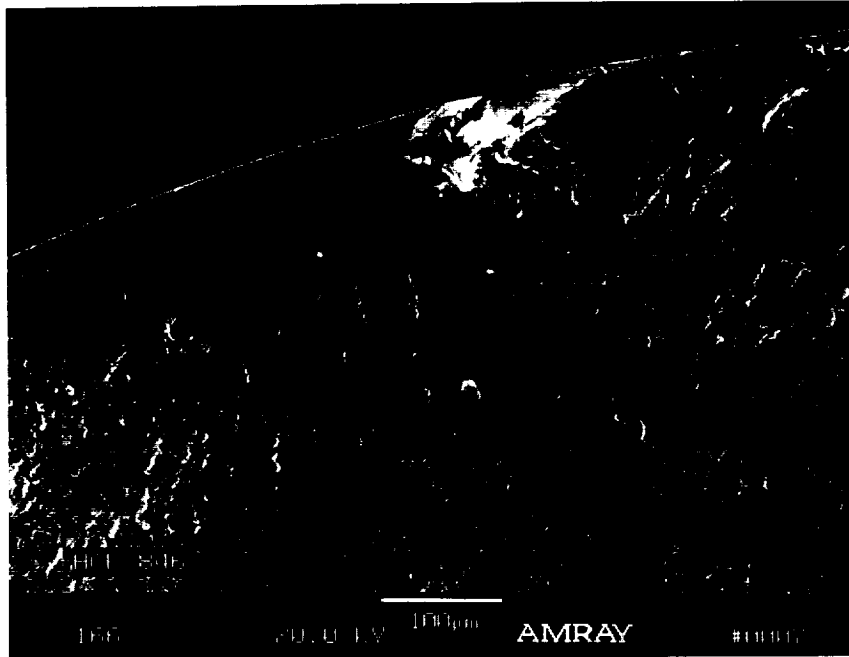


Figure 139. HCF Crack Initiation at 100  $\mu\text{m}$  Long (111) Facet From Figure 135; Conditions – PWA 1484 HT 4, 20°C (68°F), 34.5 MPa (5 ksi) Hydrogen,  $R = -1.0$  HCF

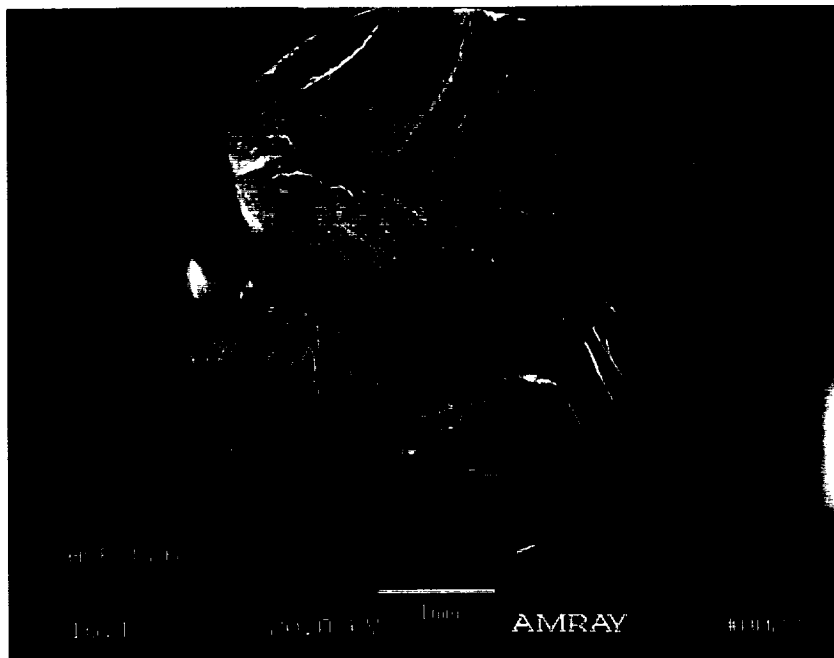


Figure 140. PWA 1482 HT 6 HCF Overall View; Crack Origin Area (At Left) Shows Prominent (111) Fracture; Conditions – PWA 1482 HT 6, 20°C (68°F), 34.5 MPa (5 ksi) Hydrogen,  $R = -1.0$  HCF

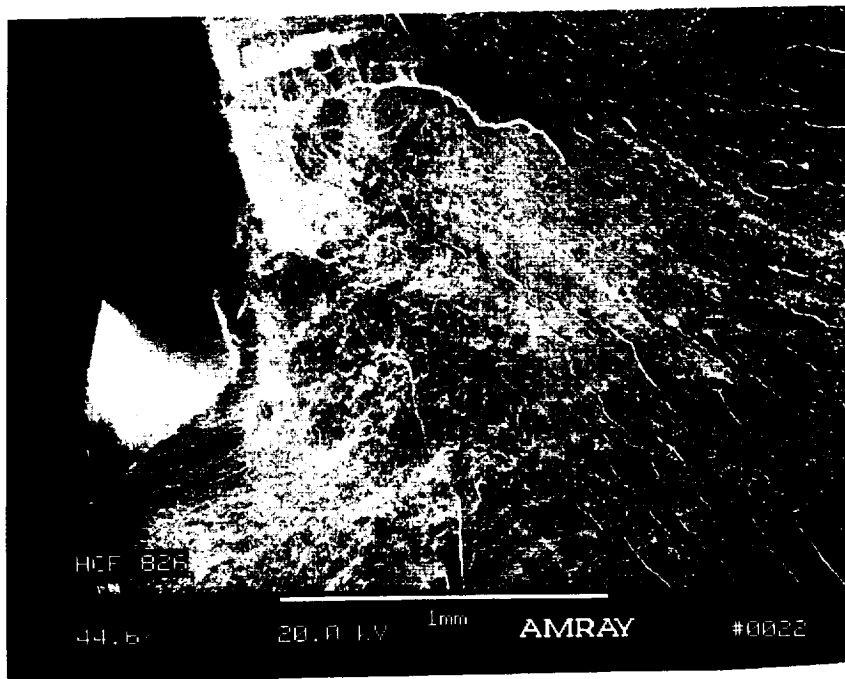


Figure 141. HCF Crack Initiation at 1mm (0.039 in.) Long (111) Facet From Figure 136; Conditions – PWA 1482 HT 6, 20°C (68°F), 34.5 MPa (5 ksi) Hydrogen,  $R = -1.0$  HCF



Figure 142. PWA 1484 HT 6 HCF Overall View; Crack Origin Area (At Right) Shows Prominent (111) Fracture; Conditions – PWA 1484 HT 6, 20°C (68°F), 34.5 MPa (5 ksi) Hydrogen,  $R = -1.0$  HCF

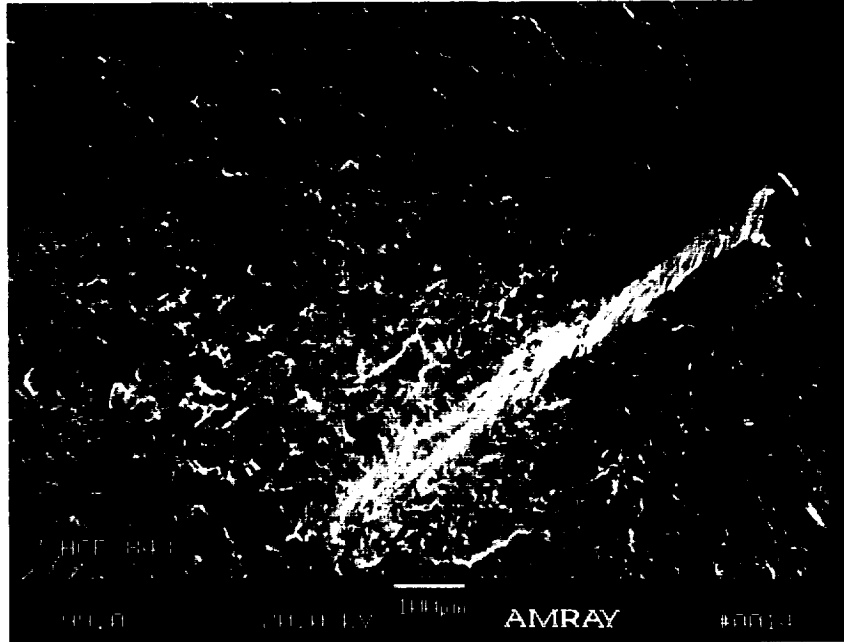


Figure 143. HCF Crack Initiation at 200 $\mu$ m Long ( $\bar{1}\bar{1}1$ ) Facet From Figure 142; Conditions – PWA 1484 HT 6, 20°C (68°F), 34.5 MPa (5 ksi) Hydrogen,  $R = -1.0$  HCF

### 2.7.5 Crack Growth Fracture

Examination of fatigue crack growth fractures from representative specimens are discussed below.

In PWA 1484 HT 1, a uniform fine cuboidal  $\gamma'$ , representing in effect a baseline, produced extremely rapid crack advance. The specimen fracture surface is shown in Figures 144 through 147.

The primary or *barrier*  $\gamma'$  (referred to by Yeom as an octet<sup>20</sup>) microstructure, which was produced by HT 4, produced the fractures shown in Figures 148 through 151.

<sup>20</sup> Yeom, S.J., Yoon, D.Y. and Henery, M.F.; *Metallurgical Transactions*; Vol 24A, pp 1275, September 1993.



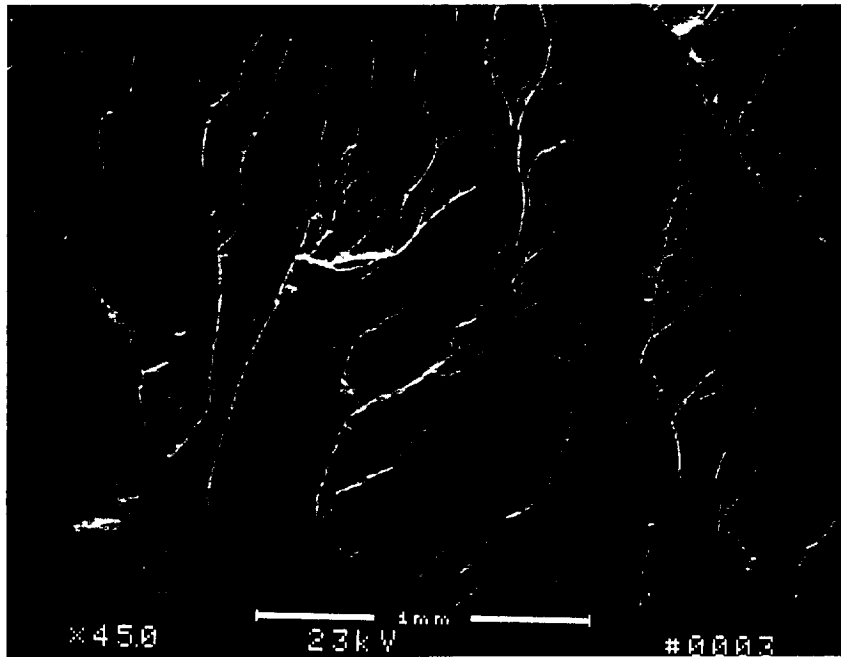


Figure 144. Fatigue Crack Growth in Hydrogen at Low Stress Intensity; Note Crack Front From Air Precrack at Top of Micrograph; Micromechanical Damage Was Extensive With Propagation on Multiple Parallel Planes; Crack Advance Was Extremely Rapid; Conditions – PWA 1484 HT 1, Fatigue Crack Growth in 20°C (68°F), 34.5 MPa (5 ksi) Hydrogen,  $R = 0.1$ , 0.16 Hz

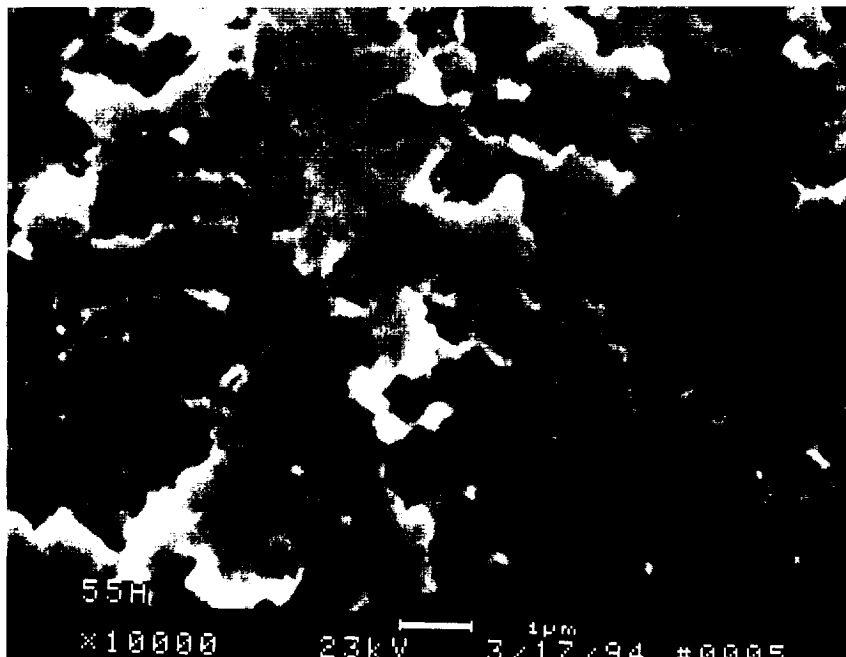
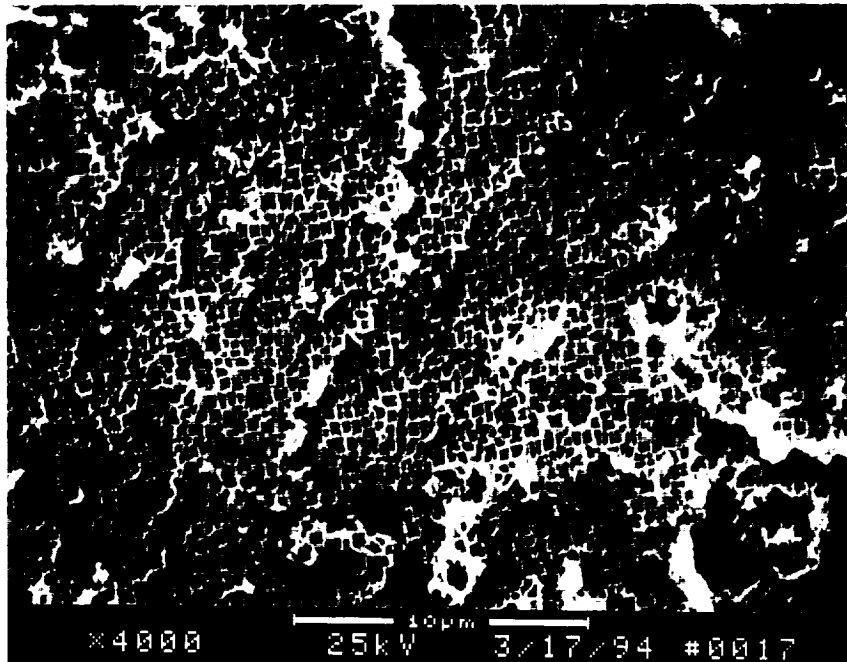
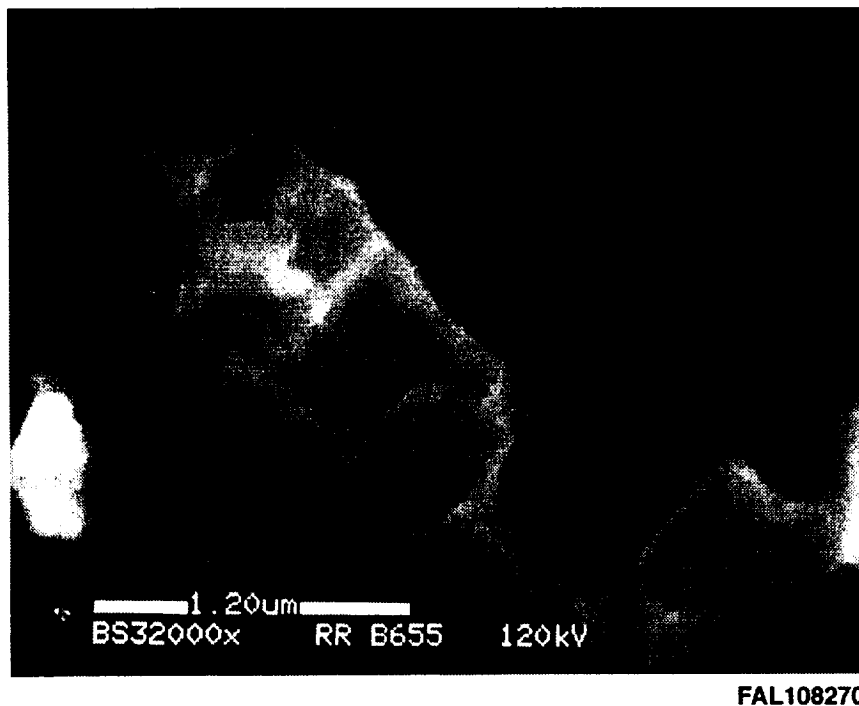


Figure 145. Microscopic Fracture Mode From Figure 144 Shows Failure Along Multiple Layers of  $\gamma'$ ; Conditions – PWA 1484 HT 1, Fatigue Crack growth in 20°C (68°F), 34.5 MPa (5 ksi) Hydrogen,  $R = 0.1$ , 0.16 Hz



*Figure 146. Microscopic Fracture Mode From Figure 145 Etched in This Case Shows Layers of  $\gamma$  Exhibiting "Stepped" Appearance Associated With Matrix Failure; Conditions – PWA 1484 HT 1, Fatigue Crack Growth in 20°C (68°F), 34.5 MPa (5 ksi) Hydrogen, R = 0.1, 0.16 Hz*



*Figure 147. SEM Mode From Scanning Transmission Electron Microscope (STEM) in High Voltage Backscatter Electron Imaging Shows Disposition of  $\gamma$  Phase (Blotches on Top of Upper Layer of Precipitates) and Step as Described in Figure 146*

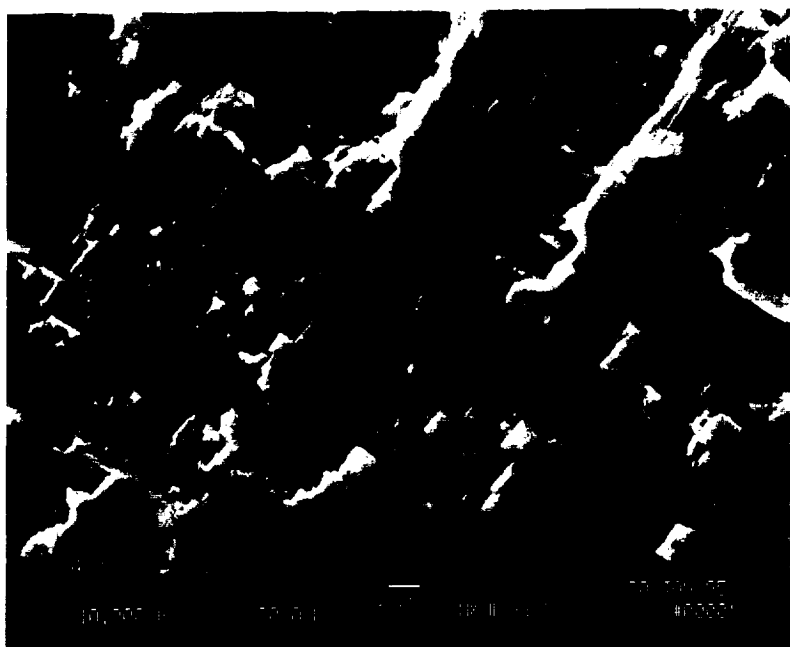


*Figure 148. FEM Imaging of HT 4 Shows Planer Fracture in Primary  $\gamma'$  (Dark Flat "X" Shape at Center) Surrounded by (111) Crystallographic Fracture in Fine Cuboidal  $\gamma'$*



*Figure 149. Enlargement of Primary  $\gamma'$  From Figure 148; PWA 1484 HT 4; Orthogonal Metallographic Sections Show Precipitate Is Ripened Octet Elongated in  $\langle 111 \rangle$  Directions (Appearing To Be  $\langle 110 \rangle$  in This  $\langle 001 \rangle$  View); Conditions – Fatigue Crack Growth in 34.5 MPa (5 ksi), 20°C (68°F), Hydrogen*

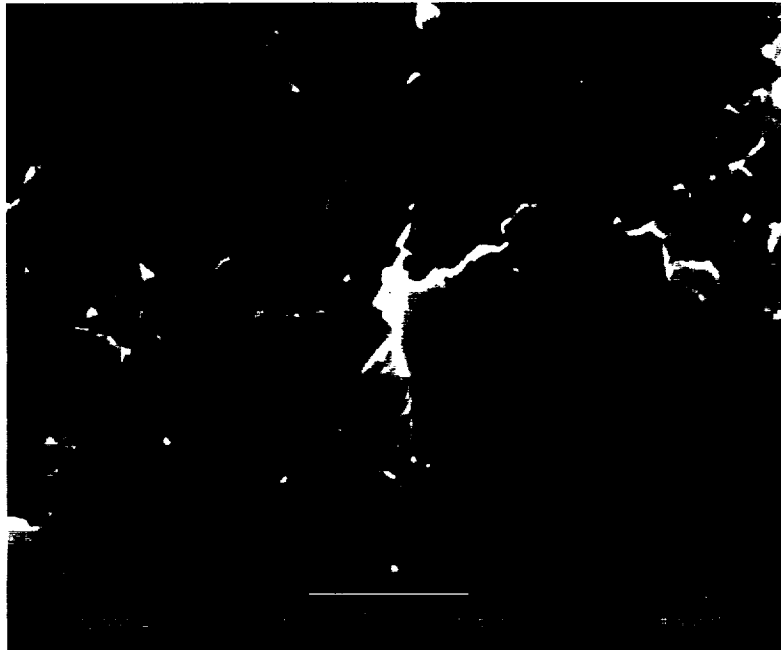


*Figure 150. Center of Octet (From Figure 149) Shows (111) Matrix Failure Revealed by Sunken "Stepped" Fracture; PWA 1484 HT 4; Conditions – Fatigue Crack Growth in 34.5 MPa (5 ksi), 20°C (68°F), Hydrogen*

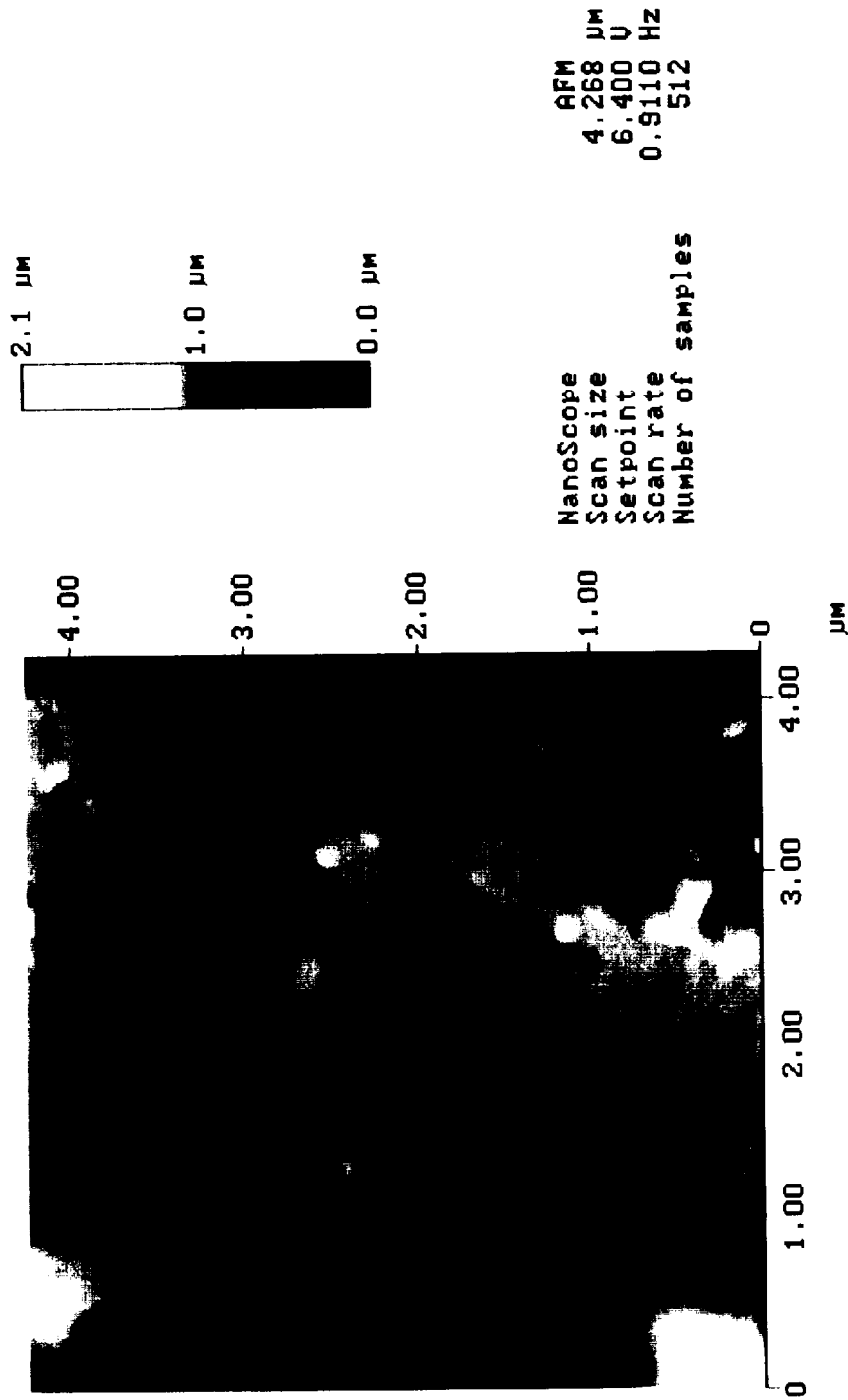
## 2.7.6 Elemental Analysis/Phase Compositions/Deformation Structures

The shearing of precipitates by dislocations culminating in (111) fracture is resisted by atomic forces within the  $\gamma'$  superlattice, namely the antiphase boundary energy (APBE) and the superlattice intrinsic stacking fault energy (SISFE). These parameters are a function of superlattice chemistry, representing the resistive force in an energy balance equation; where the rate of applied strain energy,  $de/dt$  (a function of  $\Delta K$ ,  $R$ , and frequency), represents the driving force. The resultant microscopic fracture mode is the dependent variable in this equation and determines the operative microscopic fracture mode and resultant FCG behavior.

The bimodal microstructures described in this program exhibit precipitate shearing in high-pressure hydrogen, where conventional microstructures do not. This microscopic fracture mode transition is beneficial, producing a significant reduction in crack growth rate<sup>21</sup> in hydrogen. This is evidenced by the difference in growth rate between microstructures HTs 4 and 6. The significantly higher volume fraction of primary  $\gamma'$  in HT 6 compared to HT 4 is likely responsible for the differing growth rates. The change is theorized to stem from differences in the bimodal microstructure's fine cuboidal  $\gamma'$  composition compared to that of a conventional microstructure, one with all fine uniform cuboidal precipitates. The staged precipitation cycle affects the  $\gamma'$  phase compositions.

<sup>21</sup> DeLuca, D.P., Jones, H.B., Cowles, B.A., and Cobia, F.D.; *Second Workshop on Hydrogen Effects on Materials Propulsion Systems*; 20-21 May 1992; Proceedings of Conference Held at NASA George C. Marshall Space Flight Center, Huntsville, AL; NASA CP-3182.

Height Angle Plane Angle Clear Calculator



pwa 1484 crack growth test specimen  
waterpro.039

Height

Figure 151. Atomic Force Microscopy (AFM) of Fatigue Crack Growth Fracture Produced in Room Temperature 34.5 MPa (5 ksi) Hydrogen; Enlargement of primary  $\gamma'$  from Figure 150; In This Case, the "Step" Is Elevated by Approximately 0.2  $\mu\text{m}$ ; (111) Matrix Failure Appears at Right Corner of Step; Blotches on Precipitate Surface Are  $\gamma$  Phase (as in Figure 147); PWA 1484 HT 6

While checking for reprecipitated  $\gamma$  in thin foils of PWA 1484 HT 4, phase composition gradients were determined for the fine cuboidal  $\gamma/\gamma'$  composition. The results are shown in Table 28. Phase compositions can be modeled by atomistic simulation techniques to relate superlattice parameters, such as antiphase boundary and superintrinsic stacking fault (APBE and SISFE) to superlattice chemistry. The results for the selected elements are plotted in Figures 152 and 153.

Table 28. Phase Composition Gradients in  $\gamma$  and Fine Cuboidal  $\gamma'$  From PWA 1484 HT 4

	Distance from $\gamma/\gamma'$ Interface (nm)	Al	Cr	Co	Ni	Mo	Hf	Ta	W	Re
$\gamma$	-200	2.80	11.16	14.28	55.14	3.72	0.33	2.03	6.25	4.29
$\gamma$	-100	2.48	11.38	13.91	56.13	3.56	0.39	1.63	6.07	4.45
$\gamma'$	100	6.42	2.14	7.46	69.71	0.71	0.59	8.70	3.83	0.45
$\gamma'$	200	6.00	2.11	7.63	70.63	0.73	0.65	8.74	3.11	0.40
$\gamma'$	400	5.78	2.00	7.62	70.15	0.90	0.80	8.98	3.18	0.59

### Deformation Structures

The foils that were produced to study reprecipitated  $\gamma$  in the primary  $\gamma'$  were intentionally obtained from controlled strain LCF specimens, so that they could also provide an opportunity to view the underlying deformation structures associated with bimodal microstructures. In general, the foils showed dislocations at the interface of the primary  $\gamma$  and within the primary  $\gamma'$  (Figures 154 through 156), but relatively light concentrations in the areas of fine  $\gamma'$ .

### Interdendritic Mismatch

The high gradient casting process not only affects dendrite arm spacing, but also interdendritic misorientation. Increased amounts of dendritic misorientation are felt to be beneficial under certain circumstances, specifically Mode II (111) crystallographic fatigue crack initiation and propagation. This is so because the only microstructural element acting as an impediment to crack advance in (111) shear, other than  $\gamma$  and  $\gamma/\gamma'$  interfaces, is dendritic mismatch.

As such, Laue' x-ray analysis was employed to characterize the degree of mismatch as a function of casting thermal gradient. PWA 1484 cast bars were selected for the measurement. Castings produced under the high thermal gradient casting conditions are started at a conventional gradient approximately equal to 30°C/cm (140°F/in.) and quickly increased to approximately 57°C/cm (260°F/in.). Laue' back reflection x-ray diffraction was conducted on each end of the cast PWA 1484 bar and compared.

Five Laue' photographs were taken across each (001) section (perpendicular to the growth direction, space approximately 5 mm (0.20 in.) apart.

The analysis showed more long range and local misorientation at the high gradient end of the bar than at the low gradient end. At the low gradient end, the average total mismatch was 0.6 degree (average tilt mismatch was 0.5 degree and average rotation mismatch was 0.2 degree). At the high gradient end the average total mismatch was 2.4 degrees (average tilt mismatch was 2.2 degrees and average rotational mismatch was 0.5 degree).

### 2.7.7 Summary

The bimodal microstructures show (111) precipitate fracture in the fine cuboidal  $\gamma'$ . Essential fracture details of the primary  $\gamma'$  are unresolved at high magnification through SEM/FEM and replica TEM<sup>22</sup>, as only a suggestion of structure is revealed. The AFM compliments the images provided by SEM/FEM and TEM, and together support the observations that matrix failure is in some cases (111) fracture of the  $\gamma$  phase.

---

<sup>22</sup> Scanning Transmission Electron Microscopy (STEM) has been experimented with for high-magnification work with mixed results in P&W's Independent Research and Development Programs. The practice is hindered by the additional costs associated with extracting specimens from the fracture surfaces of interest.

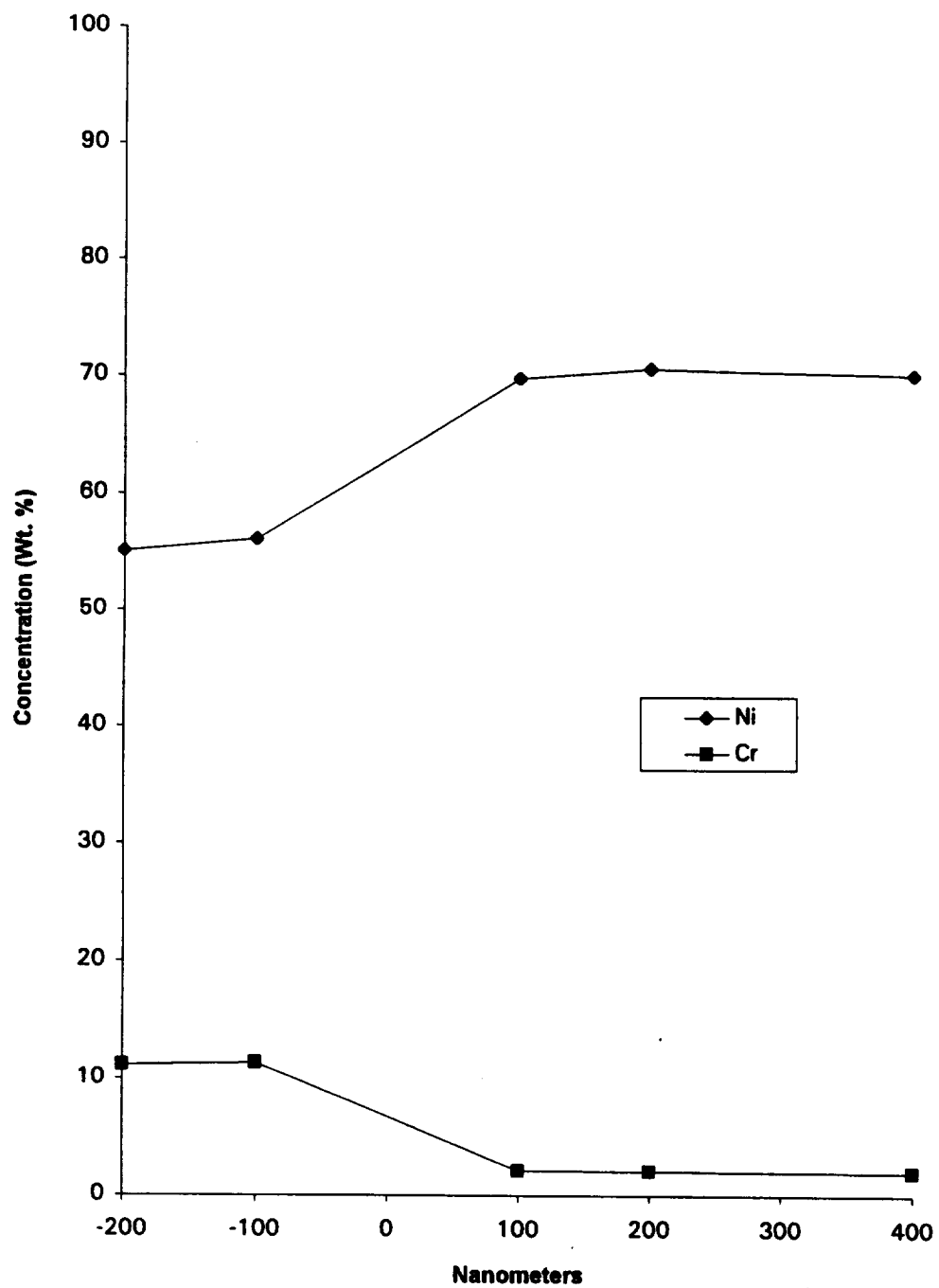


Figure 152.  $\gamma/\gamma'$  Phase Composition gradients for Ni and Cr in PWA 1484 HT 4;  $\gamma/\gamma'$  Interface is at zero nanometers



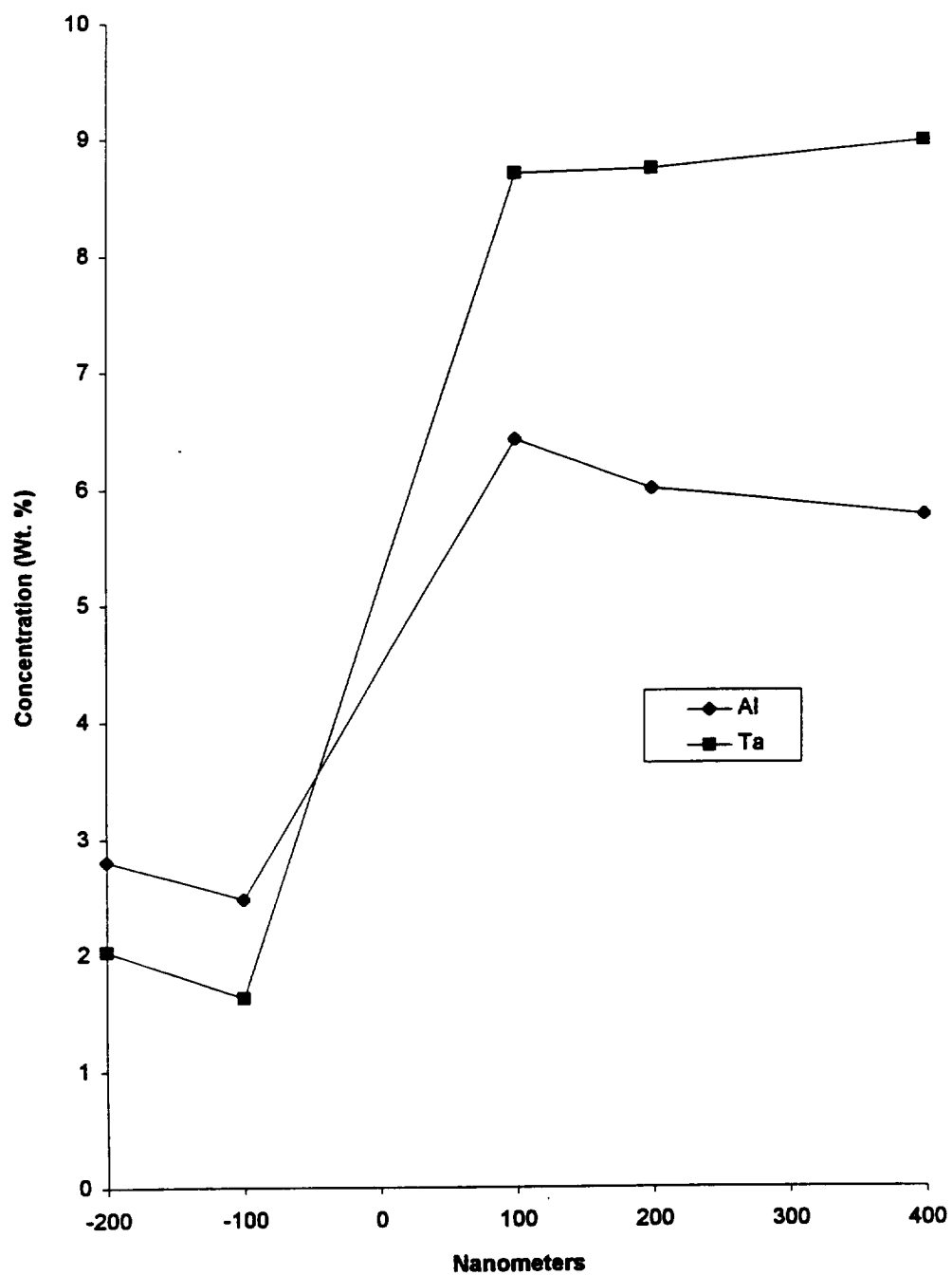
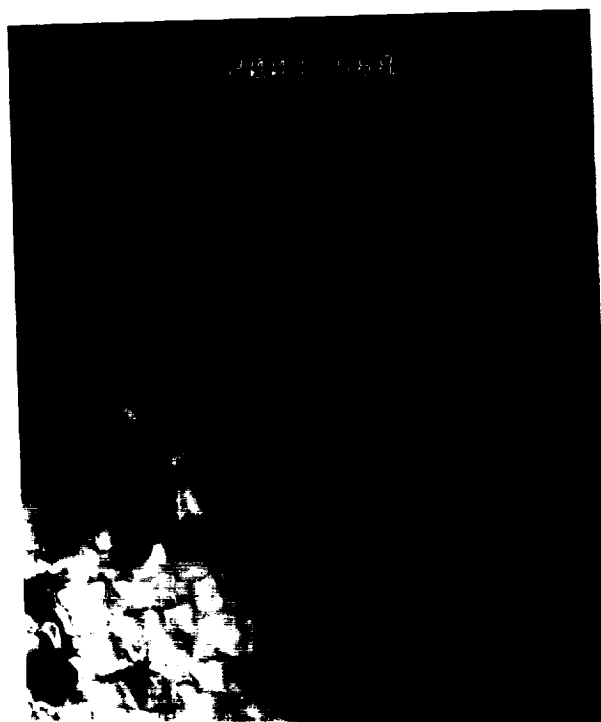
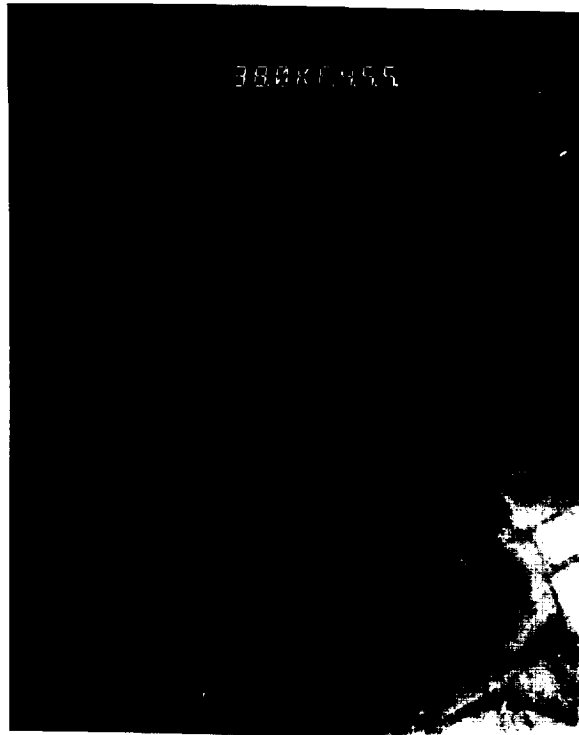


Figure 153.  $\gamma/\gamma'$  Phase Composition Gradients for Al and Ta in PWA 1484 HT 4;  $\gamma/\gamma'$  Interface Is at zero nanometers



*Figure 154. Fine Cuboidal  $\gamma$  Covers Lower Left Half of Micrograph; Overaged Octet (Primary  $\gamma$ ) At Upper Right; Octet/ $\gamma$  Interface Is Delineated by High Dislocation Concentration; Numerous Dislocations Can Be Observed Within Octet; Conditions – Controlled Strain LCF,  $\Delta\epsilon_f = 1.5\%$ ,  $20^\circ\text{C}$  ( $68^\circ\text{F}$ ),  $34.5\text{ MPa}$  ( $5\text{ ksi}$ ) Hydrogen,  $R = -1$ , Load Axis  $\langle 001 \rangle$ , Zone Axis Approximately  $\langle 001 \rangle$ , Magnification  $20,000\times$*



*Figure 155. Higher Magnification of Interface Shows Concentrated Dislocations at Octet/ $\gamma$  Interface (Left) and Near Absence of Dislocations in Cuboidal  $\gamma/\gamma'$  Array; Conditions – Controlled Strain LCF,  $\Delta\epsilon_f = 1.5\%$ ,  $20^\circ\text{C}$  ( $68^\circ\text{F}$ ),  $34.5\text{ MPa}$  (5 ksi) Hydrogen,  $R = -1$  Load Axis  $\langle 001 \rangle$ , Zone Axis Approximately  $\langle 001 \rangle$ , Magnification 30,000X.*



*Figure 156. Dislocation Structures Within Primary  $\gamma$ , Cuboidal  $\gamma'$  Can Be Observed at Upper Right Bounded by Dislocation Tangles at Interface With Octet; Deformation Substructures Within Octet Are Coincident With Fractographic Details Previously Discussed in Paragraph 2.7.4 – Fatigue Fractures; Conditions – Controlled Strain LCF,  $\Delta\epsilon_f = 1.5\%$ ,  $20^\circ\text{C}$  ( $68^\circ\text{F}$ ),  $34.5\text{ MPa}$  ( $5\text{ ksi}$ ) Hydrogen,  $R = -1$  Load Axis  $\langle 001 \rangle$ , Mag  $30,000\times$ , Zone Axis Approximately  $\langle 001 \rangle$*

### 3. SUMMARY

A summary of the specific accomplishments for the program is provided in the following paragraphs.

#### 3.1 PROCESSING

Advanced processing approaches have been successfully demonstrated with two single-crystal alloys. These processes include:

- Procurement of two 227 kg (500 lb) heats of certified chemistry PWA 1482 and PWA 1484.
- Demonstration of high thermal gradient casting of low carbon PWA 1482 and PWA 1484.
- Establishment of hot isostatic pressing (HIP) parameters for both single-crystal alloys.
- Development of solution heat treatment (HT) parameters that provide 100 percent gamma prime ( $\gamma'$ ) solutioning, including all eutectic  $\gamma/\gamma'$  phases islands.
- Development of post-solution HT parameters that produced seven variations of  $\gamma'$  precipitate morphology in PWA 1484 and two in PWA 1482 for subsequent mechanical property testing and evaluation.
- Two general types of  $\gamma'$  microstructures were developed in PWA 1484; both were pore free and eutectic-free. The principal difference between the two was the  $\gamma'$  precipitate morphology. Variations on (1) a fine cuboidal  $\gamma'$  precipitate morphology and (2) a bimodal  $\gamma'$  precipitate morphology were developed.
- The first group, HTs 1 and 2 possessed microstructures ranging from the conventional fine cuboidal  $\gamma'$  precipitate morphology to a coarse, less geometrically ordered structure. The second group, HTs 3 through 7, exhibited a bimodal  $\gamma'$  structure as previously described.
- These microstructures were evaluated under the Section 2/Paragraph 2.5 – *Hydrogen Test – Alternate Microstructure Screening* for their relative hydrogen capability in tensile, notched low-cycle fatigue (LCF) and fatigue crack growth (FCG) tests conducted in 34.5 MPa (5 ksi) hydrogen at 20°C (68°F).
- Based on this study, two microstructures were later chosen (down selected) from these screening test results for application to both PWA 1484 and PWA 1482. An alloy/process comparison was then made in testing that was covered in the Section 2/Paragraph 2.6 – *Program Test Matrix*.

#### 3.2 ALLOY CAPABILITY

Tensile fatigue and crack growth results obtained from the Section 2/Paragraph 2.5 – *Hydrogen Test – Alternate Microstructure Screening* include the following:

##### 3.2.1 Tensile

- Screening of HTs 1 through 3 showed that the greater the departure from a geometrically ordered fine uniform cuboidal  $\gamma'$  morphology, the more tensile ductility was degraded.
- For all HTs 1 through 3, ductility was low, ranging from 2.6 percent down to 1.6 percent elongation. Yield and ultimate strength showed either no effect as in HT 1 or, in the case of HT 2, a 1.0 percent increase in strength. No distinct yield point was observed with these microstructures, as yield and ultimate strength occurred simultaneously, consistent with nonductile behavior.
- The microstructures produced with bimodal  $\gamma'$  precipitate morphologies (HTs 4 through 7) showed generally lower strength and better ductility than the former group of microstructural variations. This tradeoff of strength for ductility was accompanied by the appearance of a distinct tensile yield point.

##### 3.2.2 Notched Low-Cycle Fatigue

- Notched LCF tests, run under the *Alternate Microstructure Screening* study on HTs 1 through 7, showed that all seven HTs produced more than an order of magnitude improvement over PWA 1480 and three orders of

magnitude improvement over directionally-solidified (DS) columnar-grained MAR-M-246+Hf, which is the current blade alloys used in the SSME. This testing was conducted at a single stress level (620.6 MPa [90 ksi]) in 34.5 MPa (5 ksi) hydrogen at room temperature.

### 3.2.3 Crack Growth

- Heat Treatments 1 through 3 generally exhibited growth rates too rapid to be considered for further development. The only microstructures showing promise were the bimodal  $\gamma'$  structures.
- Of the bimodal  $\gamma'$  structures, PWA 1484 HT 6 is more than 10X better than PWA 1480 at 8 MPa  $\sqrt{m}$ . The PWA 1484 HT 6 crack growth rate curve crossed the PWA 1480 curve at 20 MPa  $\sqrt{m}$ . Above 20 MPa  $\sqrt{m}$ , PWA 1480 is superior to PWA 1484 HT 6. Below this point PWA 1484 has the advantage.
- PWA 1484 HT 4 fatigue crack growth capability was inferior to PWA 1480 at all stress intensities.

## 3.3 PROGRAM TEST MATRIX

The *Program Test Matrix* evaluated HTs 4 and 6 applied to PWA 1482 and PWA 1484 at room and elevated temperatures in air and hydrogen. Where important differences existed between HTs 4 and 6, these were fully documented; however, small differences are not necessarily addressed in these conclusions due to the limited number of tests conducted.

### 3.3.1 Yield Strength

- In 20°C (68°F) hydrogen, PWA 1482 HT 4 strength was greater than HT 6, which is consistent with PWA 1484 behavior.
- In 649°C (1200°F) hydrogen, the difference in yield strengths for the two HTs is less pronounced than at 20°C (68°F).
- In hydrogen, yield strengths for the two alloys were similar; however both were significantly lower than PWA 1480. The higher volume fraction of primary  $\gamma'$  (HT 6) carried a strength penalty in both alloys.
- Ultimate strength in hydrogen for PWA 1482 was equal to or higher than PWA 1484; however, this also was considerably lower than PWA 1480.
- In 649°C (1200°F) air, PWA 1482 yield strength was similar to PWA 1484 for both HT 4 and 6 and 200 MPa (30 ksi) weaker than PWA 1480.
- Air ultimate tensile strength for PWA 1482 was higher than PWA 1484.
- PWA 1482 ductility (elongation and area reduction) is lower than PWA 1484 with little effect of heat treatment observed. Above 649°C (1200°F), PWA 1484 is much more ductile than PWA 1480.

### 3.3.2 Creep Stress/Rupture

- PWA 1484 creep capability is much better than PWA 1480, and HT 4 has a distinct advantage over HT 6.
- PWA 1482 creep/stress rupture capability is not as good as PWA 1480.<sup>23</sup> PWA 1482 HTs 4 and 6 creep rates were nearly identical, suggesting this alloy's creep/stress rupture capability was not sensitive to differing volume fractions of primary  $\gamma'$  as was PWA 1484.

<sup>23</sup> PWA 1484 was formulated specifically for superior creep to PWA 1480 and PWA 1482. the improved creep behavior in PWA 1484 is due to the addition of rhenium.

### 3.3.3 Fatigue

- High-Cycle Fatigue

- In 34.5 MPa (5 ksi) hydrogen at room temperature, smooth HCF life for both PWA 1482 and PWA 1484 is between two and three orders of magnitude (100X to 1,000X) greater than PWA 1480. The fatigue strengths of PWA 1482 and PWA 1484 are more than twice the strength of PWA 1480.
- Although PWA 1482 and PWA 1484 were not specifically evaluated in air HCF testing, an interesting comparison can be made. Both advanced processed alloys have (depending on stress) 10X to 20X better life in hydrogen than PWA 1480 in air and almost twice the fatigue strength. HCF gains of this magnitude are unprecedented and suggest that modified PWA 1484 is essentially undebited by hydrogen in room temperature HCF. This benefit will likely carry over to air breathing applications.

- Strain Controlled Low-Cycle Fatigue

- In controlled strain tests conducted in high-pressure hydrogen at room temperature, smooth LCF lives for both PWA 1482 and PWA 1484 are more than 10X longer than PWA 1480.
- Hydrogen capability for PWA 1484 is roughly equal to PWA 1482 at 1.2 percent strain. Above this level, PWA 1482 exhibits a significant advantage over PWA 1484, which is likely due to the strength advantage in hydrogen exhibited by PWA 1482.
- In controlled strain tests conducted in air, smooth LCF results show PWA 1484 to possess an approximate 2X advantage over PWA 1482.<sup>24</sup> PWA 1484 is slightly better than PWA 1480 at 1.6 percent strain. PWA 1484 LCF life is more than 10X greater than PWA 1480 at 1.0 percent strain.

- Notched Low-Cycle Fatigue

- In 34.5 MPa (5 ksi) hydrogen at room temperature, PWA 1482 and PWA 1484 notched LCF lives range from 4X to more than 10X greater than PWA 1480, depending on stress.
- In room temperature air, notched LCF lives for both PWA 1482 and PWA 1484 are slightly lower than PWA 1480. These sample sizes are small; however, and this difference is probably due to normal fatigue data variability. No important difference exists between PWA 1484 and PWA 1482.

- Fatigue Crack Growth

- Room temperature 34.5 MPa (5 ksi) hydrogen crack growth properties of PWA 1484 HT 6 are significantly better than HT 4.
- PWA 1484 HT 6 has similar crack growth properties to PWA 1480 in high-pressure hydrogen at room temperature.

### 3.4 MECHANISTIC ASPECTS

- In PWA 1484, the higher volume fraction of primary  $\gamma'$  in HT 6 appears detrimental to creep either indirectly by lowering strength or directly by affecting creep deformation mechanisms.
- With respect to fatigue, since all seven  $\gamma'$  precipitate variations showed >10X better life in hydrogen than PWA 1480 regardless of  $\gamma'$  structure, it appears that the single most potent microstructural effect appears to be the elimination of microstructural discontinuities (eutectics, porosity, carbides).
- Most fatigue failures were initiated by microscopic Stage I crystallographic facets or at locations where no point source origin could be identified (leaving surface finish suspect).
- The fact that the pore-free, eutectic-free microstructures provided no benefit in air LCF is not surprising.

<sup>24</sup> PWA 1484 tests showed less inelastic strain than PWA 1482 at equivalent total strain.

Micropores and eutectics are generally not operative defects in 26°C (79°F) air. Gayda *et. al.*<sup>25</sup> has shown that eliminating microsporosity in PWA 1480 was ineffective in reducing the hydrogen-to-air debit in fatigue in a previous study. Fatigue cracks in the PWA 1482 specimens, tested in hydrogen, were surface connected, initiating at microscopic Stage I facets or no specific point source.

- Both PWA 1482 and PWA 1484 bimodal microstructures exhibited a significant amount of microscopic (111) fracture, typical of conventional high volume fraction  $\gamma'$  strengthened superalloys with fine uniform cuboidal  $\gamma'$  microstructures.

### 3.5 OVERALL SUMMARY

In reusable space propulsion systems, the most important quality that an otherwise capable rocket turbine alloy can possess is superior durability. In this program, two alloys with fatigue capability, superior to that of the most advanced blade material currently available (PWA 1480), were successfully demonstrated.

The current Space Shuttle Main Engine (SSME) High Performance Fuel Turbopump (HPFTP) blade alloy directionally-solidified (DS) MAR-M-246+Hf was compared to a number of alternate blade alloys, including PWA 1480 in the SSME Alternate Turbopump (AT) Program (NASA-MSFC Contract No. NAS8-36801).

The most pronounced hydrogen degradation was observed at 26°C (79°F) in 34.5 MPa (5 ksi) hydrogen for smooth and notched fatigue, where life was decreased by an order of magnitude or more.

Those tests showed PWA 1480 to exhibit a 10X advantage over DS MAR-M-246+Hf. The advanced processed PWA 1484 microstructures developed in the current program in some cases exhibit a 100X improvement over PWA 1480 fatigue life.

Shuttle engine life cycle cost (LCC) is significantly impacted by turbine airfoil inspection interval requirements. Increasing the number of missions between inspections can have a significant effect on system LCC. Modified PWA 1484 has the potential of greatly reducing system LCC.

<sup>25</sup> Gayda, T.P. and Dreshfield, R. L.; *Hydrogen Effects on Material Behavior*; Moody, N.R. and Thompson, A.W., eds.; TMS, Warrendale, PA, pp 591-601, 1989.



#### 4. CONCLUSIONS

The following conclusions are provided:

- The advanced single-crystal processing methods developed in this program are production viable methods for the manufacture of turbine hardware.<sup>26</sup>
- Hot isostatic pressing (HIP) eutectic-free bimodal gamma prime ( $\gamma'$ ) microstructures have been shown to be superior to conventional microstructures in hydrogen applications regardless of casting form.<sup>27</sup>
- Reduction of intrinsic microstructural discontinuities (pores, eutectics, carbides) significantly improves fatigue properties in hydrogen.
- Bimodal  $\gamma'$  precipitate microstructures are needed to reduce the hydrogen induced increase in fatigue crack growth (FCG) rate.

---

<sup>26</sup> Modified PWA 1484 thermal processing parameters successfully transitioned (HT 6) from this NASA contract to the Space Shuttle Main Engine (SSME) Alternate Turbopump (AT) Program for use as high-pressure fuel turbopump (HPFTP) blade and vane material. Howmet Dover successfully demonstrated vane/blade casting and thermal processing trials for the fuel pump 1st- and 2nd-stage fuel vanes and 1st-stage blades. PWA 1484 HT 6 High-Pressure Fuel Turbopump (HPFTP) 2nd-stage vanes were procured for SSME-AT development engine testing.

<sup>27</sup> In a series of company funded research programs, the HIP eutectic-free bimodal  $\gamma'$  microstructures studied in this contract have been evaluated in equiaxed, columnar grain, and single-crystal alloys. Pratt & Whitney's Space Propulsion (SP) alloy PWA-SP 1489, a HIP eutectic-free bimodal  $\gamma'$  version of HIP Microcast Mar-M-247, is targeted for five oxidizer pump applications because of its superior durability in hydrogen.



## 5. SPECIFIC RECOMMENDATIONS

Recommendations include the following:

1. PWA 1484 Heat Treatments (HTs) 4 and 6 warrant further mechanical property characterization. A comprehensive specimen test program is recommended.<sup>28</sup>

2. Because hot isostatic pressing (HIP) eutectic-free bimodal gamma prime ( $\gamma'$ ) microstructures have been shown to be superior to conventional microstructures in hydrogen, it is recommended that these advanced processing approaches be considered, where applicable (e.g., cast, high volume fraction, cuboidal  $\gamma'$  strengthened Ni base superalloys), when superior durability is a requirement.

3. A modified chemistry PWA 1480 (within PWA 1480 specifications) that possesses a wider solutioning window has been the subject of limited testing at Pratt & Whitney (P&W). This alloy can be produced HIP eutectic-free in a production environment and has been evaluated with a bimodal precipitate structure. Fatigue and fracture gains, similar to those achieved in this program, were demonstrated with this modified version of PWA 1480. It is recommended that a characterization be conducted to combine this program's enhanced durability approaches with PWA 1480's intrinsically high strength.

4. Rotating structures, such as turbine blades, are self loaded through centrifugal force. This places an increased demand on the platform and attachment areas, where numerous stress concentrations are present. A low-density superalloy produced in an anisotropic casting form (for high-specific strength) could show a significant increase in thrust-to-weight ratio (largely by allowing lighter turbine disk designs). This blade alloy system could be further augmented with the superior durability shown by the advanced processing approaches developed in the present study. It is recommended that the development of a high-specific strength hydrogen resistant turbopump blade alloy (based on the program microstructures) be undertaken.

5. The mechanism by which improved crack-growth resistance in hydrogen is achieved is through the restoration of the normal air fracture mode, which has been disrupted by hydrogen. This appears to come about by some effect on fault energies within the  $\gamma'$  superlattice.<sup>29</sup> A study of the relationships existing between superlattice elemental composition, fault energies, and submicroscopic fracture mode is recommended. Specifically, atomistic simulations of the program alloys  $\gamma'$  compositions should be conducted.

6. Several advanced rocket concepts include turbomachinery operating at temperatures well below those of the SSME. In hydrogen fueled systems,  $\gamma'$  alloys are at a disadvantage due to their inherent tendency for strain localization in the matrix phase, exacerbated by hydrogen, resulting in matrix failure. Lower temperatures permit alternative alloy systems other than high volume fraction  $\gamma'$  strengthened superalloys.  $\gamma'$  alloys (such as INCO 718) possess an inherent immunity to this mechanism of degradation,<sup>30</sup> however, since they are exclusively used in equiaxed form, this strength is not realized as intergranular failure becomes the limiting factor. A high strength  $\gamma'$  single-crystal alloy has been the subject of limited testing in air and high-pressure hydrogen at P&W. The alloy has shown superior hydrogen high-cycle fatigue (HCF) and a 275 MPa (40 ksi) room temperature strength advantage as compared to PWA 1480. Most notably the microscopic fatigue fracture is the same in air and room temperature high-pressure hydrogen. It is recommended that a  $\gamma'$  strengthened single-crystal alloy be investigated.

7. The microstructural alterations in the program alloys were suggested by studying microscopic fracture modes at very high magnification. This additional insight leads to more questions about mechanistic details occurring on an increasingly minute level. Pratt & Whitney views this approach to fracture research based alloy develop-

<sup>28</sup> During the course of this program, the NASA/P&W SSME Alternate Turbopump (AT) Program requested the transfer of all of this program's PWA 1484 cast bars to the AT Program for mechanical property characterization as a fuel turbopump vane alloy.

<sup>29</sup> Baskes, M.I., Angelo, J.E., and Moody, N.R.; *Atomistic Calculations of Hydrogen Interactions With Ni<sub>3</sub>Al Grain Boundaries and Ni/Ni<sub>3</sub>Al Interfaces*; Sandia National Laboratories Report, SAND94-8741 • YX-41, Albuquerque, NM and Livermore, CA; Contract DE-AC04-94AL85000; January 1995.

<sup>30</sup> DeLuca, D.P. and Hatala, R.W.; *Single-Crystal PWA 1472 in High-Pressure Hydrogen*; Superalloys 718, 625, and 706 and Various Derivatives; Loria, E.A., ed., TMS, Warrendale, PA, 1994.

ment as a critical technology to be increasingly applied to present and future problems in materials mechanics. The adoption of atomic force microscopy (AFM) to study nanoscopic fracture features was attempted in this study. This is a relatively new application of AFM, and preliminary results are encouraging. It is recommended that this technique be pursued in future investigations of the micromechanics of the fatigue and fracture processes.

8. Thread sizes on single-crystal specimens that are intended for hydrogen environment testing should be larger than standard air specimen threads to reduce the possibility of thread failures.

## **APPENDIX A — HEAT CERIFICATION**



**SPECIAL METALS CORPORATION**  
MIDDLE SETTLEMENT ROAD.  
NEW HARTFORD, NEW YORK 13413

# CERTIFICATE OF TEST

1110

# CERTIFICATE OF TEST

HEAT NO		SIZE				ALLOY		SMC ORDER NO		CUSTOMER ORDER NO		WEIGHT		DATE MO/DAY/YR	
D54223		2 3/4" DIA.				PWA 1482 A		PHA-13 RESII		N0614884				6-10-92	
C	PN	SI	CR	NI	CO	FE	MO	W	V	NB	TI	AL	B	ZR	
0.0039	0.01	0.03	8.95	BAL	5.02	0.017	0.96	6.68	0.01	0.01	1.05	5.57	0.001	0.001	
S	P	CU	TA	HF	AG-PPM	PB-PPM	BI-PPM	CA-PPM	O-PPM	N-PPM	SN-PPM	CD-PPH	SB-PPM	2M-PPM	
0.0004	0.002	0.01	6.00	0.17	*5	*5	*0.5	*50	4	1	*20	*50	*20	*20	*20

$$N_{r,3B} = 2.181$$

ALL MATERIAL CROPPED AND CONDITIONED INGOT.  
"DENOTES LESS THAN NUMBER.  
CHEMISTRY WT & UNLESS DESIGNATED PPM.

HEAT TREATMENT	TYPE SAMPLE	TEMP ° F	STRESS/YIELD PSI	0.2% YIELD PSI	LIFE HRS	GAGE LGTH	ELONG %	RA %

GRAIN SIZE: \_\_\_\_\_

HARDNESS: \_\_\_\_\_

This is to certify that the above values are true and accurate to the best of my knowledge and belief

**PWA 1482A, CHEMISTRY ONLY**

26-01-92

PRATT AND WHITNEY AIRCRAFT  
DISBURSEMENT ACCOUNTING  
H.S. 182-05, 400 MAIN STREET  
EAST HARTFORD, CT 06108

# CERTIFICATE OF TEST

SPECIAL METALS CORPORATION

MIDDLE SETTLEMENT ROAD,  
NEW HARTFORD, NEW YORK 13413



HEAT NO	SIZE				ALLOY		SMC ORDER NO		CUSTOMER ORDER NO		WEIGHT		DATE MO/DAY/YR	
D54224	2 3/4" DIA.				PWA 1482A		PWA-13 RESH		N0614884				6-10-92	
C	MN	SI	CR	NI	CO	FE	MO	W	V	NB	TI	AL	B	ZR
0.0018	0.01	0.03	8.80	BAL	5.04	0.026	0.94	6.75	0.01	0.01	1.05	5.54	0.001	0.001
S	P	CU	TA	HIF	AG-PPM	PB-PPM	BI-PPM	O-PPM	N-PPM	SN-PPM	CD-PPM	ZN-PPM	SB-PPM	CA-PPM
0.0005	0.002	0.01	5.98	0.18	*5	*2	*0.3	7	2	*20	*50	*20	*20	*50

N<sub>0</sub>3B = 2.158

MATERIAL CROPPED AND CONDITIONED INGOT.  
\*DENOTES LESS THAN NUMBER.  
CHEMISTRY WT % UNLESS DESIGNATED PPM.

HEAT TREATMENT	TYPE SAMPLE	TEMP °F	STRESS/ULT PSI	0.2% YIELD PSI	LIFE MRS	RAGE LGTH	ELONG %	RA %
GRAIN SIZE:								
HARDNESS:								

PWA 1482 A, CHEMISTRY ONLY

This is to certify that the above values are true and accurate  
to the best of my knowledge and belief

*[Signature]* 6 '92





PRATT AND WHITNEY AIRCRAFT  
DISBURSEMENT ACCOUNTING  
M.S. 182-05, 400 MAIN STREET  
EAST HARTFORD, CT 06108

# CERTIFICATE OF TEST

SPECIAL METALS CORPORATION

MIDDLE SETTLEMENT ROAD,  
NEW HARTFORD, NEW YORK 13413



HEAT NO		SIZE			ALLOY		SMC ORDER NO		CUSTOMER ORDER NO		WEIGHT		DATE MO/DAY/YR	
D54229		2 3/4" DIA.			PWA 1484E		PWA-12 RESH		N0614884				6-19-92	
C	MN	SI	CR	NI	CO	FE	MO	W	V	NB	TI	AL	B	ZR
0.0045	0.004	0.05	4.93	BAL	10.08	0.02	1.88	5.91	0.01	0.05	0.017	5.66	0.0023	0.002
S	P	CU	TA	HF	RE	AG-PPH	PB-PPH	BI-PPH	O-PPH	N-PPH	MG-PPH	SN-PPH	CD-PPH	ZN-PPH
0.0004	0.003	0.01	8.74	0.12	2.95	*5	*1	*0.3	3	1	18	*20	*50	*20

N<sub>0</sub>3B = 2.108

FACTOR 1 = 48.025

FACTOR 2 = 2.114

100% VIRGIN MATERIAL. VIM MELTED. MATERIAL CROPPED AND CONDITIONED.

\*DENOTES LESS THAN NUMBER.

CHEMISTRY WT % UNLESS DESIGNATED PPM.

SB-PPH

\*20

HEAT TREATMENT	TYPE SAMPLE	TEMP °F	STRESS/UTL PSI	0.2% YIELD PSI	LIFE HRS	GAGE LGTH	ELONG %	RA %
HARDNESS:								
GRAIN SIZE:								

PWA 1484E, CHEMISTRY ONLY. (EXCEPTION C)

This is to certify that the above values are true and accurate to the best of my knowledge and belief

*Signature* 6-19-92

## **APPENDIX B — TEST MATRIX SPECIMENS**



Specimen Type	Material Spec.	Sample No.	Heat Treat	Bar S/N	Heat No.	$\alpha$
Smooth Tensile	PWA 1482	4-1	4	154143	J203	4
Smooth Tensile	PWA 1482	4-2	4	154144	J203	1
Smooth Tensile	PWA 1482	4-3	4	154146	J203	4
Smooth Tensile	PWA 1482	4-4	4	829201	J203	1
Smooth Tensile	PWA 1482	4-5	4	829203	J203	4
Smooth Tensile	PWA 1482	4-6	4	768810	P1030	3
Smooth Tensile	PWA 1482	4-7	4	768811	P1030	1
Smooth Tensile	PWA 1482	4-8	4	768903	P1030	6
Smooth Tensile	PWA 1482	4-9	4	768904	P1030	4
Smooth Tensile	PWA 1482	4-10	4	768905	P1030	2
Smooth LCF	PWA 1482	4-1	4	82953	J203	5
Smooth LCF	PWA 1482	4-2	4	82954	J203	2
Smooth LCF	PWA 1482	4-3	4	82955	J203	5
Smooth LCF	PWA 1482	4-4	4	82956	J203	6
Smooth LCF	PWA 1482	4-5	4	156012	P1030	
Smooth LCF	PWA 1482	4-6	4	156085	P1032	
Smooth LCF	PWA 1482	4-7	4	156102	P1032	
Smooth LCF	PWA 1482	4-8	4	156103	P1032	
Smooth HCF	PWA 1482	4-1	4	154147	J203	5
Smooth HCF	PWA 1482	4-2	4	154149	J203	4
Smooth HCF	PWA 1482	4-3	4	829202	J203	2
Smooth HCF	PWA 1482	4-4	4	768812	P1030	1
Smooth HCF	PWA 1482	4-5	4	768901	P1030	5
Smooth HCF	PWA 1482	4-6	4	768906	P1030	4
Notched LCF	PWA 1482	4-1	4	154143	J203	4
Notched LCF	PWA 1482	4-2	4	154144	J203	1
Notched LCF	PWA 1482	4-3	4	154145	J203	4
Notched LCF	PWA 1482	4-4	4	154146	J203	4
Notched LCF	PWA 1482	4-5	4	829203	J203	4
Notched LCF	PWA 1482	4-6	4	768810	P1030	3
Notched LCF	PWA 1482	4-7	4	768811	P1030	1
Notched LCF	PWA 1482	4-8	4	768903	P1030	6
Notched LCF	PWA 1482	4-9	4	768904	P1030	4
Notched LCF	PWA 1482	4-10	4	768905	P1030	2
Creep	PWA 1482	4-1	4	82953	J203	5
Creep	PWA 1482	4-2	4	82955	J203	5
Creep	PWA 1482	4-3	4	82956	J203	6
Crack Growth	PWA 1482	4-1	4	8	J203	2
Crack Growth	PWA 1482	4-2	4	8	J203	2
Collared LCF	PWA 1482	4-1	4	154149	J203	4
Collared LCF	PWA 1482	4-2	4	154149	J203	4
Collared LCF	PWA 1482	4-3	4	829201	J203	1
Collared LCF	PWA 1482	4-4	4	768817	P1030	
Collared LCF	PWA 1482	4-5	4	768901	P1030	5
Collared LCF	PWA 1482	4-6	4	768906	P1030	4

Specimen Type	Material Spec.	Sample No.	Heat Treat	Bar S/N	Heat No.	$\alpha$
Smooth Tensile	PWA 1482	6-1	6	154131	J203	4
Smooth Tensile	PWA 1482	6-2	6	154134	J203	4
Smooth Tensile	PWA 1482	6-3	6	154135	J203	4
Smooth Tensile	PWA 1482	6-6	6	154136	J203	3
Smooth Tensile	PWA 1482	6-4	6	154139	J203	4
Smooth Tensile	PWA 1482	6-5	6	154141	J203	3
Smooth Tensile	PWA 1482	6-7	6	768801	P1030	2
Smooth Tensile	PWA 1482	6-8	6	768802	P1030	4
Smooth Tensile	PWA 1482	6-9	6	768803	P1030	4
Smooth Tensile	PWA 1482	6-10	6	768804	P1030	6
Smooth Tensile	PWA 1482	6-11	6	768807	P1030	3
Smooth LCF	PWA 1482	6-1	6	82945	J203	2
Smooth LCF	PWA 1482	6-2	6	82947	J203	3
Smooth LCF	PWA 1482	6-3	6	82948	J203	0
Smooth LCF	PWA 1482	6-4	6	82951	J203	5
Smooth LCF	PWA 1482	6-5	6	156011	P1030	
Smooth LCF	PWA 1482	6-6	6	156066	P1030	
Smooth LCF	PWA 1482	6-7	6	156074	P1032	
Smooth LCF	PWA 1482	6-8	6	156083	P1032	
Smooth HCF	PWA 1482	6-1	6	154132	J203	1
Smooth HCF	PWA 1482	6-2	6	154139	J203	4
Smooth HCF	PWA 1482	6-3	6	154142	J203	2
Smooth HCF	PWA 1482	6-4	6	768805	P1030	2
Smooth HCF	PWA 1482	6-5	6	768806	P1030	4
Smooth HCF	PWA 1482	6-6	6	768808	P1030	7
Notched LCF	PWA 1482	6-1	6	154131	J203	4
Notched LCF	PWA 1482	6-2	6	154134	J203	4
Notched LCF	PWA 1482	6-3	6	154135	J203	4
Notched LCF	PWA 1482	6-4	6	154136	J203	3
Notched LCF	PWA 1482	6-5	6	154141	J203	3
Notched LCF	PWA 1482	6-6	6	768801	P1030	2
Notched LCF	PWA 1482	6-7	6	768802	P1030	4
Notched LCF	PWA 1482	6-8	6	768803	P1030	4
Notched LCF	PWA 1482	6-9	6	768809	P1030	5
Notched LCF	PWA 1482	6-10	6	768809	P1030	5
Creep	PWA 1482	6-1	6	82948	J203	0
Creep	PWA 1482	6-2	6	768804	P1030	6
Creep	PWA 1482	6-3	6	768807	P1030	3
Crack Growth	PWA 1482	6-2	6	8	J203	2
Collared LCF	PWA 1482	6-1	6	154132	J203	1
Collared LCF	PWA 1482	6-2	6	154133	J203	0
Collared LCF	PWA 1482	6-3	6	154142	J203	2
Collared LCF	PWA 1482	6-4	6	768805	P1030	2
Collared LCF	PWA 1482	6-5	6	768806	P1030	4
Collared LCF	PWA 1482	6-6	6	768808	P1030	7

<b>Specimen Type</b>	<b>Material Spec.</b>	<b>Sample No.</b>	<b>Heat Treat</b>	<b>Bar S/N</b>	<b>Heat No.</b>	<b><math>\alpha</math></b>
Smooth Tensile	PWA 1484	4-1	4	1530204	1033	3
Smooth Tensile	PWA 1484	4-2	4	1530207	1033	6
Smooth Tensile	PWA 1484	4-3	4	1530208	1033	4
Smooth Tensile	PWA 1484	4-4	4	1530210	1033	5
Smooth Tensile	PWA 1484	4-5	4	1530211	1033	4
Smooth Tensile	PWA 1484	4-6	4	1530212	1033	4
Smooth Tensile	PWA 1484	4-7	4	1531011	1034	2
Smooth Tensile	PWA 1484	4-8	4	1531103	1034	4
Smooth Tensile	PWA 1484	4-9	4	1531106	1034	5
Smooth Tensile	PWA 1484	4-10	4	1531107	1034	5
Smooth Tensile	PWA 1484	4-11	4	1531108	1034	
Smooth Tensile	PWA 1484	4-12	4	1531110	1034	2
Smooth LCF	PWA 1484	4-1	4	155023	1033	1
Smooth LCF	PWA 1484	4-2	4	155024	1033	4
Smooth LCF	PWA 1484	4-3	4	155025	1033	6
Smooth LCF	PWA 1484	4-4	4	155026	1033	6
Smooth LCF	PWA 1484	4-5	4	155038	1034	1
Smooth LCF	PWA 1484	4-6	4	155041	1034	3
Smooth LCF	PWA 1484	4-7	4	155042	1034	4
Smooth LCF	PWA 1484	4-8	4	155043	1034	3
Smooth HCF	PWA 1484	4-1	4	1530205	1033	4
Smooth HCF	PWA 1484	4-2	4	1530206	1033	2
Smooth HCF	PWA 1484	4-3	4	1530209	1033	4
Smooth HCF	PWA 1484	4-4	4	1531104	1034	3
Smooth HCF	PWA 1484	4-5	4	1531105	1034	5
Smooth HCF	PWA 1484	4-6	4	1531109	1034	5
Notched LCF	PWA 1484	4-1	4	1530207	1033	6
Notched LCF	PWA 1484	4-2	4	1530208	1033	4
Notched LCF	PWA 1484	4-3	4	1530210	1033	5
Notched LCF	PWA 1484	4-4	4	1530211	1033	4
Notched LCF	PWA 1484	4-5	4	1530212	1033	4
Notched LCF	PWA 1484	4-6	4	1531008	1034	4
Notched LCF	PWA 1484	4-7	4	1531011	1034	2
Notched LCF	PWA 1484	4-8	4	1531103	1034	4
Notched LCF	PWA 1484	4-9	4	1531106	1034	5
Notched LCF	PWA 1484	4-10	4	1531107	1034	5
Creep	PWA 1485	4-1	4	155025	1033	6
Creep	PWA 1486	4-2	4	1530204	1033	3
Creep	PWA 1487	4-3	4	1531110	1034	2
Crack Growth	PWA 1484	4-1	4	77	1034	3
Crack Growth	PWA 1484	4-2	4	77	1034	3
Collared LCF	PWA 1484	4-1	4	1530205	1033	4
Collared LCF	PWA 1484	4-2	4	1530206	1033	2
Collared LCF	PWA 1484	4-3	4	1530209	1033	4
Collared LCF	PWA 1484	4-4	4	1531104	1034	3
Collared LCF	PWA 1484	4-6	4	1531109	1034	5
Collared LCF	PWA 1484	4-5	4	1531105	1034	5

<b>Specimen Type</b>	<b>Material Spec.</b>	<b>Sample No.</b>	<b>Heat Treat</b>	<b>Bar S/N</b>	<b>Heat No.</b>	<b><math>\alpha</math></b>
Smooth Tensile	PWA 1484	6-1	6	1530101	1033	2
Smooth Tensile	PWA 1484	6-2	6	1530106	1033	5
Smooth Tensile	PWA 1484	6-3	6	1530107	1033	1
Smooth Tensile	PWA 1484	6-4	6	1530202	1033	3
Smooth Tensile	PWA 1484	6-5	6	1530203	1033	5
Smooth Tensile	PWA 1484	6-6	6	1530910	1034	5
Smooth Tensile	PWA 1484	6-7	6	1530911	1034	5
Smooth Tensile	PWA 1484	6-8	6	1531002	1034	4
Smooth Tensile	PWA 1484	6-9	6	1531004	1034	4
Smooth Tensile	PWA 1484	6-10	6	1531007	1034	6
Smooth LCF	PWA 1484	6-1	6	155012	1033	6
Smooth LCF	PWA 1484	6-2	6	155013	1033	2
Smooth LCF	PWA 1484	6-3	6	155016	1033	2
Smooth LCF	PWA 1484	6-4	6	155017	1033	6
Smooth LCF	PWA 1484	6-5	6	155031	1034	1
Smooth LCF	PWA 1484	6-6	6	155032	1034	2
Smooth LCF	PWA 1484	6-7	6	155034	1034	2
Smooth LCF	PWA 1484	6-8	6	155036	1034	2
Smooth HCF	PWA 1484	6-1	6	1530103	1033	4
Smooth HCF	PWA 1484	6-2	6	1530105	1033	3
Smooth HCF	PWA 1484	6-3	6	1530201	1033	3
Smooth HCF	PWA 1484	6-4	6	1530812	1034	4
Smooth HCF	PWA 1484	6-5	6	1530909	1034	5
Smooth HCF	PWA 1484	6-6	6	1531006	1034	3
Notched LCF	PWA 1484	6-1	6	1530101	1033	2
Notched LCF	PWA 1484	6-2	6	1530106	1033	5
Notched LCF	PWA 1484	6-3	6	1530107	1033	1
Notched LCF	PWA 1484	6-4	6	1530202	1033	3
Notched LCF	PWA 1484	6-5	6	1530203	1033	5
Notched LCF	PWA 1484	6-6	6	1530910	1034	5
Notched LCF	PWA 1484	6-7	6	1530911	1034	5
Notched LCF	PWA 1484	6-8	6	1531002	1034	4
Notched LCF	PWA 1484	6-9	6	1531004	1034	4
Notched LCF	PWA 1484	6-10	6	1531007	1034	6
Creep	PWA 1484	6-1	6	155015	1033	2
Creep	PWA 1484	6-2	6	155033	1034	7
Creep	PWA 1484	6-3	6	155035	1034	5
Crack Growth	PWA 1484	6-1	6	77	1034	3
Crack Growth	PWA 1484	6-2	6	77	1034	3
Collared LCF	PWA 1484	6-1	6	1530103	1033	4
Collared LCF	PWA 1484	6-2	6	1530105	1033	3
Collared LCF	PWA 1484	6-3	6	1530201	1033	3
Collared LCF	PWA 1484	6-4	6	1530812	1034	4
Collared LCF	PWA 1484	6-5	6	1530909	1034	5
Collared LCF	PWA 1484	6-6	6	1531006	1034	3



**APPENDIX C — NOTCHED LOW-CYCLE FATIGUE FRACTURES FROM HEAT TREATMENTS 1  
THROUGH 7 PRODUCED AT 20°C (68°F) IN 34.5 MPA (5 KSI) HYDROGEN**



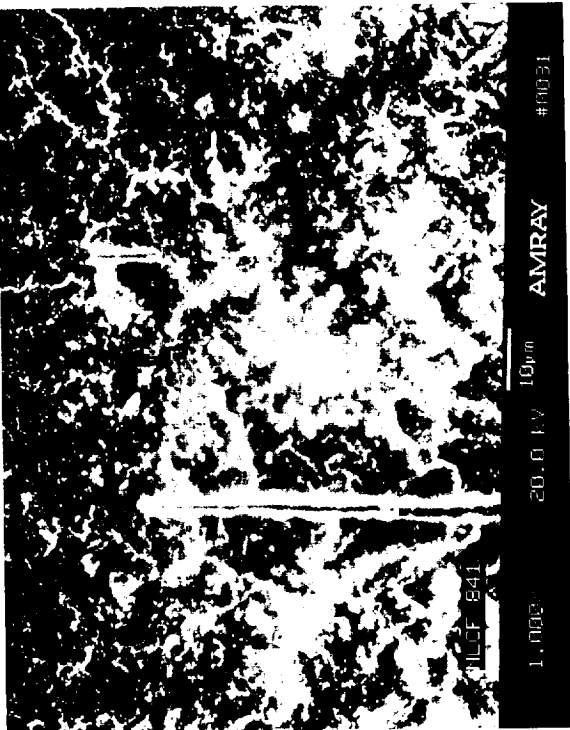
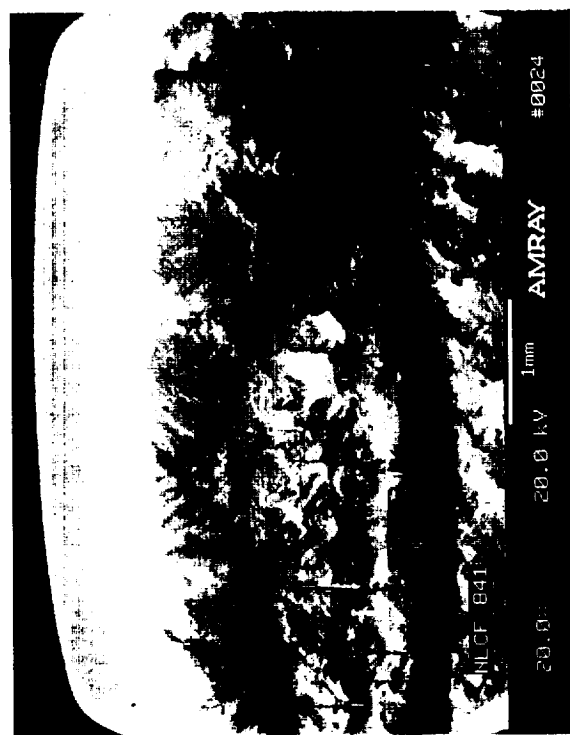


Figure 157. Heat Treatment 1

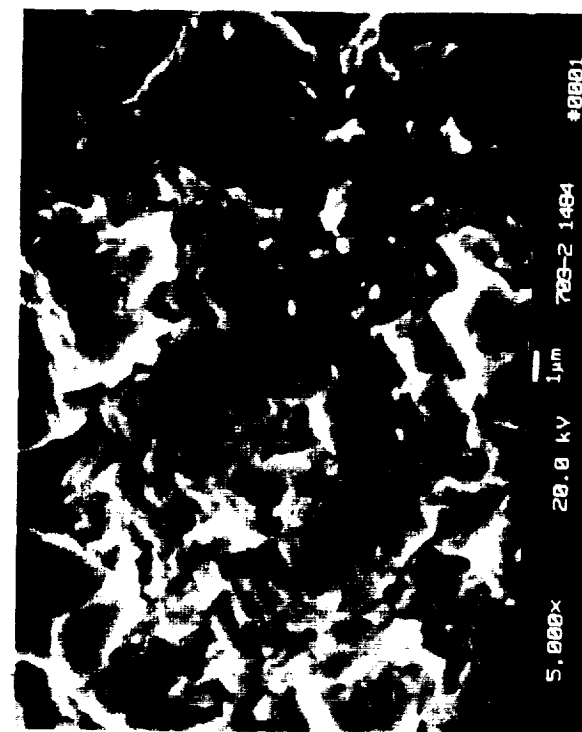
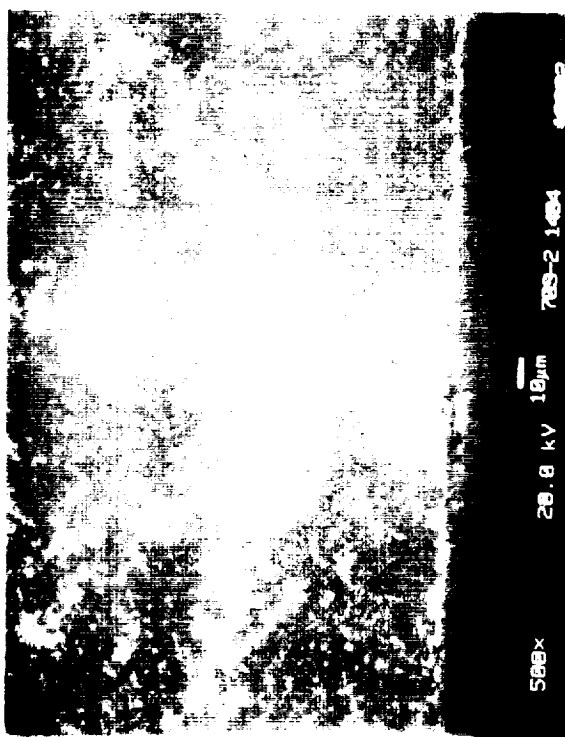
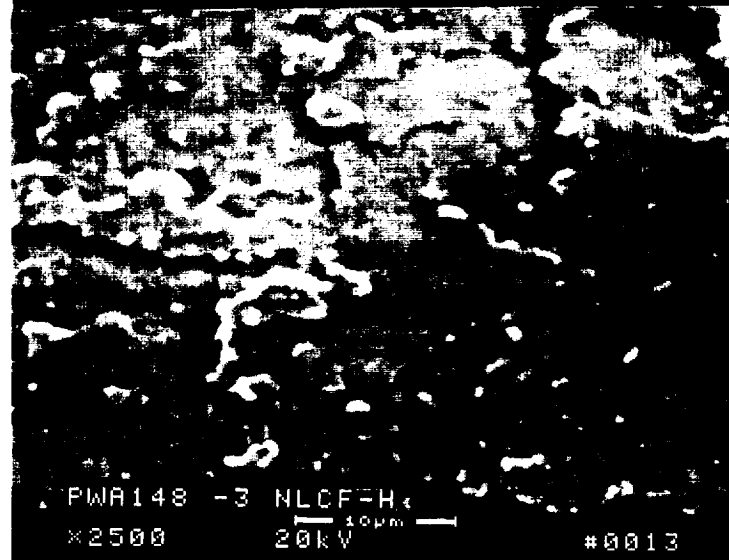
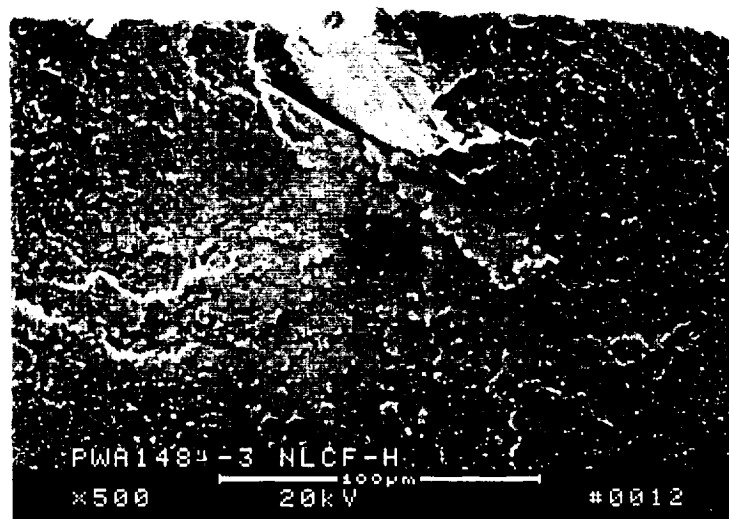
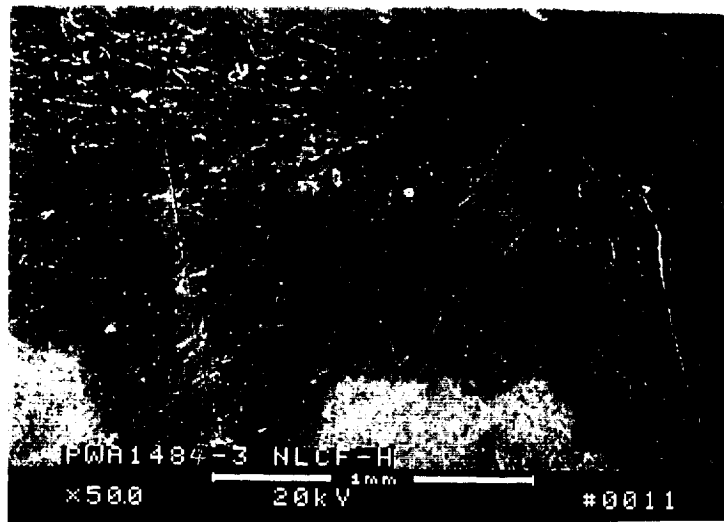


Figure 158. Heat Treatment 2



*Figure 159. Heat Treatment 3*

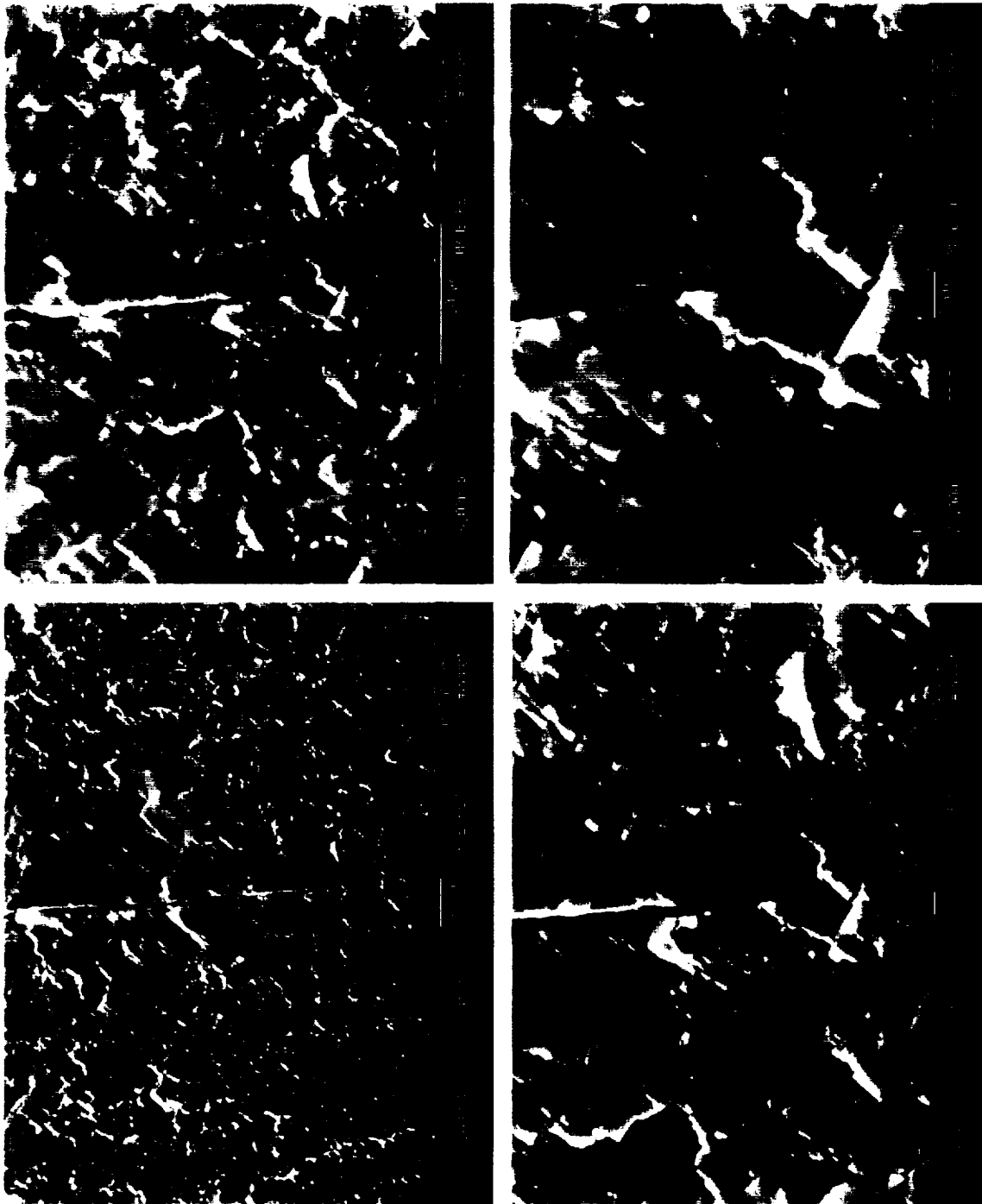


Figure 160. Heat Treatment 4

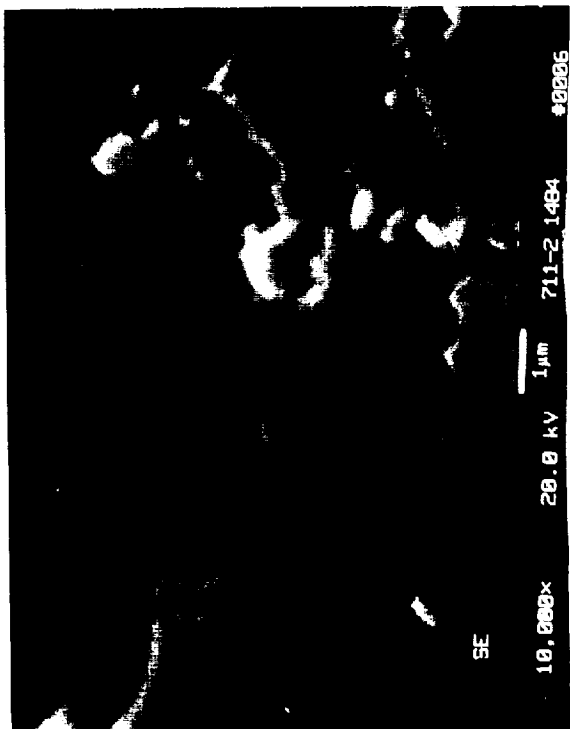
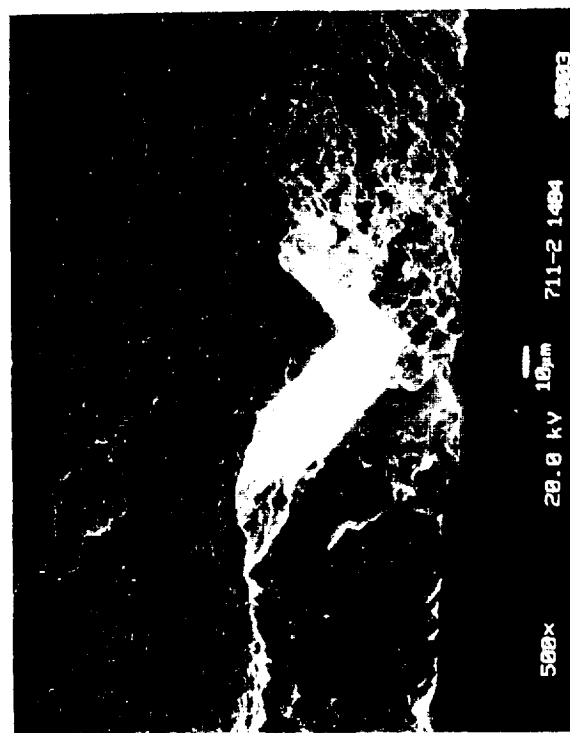


Figure 161. Heat Treatment 5

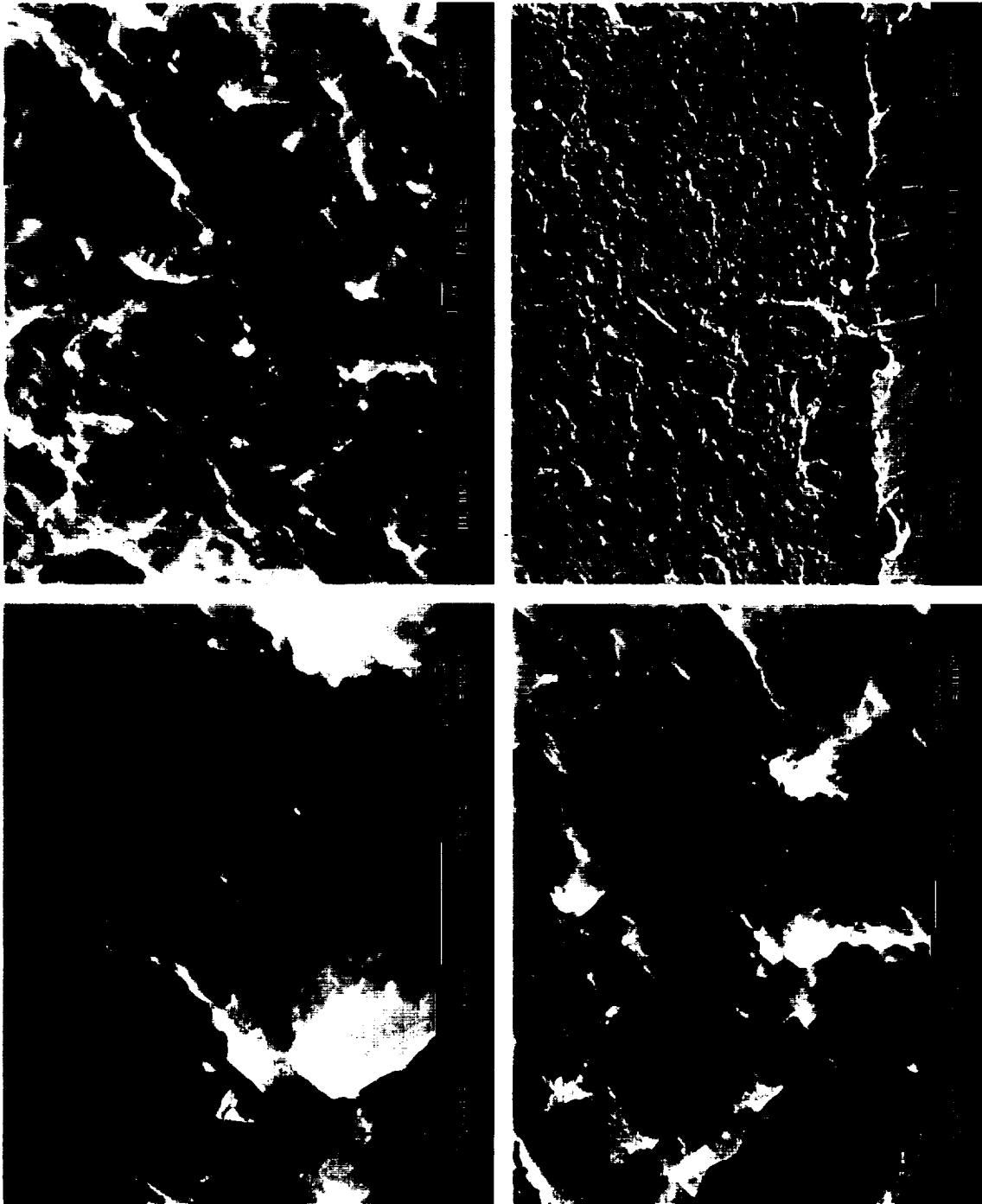


Figure 162. Heat Treatment 6



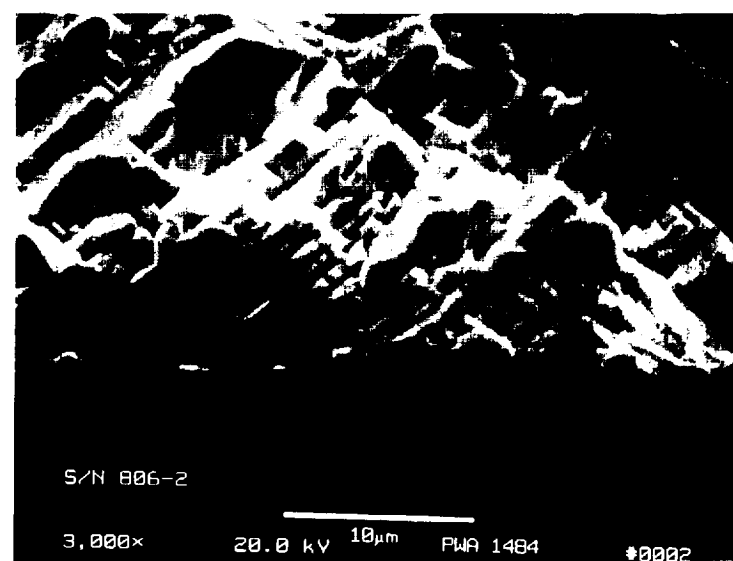
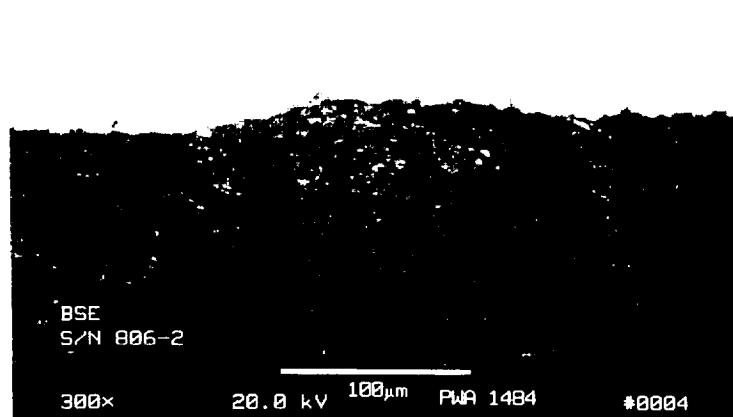
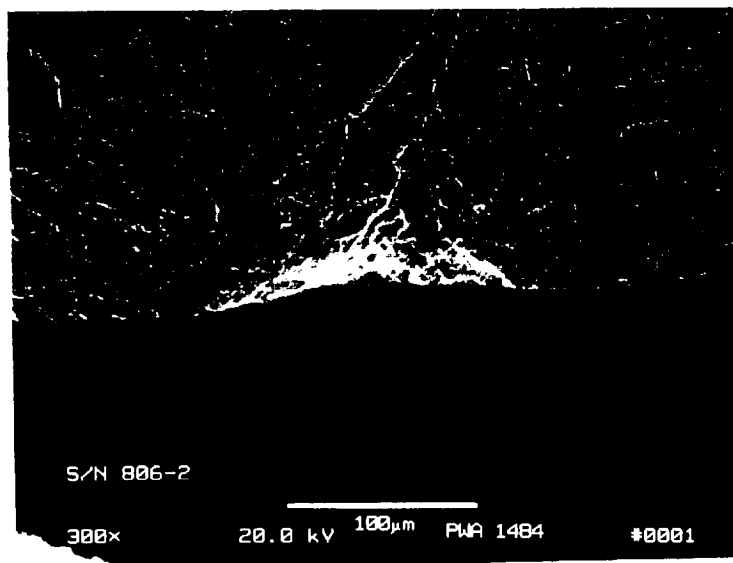


Figure 163. Heat Treatment 7





